

NUMERICAL ANALYSIS OF HERTZIAN AND
NON-HERTZIAN WHEEL-RAIL CONTACTS

Robert Fredrick Harder

B.S., Michigan Technological University, 1982
M.S., Michigan Technological University, 1986


A dissertation presented to the faculty of the
Oregon Graduate Institute of Science & Technology
in partial fulfillment of the
requirements for the degree of
Doctor of Philosophy
in
Materials Science and Engineering
July 1995

The dissertation "Numerical Analysis of Hertzian and Non-Hertzian Wheel-Rail Contacts" by Robert F. Harder has been examined and approved by the following Examination Committee:

Dr. Lemmy Meekisho, Thesis Advisor
Assistant Professor

Dr. William E. Wood
Professor and Department Head

 Dr. Paul Clayton
Professor

 Dr. Jack H. Devletian
Professor

ACKNOWLEDGEMENTS

I would like to acknowledge the support and guidance of my advisor and friend Dr. Lemmy Meekisho, without which this work could neither have been initiated nor completed. His many insightful suggestions, as well as his gentle, yet wise counsel have been greatly appreciated during these past three and a half years.

I am also very appreciative of the time and effort that the thesis committee, Dr. Lemmy Meekisho, Dr. Bill Wood, Dr. Jack Devletian, and Dr. Paul Clayton, has invested in reviewing this document and examining both its contents and my presentation. A special thanks to Dr. Bill Wood and Dr. Paul Clayton. To Dr. Wood for working out many of the details that it took to get me back into my Ph.D. study after being removed from it for four years. To Dr. Clayton for stimulating my interest in the subject of Tribology and providing the practical insight necessary for understanding this work within the “big picture” of track - train engineering.

The support, ideas and funding provided by Gunderson, Inc., Oregon Steel Mills and the Oregon Metals Initiative (OMI) were critical to the accomplishment of this thesis. The many discussions I have had with Gary Kaleta, Greg Saxton, Jon Zaer and Jim Pileggi of Gunderson, Inc. during the course of my study has broadened my understanding of materials, mechanics and rail car dynamics. I greatly appreciate their efforts and patience in this regard.

A special thanks to Dr. Burton Paul and Dr. C. Liu for sharing their computer algorithms, and Dr. Francis Kennedy and Dr. S. Kumar for spending time and energy providing thoughtful answers to my many questions.

I am also appreciative of the time that Drs. R. Viskanta and S. Ramadhyani invested in me during my years in the “doctoral proving ground” of Purdue University. To those dear classmates who I will always remember (John Weaver, Mark Christiansen, Vic Mahoney, Kirby Chapman, Dave Vader, Dave Zumbrennen, and Bill Valentine), many thanks!

I will to express my sincere thanks to the George Fox College community for helping bear the burden of this added load during the past four years. A special thanks to President Ed Stevens, Dr. Dirk Barram, and Dr. Hank Helsabeck for your assistance, encouragement and prayers. To my colleague John Johnson - thanks for your mathematical insights. To the library staff, especially Mr. Chuck Church, thanks for your tireless efforts. To my many students, especially Mike Timmons and Dan Pringle - you guys were there when I really needed you, thanks so much. Also, to my secretary and sister Linnea Stahlnecker, thanks for putting up with me and putting all the details of this document into a readable format!

I gratefully acknowledge the prayers, encouragement and continued sacrifice of my wife, Cynthia Ann Harder, who has supported me through both failures and successes, in sickness as well as health. Without her patience, understanding, and love, this work would never have been realized. To my daughters: Jocelyn Rose, Naomi Rachelle, Anja Renee, Esther Rhiana and Hanna Roux, thank you for your patience and prayers - you are both my joy and my motivation.

Most importantly I must acknowledge the ever-present source of strength, endurance, hope and peace in my life - Jesus Christ the only Son of God. For, “I can do all things through Him who strengthens me”. Philippians 4:13

DEDICATION

Dedicated to my mother and father,
Caroline E. Harder and Robert C. Harder, P.E.

TABLE OF CONTENTS

ACKNOWLEDGEMENTS	iii
DEDICATION	v
TABLE OF CONTENTS	vi
LIST OF TABLES	x
LIST OF FIGURES	xi
NOMENCLATURE	xix
ABSTRACT	xxiii
1. INTRODUCTION	1
1.1 Rail Car Dynamics	1
1.2 Wheel-Rail Contact	3
1.3 Outline of the Dissertation	4
2. BACKGROUND	7
2.1 The Normal Problem	7
2.1.1 Hertzian Contact Geometries	7
2.1.2 Non Hertzian Contact Geometries	11
2.2 The Tangential Problem	12
2.2.1 Creepage Kinematics	13
2.2.1.1 Longitudinal Creepage	14
2.2.1.2 Lateral Creepage	15

2.2.1.3	Spin Creepage	15
2.2.2	Creepage Kinetics	16
2.2.2.1	Linear Creep Force Regime	16
2.2.2.2	Nonlinear Creep Force Regime	17
2.2.2.3	Full Slip Regime	18
2.2.3	Complete Creep Force-Creepage Theories	18
2.2.3.1	Variational Methods	19
2.2.3.2	Heuristic Models	20
2.2.3.3	Iterative Techniques	22
2.3	Rough and Inelastic Surfaces	25
2.3.1	Surface Roughness	25
2.3.2	Surface Contamination	26
2.3.3	Plasticity Effects	27
2.4	Contact Patch Friction Work	29
2.4.1	Global Work	29
2.4.2	Local Work Distribution	30
2.4.3	Local Heat Flux	32
3.	PROCEDURES AND RESULTS	56
3.1	Counterformal Hertzian Contacts	56
3.1.1	Closed form solution to Patch Geometry	56
3.1.2	Iterative Solution for Two Axis of Symmetry-COUNTAC2	57
3.1.2.1	Code Implementation	58
3.1.2.2	Code Verification	59

3.1.3	Creep Force - Creepage Algorithms	60
3.1.3.1	Code Implementation	60
3.1.3.2	Sparse Matrix Solution	61
3.1.3.3	Code Verification	63
3.2	Counterformal Non-Hertzian Contacts	63
3.2.1	Iterative Solution for One Axis of Symmetry - COUNTAC1	63
3.2.1.1	Code Implementation and Verification	65
3.2.2	Creep Force - Creepage Algorithms -ROLCREEP	66
3.2.3	Code Implementation and Verification	66
3.3	Wheel - Rail Model - 136RE X AAR1-B	67
3.3.1	Wheel-Rail Surface Geometries	68
3.3.2	Three Regimes of Contact	68
3.3.3	Centralized Rail Crown Contact (Position #1)	69
3.3.3.1	Normal Hertzian Solution	69
3.3.3.2	Tangential Hertzian Solution	69
3.3.4	Gauge-side Rail Head Contact (Position #3)	72
3.3.4.1	Normal Hertzian Solution	72
3.3.4.2	Tangential Hertzian Solution	72
3.3.5	Transition Zone Contact (Position #2)	73
3.3.5.1	Non-Hertzian Solution to the Normal Problem	73
3.3.5.2	Non-Hertzian Solution to the Tangential Problem	74
3.3.5.3	Ellipticizing Non-Hertzian Contacts	75
3.3.5.4	Non-Hertzian vs. Ellipticized - Normal Results	78

3.3.5.5	Ellipticized Solution to the Tangential Problem	78
3.3.5.6	Non-Hertzian vs. Ellipticized Tangential Results	79
3.4	Contact Patch Friction Work	79
3.4.1	Global Patch Work	80
3.4.1.1	Friction Work Surfaces	80
3.4.1.2	Surface Equations	81
3.4.2	Local Patch Work Computations	82
3.4.3	Friction Work Distribution	82
4.	DISCUSSIONS	135
4.1	Generalized Creep Force - Creepage Behavior	135
4.2	Ellipticized Non-Hertzian Contacts	139
4.3	Contact Patch Friction Work	143
5.	CONCLUSIONS	159
6.	SUGGESTIONS FOR FUTURE WORK	161
	REFERENCES	164
	APPENDIX A	175
	APPENDIX B	184
	APPENDIX C	187
	APPENDIX D	209
	APPENDIX E	223
	VITA	227

LIST OF TABLES

2.1	Coefficients m and n for different values of θ	34
2.2	Overview of Contact Mechanics Computer Codes	35
3.1	Comparison of Contact Parameters Resulting from COUNTAC2 with Hertz Theory.	84
3.2	Coefficients for the Creep Force - Creepage Surface Equations of Position #1	85
3.3	Coefficients for the Creep Force - Creepage Surface Equations of Position #3	85
3.4	Coefficients for the Creep Force - Creepage Surface Equations of Position #2, Ellipticized	86
3.5	Range of Input Parameters for Global Parametric Friction Work Study	86
3.6	Coefficient for the Friction Work Surface Equation of Position #1	87
3.7	Coefficient for the Friction Work Surface Equation of Position #2	87
3.8	Coefficient for the Friction Work Surface Equation of Position #3	87
4.1	Coefficients for Longitudinal Creep Force Approximating function of Equation (3.8)	149
4.2	Coefficients for Lateral Creep Force Approximating function of Equation (3.9)	149
4.3	Speed and Accuracy Test Data for Computer Codes	150

LIST OF FIGURES

1.1	Schematic diagram illustrating wheelset - torsional / track longitudinal interaction [26].	5
1.2	A wheelset force diagram including creep and flange forces [27].	5
1.3	Types of wheel-rail contact: (a) New wheel - counterformal; and (b) Worn wheel - conformal contact [40].	6
2.1	Two elastic bodies in frictional rolling contact.	
2.2	Tractive rolling with slip and stick zones indicated [40].	36
2.3	The creepages: (a) a wheelset on a track; and (b) illustration of camber spin [44].	37
2.4	Creep force - creepage diagram according to Carter [39].	38
2.5	Creep force - creepage diagram and contact ellipse for the linear regime.	39
2.6	Creep force - creepage diagram and contact ellipse for the non-linear regime.	40
2.7	Creep force - creepage diagram and contact ellipse for the full slip regime.	41
2.8	Measured and theoretical surface traction stresses for circular contact patch [46].	42
2.9	The idea of the simplified theory [44].	42
2.10	Contact position on the rail head for various wheelset positions - both ellipticized and actual geometries [56].	43

2.11	Comparison of complete creep force - creepage theories.	
	(a) spin $\leq 10\%$ and (b) $10\% \leq \text{spin} < 25\%$ [57].	44
2.12	Non-Hertzian wheel - rail contact patch [75].	45
2.13	Longitudinal traction distribution for non-Hertzian patch.	
	$u_x = 0.0003$, $N = 1400$ pounds, $\frac{F_x}{\mu N} = 0.6$ $m = 0.2$ [75]	46
2.14	Longitudinal creepage curve for elastically similar bodies with elliptic contact. ($a/b = 2.89$, $\nu = 0.28$, $\nu_y = \phi = 0$) [35].	47
2.15	Longitudinal traction along x-axis for rolling contact of elliptic patch, (circle - Kalker's nonlinear theory; square Paul and Liu [35]).	
	(a) $\eta_x = 0.3$, and (b) $\eta_x = 0.6$	48
2.16	Shape of a non-Hertzian contact patch [64].	49
2.17	Pressure along y-axis for the contact patch of Figure 2.16 [64].	50
2.18	Nondimensional contact pressure p^* versus nondimensional radial coordinate ρ . (a) light load; and (b) heavy load (note change in scales) [82].	51
2.19	Influence of surface roughness (a) on the minimum contact pressure $p(0)$ compared with the maximum Hertzian pressure p_0 ; and (b) on the effective contact radius a^* compared with the Hertz radius a_0 [31].	52
2.20	High rail surface showing possible contact areas [106].	53
2.21	Typical traction distribution with separatrix location and regions of slip and stick.. . . .	54

2.22	Contact patch domain indicating local traction	
	\bar{T} and slip \bar{s} vectors at cell location i, j	55
3.1	Wheel and rail radii of curvatures.	88
3.2	Mesh development and contact boundary (a) interpenetration curve and first iteration; and (b) first iteration and final boundary.	89
3.3	Comparison of contact patch geometry as predicted by COUNTAC2 and Hertz theory.	90
3.4	Comparison of contact patch pressure distribution as predicted by COUNTAC2 and Hertz theory.	91
3.5	Lateral creep force - creepage curve comparison between modified DUVOROL and Kalker's original data [53].	92
3.6	Comparison of separatrix locations for a circular contact as predicted by modified DUVOROL, data from Liu [35].	93
3.7	Rail and wheel profiles for a 140 RE X SIG (Schweitzerische Industril - Gesellschaft) Metroliner.	94
3.8	Profile of a new 136RE (136 pound per yard) rail.	95
3.9	Profile of a new AAR1-B wide flange wheel.	96
3.10	Three regimes of contact (positions #1, #2, #3) for a new 136RE X AAR1-B rail wheel combination.	97
3.11	Results of the <i>normal</i> Hertzian solution as a function of wheel load for contact position #1.	98
3.12	Longitudinal creep force - creepage surface plot for contact position #1 ($a/b = 1.22$) ($UXN = \eta_x$, $UYN = \eta_y$)	99

3.13	Lateral creep force - creepage surface plot for contact position #1 (a/b = 1.22) (UXN = η_x , UYN = η_y)	100
3.14	Results of the <i>normal</i> Hertzian solution as a function of wheel load for contact position #3.	101
3.15	Longitudinal creep force - creepage surface plot for contact position #3 (a/b = 5.88) (UXN = η_x , UYN = η_y)	102
3.16	Lateral creep force - creepage surface plot for contact position #3 (a/b = 5.88) (UXN = η_x , UYN = η_y)	103
3.17	Results of the <i>normal</i> non-Hertzian solution as a function of wheel load for contact position #2.	104
3.18	Non-Hertzian contact patch geometries as a function of wheel load for contact position #2 (half symmetry).	105
3.19	Non-Hertzian contact patch pressure distribution (3-D) for a 12,342 pound wheel load at position #2. (pmax = 0.255 * 10 ⁶ psi, Xnorm = 0.2591 in.)	106
3.20	Non-Hertzian contact patch pressure distribution (2-D) for a 26,535 pound wheel load at position #2 (xnorm = .3038 inches, legend signifies variation in $\frac{P}{p_{max}}$)	107
3.21	Separatrix location for a non-Hertzian contact of position #2 with a wheel load of 12,342 pounds ($v_x = 0.15\%$, $v_y = \phi = 0.0$, xnorm = .259 inches, triangle - leading edge; square - trailing edge; dots - separatrix)	108

3.22	Separatrix location for a non-Hertzian contact of position #2 with a wheel load of 12,342 pounds ($v_x = 0.35\%$, $v_y = \phi = 0.0$, $x_{norm} = .259$ inches, triangle - leading edge; square - trailing edge; dots - separatrix)	109
3.23	Longitudinal slippage distribution for non-Hertzian contact of position #2 with a wheel load of 12,342 pounds ($v_x = 0.35\%$, $v_y = \phi = 0.0$, $x_{norm} = .2591$ inches, $f = 0.3$, $\psi = 0.0035$).	110
3.24	Longitudinal surface shear traction distribution for non-Hertzian contact of position #2 with a wheel load of 12,342 pounds ($v_x = 0.15\%$, $v_y = \phi = 0.0$, $x_{norm} = .2591$ inches, $f = 0.3$, $\psi = .255 * 10^6$ psi).	111
3.25	Non-Hertzian contact patch geometry for a wheel load of 12,342 pounds at position #2 - half symmetry with grid.	112
3.26	Non-Hertzian contact patch geometry for a wheel load of 12,342 pounds at position #2 - half symmetry showing actual area.	113
3.27	Contact patch geometry for both actual non-Hertzian and ellipticized contact for position #2 at 12,342 pounds of wheel load.	114
3.28	Contact patch pressure distribution for both actual non-Hertzian and ellipticized contacts for position #2 at 12,342 pounds of wheel load.	115
3.29	Polynomial curve fit of non-Hertzian contact geometries for position #2.	116

3.30	Effect of wheel load on non-Hertzian contact patch geometric parameters for position #2.	117
3.31	Effect of wheel load on non-Hertzian contact patch pressure for position #2.	118
3.32	Longitudinal creep force - creepage surface plot for ellipticized contact position #2 ($a/b = 5.88$) ($U_{XN} = \eta_x$, $U_{YN} = \eta_y$)	119
3.33	Lateral creep force - creepage surface plot for ellipticized contact position #3 ($a/b = 5.88$) ($U_{XN} = \eta_x$, $U_{YN} = \eta_y$)	120
3.34	Comparison of creep force - creepage behavior for ellipticized and non-Hertzian contact at position #2 (load = 26,535 pounds, $v_y = \phi = 0$).	121
3.35	Global friction work surface plot ($a/b = 1.0$, $\chi_z = 0.2$, longitudinal creepage = η_x , lateral creepage = η_y , friction work = $W'_{gd}(J / m)$).	122
3.36	Global friction work surface plot ($a/b = 1.0$, $\chi_z = 0.8$, longitudinal creepage = η_x , lateral creepage = η_y , friction work = $W'_{gd}(J / m)$).	123
3.37	Global friction work surface plot ($a/b = 1.0$, $\chi_z = 6.5$, longitudinal creepage = η_x , lateral creepage = η_y , friction work = $W'_{gd}(J / m)$).	124
3.38	Global friction work surface plot ($a/b = 6.75$, $\chi_z = 0.8$, longitudinal creepage = η_x , lateral creepage = η_y , friction work = $W'_{gd}(J / m)$).. . . .	125

3.39	Generalized global friction work surface for position #1 ($UXN = \eta_x$, $UYN = \eta_y$).	126
3.40	Generalized global friction work surface for position #2 ($UXN = \eta_x$, $UYN = \eta_y$).	127
3.41	Generalized global friction work surface for position #3 ($UXN = \eta_x$, $UYN = \eta_y$).	128
3.42	Local traction distribution for ellipticized contact of position #2 (load = 26,535 pounds, $a/b = 2.16$, $v_x = 0.6\%$, $v_y = \phi = 0.0$, $xnorm = 0.3360$ inches, legend signifies variations in local traction T_x).	129
3.43	Longitudinal slippage distribution for ellipticized contact of position #2 (load = 26,535 pounds, $v_x = 0.6\%$, $v_y = \phi = 0.0$, $xnorm = 0.3360$ inches, legend signifies variations in local slippage s_x).	130
3.44	Local traction distribution for non-Hertzian contact of position #2 (load = 26,535 pounds, $v_x = 0.6\%$, $v_y = \phi = 0.0$, $xnorm = 0.3038$ inches, legend signifies variations in local traction T_x).	131
3.45	Longitudinal slippage distribution for non-Hertzian contact of position #2 (load = 26,535 pounds, $v_x = 0.6\%$, $v_y = \phi = 0.0$, $xnorm = 0.3038$ inches, legend signifies variations in local slippage s_x).	132
3.46	Local friction work distribution for ellipticized contact of position #2	

	(load = 26,535 pounds, $v_x = 0.6\%$, $v_y = \phi = 0.0$, $x_{norm} = 0.3360$ inches, legend signifies variations in local friction work W_{ij}').	133
3.47	Local friction work distribution for non-Hertzian contact of position #2 (load = 26,535 pounds, $v_x = 0.6\%$, $v_y = \phi = 0.0$, $x_{norm} = 0.3038$ inches, legend signifies variations in local friction work W_{ij}').	134
4.1	General behavior of dimensionless creep forces (a) FXN versus η_x ; and (b) FYN versus η_y	151.
4.2	Effect of patch aspect ratio (a/b) on the creep force - creepage curve.	152
4.3	Effect of the dimensionless spin parameter χ_z on the creep force - creepage curve.	153
4.4	The idea of the geometric distortion parameter Γ	154
4.5	Non-Hertzian and ellipticized contact patch geometry for position #2 at a wheel load of 26,535 pounds.	155
4.6	Polynomial curve fits and ANI for ellipticized and non-Hertzian contact of position #2 at a wheel load of 26,535 pounds.	156
4.7	Non-Hertzian contact patch friction work comparison of local summation to global work (position #2, load = 26,535 pounds, $v_y = \phi = 0.0$).	157
4.8	Non-Hertzian contact patch creepage effects on slip region (position #2, load = 26,535 pounds, $v_y = \phi = 0.0$).	158

NOMENCLATURE

Symbol	Meaning
\bar{a}	half length of the strip of maximum pressure for a non-Hertzian contact patch
\bar{b}	contact patch width, non-Hertzian contact through centroid of pressure
a, b	semi-diameters of an elliptic contact patch, with "a" in the rolling direction, and "b" transverse to the rolling direction.
c	\sqrt{ab}
A	area
A, B	coefficients in the equation for initial surface separation, also dimensionless patch semi-diameters a/c, b/c
C_{11} C_{22} C_{23}	Kalker's creepage coefficients
E	Young's modulus
E*	effective modulus
F	force
G	shear modulus
$\hat{i}, \hat{j}, \hat{k}$	unit vectors in (x, y, z) directions
I	moment of inertia
J	polar moment of inertia
l	characteristic length

m, n	tabulated functions of (B/A)
M	spin moment
p	pressure
P_m	peak pressure
\overline{P}	thermal power
N	normal force (wheel load)
q''	surface heat flux
r	distance
R	surface radius
s	slippage
t	time
T	traction
V_o	rolling velocity
W	work
X	longitudinal translation
\ddot{X}	longitudinal acceleration
x, y, z	orthogonal cartesian coordinates
α	yaw angle (wheelset angle of attach); roughness parameter
$\dot{\alpha}$	time rate-of-change of yaw
χ_z	dimensionless spin creepage
γ	cone angle of wheel with respect to axle
Γ	geometric distortion parameter

δ	rigid body approach
δ_0	bulk compression
ε	normalizing parameter
ξ	creepage vector
K_s	asperity summit curvature
η_x, η_y	dimensionless longitudinal and lateral creepage
λ	convergence parameter
μ	coefficient of friction; roughness parameter
v_x, v_y	longitudinal and lateral creepages
ϕ	spin creepage
θ	angular displacement of wheelset
$\dot{\theta}$	angular velocity of wheel set
$\ddot{\theta}$	angular acceleration of wheelset
ν	Poisson's ratio
ρ	effective rolling radius
Ψ	angle between the normal planes containing the curvatures $\frac{1}{R_1}$ and $\frac{1}{R_2}$
σ_s	standard distribution of summit heights
ξ	asperity density (number of summits per unit area)
ω	relaxation scaling factor
Ω	contact patch domain

Subscript	Meaning
c	circumferential
cl	left contact
d	dimensionless
g	global
h	Hertzian
l	local
m	maximum
nh	non-Hertzian
t	track, translational
tl	left track
tr	right track
R	resultant
s	sliding
w	wheel
wl	left wheel
wr	right wheel
XNL	x direction non-linear
YNL	y direction non-linear
x, y, z	orthogonal coordinate directions
1, 2	rolling bodies
i, j	indices of (x, y)

ABSTRACT
**NUMERICAL ANALYSIS OF HERTZIAN AND
NON-HERTZIAN WHEEL-RAIL CONTACTS**

Robert F. Harder
Oregon Graduate Institute of Science & Technology
Supervising Professor: Lemmy L. Meekisho

Improved rail car designs which can provide faster, safer and more economical transportation, often require a significant amount of dynamic analysis and simulation. Of the many important processes that simultaneously occur during the rolling of wheels on rails, one of the most important is that of the contact mechanics at the wheel-rail interface. The forces which develop within the contact patch are ultimately responsible for coupling the dynamics of the rail car to the geometry of the rail. This work seeks to understand the mechanics of wheel-rail contacts and to define the governing parameters in a generalized format which can be used for dynamic rail car simulation. Emphasis is given to non-Hertzian contact geometries and the tribological implications of frictional work.

The mechanics of both Hertzian and non-Hertzian contacts were studied with the aid of a variety of computational tools. A detailed parametric analysis was performed for a 136RE X AAR1-B rail-wheel combination. Three different regimes of contact were identified (assuming unworn profiles) between the rail crown and gauge corner. Two were Hertzian and the other was non-Hertzian. Solution to the *normal* problem for each regime of contact was obtained over a wide range of wheel loads. Using the results of the *normal* problem, solutions to the *tangential* problem were obtained for each regime of contact for a wide range of creepages. This was accomplished for the non-Hertzian contact by using both a non-Hertzian algorithm as well as postulating the existence of an *ellipticized* non-

Hertzian contact and treating it with classic Hertzian methods. This latter method showed that the non-Hertzian nature of wheel-rail contacts does not significantly alter the classic creep force - creepage behavior (for non-Hertzian contacts having a geometric distortion of $\Gamma \leq 64\%$).

Results of the parametric analysis also revealed a set of generalized surface equations capable of approximating both longitudinal and lateral creep force as a function of the creepages and patch aspect ratio. The form of these equations was found to be most accurately represented by the hyperbolic tangent function. Speed and accuracy tests of the approximating functions showed favorable results when compared to other codes that were based on complete creep force - creepage theories.

Generalized approximating equations were also obtained which accurately represented the behavior of global contact patch friction work. The distribution of local patch friction work was also obtained for both Hertzian and non-Hertzian contacts. Due to the asymmetry of traction and slip profiles for the non-Hertzian patch, a unique bi-modal patch friction work profile was obtained.

CHAPTER I

INTRODUCTION

1.1 Rail Car Dynamics

Rail car dynamics have long been identified as a major cause of train accidents. Over the past several decades, derailments due to rail car dynamic instabilities have shown a steadily upward trend in both the number of derailments and in the dollar damage resulting from these derailments [1]. As the rail transportation industry seeks to increase market potential in both freight and passenger transport, operational efficiency and safety will become key factors in need of optimization. However, these two parameters are tightly coupled, in that operating efficiency is a function of maximum rail car load capacity and speed, while operational safety is dependent upon successful curve negotiation and braking. Hence the need for improved rail car designs, which should be one of the natural results of rail car dynamic modeling.

Numerous mathematical models for predicting the dynamic performance of rail cars have been reported in the literature [2-17]. Methodologies including finite element, finite difference as well as analog computer simulation techniques abound. Models range from a single wheelset having three degrees of freedom [18], to complete rail car models (car body, trucks, suspensions and wheelsets) on the order of 23 degrees of freedom [19], to commercial codes such as NUCARS (New and Untried Car Analytic Regime Simulator) [20, 21], which provides dynamic modeling capability for multiple interconnected rail cars.

Regardless of model methodology or complexity, the governing equations of rigid body motion for multidimensional rail car dynamics are well understood and a variety of general dynamic analysis packages (ie. ADAMS, ADINA, DYNA CODES-LLL) could be adopted for the purposes of model development. However, if a reliable dynamic rail car model is to be developed, an accurate physical understanding and quantitative prediction of the wheel/rail contact forces must be achieved. These forces which act at the interface of the wheel and rail are ultimately what control incipient derailment [22].

Regarding derailment, several different modes have been identified as resulting from excessive forces between the wheel and rail [23-25]. The three primary modes include: gage widening derailment, track panel shift, and wheel climb derailment. All three modes are a strong function of lateral contact force magnitude, which becomes especially severe during curving.

When considering the governing equations of rail car dynamics, it can be shown [26] that the wheel and rail interfacial forces only appear in the wheelset equations of motion (Figure 1.1 and 1.2). These are indicated below in equations (1.1) and (1.2):

$$J_{wl}\ddot{\theta}_{wl} + F_{cl}R_{wl} + K_w(\theta_{wl} - \theta_{wr}) = 0 \quad (1.1)$$

$$I_{tl}\ddot{X}_{tl} + F_{cl} + K_t(X_{tl} - X_{tr}) = 0 \quad (1.2)$$

What is not indicated by these wheelset equations, is that the wheel/rail tractive forces (F_{cl}) and spin moment which exist within the contact domain are a function of the wheelset position and motion relative to the rails. They are also known to be a function of wheel conicity and rail head geometry [27, 28]. Thus the contact forces are a function of the rail car dynamics, and the rail car dynamics are dependent on the contact forces.

1.2 Wheel-Rail Contact

When the surfaces of two perfectly rigid bodies are brought into contact with each other, a mathematical point (or possibly a line) of contact exists between them. As these non-deformable bodies are pressed together with an applied force, an infinite stress would be created on the interfacial region of zero area. However, as a natural consequence of material elasticity, the contact of real bodies results in an interfacial area of finite size, which increases as the applied loading increases. This leads to finite magnitudes of contact stress over the interface region (or contact patch).

An understanding and quantitative prediction of the forces which develop at the interface between two bodies in contact requires some knowledge about the geometry of the contact region over which the contact forces are distributed. Bodies which have dissimilar profiles are said to be *non-conforming*. The area of contact between such bodies is generally small compared with the dimensions of the bodies, and not greatly influenced by the shape of the bodies at a distance from the contact patch [31]. One example of non-conforming (or antiformal) contact is that which occurs between a new wheel and rail at a location well removed from the flange. Bodies having similar profiles are classified as *conformal*. Conformal contacts generally have contact patch dimensions which are not small compared to the principal body dimensions and cannot be approximated by a plane surface [32]. Such contacts are formed by bodies which “fit” closely together without deformation. One example of a conformal contact is that of a rail corner within the throat of a wheel flange. Other examples are a circular pin in a closely fitted hole, or a ball bearing rolling within a conformal groove. Examples of non-conforming and conformal contacts are shown in Figures 1-3a and 1-3b respectively.

1.3 Outline of the Dissertation

In this dissertation, a numerical investigation of wheel-rail contact is conducted. Chapter 2 is a literature survey on wheel-rail contact mechanics and contact force modeling techniques, along with relevant background about various computational algorithms for analyzing the rolling contact behavior of elastic bodies. In Chapter 3, the numerical results are outlined: counterformal Hertzian and non-Hertzian contacts (both normal and tangential solutions), as well as the complete solution of the creep force-creepage behavior for a 136RE X AAR1-B wheel-rail combination over a wide range of operating conditions. The important results are discussed in Chapter 4, and the main conclusions obtained from this study are listed in Chapter 5. Chapter 6 outlines possible future research direction with regard to wheel-rail contact analysis.

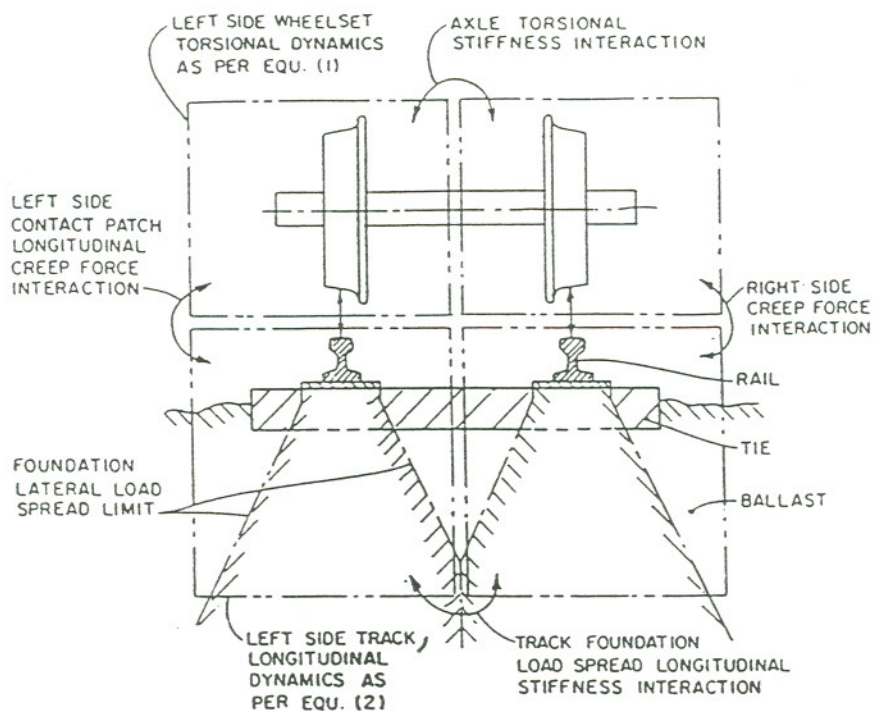


Figure 1.1 Schematic diagram illustrating wheelset - torsional / track longitudinal interaction [26].

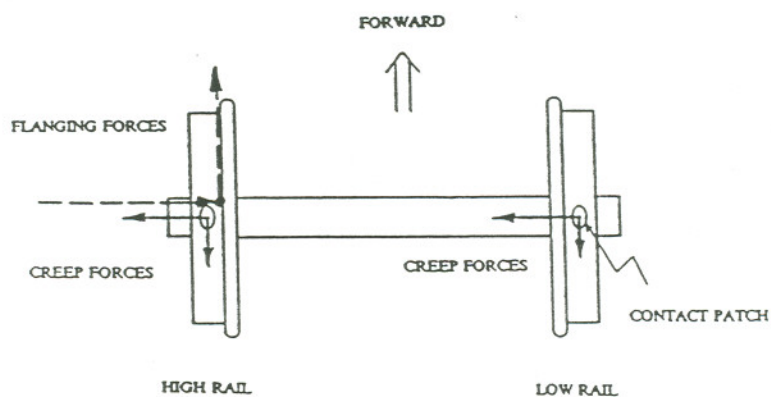


Figure 1.2 A wheelset force diagram including creep and flange forces [27].

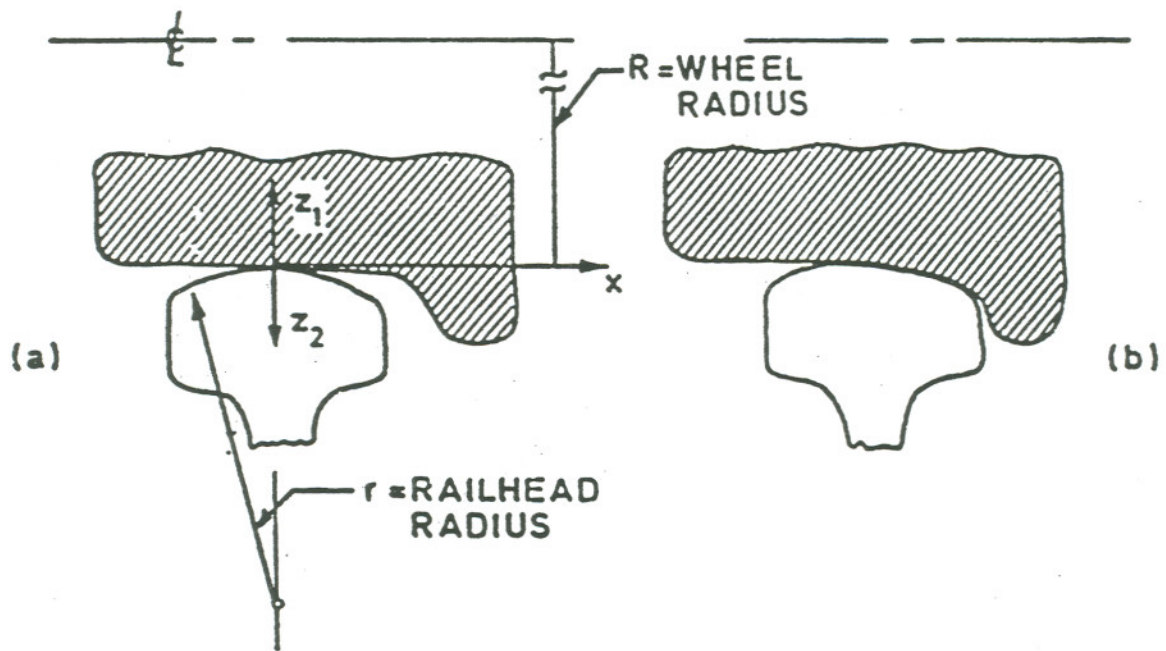


Figure 1.3 Types of wheel-rail contact: (a) New wheel - counterformal; and (b) Worn wheel - conformal contact [40].

CHAPTER 2 BACKGROUND

2.1 The Normal Problem

As shown by Kalker [33] the problem of rolling contact may be separated into two parts, the *normal problem* and the *tangential problem*. However, this is only valid for contacting bodies having the same elastic constants [34], because only then will the tangential tractions produce equal and opposite normal displacements on the two contacting surfaces.

The goals of the normal problem are to determine the size and shape of the contact region and the normal contact pressure distribution [35].

2.1.1 Hertzian Contact Geometries

The work of Hertz [36] was the first reliable mathematical solution to the normal problem. Hertz's theory is only valid for contacting surfaces which satisfy the following conditions:

- (1) The bodies are homogeneous, isotropic, obey Hooke's law, and experience small strains and rotations (ie. the linear theory of elasticity applies).
- (2) The contacting surfaces are frictionless.
- (3) The dimensions of the deformed contact patch remain small compared to the principal radii of curvature of the undeformed surfaces.

- (4) The deformations are related to the stresses in the contact zones as predicted by the linear theory of elasticity for half-spaces (Boussinesq's influence functions are valid).
- (5) The contacting surfaces are continuous, and may be represented by second degree polynomial (quadratic surfaces) prior to deformation.

For the general case of compression between two elastic bodies having quadratic surface curvatures, the surfaces near the point of contact (Figure 2.1) may be described by equations 2.1 and 2.2.

$$z_1 = A_1x^2 + A_2xy + A_3y^2 \quad (2.1)$$

$$z_2 = B_1x^2 + B_2xy + B_3y^2 \quad (2.2)$$

By adding these equations together and rearranging, the distance between any two such points C and D may be obtained as a function of the general constants A and B.

$$(z_1 + z_2) = Ax^2 + By^2 \quad (2.3)$$

Here the constants A and B depend on the magnitudes of the radii of curvature of the surfaces in contact and the angle between the planes of principal curvature, such that:

$$A + B = \frac{1}{2} \left[\frac{1}{R_1} + \frac{1}{R_{1'}} + \frac{1}{R_2} + \frac{1}{R_{2'}} \right] \quad (2.4)$$

$$B - A = \frac{1}{2} \left[\left(\frac{1}{R_1} - \frac{1}{R_{1'}} \right)^2 + \left(\frac{1}{R_2} - \frac{1}{R_{2'}} \right)^2 + 2 \left(\frac{1}{R_1} - \frac{1}{R_{1'}} \right) \left(\frac{1}{R_2} + \frac{1}{R_{2'}} \right) \cos 2\psi \right]^{1/2} \quad (2.5)$$

As presented in [37], since $(z_1 + z_2)$ of equation (2.3) must be positive, then A and B

must also be positive, and if the bodies are pressed together in a direction normal to the tangent plane at 0, the surface will have an elliptical boundary such that:

$$(x/a)^2 + (y/b)^2 = 1 \quad (2.6)$$

with semidiameters given by:

$$a = m \sqrt[3]{\frac{3\pi}{4} \frac{\rho(k_1 + k_2)}{(A + B)}} \quad (2.7)$$

$$b = n \sqrt[3]{\frac{3\pi}{4} \frac{\rho(k_1 + k_2)}{(A + B)}} \quad (2.8)$$

where k_1 and k_2 are material constants for the respective bodies.

$$k_1 = \frac{1 - \nu_1^2}{\pi E_1} \quad (2.9)$$

$$k_2 = \frac{1 - \nu_2^2}{\pi E_2} \quad (2.10)$$

The coefficients m and n are obtained depending on the ratio of $(B-A) : (A + B)$ as indicated in Table 2.1, where this ratio may be described by the term θ .

$$\theta = \cos^{-1} \left[\frac{B-A}{A+B} \right] \quad (2.11)$$

As shown in Table 2.1 for values of θ from 0 to 90°, the ratio of m/n is identical to the elliptical aspect ratio of the Hertzian contact patch a/b , which is reported extensively in the literature as a means for characterizing contact patch shape.

It has also been shown [52] that an alternative description for θ may be defined as

follows:

$$\theta = \cos^{-1} [k^2 (D' - C') / E'] \quad (2.12)$$

where, D' , C' and E' are complete elliptic integrals of argument k^2 ,

$$D' = \int_0^{\pi/2} \sin^2 \beta (1 - k^2 \sin^2 \beta)^{-1/2} d\beta \quad (2.13a)$$

$$C' = \int_0^{\pi/2} \sin^2 \beta \cos^2 \beta (1 - k^2 \sin^2 \beta)^{-3/2} d\beta \quad (2.13b)$$

$$E' = \int_0^{\pi/2} (1 - k^2 \sin^2 \beta)^{-1/2} d\beta \quad (2.13c)$$

and,

$$k^2 = (1 - a/b)^2 \quad (2.14)$$

These are listed in tabular form in [52], appendix E.

Hertz also showed the pressure distribution to be ellipsoidal, where the pressure at any point (x, y) within the contact patch is described by:

$$p(x, y) = p_m \sqrt{1 - \left(\frac{x}{a}\right)^2 - \left(\frac{y}{b}\right)^2} \quad (2.15)$$

where the magnitude of maximum pressure, p_m which was located at the center of the contact patch was found to be 1 1/2 times the average pressure on the surface of the contact.

$$p_m = \frac{3N}{2\pi ab} \quad (2.16)$$

2.1.2 Non-Hertzian Contact Geometries

When the contact conditions between a given pair of surfaces are found to violate any one of the five Hertz conditions listed in section 2.1.1, a non-Hertzian contact results. Such a contact will necessarily have a non-elliptical shape and non-ellipsoidal pressure distribution [31].

For the general problem of wheel rail contact, conditions (1) and (4) will always apply, provided that standard wheel and rail materials are being considered and that analysis is limited to the elastic range. Condition (2) involves the resultant tangential tractions which are generated due to the normal contact of curved surfaces. If the contacting materials are dissimilar, the tangential displacements will be as well, and slip will take place. However the elastic properties of most rail and wheel materials are similar enough so that the resulting tangential tractions on each surface (due to normal loading only) will be negligible. The result being a frictionless effect at the interface which would allow condition (2) to be satisfied, as well as the decoupling of the normal and tangential problems.

Conforming surfaces which are in contact, result in contact patch geometries which occupy an appreciable fraction of the contacting bodies themselves. As a result, they may not be regarded as elastic half spaces and therefore Hertz treatment becomes invalid (ie. condition (3) is violated). Examples of conformal contacts would be a pin in a hole with small clearance, or a ball in a spherical socket. In addition, it has been found that under high flange wear conditions, both wheel and rail can wear to a similar matching profile [119]. Such a conformal contact has been termed a "low stress" contact, as the load is distributed over a relatively large area. These contacts occur between wheel and rail on the

high leg of sharp curves or where there is relative rail and wheel flange contact at discontinuities on straight track (Figure 1-3). Under the majority of tangent track operations however, the contact area is quite small in comparison to the undeformed surface curvatures, and therefore Hertz restriction (3) may be applied.

Regarding the specific geometric description of the contacting surfaces prior to deformation, if they may be described by second order polynomials, then the resultant patch geometry will be elliptical. However, if the surfaces are discontinuous at the location of contact, or if higher order terms are necessary for describing the curvature, restriction (5) must be relaxed. For actual wheel and rail surfaces, it is possible that a number of different radii of curvature will be required in order to describe the surface geometry at any axial station along the track, which would necessitate a number of different locations for non-Hertzian contact patches.

As will be shown in section 3.2, non-Hertzian contact problems do not permit analytical solutions in closed form. As a result, a number of numerical techniques have been developed in order to predict contact patch geometry and pressure distribution.

2.2 The Tangential Problem

The tangential problem was first attempted by Reynolds [38] in a remarkable paper on frictional rolling contact between two elastic bodies. He was the first to identify a limiting region of adhesion within the contact patch, and recognized that as a consequence, regions of both “stick” and “slip” existed within the contact patch. The first complete mathematical treatment of the tangential problem was reported by Carter [39]. He provided a theoretical description of the slip/stick zones for elastic cylinders under tractive rolling, as he qualified the distribution of tangential forces (Figure 2.2) and surface strains within the contact patch.

Within the “locked” (or adhesion region) of the contact patch, the axial strain difference between the wheel and rail was found to be a constant (for any particular set of rolling conditions). Carter called this phenomena *creepage*. Specifically, in the axial (or rolling) direction, the term longitudinal creepage is used. Johnson [31], later obtained a description of lateral (or transverse) and spin creepages.

2.2.1 Creepage Kinematics

Creepage has kinematical significances. It is the relative mean slip velocity of the two surfaces. The longitudinal creepage may specifically be described as a fraction of the forward velocity of a rigid wheel rolling on a rigid surface [35]. For an elastic wheel deformed due to loading, the resulting circumference of the rolling wheel in the deformed state is larger than the undeformed (or rigid) wheel, by a percentage equal to the “creep ratio” or longitudinal creepage. (Perfectly rigid wheels and rails would not experience this effect). Lateral creepage, which occurs in the direction of the axle, may similarly be described as “the ratio of lateral displacement per wheel revolution, to the circumference of the wheel” [40]. Johnson [41-43] has performed numerous laboratory experiments using this method and has accurately obtained creep curves for a variety of rolling elements and surfaces.

Kalker [44] obtained a generalization of Carter’s notion of creepage. He pointed out that it was a rigid body motion in the plane of contact, where the corresponding velocity is a translation and a rotation within the osculating plane. The rotation is taken about the common normal at the center of the contact area. Kalker defined this rigid body motion as given in equation (2.17) and called it the *rigid slip*.

$$\xi \mathbf{V}_o = (v_x - \phi y) V_o \hat{i} + (v_y + \phi x) V_o \hat{j} \quad (2.17)$$

A physical description of equation (9) follows directly from the schematic of the wheelset-track system shown in Figure 2.3. As indicated, (following the definitions of Kalker [44]) the wheel set makes a *yaw angle* α with the rails, where the time rate-of-change of yaw angle due to vehicle turning rate is given as $\dot{\alpha}$. The lateral component of wheelset velocity is given as \dot{y} , and the translational velocity as \mathbf{V}_T . At the origin of the coordinate system shown, the wheelset has circumferential velocity \mathbf{V}_c , which can be related to the wheel's angular velocity, $\dot{\theta}$ via rotational dynamics by,

$$\dot{\theta} = \frac{V_c}{R_w} \quad (2.18)$$

where R_w is the rolling radius of the wheel.

2.2.1.1 Longitudinal Creepage

Due to the conical shape of railroad wheels, the difference in effective rolling radii at any instant in time, gives rise to a longitudinal (x-direction) component of creepage, v_x (ie. the two conical frustrums are connected rigidly via a fixed shaft which ensures a high degree of rotational compliance between them, as a result, any differences in rolling radii of the wheels, produces an excessive elastic compliance or possible slip in the longitudinal direction within the contact patch of one or the other rolling contacts.) Other contributions to the longitudinal creep term may be physically associated with the tractive forces due to

acceleration or braking couples, and as Kalker [44] points out “very importantly, through the rotation $\dot{\alpha}$ of the yaw angle α , by which the left wheel moves with a different velocity over the rail than the right wheel”.

2.2.1.2 Lateral Creepage

The lateral creepage, v_y is due in part to the time rate-of-change of wheelset y - coordinate position, \dot{y} which could arise in steady curving, or from “hunting” (a guidance instability which occurs within certain velocity regimes on tangent track, due to conicity) or possibly transient load shifts. There is also a contribution to lateral creepage due to the vectoral difference in wheelset translational velocity V_T and wheel circumferential velocity V_c , which arises due to wheelset yaw (of angle α). This velocity difference has a component in the y -direction, which would not exist if the wheels were exactly aligned with the track.

2.2.1.3 Spin Creepage

The spin creepage (or spin), may be described [11] by two separate terms as indicated in equation (2.19).

$$\phi = \frac{\dot{\alpha}}{V_o} + \frac{\sin \gamma}{R_w} \quad (2.19)$$

Physically, spin arises due to any net rotation (or twisting) of the contact interface

about the z-direction. As shown in equation (2.19), the normalized yaw velocity has a vectorial component orthogonal to the contact plane at any instant of time, which is responsible for the first term in that equation. The second term is referred to as “camber spin” in the automotive industry, and arises due to the fact that the “common normal at the point of contact is tilted at the cone angle γ to the axis of rotation, and the wheel therefore has an angular velocity of spin $(\dot{\theta} \sin \gamma)$ relative to the rail” [31].

2.2.2 Creepage Kinetics

Creepage also has kinetic significance. Carter [39] was the first to arrive at a mathematical relationship between creep force and creepage. His analysis was concerned with the effects of acceleration, braking and frictional losses for a locomotive drive wheel. The results of Carter’s *creep-force/creepage* law are shown in Figure 2.4, where the abscissa is Carter’s creepage coefficient and the ordinate is dimensionless creep (friction) force. Although Carter’s work was limited to two dimensional contacting bodies, the general shape of his creep force - creepage curve was later verified by Vermeulen and Johnson [45] for three dimensional contacting surfaces. As indicated, the curve has three distinct regimes which correspond to three separate categories of rolling contact. These may be described as follows: (1) Linear regime, (2) Non-linear regime, (3) Full slip regime, and are shown in Figures 2.5 - 2.7 respectively, with the associated contact patch areas of slip and stick.

2.2.2.1 Linear Creep Force Regime

Within the linear regime the coefficient of friction is sufficiently high, to preclude slip

from occurring within the contact area. Therefore this region is one of pure rolling, and the entire contact patch may be identified as being a “stick” region. Graphically, the upper limit of this regime may be located where the creep force-creepage curve begins to depart from a linear asymptote as shown in Figure 2.5. The slope of the curve within this region is called the “creepage coefficient”, where any amount of creepage is due to material deformation (ie. differences in surface strain) on the adjacent contacting bodies [46]. This gradient is determined by the geometry of the contact area and the deformation properties of the material, but not by the coefficient of sliding friction. The creepage coefficients are constants of proportionality between the tractive force and relative surface velocity (displacement). For Hertzian contacts, these coefficients (gradients) are constants which are a function of: contact ellipse semi-diameters, Poisson’s ratio and shear modulus. This regime is important in analyzing the linear stability of rail car motion on tangent track and identifying “hunting” limits [47]. A number of linear theories have been developed based on the work of Carter. The first was that of dePater [34], and later Kalker [33]. The linear theory of Kalker has been the most popular. It assumes that the contact area is Hertzian elliptic, and that rolling takes place in the direction of one of the axes of the contact ellipse. Given that the ratio a/b of the elliptical axes and Poisson’s ratio are known *a priori*, the creepage coefficients may be obtained in tabular form [11].

2.2.2.2 Nonlinear Creep Force Regime

The non-linear regime of the creep force-creepage curve begins at the end of the linear region, and ends at the horizontal asymptote of the full slip (or saturation) regime. In 1958, Johnson generalized Carter’s result to accommodate circular contacts with longitudinal and lateral creepage without spin [48]. Later this theory was generalized for

elliptical contacts, resulting in a third order creep-force law [45]. Within the non-linear region, both adhesion and slip zones co-exist within the contact patch. The boundary which separates them is called the “separatrix”, which is coincident with the trailing edge of the contact patch for the linear regime, but gradually proceeds towards the leading edge as creepage increases (Figure 2.6) [40]. This behavior of the “slip” region was verified experimentally by Haines and Ollerton, using a photoelastic technique known as the “frozen stress method” [46]. The distribution of tractive forces over the contact patch is shown in Figure 2.8, (results of Haines and Ollerton’s experimental work). As indicated, the traction increases over the patch, beginning with zero at the leading edge, and becoming saturated at the Coulomb maximum value ($\mu P(x)$) from the separatrix to the trailing edge. Quantitative information regarding creep force-creepage behavior within the non-linear regime is important for predicting rail car curving behavior and non-linear stability analysis. Although numerous analytical treatments have been applied, thus far only approximate relationships have been reported [31].

2.2.2.3 Full Slip Regime

Within the full slip regime, gross sliding occurs between the two contacting bodies and the separatrix becomes coincident with the leading edge of the contact patch. This regime of contact is especially important for dynamic as well as tribological analysis of severe curving and locomotive hill climb and start up acceleration conditions [49].

2.2.3 Complete Creep Force-Creepage Theories

A number of “complete theories” have been reported for predicting the creep force -

creepage relationship over the entire regime of rolling contact between two elastic bodies. Kalker [50] developed a full three dimensional theory based on the principle of virtual work, valid for Hertzian contacts.

2.2.3.1 Variational Methods

Using the variational principle developed by Duvant and Lions [51], Kalker's "Exact Hertzian Theory" sought to maximize the complementary energy (an approach which is mathematically and physically equivalent to minimizing the total potential energy) within the contact patch domain [52]. The result of this procedure is to obtain the location of the separatrix. Once defined, the normal and tangential solutions are then carried out to predict the appropriate pressure distribution and tractive forces for given values of creepage and/or spin. The resulting computer program called "DUVOROL" was written in the ALGOL 60 computer language and was used to generate the British rail table book of creep force - creepage values. This program was later converted to a FORTRAN code by Goree and Law [53].

Kalker later [54, 55, 58] developed an approximate theory which treated the wheel and rail as a set of elastic springs. The associated physical model is that of a very thin elastic layer mounted on a rigid substrate. A schematic which depicts this is shown in Figure 2.9. This "Simplified Theory" is valid only for Hertzian contacts with similar elastic constants. By assuming similar values of Poission's ratio and shear moduli for the contacting bodies, the stresses in the shear and normal directions become uncoupled. This allows for the normal and tangential solutions to be obtained independent of each other, hence speeding up the computations. In addition, with the simplified theory the surface displacement of any given location within the contact patch depends only on the surface traction *at the same*

point, whereas in Exact Hertzian Theory, the surface tractions at *all points* contribute to the surface displacement. By introducing “flexibility parameters” a computer program called “FASTSIM” was developed, which although widely used, may be as much as 15% in error when compared to exact methods [44]. However, Goree [53] points out “for small or large values of a/b the Simplified Theory frequently gives better results, as the Exact Hertzian Theory (DUVOROL) often experiences numerical divergence difficulties for extreme values of a/b . In no instance was a significant improvement noted with the Exact Hertzian Theory.”

Kalker also developed an “exact” code to predict creep force - creepage for the entire regime which is valid for both Hertzian elliptic as well as non-Hertzian contact patches [52, 80]. Although about 400 times slower than FASTSIM, this exact code (called “CONTACT”) may be used for non-elliptic contacts. Its primary function is the validation of other “approximate theories”. The “Exact non-Hertzian Theory” of CONTACT is identical to that of DUVOROL with the exception being that of accommodating non-elliptic contact patches. In some cases non-Hertzian contact problems have been approximated as “ellipticized” contacts and subsequently treated with Hertzian codes [52, 56]. One example is indicated in Figure 2.10, where eight different lateral stages of a wheelset/track system are shown with corresponding contact geometries.

2.2.3.2 Heuristic Models

Another complete theory for predicting creep force - creepage for elastic bodies in rolling contact is due to Shen, Hendrick and Elkins (S.H.E.) [57]. Their “heuristic” model was developed based on the approximate expression of Vermeulen and Johnson [45]. This was done by implementing more accurate creep coefficients via Kalker’s linear theory [44]

and including a term to account for spin creepage. The basic methodology of the “Heuristic Model” limits it to Hertzian contact problems. As inputs, the patch semi-diameters, elastic constants, normal patch, load and creepages are required. The S.H.E. code (called “C FORCE”) first calculates the patch force based on the Kalker linear theory [33] (equations (2.20) to (2.22)).

$$F_x = abGC_{11}v_x \quad (2.20)$$

$$F_y = -abG(C_{22}v_y + \sqrt{ab} C_{23} \phi) \quad (2.21)$$

$$F_{R'} = (F_x^2 + F_y^2)^{1/2} \quad (2.22)$$

where C_{11} , C_{22} and C_{23} are the Kalker creepage coefficients. The linear resultant force $F_{R'}$ is then reduced to a non-linear value as per the third order law of Vermeulen-Johnson as in equation (2.23).

$$F_R = \begin{cases} \mu N \left[\left(\frac{F_{R'}}{\mu N} \right) - \frac{1}{3} \left(\frac{F_{R'}}{\mu N} \right)^2 + \frac{1}{27} \left(\frac{F_{R'}}{\mu N} \right)^3 \right]; & \text{for } F_{R'} \leq 3 \mu N \\ \mu N & ; \text{for } F_{R'} \geq 3 \mu N \end{cases} \quad (2.23)$$

The non-linear creep forces which result are obtained by means of a reduction parameter ε as in equations (2.24 to 2.26).

$$\varepsilon = \frac{F_R}{F_{R'}} \quad (2.24)$$

$$F_{XNL} = F_X \varepsilon \quad (2.25)$$

$$F_{YNL} = F_Y \varepsilon \quad (2.26)$$

The “Heuristic” model has been used by a number of investigators for dynamic rail car simulation due to its very high computational speed, minimal computer memory requirements and reasonable accuracy. Kalker [44] reports the S.H.E. method to be 100 times faster than FASTSIM (“the very fast calculator of the Hertzian simplified theory”). Regarding accuracy, Figure 2.11 has been included as a comparison of three creep force models: FASTSIM, DUVOROL and Heuristic Model, for a Hertzian contact of $a/b = 2.0$. Figure 2.11(a) is for the case of lateral and longitudinal creepage with small spin ($<10\%$) and 2.11(b) for intermediate spin ($>10\%$, $<35\%$). As indicated, as the amount of spin creepage is increased, so is the level of error in the Heuristic model.

By restricting comparisons to a range of steady state curving based on field results [59, 60], the maximum difference between DUVOROL and the Heuristic Model was 10.1%. For this same range of motion, the differences between DUVOROL and FASTSIM were as much as 6.2%. Kalker duly points out, however, that under the conditions of pure spin (lateral creepage = longitudinal creepage = 0), “the S.H.E. model fails miserably the moment it escapes the linear regime of the creep force - creepage curve” [44].

2.2.3.3 Iterative Techniques

A final theory to be considered for predicting the creep force - creepage relationship between three dimensional elastic bodies in contact is due to Paul [32, 49, 61- 77]. By utilizing a form of the strip theory developed by Haines and Ollerton [46] and expounded on by Kalker [33], Paul developed a complete theory valid within all three regimes of

rolling contact. The earlier work of Paul focussed on obtaining a solution to the normal problem (contact patch geometry, pressure distribution and total force) for both Hertzian and non-Hertzian counterformal contacts, as well as conformal (closely fitting) surface geometries [64, 65, 67]. Computer programs corresponding to each of these normal problems (written in FORTRAN 77) are: COUNTAC2 (two axis of symmetry) for Hertzian contacts, COUNTAC1 (one axis of symmetry) for non-Hertzian contacts and CONFORM for conformal contact problems.

After obtaining solution methodologies for all possible categories of normal contacts for wheel/rail systems, Paul sought a solution technique for the tangential problem. A modified strip theory was adopted for this purpose, primarily because it was well suited for determining the separatrix location (Figures 2.12 and 2.13) for arbitrary contact patch geometries [78]. The resulting tangential code called ROLCREEP and subsequently SLIDFORCE were developed by Liu and Paul [49] in 1988.

ROLCREEP is a “complete” code in that it is valid for all three rolling regimes. SLIDFORCE, however, was specifically designed for analyzing the problem of gross sliding contacts only. Results obtained for a Hertzian contact using both ROLCREEP and FASTSIM (Kalker Simplified) and DUVOROL (Kalker Non-Linear) are shown in Figure 2.14. As indicated, there is excellent agreement between them. Similar agreement is indicated by the traction distribution of Figure 2.15.

For non-Hertzian contacts Paul was unable to validate his work, as there are no known experimental results published for non-Hertzian situations. Kalker [79] has generated some “preliminary” geometry predictions along with the separatrix locations (via CONTACT). However “a crude approximation of the creepages was used”. For the non-Hertzian patch geometry of Paul and Hashemi [64] shown in Figure 2.16(a), and pressure

distribution of Figure 2.16(b), COUNTAC1 was utilized for the non-Hertzian normal problem, while the tangential solution was obtained via ROLCREEP. These are the first known complete solutions for non-Hertzian contact geometries.

The work of Paul appears to be quite general and well documented, however a fundamental problem exists when moderate to large values of spin creepage are encountered. Since an iterative technique (Newton-Raphson) is utilized for locating the separatrix, a suitable initial guess is crucial for successful convergence. However the initial traction distribution assumed within the slipped region corresponds to one of pure rigid body translation (without rotation). Therefore, as long as ϕ is small (Liu reports $\lambda \leq 0.1$ for non-Hertzian patches) ROLCREEP will achieve convergence, where λ is defined in equation (19) [35].

$$\lambda \equiv \frac{\bar{a}^3 E \phi}{\mu N (1 - \nu^2)} \quad (2.27)$$

Liu suggested that this limitation may be overcome by allowing ROLCREEP to begin with an acceptable value of small spin and the desired creepage values and divide the problem into a series of steps. With each step the solutions of the previous step would be used as initial guesses, where the creepages would remain constant, but the spin gradually increased. The problem would be repeated until the desired value of spin was achieved. Such a modification to ROLCREEP may become necessary when flange contact situations are encountered, where spin values as high as 80% have been reported during severe flanging [57].

The major features of each theory previously reviewed have been summarized in Table 2.2.

2.3 Rough and Inelastic Surfaces

With regards to the technical nature of three-dimensional surfaces encountered in actual rolling contact situations, several of the simplifying assumptions (common to all of the previously reviewed theories) have been addressed in the literature and are worth noting. The first is that of surface roughness, and the effects of assuming the contacting surfaces to be “smooth”.

2.3.1 Surface Roughness

“*Real* surfaces are always rough, with a vertical scale which can be almost anything, but with one universal feature - some of the roughnesses are higher than others” [81]. For the problem of wheel/rail contact, consideration should be given to the special case of elastic contact between rough curved surfaces. In qualitative terms, the surface asperities provide a much more compliant base, so under normal loading conditions the load is spread out over a wider area than that predicted by Hertz. Johnson [31] refers to this as the “real” area of contact. Since the “real” contact area is larger than the Hertz predicted area under these conditions, the peak pressure would be less. Figure 2.18(a) indicates this to be true under “light” loading conditions, however at higher loads (Figure 2.18(b)) Hertzian values of both pressure and contact area are essentially the same [82]. A generalization of these results is included in Figure 2.19(a) and (b) where parameters α and μ are defined by equations (2.28) and (2.29)

$$\alpha \equiv \frac{\sigma_s}{\delta_0} = \sigma_s \left[\frac{16 RE^{*2}}{9N^2} \right]^{1/3} \quad (2.28)$$

$$\mu = \frac{8}{3} \xi_s \sigma_s (2R/K_s)^{1/2} \quad (2.29)$$

As shown, “the Hertz theory for smooth surfaces can be used with only a few percent error provided the parameter α is less than about 0.05” [31].

With respect to the tangential forces transmitted across a “rough” surface interface, O’Conner and Johnson [83] found roughness to have a negligible effect under sliding conditions. In rolling contact, Johnson [31] reports the influence of roughness on creep to be small. This is also supported by Krause and Poll [84] where for the conditions of their test rig (surface pressure = 500N/mm²), “an increase in creep caused by greater surface roughness was not evident”.

2.3.2 Surface Contamination

Real surfaces are in mutual contact at discrete asperities and thus interfacial materials are also expected to be present. When considering the wheel/rail system, contamination of the contact surfaces may result from oxidation, foreign matter (oil, sand), environmental conditions (rain, snow, ice, temperature-humidity effects), and trackside or on-board lubrication (grease-sand mixtures) [84, 88]. In general, the presence of contaminants within the contact region has been found to cause a reduction in the coefficient of sliding friction [84, 85], however, initial gradients of the traction-creep relationships remained unchanged [84, 86]. This is a confirmation of Kalker’s [33] theory, in that creep relationships and the coefficients of sliding friction are independent quantities. Two reported contradictions to this are cited [87, 88]. In each of these cases the authors conclude that creep coefficients in the vanishingly small creepage regime can be decreased due to contaminants.

2.3.3 Plasticity Effects

During repeated rolling contact the elastic limit of the material is likely to be exceeded (initially at least) leading to plastic flow and residual stresses. The material is therefore subjected to a combination of the contact stresses due to the current load together with the residual stresses introduced during previous passes of the load [102]. Although in the early stages of the loading history plastic deformation may occur, it is possible for the steady state stresses to be entirely within the elastic limit. This process is known as “shakedown” [31].

Three separate effects contributing to the shakedown process in rolling contact as outlined by Johnson [105] are:

- 1) Residual stresses introduced during the early passes are protective and make plastic deformation less likely during subsequent passes.
- 2) Plastic deformation in the early passes may cause the material to strain-harden, thereby raising the elastic limit.
- 3) Plastic deformation may make the surface profiles more conforming so that, even under a constant load, the intensity of the contact stress is reduced.

He does note however, that the influence of plastic deformation (effect (3)) on the contact area and resultant contact pressure distribution, would be “difficult to calculate precisely but is certainly not large” [103].

Although the concept of material shakedown has been verified for a variety of materials under laboratory conditions, analytical techniques for accurately predicting such behavior are still under development [104]. This is due in part because both the shakedown limit as well as the nature of deformation which takes place when the load exceeds the shakedown limit, are dependent upon the strain hardening characteristics of the material and how

accurately then may be modelled (i.e. elastic - perfectly plastic, linear kinematic hardening, non-linear kinematic hardening, etc.). With respect to field conditions and practical applications, Kalousek et. al. [106] reports that an “open system” of wheel/rail contact which results due to wheels of different cross-sectional profiles and diameters yields a wide range of contact geometries (Figure 2.20). Moreover, when this is “combined with a wide range of contact forces occurring on high capacity railway lines, it does not permit the shakedown state to be satisfied, thereby causing severe plastic deformation and wear” [106].

A large body of literature currently exists which deals with inelastic material response under rolling contact conditions. Much of the pioneering effort is due to Johnson and his colleagues at Cambridge University [31, 103-105]. Most of the inelastic contact research being done has been motivated by the need to understand wheel/rail wear and failure mechanisms.

Regarding the influence of plastic deformations on the traction-creep relationships for rolling contact, very little work has been reported. Krause and Poll [84] was the only reference located which specifically addressed the issue. In their work, two rolling/sliding friction test rigs were used for comparing the creep force/creepage relationships (within the linear regime) of a 16 Mn Cr 5 steel in a non-hardened (HV = 213) and case hardened (HV = 802) condition. Their conclusion was that “an influence of plastic deformation could not be determined from the comparison between hardened and unhardened rolling bodies at a maximum surface pressure of 500 N/mm².” It is unknown whether or not the effects of plastic flow influence the creep force - creepage behavior outside the linear regime. However, it would seem reasonable that if plastic creep occurred, it would lead to higher values of creepage for a given friction force than would theoretically be calculated.

All of the creep force - creepage algorithms to date treat both contacting materials as linear elastic.

2.4 Contact Patch Friction Work

According to Johnson [92], “micro-slip is an irreversible process”. The implications of this are that frictional energy, (or work) is lost during the rolling process. The “heat” or thermal energy which is dissipated within the slip region of the contact patch has been primarily attributed to plastic deformation of near-surface regions of the two contacting bodies [126]. As a result of thermal resistance the local temperature would increase, possibly influencing both the friction as well as the wear rate [93-102]. In addition, the thermal energy expended due to sliding contact results in some degree of thermal deformation of the surface (within the immediate vicinity of the contact) and may indeed alter the contact patch geometry and separatrix location (in comparison to that predicted by a purely mechanical analysis) [99, 107].

2.4.1 Global Work

In the analysis of rail car dynamics, the magnitude of contact patch work has been used as a principal curing performance index (ie. indicator for the onset of derailment) [17]. The contact patch work has been defined as the dot product of creep force and creepage vectors (2.30),

$$W = \int \vec{F} \cdot d\vec{r} = V_o \Delta t \int \vec{F} \cdot d\vec{\xi} \quad (2.30)$$

where the resultant creep force vector is defined in equation (2.31), and the creepage vector by equation (2.32).

$$\vec{F} = F_x \hat{i} + F_y \hat{j} \quad (2.31)$$

$$\vec{\xi} = v_x \hat{i} + v_y \hat{j} \quad (2.32)$$

Taking into account the effects of spin moment and recognizing the $V_o \Delta t$ term in equation (2.30) to be equal to the distance rolled, then the *global* contact patch friction work per distance rolled may be described by equation (2.33) and has units of work per unit distance, or force.

$$W'_g = \frac{W}{V_o \Delta t} = [F_x v_x + F_y v_y + M_z \phi] \quad (2.33)$$

When summed over all contact patches, this index represents the additional work per unit distance rolled along the track required for the vehicle to negotiate a curve.

The index of global work has also been used by investigators interested in the wear of wheels and rails. Although comprehensive verification of wear indices has been limited, tests by British Rail have shown that under certain wear regimes, wear rate is proportional to the work done in the contact patch [109, 127].

2.4.2 Local Work Distribution

The index of global patch work is an overall, or integrated measure of wear in the contact patch, however, there has been strong interest by several investigators to obtain a measure of the wear distribution over the contact patch [89, 90]. Under slip-stick rolling condition, no relative motion occurs in the adhesion region of the patch and therefore no energy is dissipated there either. Thus the distribution of wear within the contact patch becomes a function of separatrix location, and size of slip domain.

For a contact patch with regions of both slip and stick, the local surface shear traction distribution (shear stress) is known to vary in a manner characteristic of that shown in Figure 2.21. As indicated, it reaches a local maximum at the separatrix and falls in accordance with $\mu p(x,y)$ (Coulomb saturation) from the separatrix to the trailing edge. Then for a contact domain Ω identified by the elliptic “footprint” of Figure 2.22, with discrete cell locations identified by indices i and j in the longitudinal and lateral directions respectively, the local shear traction vector \bar{T}_{ij} and slip vector \bar{s}_{ij} are defined by equations (2.34) and (2.35),

$$\bar{T}_{ij} = (T_x \hat{i} + T_y \hat{j})_{ij} \quad (2.34)$$

$$\bar{s}_{ij} = (s_x \hat{i} + s_y \hat{j})_{ij} \quad (2.35)$$

where T has units of force per unit area and s is dimensionless.

The local work per unit distance rolled at the cell ij then becomes:

$$W'_{ij} = [(\bar{T} \cdot \bar{s}) * A_{\text{cell}}]_{ij} \quad (2.36)$$

which would provide a local work map or distribution when computed for all cells within Ω , where by definition $W'_{ij} = 0$ in the adhesion region, since the slippage, $\bar{s} = 0$ there.

If the local work values for each cell are summed over the entire contact (2.37), a measure of total (or integrated) contact patch work would be obtained, which would be similar (but, not in all cases identical) to the W'_g *global* work term of section 2.4.1.

$$W'_{\text{Local sum}} = \sum_{\Omega_{\text{slip}}}^{n_{\text{Total}}} (\vec{T}_{ij} \cdot \vec{s}_{ij}) A_{\text{cell } ij} \quad (2.37)$$

2.4.3 Local Heat Flux

In order to quantify the thermal effects of contact patch work on wear, potential phase transformations and material properties, the heat flux distribution resulting from the rolling/sliding process must be understood [110-119]. Recall that power may be defined by :

$$\bar{P} = \frac{\partial W}{\partial t} \quad (2.38)$$

where thermal power per unit area is defined as heat flux (2.39).

$$q'' = \frac{\bar{P}}{A} \quad (2.39)$$

Since non-conservative work (friction work) dissipated per unit time equals thermal power, the local heat flux distribution may be obtained from equation (2.40)

$$q''_{ij} = \left[W'_{ij} \left(\frac{1}{A_{\text{cell } ij}} \right) \right] V_o \quad (2.40)$$

which may be re-arranged into the following equation by using (2.36).

$$q''_{ij} = (\vec{T} \cdot \vec{s})_{ij} V_o \quad (2.41)$$

where V_o in each case is the rolling velocity. Thus by having the traction and slip distributions available, the heat flux distribution may be predicted. For problems where a

uniform heat source moving at velocity V_0 is assumed, there would be no need to use equation (2.41). However, for non-uniform heat sources (ie. non-Hertzian contacts), the temperature maps cannot be accurately obtained without the application of equation (2.41).

Table 2.1 Coefficients m and n For Different Values of Θ

θ	30°	35°	40°	45°	50°	55°	60°	65°	70°	75°	80°	85°	90°
m	2.73	2.39	2.13	1.92	1.75	1.61	1.48	1.37	1.28	1.20	1.12	1.06	1.00
n	0.49	0.53	0.56	0.60	0.64	0.67	0.71	0.75	0.80	0.84	0.89	0.94	1.00
a/b	5.53	4.52	3.76	3.18	2.73	2.37	2.07	1.81	1.60	1.42	1.26	1.12	1.00

Table 2.2. Overview of Computer Codes

Author	Release Date	Program	Creepage Regime	Surface Geometry	Contact Geometry	Comments
Kalker [33]	1967	LINEAR	LINEAR	COUNTER-FORMAL	HERTZIAN	Look-up TABLE FORMAT [33, 44]
Kalker [50]	1970	DUVOROL	Complete	COUNTER-FORMAL	HERTZIAN	Look-up TABLE FORMAT - B.R. Book. FORTRAN Source Code [50, 53]
Kalker [54]	1973	FASTSIM	Complete	COUNTER-FORMAL	HERTZIAN	FORTRAN Source Code [54, 55, 58]
Kalker [52, 79]	1982	CONTACT	Complete	COUNTER-FORMAL	NON-HERTZIAN	General, Computationally Intensive. Code Sold by Kalker.
Shen, Hendrick & Elkins [57]	1983	C FORCE	Complete	COUNTER-FORMAL	HERTZIAN	Very Fast. Easily Programmed via Table [33, 44]. Small Spin Only
Paul and Hashemi [63]	1977	COUNTACT -2	N/A	COUNTER-FORMAL	HERTZIAN	Solves the Normal Problem Only. 2 axes of symmetry
Paul and Hashemi [64]	1978	COUNTACT -1	N/A	COUNTER-FORMAL	NON-HERTZIAN	Solves the Normal Problem Only. 1 axis of symmetry
Liu and Paul [35]	1988	ROLCREEP	Complete	COUNTER-FORMAL and CON-FORMAL	HERTZIAN and NON-HERTZIAN	Very General. Limited to Small Spin.
Liu and Paul [49]	1988	SLIDFORCE	Saturation Only	COUNTER-FORMAL	HERTZIAN and NON-HERTZIAN	Designed for Gross Sliding Problems.

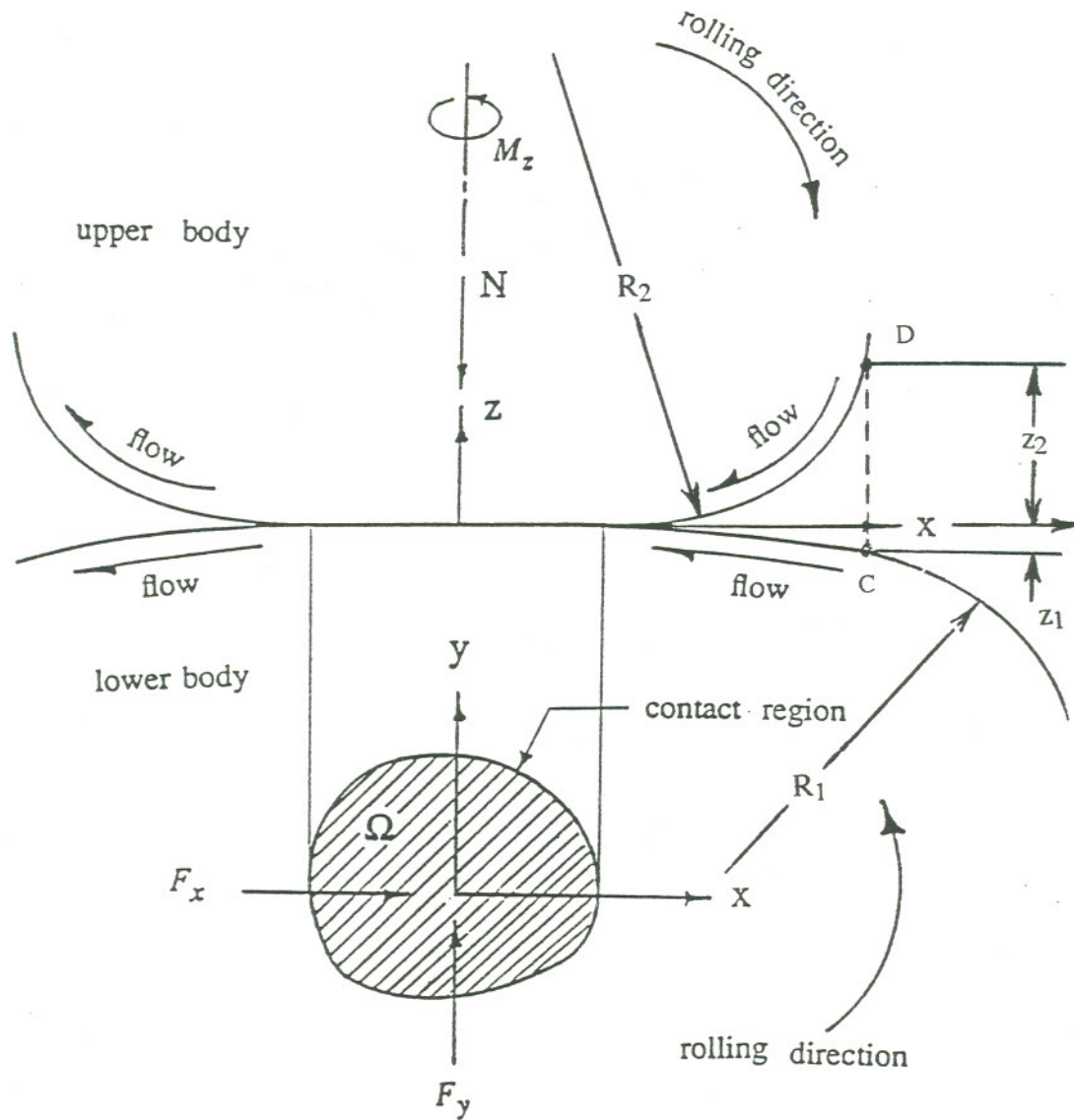


Figure 2.1 Two elastic bodies in frictional rolling contact.

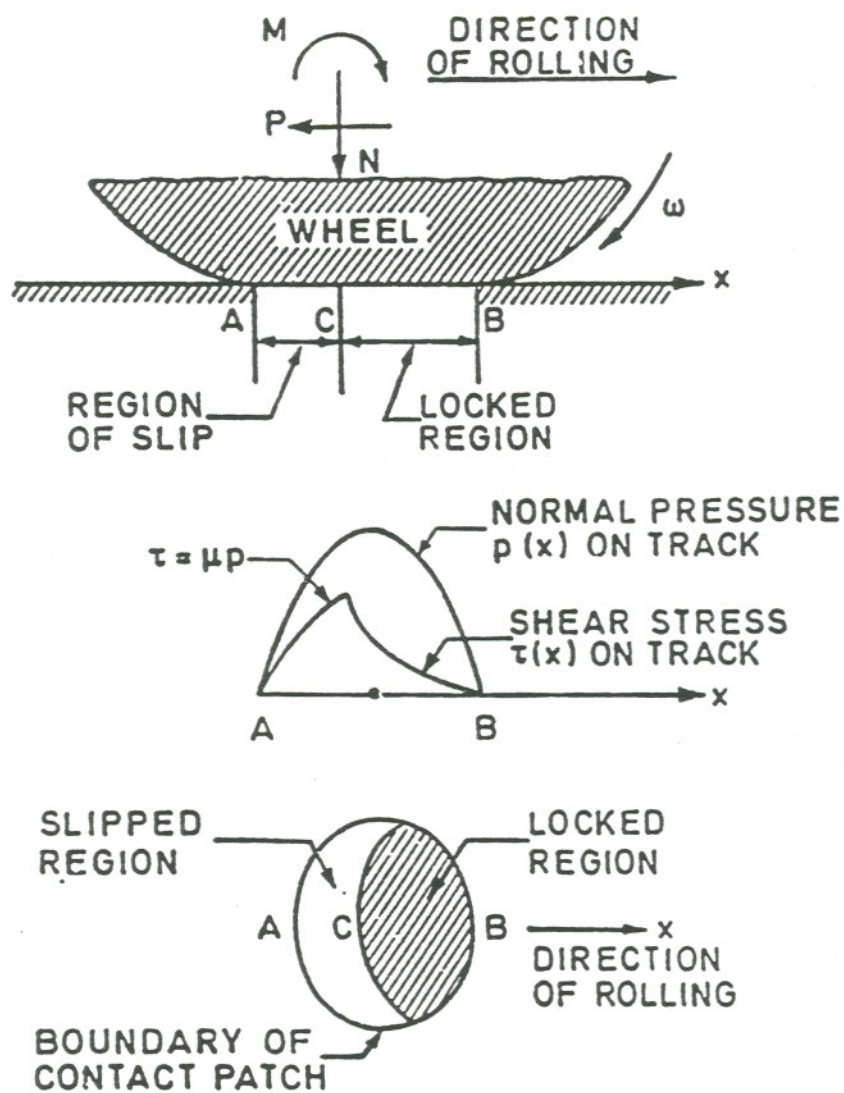


Figure 2.2 Tractive rolling with slip and stick zones indicated [40].

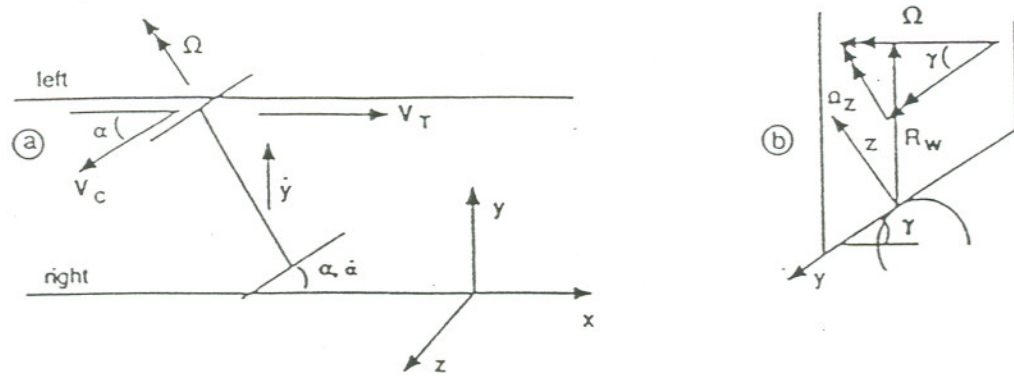


Figure 2.3 The creepages: (a) a wheelset on a track; and (b) illustration of camber spin [44].

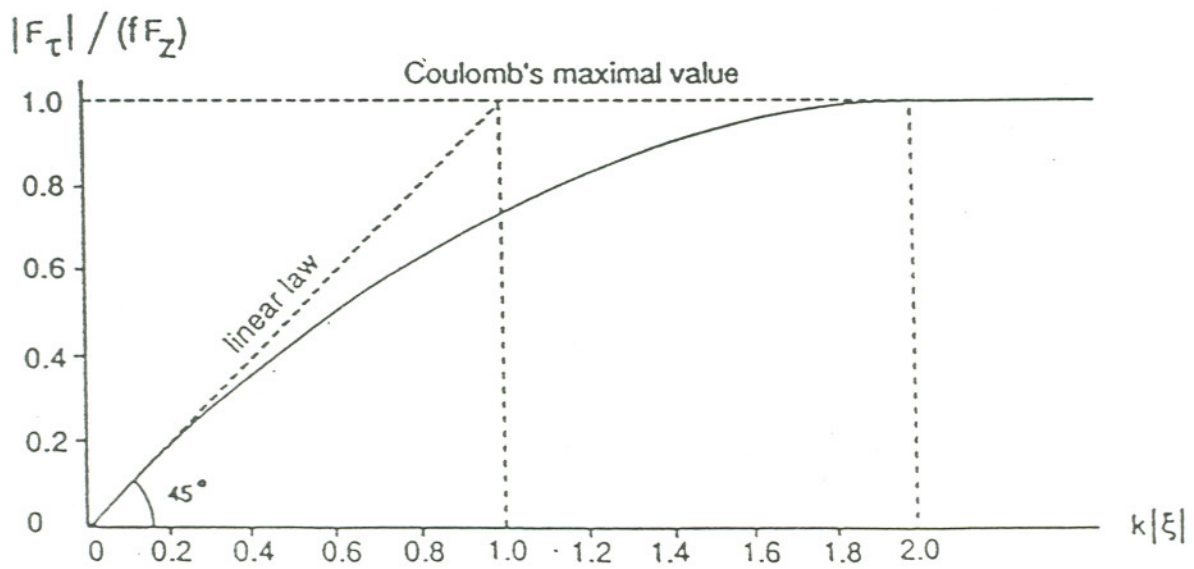


Figure 2.4 Creep force - creepage diagram according to Carter [39].

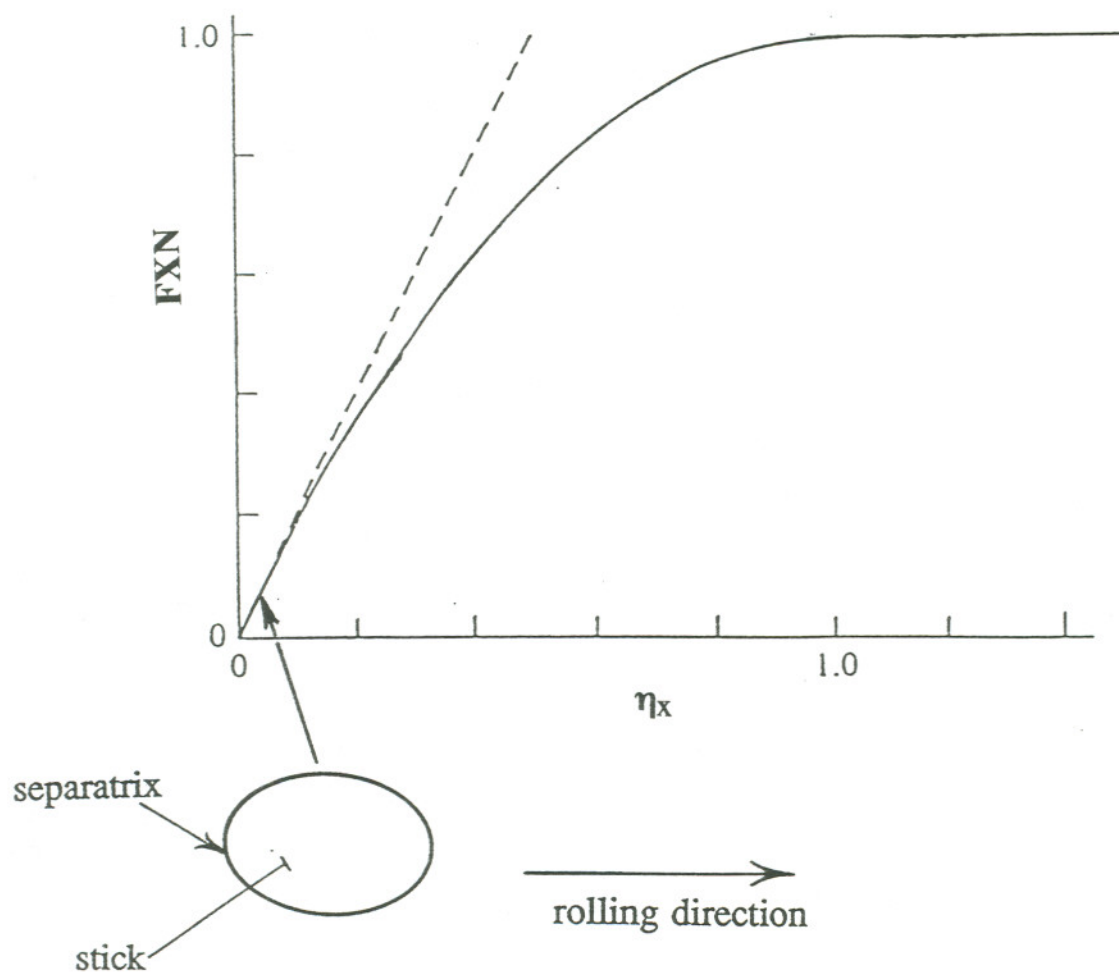


Figure 2.5 Creep force - creepage diagram and contact ellipse for the linear regime.

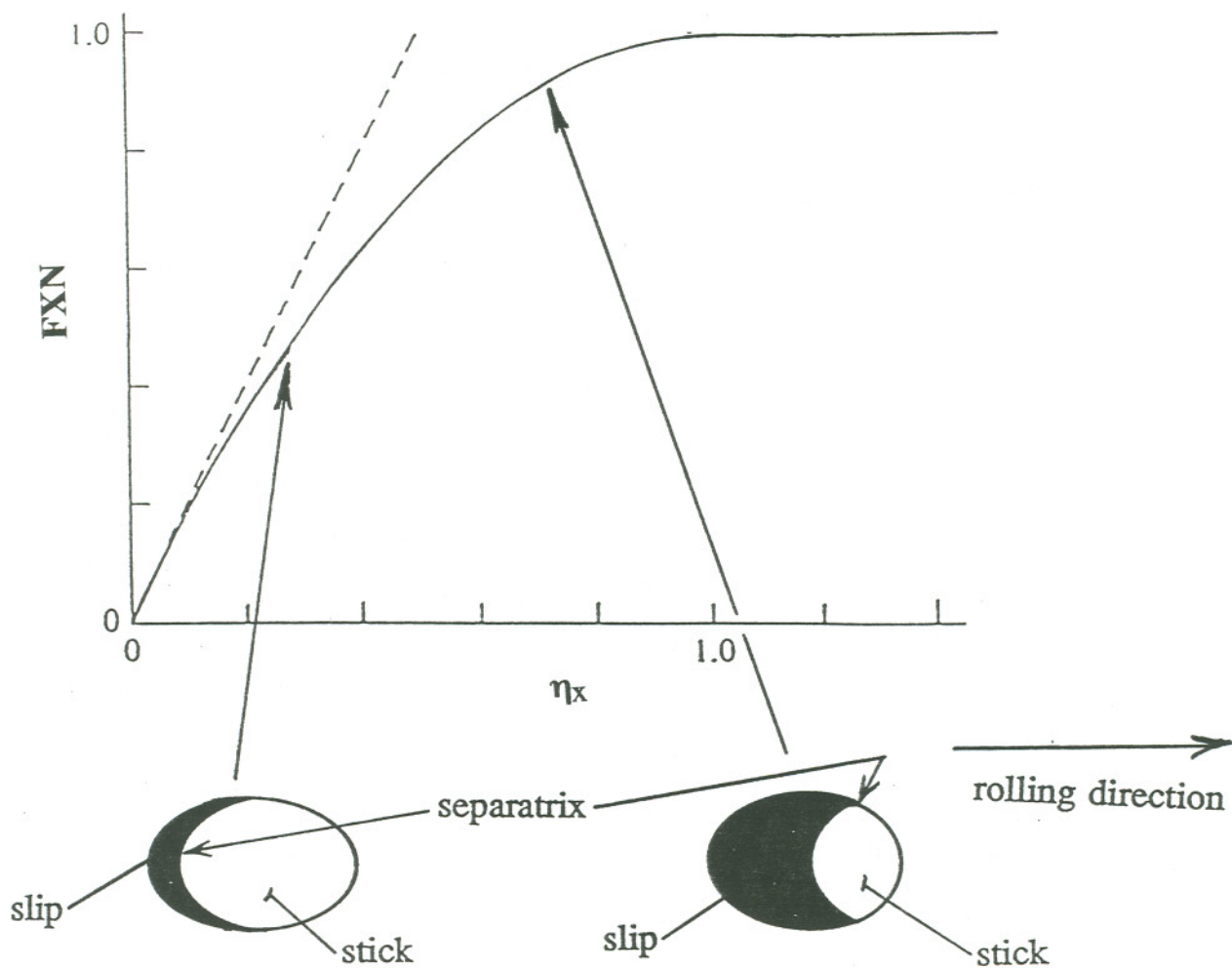


Figure 2.6 Creep force - creepage diagram and contact ellipse for the non-linear regime.

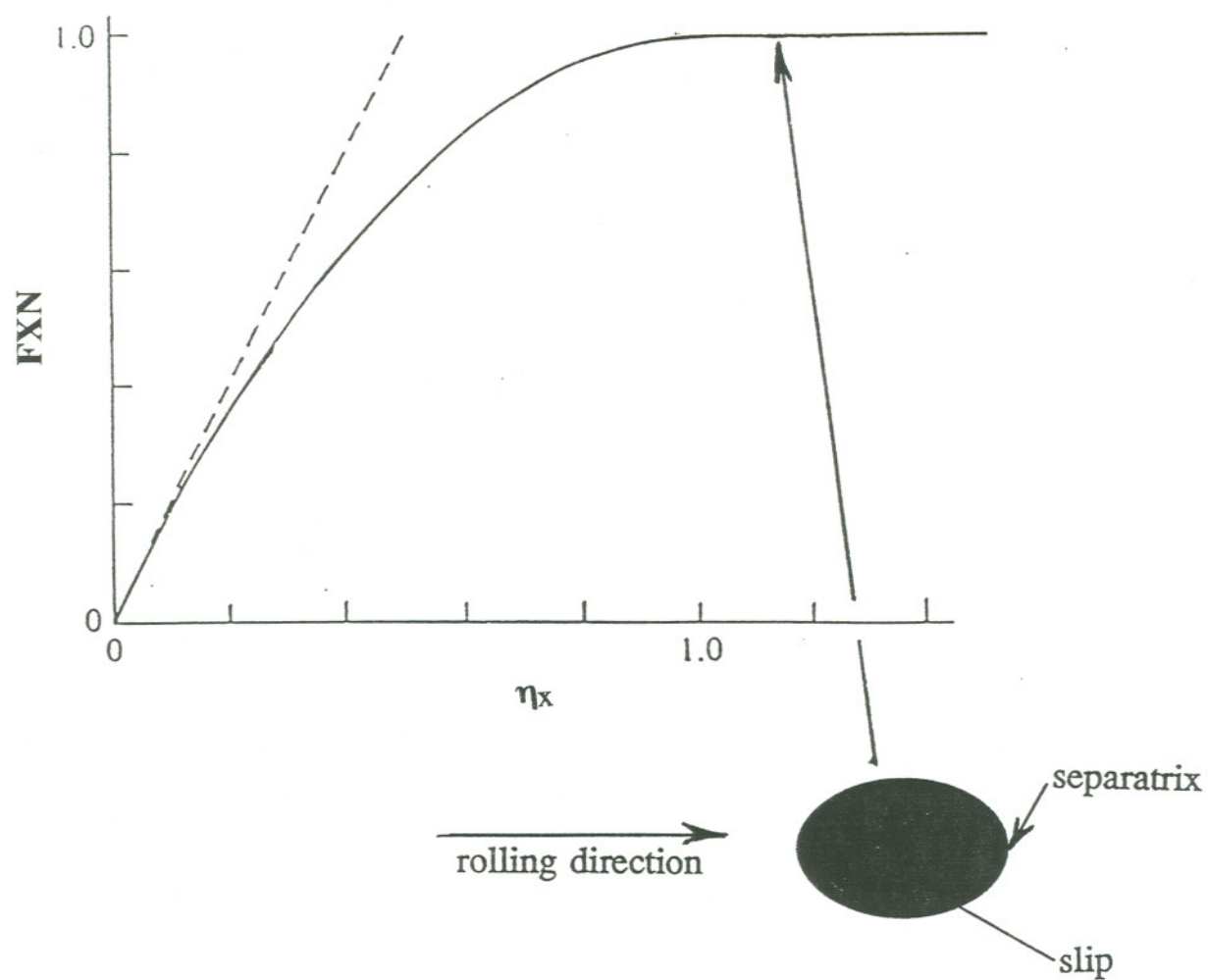


Figure 2.7 Creep force - creepage diagram and contact ellipse for the full slip regime.

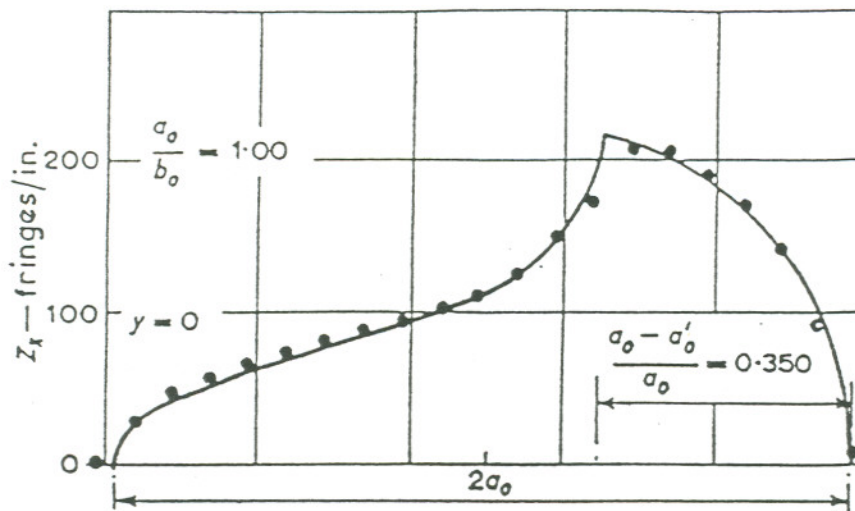


Figure 2.8 Measured and theoretical surface traction stresses for circular contact patch [46].

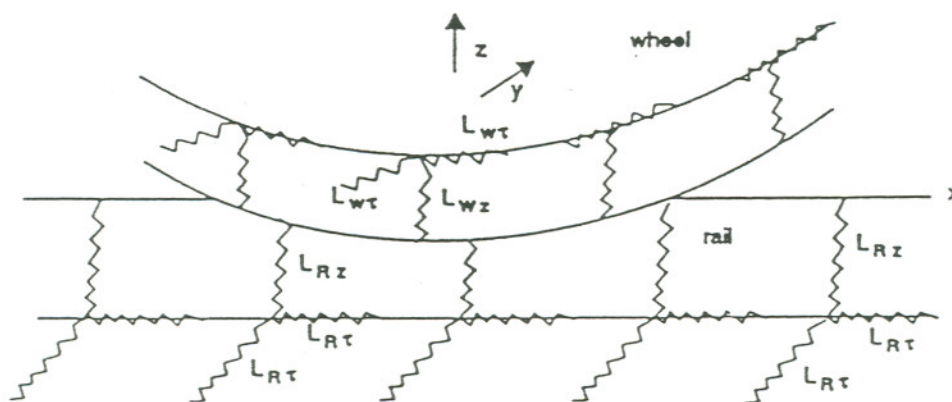


Figure 2.9 The idea of the simplified theory [44].

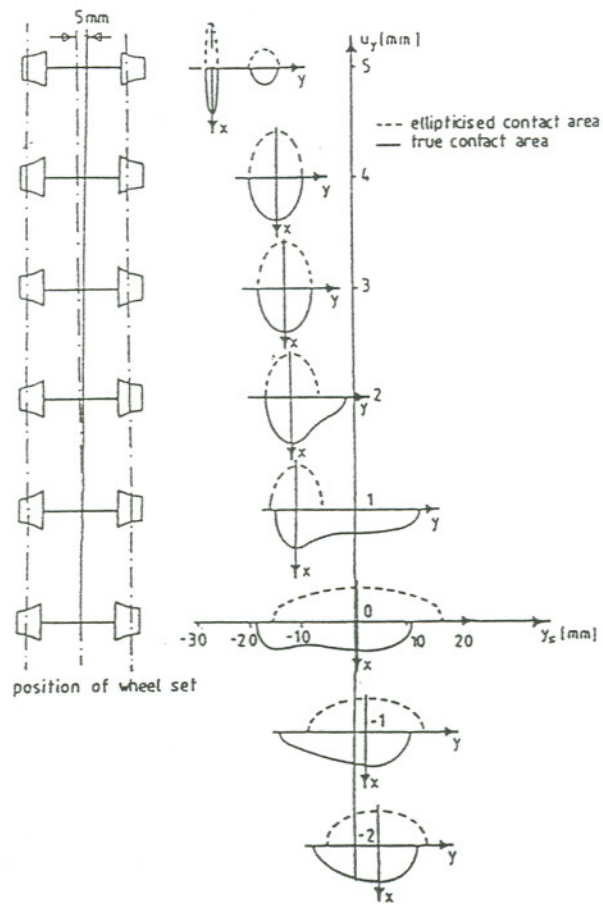
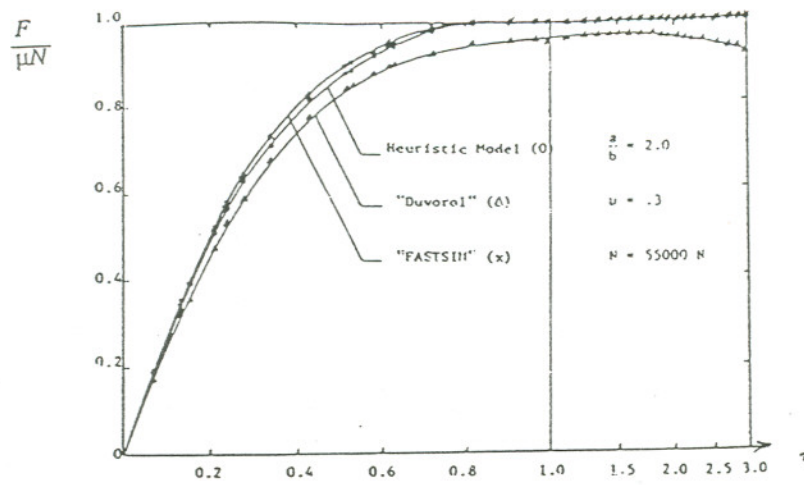
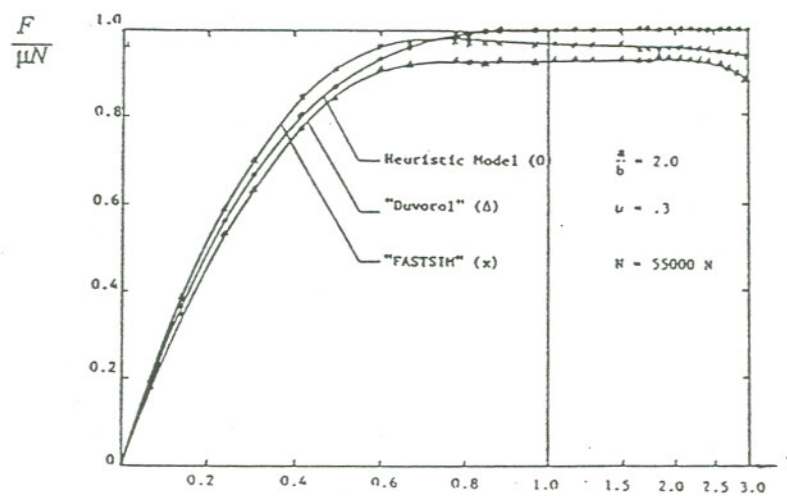


Figure 2.10 Contact position on the rail head for various wheelset positions - both ellipticized and actual geometries [56].



(a)



(b)

Figure 2.11 Comparison of complete creep force - creepage theories. (a) spin $\leq 10\%$ and (b) $10\% \leq \text{spin} < 25\%$ [57].

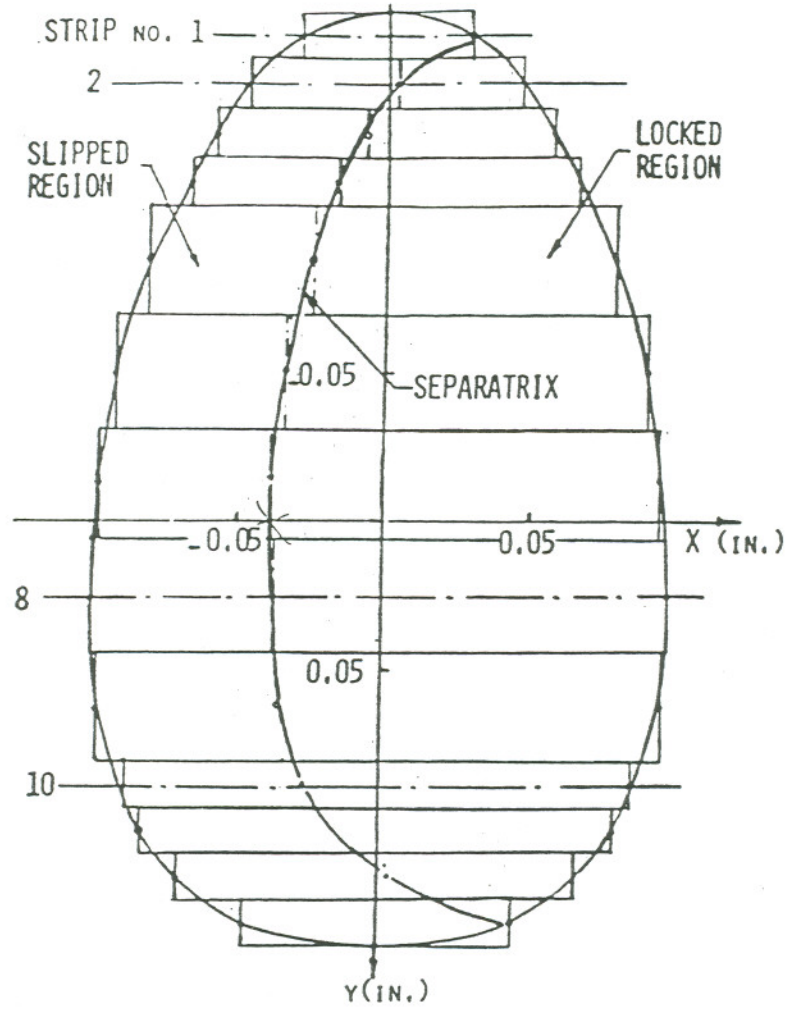


Figure 2.12 Non-Hertzian wheel - rail contact patch [75].

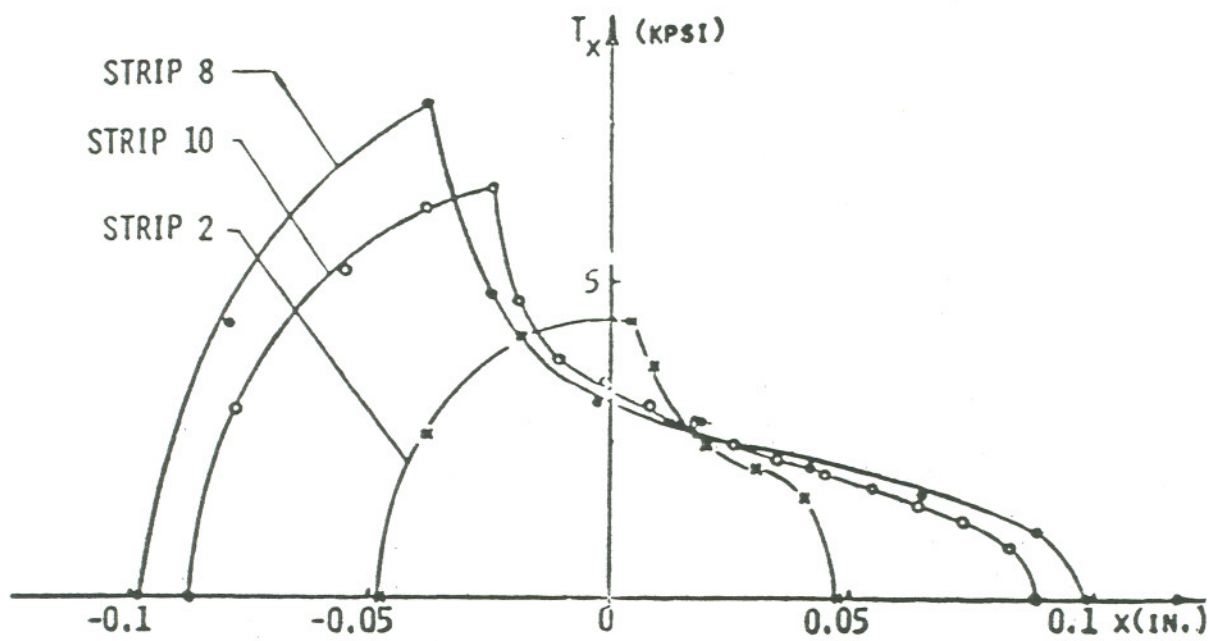


Figure 2.13 Longitudinal traction distribution for non-Hertzian patch. $\nu_x = 0.0003$, $N = 1400$ pounds, $\frac{F_x}{\mu N} = 0.6$ $\mu = 0.2$ [75].

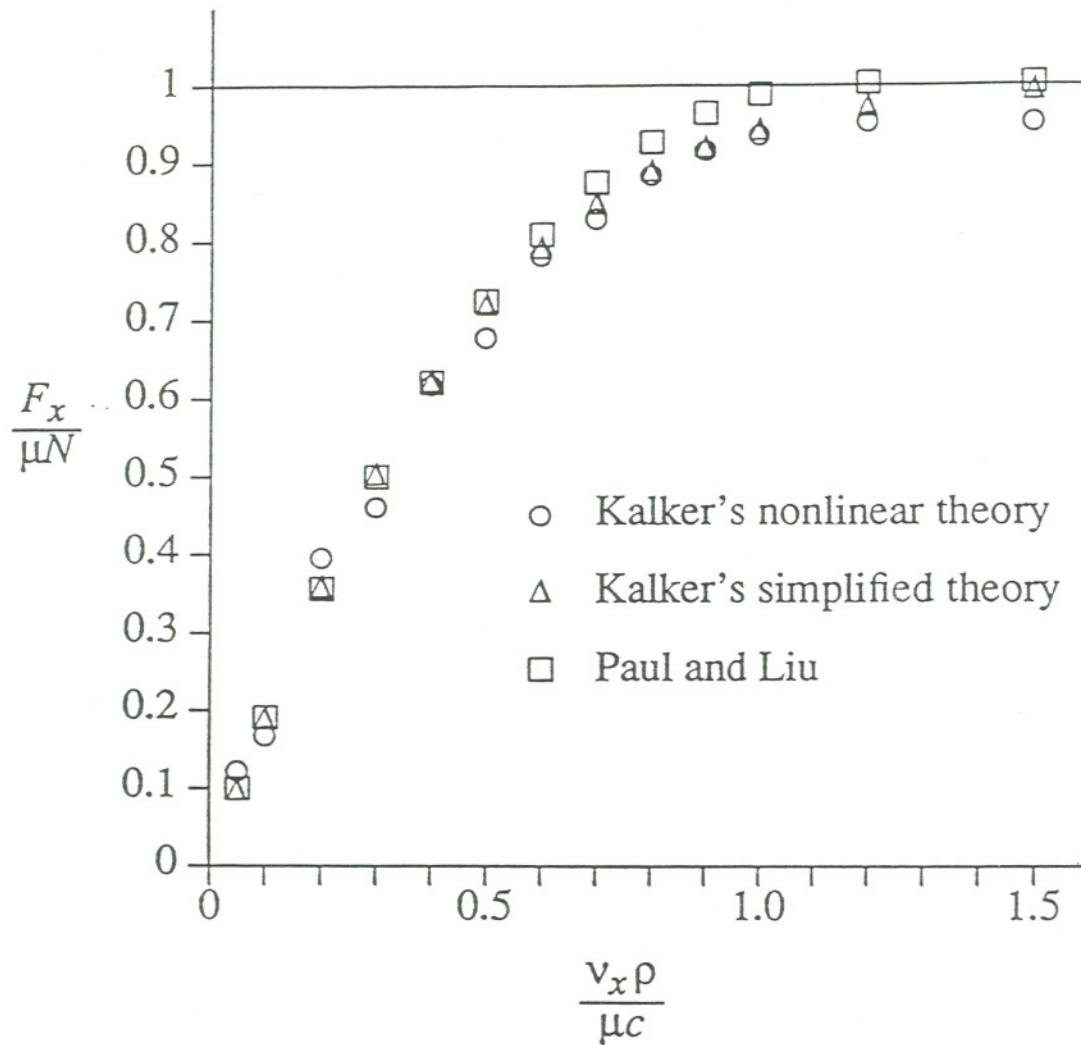


Figure 2.14 Longitudinal creepage curve for elastically similar bodies with elliptic contact. ($a/b = 2.89$, $\nu = 0.28$, $\nu_y = \phi = 0$) [35].

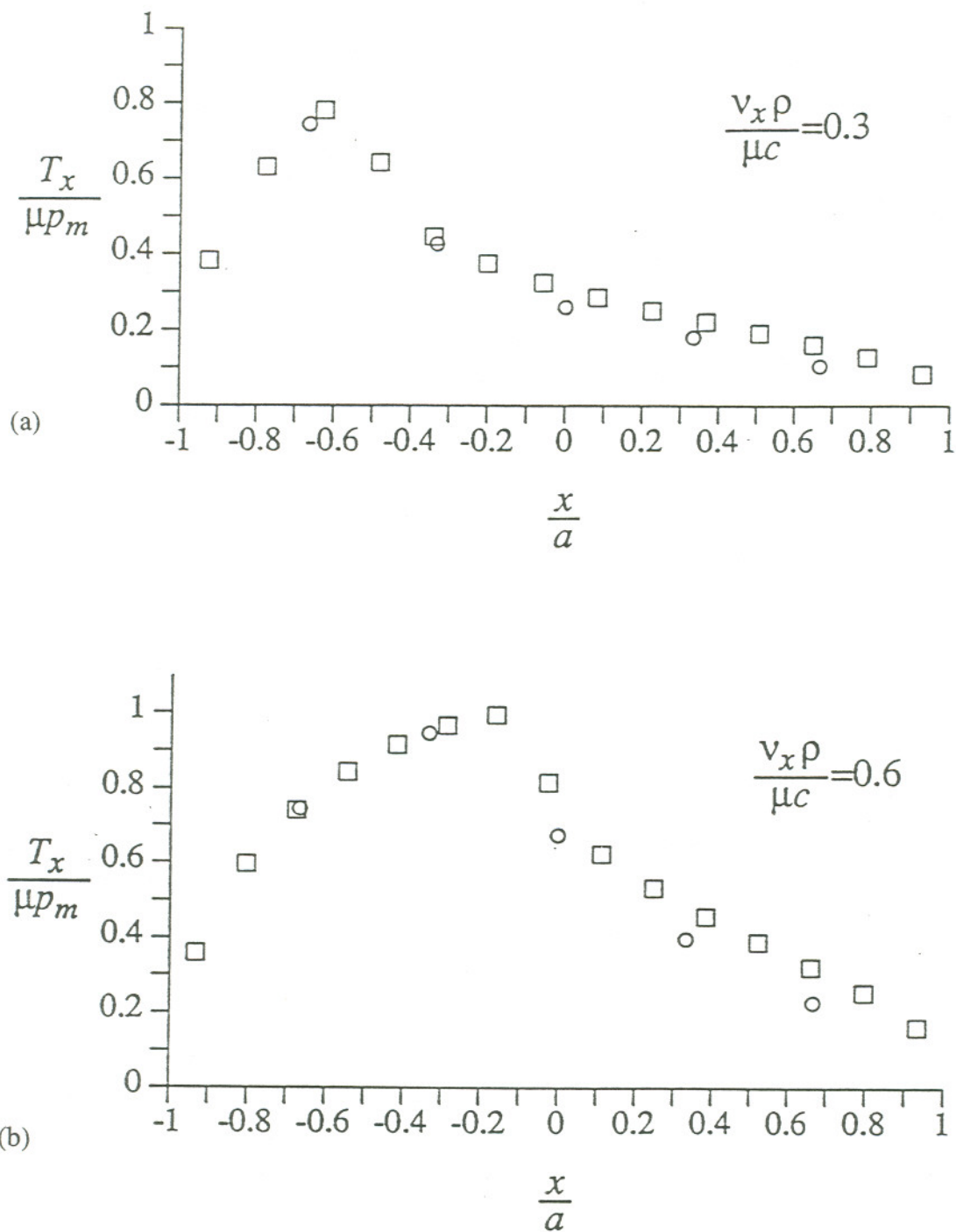


Figure 2.15 Longitudinal traction along x-axis for rolling contact of elliptic patch, (circle Kalker's nonlinear theory; square - Paul and Liu [35]). (a) $\eta_x = 0.3$, and (b) $\eta_x = 0.6$.

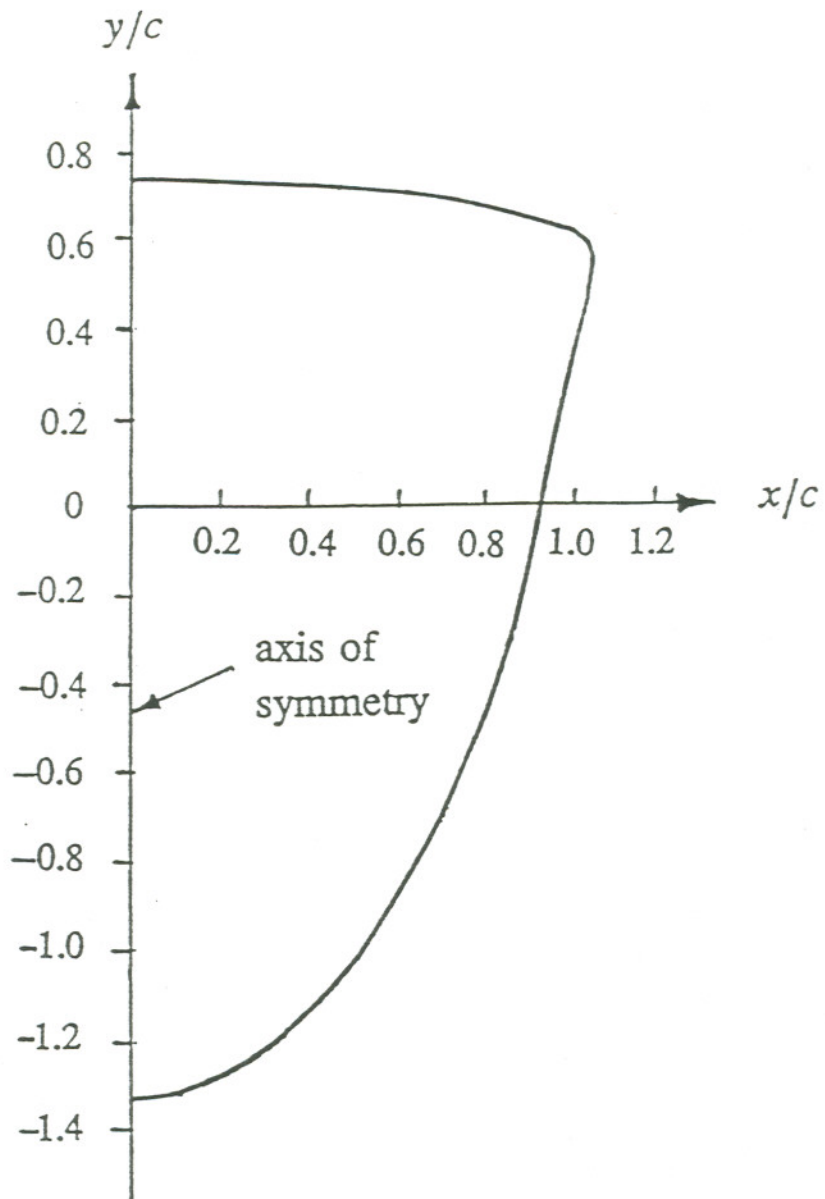


Figure 2.16 Shape of a non-Hertzian contact patch [64].

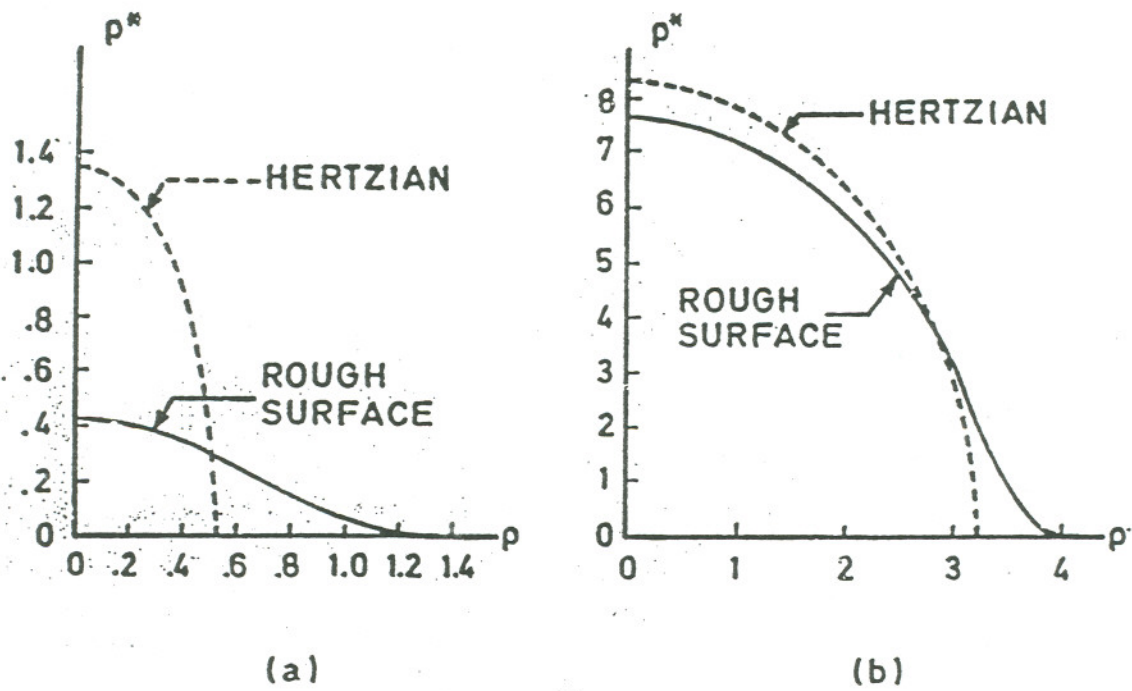


Figure 2.17 Pressure along y-axis for the contact patch of Figure 2.16 [64].

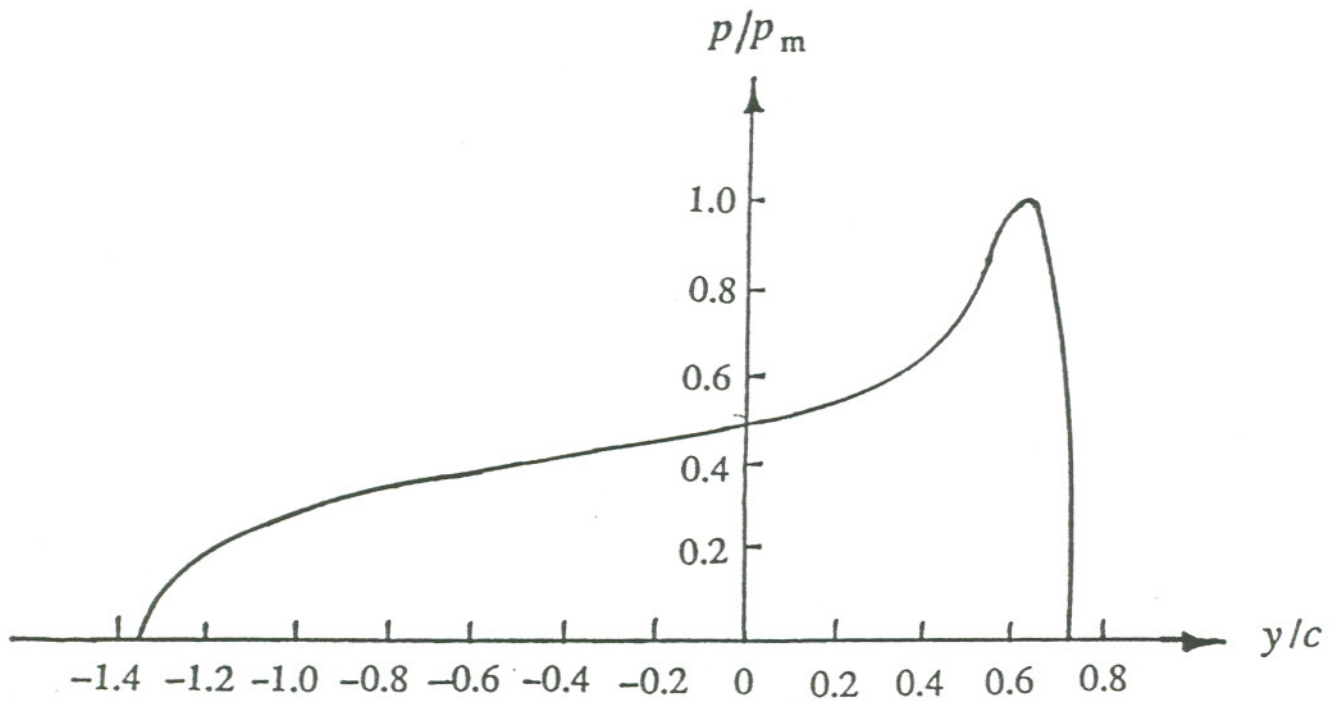


Figure 2.18 Nondimensional contact pressure p^* versus nondimensional radial coordinate ρ . (a) light load; and (b) heavy load (note change in scales) [82].

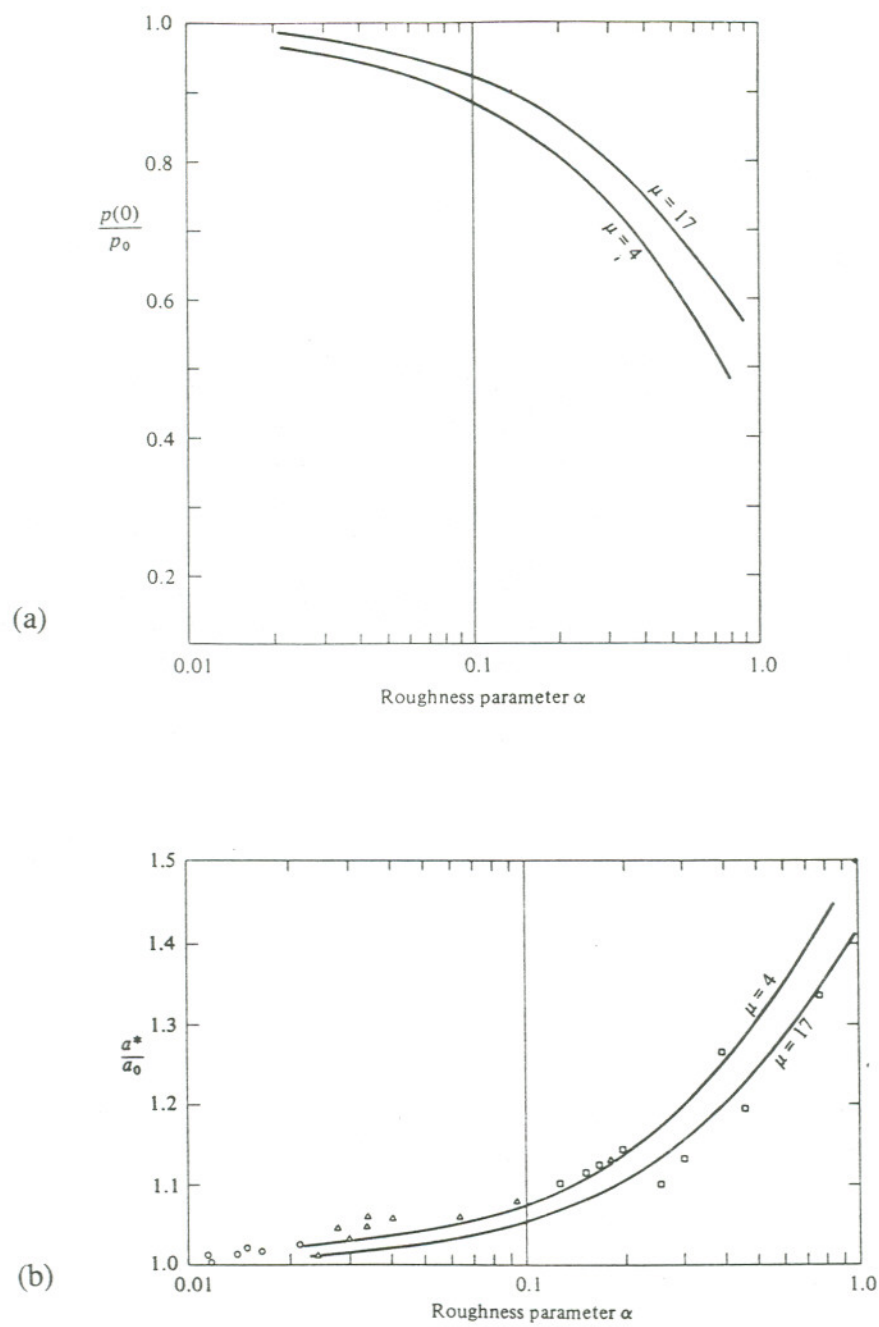


Figure 2.19 Influence of surface roughness (a) on the minimum contact pressure $p(0)$ compared with the maximum Hertzian pressure p_0 ; and (b) on the effective contact radius a^* compared with the Hertz radius a_0 [31].

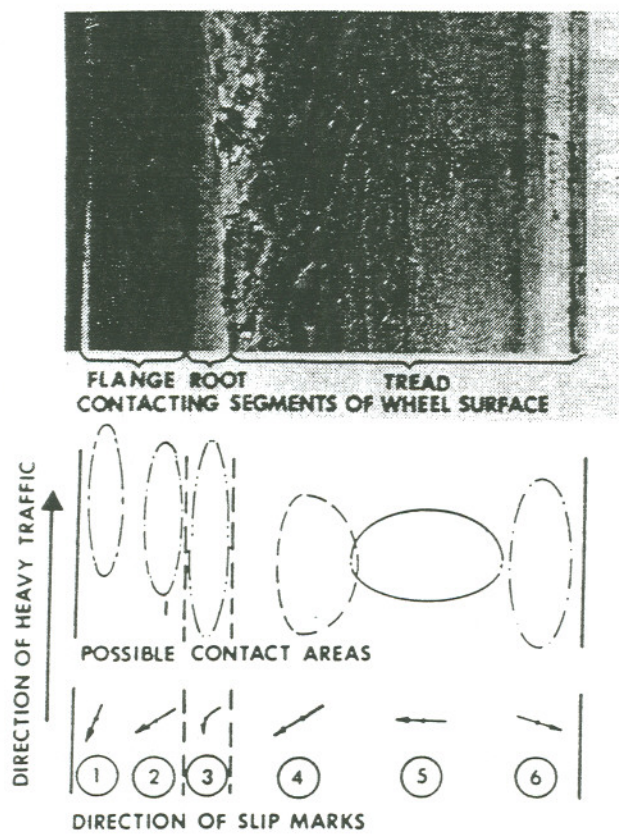


Figure 2.20 High rail surface showing possible contact areas [106].

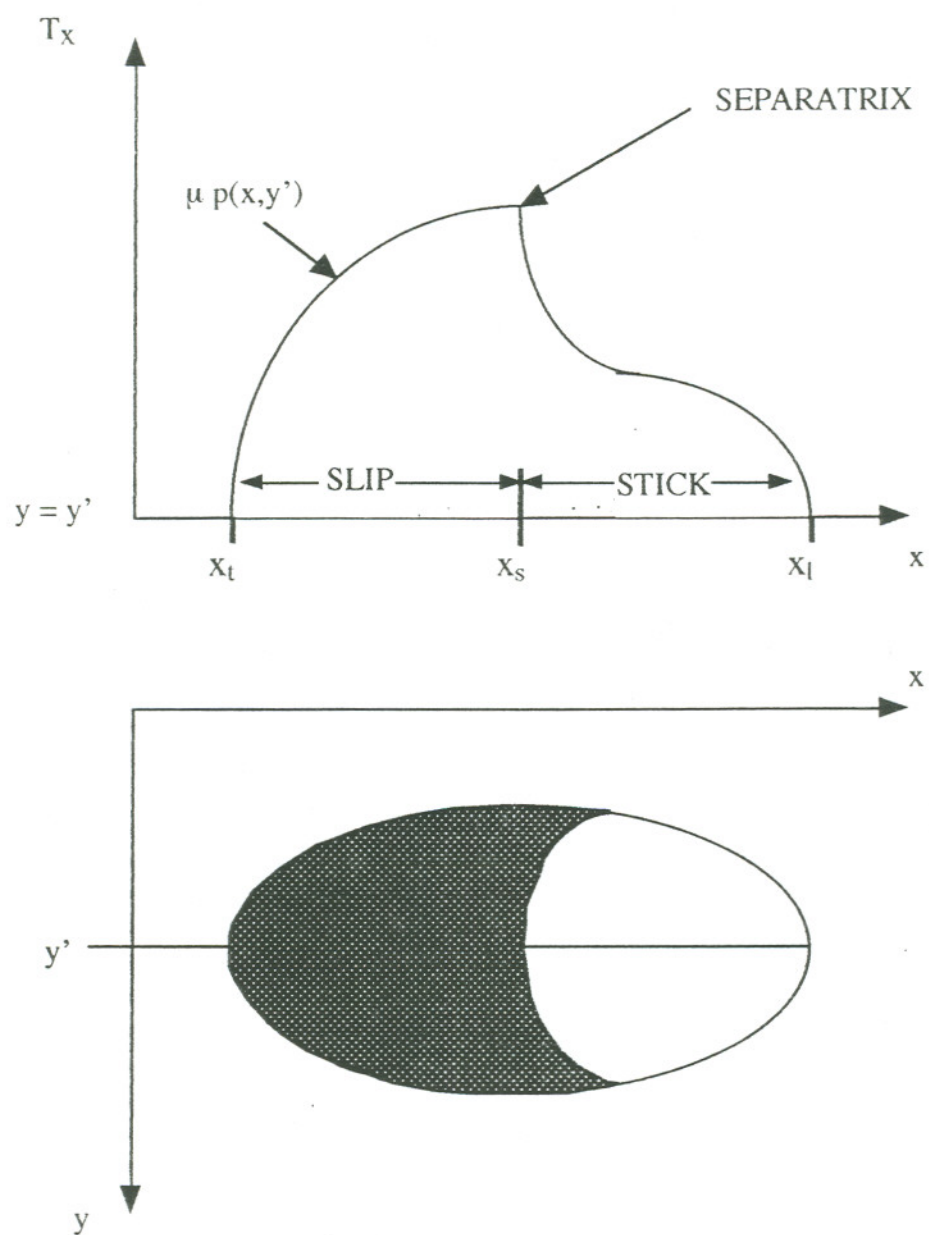


Figure 2.21 Typical traction distribution with separatrix location and regions of slip and stick.

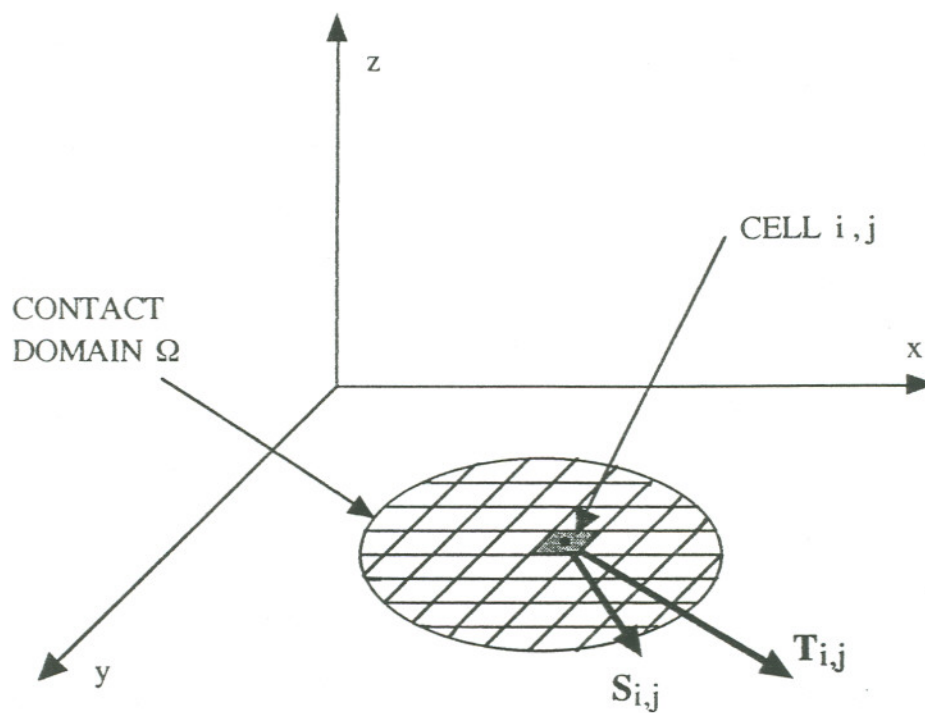


Figure 2.22 Contact patch domain indicating local traction $\bar{\mathbf{T}}$ and slip $\bar{\mathbf{s}}$ vectors at cell location i, j .

CHAPTER 3

PROCEDURES AND RESULTS

3.1 Counterformal Hertzian Contacts

In developing a complete solution to the problem of creep-force / creepage behavior of wheel / rail contacts, consideration must be given to both counterformal Hertzian, as well as non-Hertzian contacts. However, most dynamic rail car models currently require inputs of wheel-rail contact geometry which are elliptical, a characteristic unique to counterformal Hertzian contacts.

3.1.1. Closed Form Solution to Patch Geometry

Contact patch geometry is understood to be a function of wheel and rail surface curvatures at the location of contact between the bodies, as well as material properties of both wheel and rail, and normal load [37]. A procedure for obtaining a closed form solution to contact patch geometry (and hence pressure distribution) is outlined below:

- (1) Obtain the principal radii of curvature for wheel ($R_1 R'_1$) and rail ($R_2 R'_2$) at the location of contact, as in Figure 3.1.
- (2) Compute $(A + B)$ and $(B - A)$ terms from equations (2.4) and (2.5),
(where $\psi = \pi/2$ for most rolling contact problems [52]).
- (3) Obtain θ from equation (2.11).

- (4) Use this value of θ and interpolate on Table 2.1 to obtain m and n , as well as a/b .
- (5) Compute the elastic constants k_1, k_2 from equation (2.9) and (2.10).
- (6) Calculate semidiameters a and b from equations (2.7) and (2.8).
- (7) Substituting these into the elliptical formula of (2.6) the patch geometry is obtained where semidiameter a is along the x - axis, in the direction of rolling.
- (8) At this point the maximum Hertzian pressure may be obtained from equation (2.16), and the ellipsoidal pressure distribution from equation (2.15)

3.1.2. Iterative Solution for Two Axis of Symmetry - COUNTAC2

The program COUNTAC2 was developed by Paul and Hashemi [63] for the purpose of obtaining an iterative method for computing the contact patch geometry, pressure distribution and total load for various wheel and rail geometries, under a given rigid body approach. The program was written in FORTRAN 77 and is based on the modified simply discretized method [68]. Although the output generated includes the same parameters which can be predicted via the closed form procedure of 3.1.1, obtaining Hertzian results was not the primary goal for developing COUNTAC2. The main motivation was to develop the *iterative solution method* which could be compared to an acceptable standard (closed form Hertz analysis), and which could be extended to handle non-Hertzian contact problems.

3.1.2.1 Code Implementation

The FORTRAN source code for COUNTAC2 is available in the open literature [64]. After contacting the author, however, a diskette of the source code was obtained [120]. The source code was compiled on a 486 IBM compatible computer using a Microsoft FORTRAN 5.1 optimizing compiler.

Since the source code was originally written in the late 1970's, it was set up for running in a batch mode, and the input format was designed for use with a card reader. In addition, the large mainframe computer it was developed to run on (IBM 370/168) had been equipped with a library of IMSL scientific subroutines, which the source code was dependant on for operation [21].

The first modification which was made to the code was that of incorporating I/O changes which allowed for reading and writing to and from the program via data files. An additional code modification was necessary before COUNTAC2 could be compiled. This modification required obtaining a copy of the IMSL math library subroutines in order to provide the linear systems equation solver that the source code called for. Once the IMSL libraries were obtained, however, it was discovered that the subroutine LEQTIF (called for by COUNTAC2) had been discontinued. After studying the various linear systems solvers available, it was decided that an equivalent call could be made to the two IMSL double precision algorithms, DL2TRG and DLFSRG, which perform the complete LU (lower triangular / upper triangular) factorization of a real general matrix, and provide the solution to a real general system of linear equations (given the LU factorization of the coefficient matrix), respectively [121]. A copy of the modified COUNTAC2 is included in Appendix A.

3.1.2.2. Code Verification

In order to verify that the modified source code for the "PC Version" of COUNTAC2 was an accurate and reliable tool for predicting Hertzian contact patch geometry and pressure distribution, a comparison of the theoretical results (via Hertz analysis) and those obtained with COUNTAC2 was made. These are indicated in Table 3.1.

It should be noted that the inputs to COUNTAC2 include the rigid body approach δ , the coefficients A and B (as obtained from equations (2.4) and (2.5)) for use in the subroutine INSEP, as well as the candidate contact region plus the desired initial mesh arrangement. The candidate contact region is obtained by solving the equation

$$f(x,y) = \delta = Ax^2 + By^2 \quad (3.1)$$

for a locus of points (x_i, y_j) at $i, j = 1$ to n , given A, B, and δ are known. Generating an initial mesh arrangement is described in detail in [64], and basically involves plotting one quarter symmetry of the candidate contact region (interpenetration curve) and dividing it into a series of segments and further subdividing each segment into a group of cells. Once completed, the cell locations (field points) which are identified by their (x,y) orientation are tabulated and read into COUNTAC2 as input. Figures 3.2a and 3.2b show a sample of mesh development and convergence of contact boundary. Figure 3.3 and 3.4 show resultant patch geometry and pressure distribution comparisons between theory and COUNTAC2.

3.1.3 Creep Force - Creepage Algorithms

Several different creep force - creepage algorithms exist (as outlined in 2.2.3) which have been utilized for the complete creepage regime of Hertzian contacts. The fastest of these is the Heuristic model of [57]. Based on a description of the main components of the algorithm [57], a FORTRAN source code was written for the purpose of obtaining benchmark results for the fastest method of creep force prediction, which could be used at a later time for comparison. A copy of the FORTRAN source code generated (SHE.FOR) is located in Appendix B.

The most complete, widely accepted code for Hertzian creepage predictions is the "exact nonlinear theory" of Kalker [33]. Besides providing creep forces and spin moment, the algorithm based on this theory (DUVOROL) also predicts the details of separatrix location, slip and stick regions, and surface normal and shear stress distributions. As inputs, the program requires dimensionless values of contact ellipse semidiameters, creepages, and Poission's ratio.

3.1.3.1 Code Implementation

The original DUVOROL source code written in the ALGOL 60 computer language, was converted to FORTRAN by Goree [53]. This source code (1082 lines) was obtained from the literature, and entered into a 486 IBM compatible computer via a standard DOS editor and compiled using a Microsoft FORTRAN 5.1 optimizing compiler.

The code conversion work of Goree [53] which was performed in the late 70's, provided a FORTRAN version of Kalker's commercially available computer code (DUVOROL) was developed to run on an IBM-370/3165 - II mainframe computer. Again,

this posed several problems when attempting to compile and execute it on a 486.

The first modification necessary, was that of converting the code from a card reader/line printer input-output format, to that of data file I/O. An additional modification which was required before DUVOROL could be compiled, was that of obtaining the appropriate subroutines called by the main program. As was discovered, although the user's manual indicated that only two subprograms (SIGN and CONST) were needed, DUVOROL could not be compiled until three additional subroutines internal to the mainframe operating system were obtained [53].

The three intrinsic subroutines were vital to DUVOROL, in that they were responsible for the matrix operations which had to be performed on a large system of tangential displacement equations. Two of these routines (ARRAY and GMPRD) were obtained readily in the exact format necessary from an IBM system scientific library archive at Portland State University [122]. The remaining routine (GELG), which performed the actual solution to a system of general simultaneous linear equations via Gaussian elimination, however, was part of a different scientific software library and could not be located.

3.1.3.2 Sparse Matrix Solution

In order to complete the final modification necessary for running the creep-force creepage code DUVOROL, the program architecture (as well as syntax) needed to be analyzed, and an equivalent replacement algorithm for GELG needed to be developed.

Since GELG was based on a direct method for solving a system of linear equations, namely the systematic reduction procedure of Gaussian elimination, it seemed reasonable to replace it with a similar algorithm. However, difficulties in obtaining convergence, as well

as incomplete solutions due to singularities were realized. Goree [53] mentioned a similar behavior for certain aspect ratios of contact ellipse semi-diameter. After inspection of the coefficient matrix, it became apparent that in many cases, a large number of randomly located zero entries existed, which explained the convergence difficulties encountered using a direct method.

Based on the aforementioned experience, it was decided that GELG would best be replaced by an iterative (rather than direct) linear equation solver. Although these methods are unable to return the exact solution even if all of the calculations could be performed using exact arithmetic, in many instances they are more effective than direct methods since they require far less computational effort as well round-off error is reduced [123].

Of the classic iterative techniques, the two most popular are the Jacobi method and Gauss-Seidel method. A relatively new extension to these techniques, however, is that of the Successive over-relaxation (SOR) method [124]. The SOR method is similar to both the Jacobi and Gauss-Seidel methods, but it uses a scaling factor in order to provide for a rapid reduction of the approximation error.

The Jacobi and Gauss-Seidel methods both involve a process that converts a system of ($n \times n$) equations of the form $A \bar{x} = \bar{b}$ into an equivalent form $\bar{x} = T \bar{x} + c$, for some ($n \times n$) matrix T and vector \bar{c} [123]. After the initial vector $\bar{x}^{(0)}$ is selected, the sequence of approximate solution vectors is generated by computing

$$\bar{x}^{(k)} = T \bar{x}^{(k-1)} + \bar{c} \quad (3.2)$$

for each $k = 1, 2, 3, \dots$, where the exact form of equation (3.2) varies with the method chosen. The SOR method is one class of relaxation methods that computes the approximations $\bar{x}^{(k)}$ by

$$x_i^{(k)} = (1 - \omega) x_i^{(k-1)} + \frac{\omega}{a_{ii}} \left[b_i - \sum_{j=1}^{i-1} a_{ij} x_j^{(k)} - \sum_{j=i+1}^n a_{ij} x_j^{(k-1)} \right] \quad (3.3)$$

where ω is a scaling factor, which is used to speed up convergence. For ω within (0, 1), the procedure is called an under-relaxation method, while for $\omega > 1$, an over-relaxation procedure results. For accelerating the convergence of DUVOROL, a value of ω between 1.25 and 1.8 was found to be optimal.

3.1.3.3 Code Verification

After the SOR subroutine was linked to DUVOROL, the code was tested for a number of different “base-line” data to insure its accuracy. The results of lateral creep force as predicted by the modified DUVOROL are compared with Kalker’s original code predictions [53] and the experimental results of Brickle [22] as shown in Figure 3.5, for the case of lateral creepage values of -1.4 to 0.8, $A/B = 6.75$. Additional results for a circular contact patch with pure longitudinal creepage is shown in Figure 3.6 where the separatrix locations are compared with those of Liu [35].

3.2 Counterformal Non-Hertzian Contacts

Contact stress problems with load-dependent contact regions are classified as counterformal problems. When wheel-rail contact occurs at a surface location which is discontinuous (ie. at a surface point common to two different radii of curvature) the contact patch geometry will be non-Hertzian. Most dynamic rail car models assume the existence

of Hertzian contact geometries. This is not usually because wheel-rail contact necessarily results in an elliptical patch, but often times due to the relative simplicity of solution methods for Hertzian problems and the difficulty encountered in attempting to solve non-Hertzian ones [52].

3.2.1 Iterative Solution for One Axis of Symmetry - COUNTAC1

For contacting bodies with similar elastic constants, Hertz's second assumption remains valid and allows for a de-coupling of the normal and tangential analysis. However, obtaining a normal solution (ie. patch geometry and pressure distribution) cannot be achieved in closed form and requires an iterative approach [69]. The primary reason for this is that the elastic displacement field w and the pressure field p within the contact region Ω , are related by integrating the Boussinesq solution (influence of a normal point load at location x', y' on the elastic displacement at a point x, y) [37],

$$w_i(x, y) = \frac{(1 - \nu_i^2)}{\pi E_i} \iint_{\Omega} \frac{p(x', y') dx' dy'}{[(x - x')^2 + (y - y')^2]^{1/2}} \quad (i = 1, 2) \quad (3.4)$$

where the domain of integration (Ω) cannot be known *a priori* (since it is a function of load).

The iterative scheme of COUNTAC1 (similar to COUNTAC2) utilizes the concept of a family of "interpenetration curves", as an aid in establishing the contact boundary for a given pair of surfaces. By definition, the interpenetration curve is "the intersection of two (undeformed) surfaces if the vertex of body 1 is moved along axis z_2 through an arbitrary distance δ " [69], (see Figure 2.1). This family of interpenetration curves becomes

potential candidate contact patch boundaries associated with some family of applied loads.

In order to develop the FORTRAN computer code of COUNTAC1, the simply discretized method was again employed which allowed equation (3.4) to be solved over a summation of small rectangular cells within the candidate patch Ω . The inputs required for execution include: interpenetration distance, wheel and rail curvatures at the location of contact, initial mesh configuration and elastic constants. The program outputs: total wheel load, peak pressure, pressure distribution and contact patch geometry.

3.2.1.1. Code Implementation and Verification

The FORTRAN source code for COUNTAC1 is available in the open literature [64]. After contacting the author, however, a diskette of the source code was obtained [120]. The source code was compiled on a 486 IBM compatible computer using Microsoft FORTRAN 5.1 optimizing compiler.

Similar to the code COUNTAC2, COUNTAC1 required I/O charges which allowed for reading and writing from data files, as well as the same IMSL subroutines for efficient solution to the system of linear equations (see section 3.1.2.1). A copy of the modified COUNTAC1 is included in Appendix D.

In order to verify that the modification to COUNTAC1 did not alter the accuracy of its predictive capabilities, a sample problem cited in [78] was attempted. Figure 3.7 shows the location of contact for the wheel-rail combination, where the normal wheel load was 34,000 pounds. As indicated at the location of contact (O), the rail head radius of curvature changes from 10 to 1.25 inches, a discontinuity causing non-Hertzian behavior. The rail is a 140RE and the wheel is that of a SIG (Schweizerische Industriel-Gesellschaft)

Metroliner. The resulting non-Hertzian patch geometry and pressure distribution were in exact agreement with those reported in the literature [78].

3.2.2 Creep Force - Creepage Algorithms - ROLCREEP

Solution to the tangential problem of wheel-rail contact results in the prediction of longitudinal and lateral components of creep (tangential) force, resultant creep force, spin moment and separatrix location (ie. regions of slip and stick). For non-Hertzian contacts, only two codes exist which can accurately treat the tangential problem. These are the code CONTACT of Kalker [79] and ROLCREEP by Paul and Liu [35]. The cost of acquiring CONTACT was prohibitive and as a result, the code ROLCREEP was decided upon as the only realistic choice for a non-Hertzian study.

3.2.3. Code Implementation and Verification

The FORTRAN source code for the program ROLCREEP was obtained from Professor B. Paul at the University of Pennsylvania in diskette form [120]. The program consisted of 1823 lines of FORTRAN code, which included 23 subroutines for execution. One primary problem, however, was that no instructions on how to use the code had ever been recorded. Given the length and complexity of the code, it was assumed to be unusable without the aid of some form of user's manual. Initial contact with Dr. C. Liu (code author) at Tamkang University, Taiwan, was made and he indicated that a brief user's manual for ROLCREEP could be developed and made available. After several months the user's manual became available, and it provided much of the necessary information regarding the architecture and viable definitions for ROLCREEP.

When the sample problem included in the user's manual was attempted, however, a "divide by zero" error was encountered. This was a major set back which took several weeks to resolve. The nature of the error was also complicated by the fact that this was the first application in which ROLCREEP was run on a machine other than a main frame computer. This hurdle was finally overcome when the details of matrix manipulation and transfer to and from various subroutines were studied in sufficient detail so as to discern that a certain coefficient matrix was apparently being "rearranged" after it was passed to a subroutine, but prior to its arrival in the subroutine. Further investigation revealed that the subroutine was exceeding the 640 K DOS operating limit. This problem was finally solved by including the /MW option at compilation time, and executing the program under the Microsoft Windows operating system.

In order to verify that the modifications to ROLCREEP did not alter the accuracy of its predictive capabilities, a sample Hertzian problem was run and compared to the results of DUVOROL. In addition, the non-Hertzian contact patch of Figure 2.16 and 2.17 was analyzed under a variety of creepage conditions and the separatrix locations were found to be in excellent agreement with the results of Liu [35].

3.3 Wheel-Rail Model - 136RE x AAR1-B

Having developed sufficient confidence in, and competence with, the four primary numerical tools for wheel-rail contact analysis (COUNTAC2, DUVOROL, COUTAC1, ROLCREEP), the modeling of an actual wheel-rail system was undertaken. The objective of this analysis was to obtain a better understanding of the creep force - creepage behavior throughout the full range of counterformal contact of a standard wheel-rail combination under typical load conditions.

3.3.1. Wheel-Rail Surface Geometries

The specific wheel-rail combination used in this study was suggested by the project sponsor as a “popular combination relevant to their industry” [91]. The rail was a 136RE (136 pounds per yard) and the wheel, an AAR 1-B (American Association of Railways) wide flange wheel. The geometries of each were obtained from the AREA Manual for Railway Engineering [129] and are included in Figures 3.8 and 3.9 respectively. Although these are “new” unworn profiles, an analysis could be carried out in a similar fashion if the surface curvatures of worn profiles were made available. It has been assumed that the surfaces are elastic, clean and dry.

3.3.2 Three Regimes of Contact

Given the constant taper of the AAR1-B for locations other than the flange root (Figure 3.9), and that the 136RE has two different radii of curvature between the gauge corner and rail crown centerline (Figure 3.8), there will be three distinct counterformal contact geometries (each of which will vary with load). Of these three geometries, two will be Hertzian and one non-Hertzian. Figure 3.10 shows the locations of each separate regime of contact, where patch #1 and #3 are elliptic (due to a continuous radius of curvature throughout) and patch #2 is at a location shared by two separate radii of curvature and therefore is non-Hertzian by definition. Under normal tangent track operating conditions, this wheel-rail combination would experience the contact conditions associated with patch #1, #2 or #3, at any given time depending on the lateral alignment of the wheelset with respect to the track.

3.3.3 Centralized Rail Crown Contact (Position #1)

As indicated in Figures 3.8 and 3.9, the radii of curvature of rail and wheel in the lateral direction are 14 inches and ∞ , respectively. In the longitudinal direction they are $-\infty$ for the rail and 19 inches for the wheel. Given these curvatures, the elastic properties, and any value of wheel load, the normal problem for contact patch geometry, peak pressure and pressure distribution could be obtained.

3.3.3.1 Normal Hertzian Solution

In order to evaluate the creep force behavior for a realistic range of wheel loads the sponsor was again consulted. It was recommended that a wheel load range from 6000 to 36,000 pounds be considered so as to cover all reasonable conditions from empty flat cars to fully loaded double stack designs. Since contact patch geometry is load dependent, this necessitated that a separate normal solution be computed for each wheel load condition. This analysis was carried out using the procedure of 3.1.1. The results are shown in Figure 3.11. As indicated, the contact ellipse semi-diameter in the longitudinal (rolling) direction "a" grows at a faster rate than its lateral counterpart "b". Of special interest is the range on the magnitude of the parameter "c" as this will be necessary for normalizing both the ellipse diameters as well as the lateral and longitudinal creepage and spin inputs for the tangential code DUVOROL.

3.3.3.2 Tangential Hertzian Solution

After obtaining the full range of geometric parameters from the normal contact solution,

the corresponding tangential results were sought. The normal results were used as inputs for the Hertzian code DUVOROL, ($A = a/c$, $B = b/c$), along with the elastic properties. However, for any given normal condition, a wide variety of creepage combinations could exist and thus effect the creep force magnitude and separatrix location (depending on the rail car dynamics).

The creepage inputs for DUVOROL appear in the dimensionless form given by (3.5) and (3.6), for longitudinal and lateral directions respectively.

$$\eta_x = \frac{v_x \rho}{\mu c} \quad (3.5)$$

$$\eta_y = \frac{v_y \rho}{\mu c} \quad (3.6a)$$

$$\chi_z = \frac{\phi \rho}{\mu} \quad (3.6b)$$

Here c is the parameter \sqrt{ab} , μ is the coefficient of friction, ρ is the effective rolling radius (3.7), and v_x and v_y are creepages.

$$\frac{1}{\rho} = \frac{1}{4} \left(\frac{1}{R_1} + \frac{1}{R_1'} + \frac{1}{R_2} + \frac{1}{R_2'} \right) \quad (3.7)$$

In order to study an appropriate range of creepage (v_x , v_y), a corresponding range of η_x and η_y needed to be determined. As indicated by equation (3.7), for given location of contact ρ becomes fixed. For position #1, this value was 32.24 inches. As shown in Figure 3.15, for a given contact location between a fixed set of surfaces, the parameter c increases in a nonlinear fashion with respect to load from 0.128 inches at 5000 pounds, to 0.245 inches at 35,000 pounds. A coefficient of friction of $\mu = 0.3$ was selected as one representing an average of values cited in the literature for dry conditions, and the range on

v_x and v_y was chosen to have an upper limit for tangent operations of 0.5% [44, 89].

Using these values, an appropriate range on η_x and η_y for position #1 was determined to be: η_x (0, 5.0) and η_y (-5.0, 5.0), where the -5.0 lower limit on η_y results from v_y values associated with a negative angle of attack (α in Figure 2.3). After a test matrix was developed to systematically exercise DUVOROL over the range of load, geometry and creepage parameters selected, the resultant dimensionless creep force values were computed ($FXN = F_x/\mu N$, $FYN = F_y/\mu N$). The longitudinal creep forces are shown as dots in the three dimensional plot of Figure 3.12. The mesh represents a creep-force creepage surface (CFCS) for position #1. The surface fit was achieved by using a least squares surface fitting algorithm with automatic singular value decomposition (SVD) [125]. The resulting surface equation is given in (3.8) where the constants are listed in Table 3.2

$$FXN = a_0 \tanh (\eta_x \exp (a_1 |\eta_y|)) \left\{ (a_2 |\eta_y|^{3.5} - a_3 |\eta_y|^{2.0} - a_4 |\eta_y| + a_5) (\exp (|\eta_y|^{a_6}) \exp (a_7 (1 - \eta_x))) \right\} \quad (3.8)$$

A similar surface plot of the lateral creep force variation and associated CFCS is shown in Figure 3.13. The resulting surface equation is given in (3.9) where the constants are also listed in Table 3.2,

$$FYN = b_0 \tanh [b_1 \eta_y] \left\{ (b_2 \eta_x^3 - b_3 \eta_x^2 - b_4 \eta_x + b_5) \exp (\eta_x / b_6) \right\} \quad (3.9)$$

and where η_x and η_y are defined by equations (3.5) and (3.6).

3.3.4 Gauge-side Rail Head Contact (Position #3)

Wheel-rail contact geometries located at position #3 are characterized by the radii of curvatures within that regime. As indicated in Figures 3.8 and 3.9, the radii of curvature of rail and wheel in the lateral direction are 1.25 inches and ∞ , respectively. In the longitudinal direction they are $-\infty$ for the rail and 19 inches for the wheel.

3.3.4.1 Normal Hertzian Solution

For the same reasons identified in section 3.3.3.1, the normal problem was solved for position #3. Using the analysis method of section 3.1.1 for a range of 6000 to 36,000 pounds of wheel load, the trends for contact patch geometry and pressure were obtained and plotted in Figure 3.14. These results were used to compute the necessary range of input values for the tangential code DUVOROL.

3.3.4.2 Tangential Hertzian Solution

In order to study an identical range of operating conditions (ie. wheel load and creepage), the dimensionless inputs of DUVOROL needed to be determined. For position #3, the effective rolling radius (ρ) was found to be equal to 4.69 inches. From Figure 3.14, the range on c was shown to be 0.0779 inches at 5000 pounds and 0.149 inches at 35,000 pounds. Combining these with a creepage range identical to that of position #1, a range of η_x and η_y was determined for the dimensionless creepage values from equations (3.5) and (3.6), η_x (0, 2.0) and η_y (-2.0, 2.0). Figures 3.15 and 3.16 show the results of

the parametric analysis as well as the corresponding surface fits. The equations which approximate the CFCS indicated by the mesh in each plot, are described by equations which have the exact form of (3.8) and (3.9) for the longitudinal and lateral directions respectively. The constants for each equation are found in Table 3.3.

3.3.5 Transition Zone Contact (Position #2)

The 14 inch radius of curvature of the centralized rail crown of Figure 3.8, transitions to a 1.25 inch radius at a location identified as position #2 on Figure 3.10. At this location the radius of curvature is discontinuous and the contacting wheel surface encounters a portion of each of the two different rail curvatures simultaneously. The geometry of the resulting non-Hertzian contact patch is a function of both of these radii, as well as the wheel load and elastic properties of the surfaces.

3.3.5.1 Non-Hertzian Solution to the Normal Problem

The solution method for the normal part of the non-Hertzian contact problem, as outlined in section 3.2.1, was accomplished by using COUNTAC1. In order to analyze the full range of possible wheel loads, four different values of rigid body approach (δ) were selected. The results of COUNTAC1 for the load range of 5000 to 35,000 pounds are shown in Figure 3.17. The parameters \bar{a} and \bar{b} are the maximum values of half length and patch width of the non-Hertzian contact in the longitudinal (rolling) and lateral directions respectively. A detailed plot of the load-dependent contact patch geometries is shown in Figure 3.18, where the axis for half symmetry is the abscissa of the graph, which would be in the lateral direction. As indicated, the general shape of the contact patch is

preserved as the load is increased, however, a marked increase in patch area is observed.

The non-Hertzian pressure distributions associated with each of the four contact patches were found to be significantly non-ellipsoidal, yet they continued to display the half-symmetry which was characteristic of the geometries of Figure 3.18. The details of the pressure distributions for 12,342 and 26,535 pound patches are shown in Figures 3.19 and 3.20, in three and two dimensions respectively. Both plots have been constructed with the coordinate system origin located at the centroid of pressure for the patch.

3.3.5.2 Non-Hertzian Solution to the Tangential Problem

The non-Hertzian Solution to the tangential problem, outlined in section 3.2.2, was handled using the predictive capabilities of the computer code ROLCREEP. As input, the COUNTAC1 output data was required (in a modified format). This included the complete (x, y) description of the contact geometry, as well as the entire pressure field. In each case the patch was subdivided into 81 cell locations, each identified by an x_j and y_i field point location and a corresponding local pressure value P_{ij} .

Obtaining a converged solution to ROLCREEP for the load-dependent contact geometries of Position #2 (Figure 3.17), under the creepage conditions selected for positions #1 and #3 (ie. v_x (0, 0.5%), v_y (-0.5%, 0.5%)) proved to be a time consuming endeavor. For certain combinations of load and creepage, ROLCREEP took on the order of several days to converge to the tangential solution.

Results of separatrix location and corresponding regions of slip and stick for a 12,342 pound wheel load are shown in Figures 3.21 and 3.22 for pure longitudinal creepage values of 0.15% and 0.35%, respectively. In each case, the positive x coordinate is in the

direction of rolling. As the creepage is increased, the separatrix proceeds from a location nearer to the trailing edge of the contact, toward that of the leading edge. In addition, the corresponding region of slip grows while that of adhesion diminishes. The geometric growth of the slip region, as well as the magnitude of the local slippage distribution are shown in the three dimensional surface plot of Figure 3.23. The detailed information regarding local slip distribution is interesting not only from a contact dynamics perspective but also from a tribological one, as will be discussed in section 3.4. Figure 3.24 is included to give insight into the magnitude of local surface shear stress distribution. A two dimensional “slice” at any lateral (y-coordinate) location showed good agreement with the characteristic shape of shear stress as reported in the photoelastic studies of Haines and Ollerton [46] (and included in Figure 2.9).

3.3.5.3 Ellipticizing Non-Hertzian Contacts

After giving serious consideration to the length of time necessary for ROLCREEP convergence of ROLCREEP, as well as the amount of effort necessary for preparing the geometry and pressure fields needed as input data, the incompatibility of ROLCREEP as a non-Hertzian contact mechanics subprogram for a “real time” rail car dynamics simulation algorithm became very apparent. However, this did not minimize the sponsor’s need for a rail-wheel contact model capable of handling the non-Hertzian nature of discontinuous surface geometries. It was therefore proposed, that a systematic method be developed to ellipticize (that is to reconstruct as elliptical) non-Hertzian contacts similar to that of Hung [56]. A comparison between the actual non-Hertzian results and those obtained after the contact was ellipticized, would provide insight into the feasibility of such a proposal.

The method developed for ellipticizing non-Hertzian contact geometries was based on

two principles of similitude, which were necessary for retaining the key features of the contact patch. These were: (1) the area of the ellipticized contact patch will be equivalent to that of the original non-Hertzian contact geometry, (2) the centroid of pressure (location of maximum surface pressure) on both the ellipticized contact, as well as the actual non-Hertzian geometry, should be coincident.

This procedure was first carried out on the 12,342 pound contact patch of Figure 3.18. In order to realize condition (1), the actual non-Hertzian patch area needed to be obtained. This was initially accomplished by plotting the half symmetry “footprint” (Figure 3.25) of the contact patch on fine mesh graph paper and adding up the total number of rectangular cells as indicated in Figure 3.26. The area of an ellipse is given by equation (3.10).

$$A_e = \pi ab \quad (3.10)$$

By equating this area to that measured in Figure 3.26 (A_{nh} = area of non-Hertzian patch), a single equation with two unknowns a and b , is obtained (3.11).

$$A_{nh} = A_e = \pi ab \quad (3.11)$$

By invoking the second condition of similitude, the elliptical semi-diameter “ a ” is set equal to the maximum half-length of the actual non-Hertzian contact in the rolling direction (\bar{a} of Figure 3.26). This fixed the location of peak pressure common for both contacts. The resulting lateral semi-diameter of the ellipticized patch could then be obtained from equation (3.12).

$$b = \frac{A_{nh}}{\pi \bar{a}} \quad (3.12)$$

A plot of the contact patch geometry for both the actual non-Hertzian as well as the ellipticized contact is shown in Figure 3.31. Using the ellipticized semi-diameters and equation (2.15), a corresponding ellipsoidal pressure distribution was computed. A comparison of this with the actual non-Hertzian pressure distribution is shown in Figure 3.28 for a lateral section at $y = \text{constant} = 0.0$ (ordinate through the centroid of pressure).

The method for estimating non-Hertzian contact patch area was not only time consuming, but also subject to significant interpretation due to the approximation of partial cells. In order to streamline this process and also obtain a more accurate area estimate, the non-Hertzian contact patch geometries were curve-fit using ninth order polynomials. These are shown in Figure 3.29, for each of the four non-Hertzian patches of position #2. The best fit equations are listed in (3.13) to (3.16), for wheel-loads of 6714, 12,342, 26,535 and 34,855 pounds respectively.

$$y = -4405623x^7 - 2815684x^6 - 638948x^5 - 63071x^4 - 2430x^3 \\ -10x^2 + 0.964x + 0.211 \quad (3.13)$$

$$y = -1187614x^7 - 866051x^6 - 232361x^5 - 27972x^4 - 1400x^3 \\ -15.8x^2 + 0.632x + 0.261 \quad (3.14)$$

$$y = -10093043x^9 - 9568645x^8 - 3495835x^7 - 625712x^6 - 61031x^5 \\ -4467x^4 - 380x^3 - 24x^2 - 0.311x + 0.336 \quad (3.15)$$

$$y = -1053497x^8 - 975802x^7 - 35620x^6 - 66482x^5 - 6376x^4 \\ -0297x^3 - 9.3x^2 - 0.181x + 0.359 \quad (3.16)$$

Numerical integration of these equations was performed in order to obtain the desired half-

patch areas. This was accomplished by writing an algorithm which implemented Romberg integration by application of the composite trapezoidal rule with Richardson extrapolation [123]. A copy of the FORTRAN source code for this algorithm is included in Appendix E.

3.3.5.4 Non-Hertzian vs. Ellipticized - Normal Results

Having developed a systematic approach to ellipticizing non-Hertzian contacts, the next step was to investigate the behavior of the normal solution for the ellipticized contact and contrast it with the actual non-Hertzian normal solution. A summary of these results is included in Figures 3.30 and 3.31. Of specific interest are the maximum and minimum values of c (for normalizing DUVOROL creepage inputs), the ellipticized contact patch aspect ratio (a/b), and the peak pressure ratio (P_{nh}/P_h). As indicated, both the ellipticized aspect ratio and peak pressure ratio are independent of load. The significance of a load independent patch aspect ratio, was that the ratios of a/c and b/c (A and B DUVOROL inputs) were also independent of wheel load at position #2. Thus, similar to the results of Figures 3.15 and 3.16, which were valid throughout the entire load range, the ellipticized contact geometries could be conveniently handled with the Hertzian tangential code, DUVOROL.

3.3.5.5 Ellipticized Solution to the Tangential Problem

Using the results of c from Figure 3.30 and an effective rolling radius ρ via equation (3.7) (where an average curvature of 7.625 inches was used for R_1), the range of dimensionless longitudinal and lateral creepage (η_x, η_y) was computed to be (0, 3.0) and

(-3.0, 3.0) respectively. Similar to positions #1 and #3, the range of wheel load and creepage (v_x (0, 0.5%), v_y (-0.5%, 0.5%)), as well as $\mu = 0.3$ and identical elastic parameters, were used for obtaining the necessary inputs for DUVOROL to perform the Hertzian tangential analysis on the ellipticized contacts.

The results of this parametric analysis are displayed by the creep force - creepage surfaces (CFCS) plotted in Figures 3.32 and 3.33. Of specific (and most important) interest is that the shapes of these surfaces strongly resemble the CFCS's for the Hertzian contacts of positions #1 and #3. In addition to this, the same form of surface equations (3.8) and (3.9) were found to provide quantitative description of the creep force - creepage phenomenon for the longitudinal and lateral directions, respectively.

The equation constants are listed in Table 3.4.

3.3.5.6 Non-Hertzian vs. Ellipticized Tangential Results

In order to determine if the tangential solution for an ellipticized non-Hertzian contact could provide an accurate description of the actual non-Hertzian creep force - creepage behavior, a comparison was made between creep force - creepage results obtained via equation (3.8) and ROLCREEP predictions. This was done for the geometry of contact position #2 at a wheel load of 26,535 pounds, for pure longitudinal creepage values of v_x (0, 1.0%). The results are shown in Figure 3.34.

3.4 Contact Patch Friction Work

The general procedure for computing *global* and *local* distributions of contact patch

friction work have been outlined in sections 2.4.1 and 2.4.2. In order to quantify the behavior of contact patch friction work for dynamic and tribological purposes, a detailed parametric analysis was conducted utilizing the computational tools of COUNTAC1 and 2, DUVOROL and ROLCREEP, discussed previously. Of specific interest was a comparison between the magnitudes of global work for Hertzian and non-Hertzian contacts, as well as a comparison between their respective local work distributions.

3.4.1 Global Patch Work

The computation of global patch friction work was accomplished for Hertzian contacts by modifying the DUVOROL algorithm to perform the dot product of resultant creep force values and creepages. Using the dimensionless values of equations (3.5) and (3.6), a dimensionless friction work equation was obtained (3.21) which was similar to equation (2.33).

$$W'_{gd} = \frac{\rho}{\mu^2 c N} [v_x F_x + v_y F_y + \phi M_z] \quad (3.21)$$

3.4.1.1 Friction Work Surfaces

In order to understand the influence of the primary contact parameters on the behavior of global friction work, two Hertzian contacts were studied. The range of input parameters for each is given in Table 3.5. By running DUVOROL for a test matrix which included combinations of contact patch aspect ratio, creepage and spin, enough data was obtained to qualify the general behavior of contact patch friction work. The results of this series of computations are included in the three dimensional surface plots of Figures 3.35 - 3.38. Figures 3.35 to 3.37 show the variation in friction work behavior with respect to increasing

values of spin, while Figure 3.38 contrasts with Figure 3.36 the effect of contact patch aspect ratio (A/B) on friction work (all else equal).

3.4.1.2 Surface Equations

Given that the qualitative behavior of the contact patch friction work surfaces had a characteristic shape which was similar for each of the test cases studied, it seemed reasonable to attempt to quantify this behavior. This was achieved by using a surface data fitting algorithm similar to that described in section 3.3.3.2. From the form of the governing equation for friction work (2.44) it became clear that for a given contact patch (ie. curvatures and load) the independent parameters were v_x , v_y , and ϕ , thus:

$$W'_g = f(v_x, v_y, \phi, a/b) \quad (3.22)$$

Using the dimensionless parameters of equations (3.5) and (3.6), a dimensionless work function of the form (3.23) would be expected.

$$W'_{gd} = f(\eta_x, \eta_y, \chi_z, A/B) \quad (3.23)$$

The results of the surface fitting procedure for dimensionless friction work are shown in Figure 3.39. This data was for the rail-wheel combination 136RE X AAR1-B at position #1. The approximating equation which generated the “mesh” in this figure, is described by equation (3.24),

$$W'_{gd} = \frac{c_1 |\eta_y|^{2.5}}{(1 + c_2 \eta_y^2)} + \frac{c_3 |\eta_x|^{2.5}}{(1 + c_4 \eta_x^2)} + ((5 - |\eta_y|)(c_5 \eta_x + c_6 \eta_x^2)) \quad (3.24)$$

where the coefficients for this equation are listed in Table 3.6.

Equation (3.24) was also applied to the global friction work results for the non-Hertzian ellipticized contact patch of position #2, as well as to position #3 for the same wheel-rail combination. The surface approximations to these data are shown in Figures (3.40) and (3.41) respectively, where the coefficients of equation (3.24) for each of these fits and are included in Tables 3.7 and 3.8.

3.4.2 Local Patch Work Computations

Computation of local friction work was accomplished using a procedure which combined either COUNTAC2 or COUNTAC1 (depending on whether the patch was Hertzian or non-Hertzian) with a modified version of ROLCREEP. The modifications necessary for local work computations in the ROLCREEP algorithm primarily involved the implementation of equations (2.36). As indicated by this equation, the local work per distance travelled at any cell location within the contact patch is dependent upon the dot product of the local value of surface shear traction \bar{T} and slippage \bar{s} multiplied by the discretized area of the cell.

3.4.3 Friction Work Distribution

Given that the local work distribution should be a function of both \bar{T} and \bar{s} , it seemed reasonable to first obtain a physical understanding of these two phenomenon before computing work. Two contact geometries were considered for this purpose. One was a fully non-Hertzian patch and the other an ellipticized non-Hertzian geometry. Both were obtained from the 136RE x AAR1-B rail-wheel combination for a contact location of position #2 (Figure 3.10). The wheel load was fixed at 26,535 pounds and a pure

longitudinal creepage of $v_x = 0.6\%$ was imposed. The results of surface traction and local slippage distribution for the ellipticized patch are shown in Figures 3.42 and 3.43. Similar results for the non-Hertzian geometry are given in Figures 3.33 and 3.45. Of specific interest here is the asymmetry of the non-Hertzian distributions. It should also be noted that the distance used for normalizing the coordinates (x_{norm}) was 0.3360 inches for the ellipticized case, and only 0.3088 inches for the non-Hertzian plots. The resultant effect of this is, that the physical patch areas appear to have unequal magnitudes (ie. non-Hertzian area appears to be slightly larger than the ellipticized area). However, the dimensional areas are indeed equivalent between the two geometries, as this was the first condition of similitude imposed in section 3.3.5.3.

After the results of the \bar{T} and \bar{s} distribution for each patch had been obtained, the dot product algorithm was utilized in order to obtain the resultant local friction work profiles over the contact domain. These are shown in Figures 3.46 and 3.47 for the ellipticized and true non-Hertzian patches, respectively.

Table 3.1 Comparison of Contact Parameters Resulting from COUNTAC2 with Hertz Theory

Quantity	Hertz Theory	COUNTAC2	% Error
N (lbs)	1006.6	1006.6	0
P_m (psi)	0.3924×10^5	0.3941×10^5	0.43
a (inches)	0.15035	0.1620	1.66
b (inches)	0.07678	0.0767	0.2

Table 3.2 Coefficients For The Longitudinal and Lateral Creep Force - Creepage Surface Equations of Position #1

a_0	a_1	a_2	a_3	a_4	a_5	a_6	a_7	r^2
.0353	-0.717	-0.121	-3.834	17.052	28.044	0.817	0.100	0.964

b_0	b_1	b_2	b_3	b_4	b_5	b_6	r^2
0.019	0.558	-0.310	-4.784	26.808	56.856	2.384	0.989

Table 3.3 Coefficients For The Longitudinal and Lateral Creep Force - Creepage Surface Equations of Position #2

a_0	a_1	a_2	a_3	a_4	a_5	a_6	a_7	r^2
0.0618	-0.537	-0.216	-4.394	15.896	19.304	1.067	0.139	0.994

b_0	b_1	b_2	b_3	b_4	b_5	b_6	r^2
0.080	0.881	-0.366	-3.318	10.849	13.291	1.321	0.991

Table 3.4 Coefficients For The Longitudinal and Lateral Creep Force - Creepage Surface Equations of Position #3

a_0	a_1	a_2	a_3	a_4	a_5	a_6	a_7	r^2
.075	-1.053	-0.474	-5.095	13.081	18.660	0.951	0.414	0.971

b_0	b_1	b_2	b_3	b_4	b_5	b_6	r^2
0.207	1.598	0.271	0.692	1.018	5.205	75.544	0.984

Table 3.5 Range of Input Parameters for Global Friction Work Parametric Study

A/B	η_x	η_y	χ_z
1.0	0.0 - 1.4	(-)1.4 - 1.4	0.2, 0.8, 6.5
6.75			0.8

Table 3.6 Coefficients for the Global Friction Work Surface Equation of Position #1

c_1	c_2	c_3	c_4	c_5	c_6	r^2
0.3939	0.1414	0.0411	0.0095	0.2187	-0.0175	0.989

Table 3.7 Coefficients for the Global Friction Work Surface Equation of Position #2

c_1	c_2	c_3	c_4	c_5	c_6	r^2
0.8373	0.4280	-4.0E-7	-0.3086	0.1713	0.0108	0.986

Table 3.8 Coefficients for the Global Friction Work Surface Equation of Position #3

c_1	c_2	c_3	c_4	c_5	c_6	r^2
1.6417	0.9834	-11.8643	12.3277	0.4078	-0.0348	.986

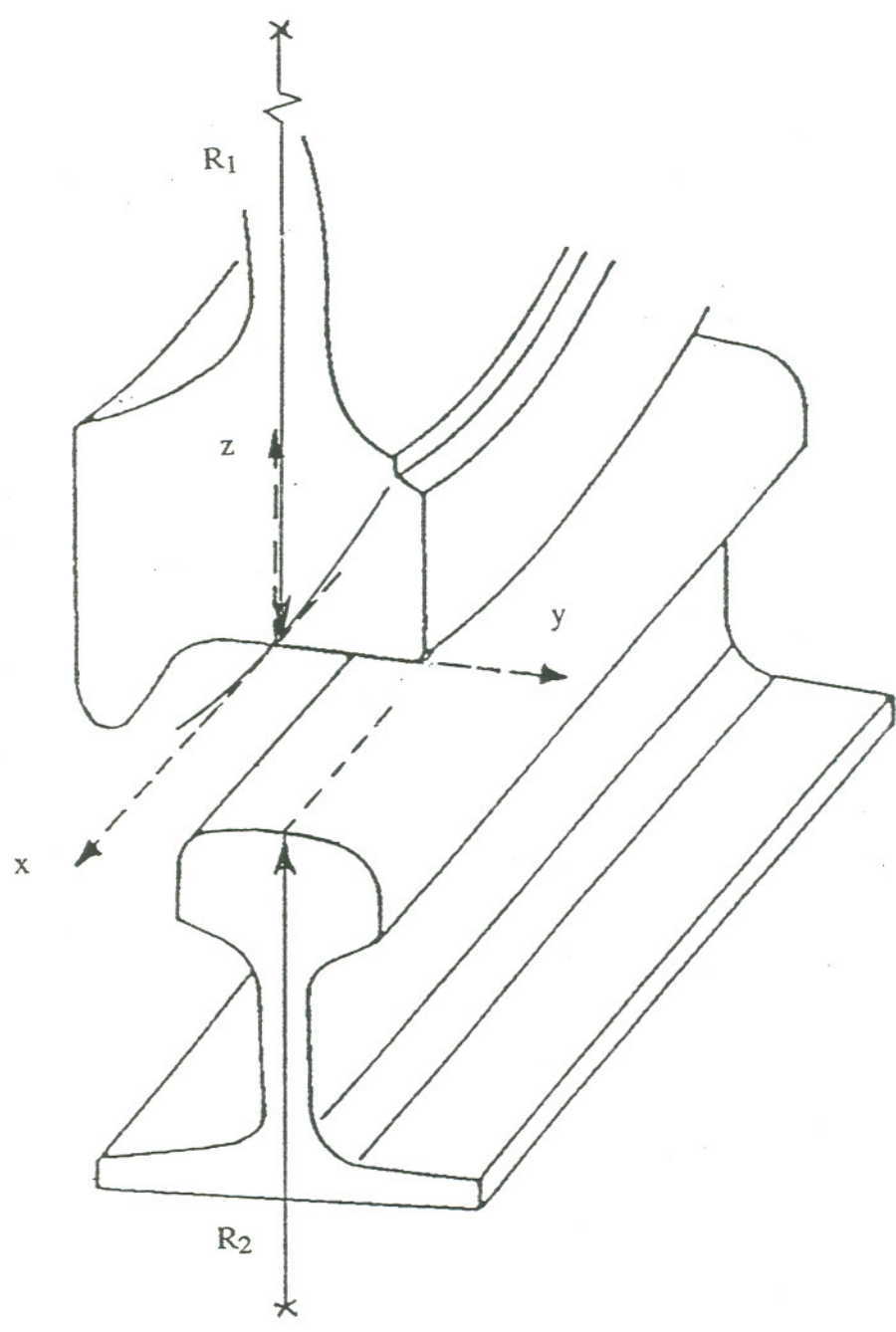


Figure 3.1 Wheel and rail radii of curvatures.

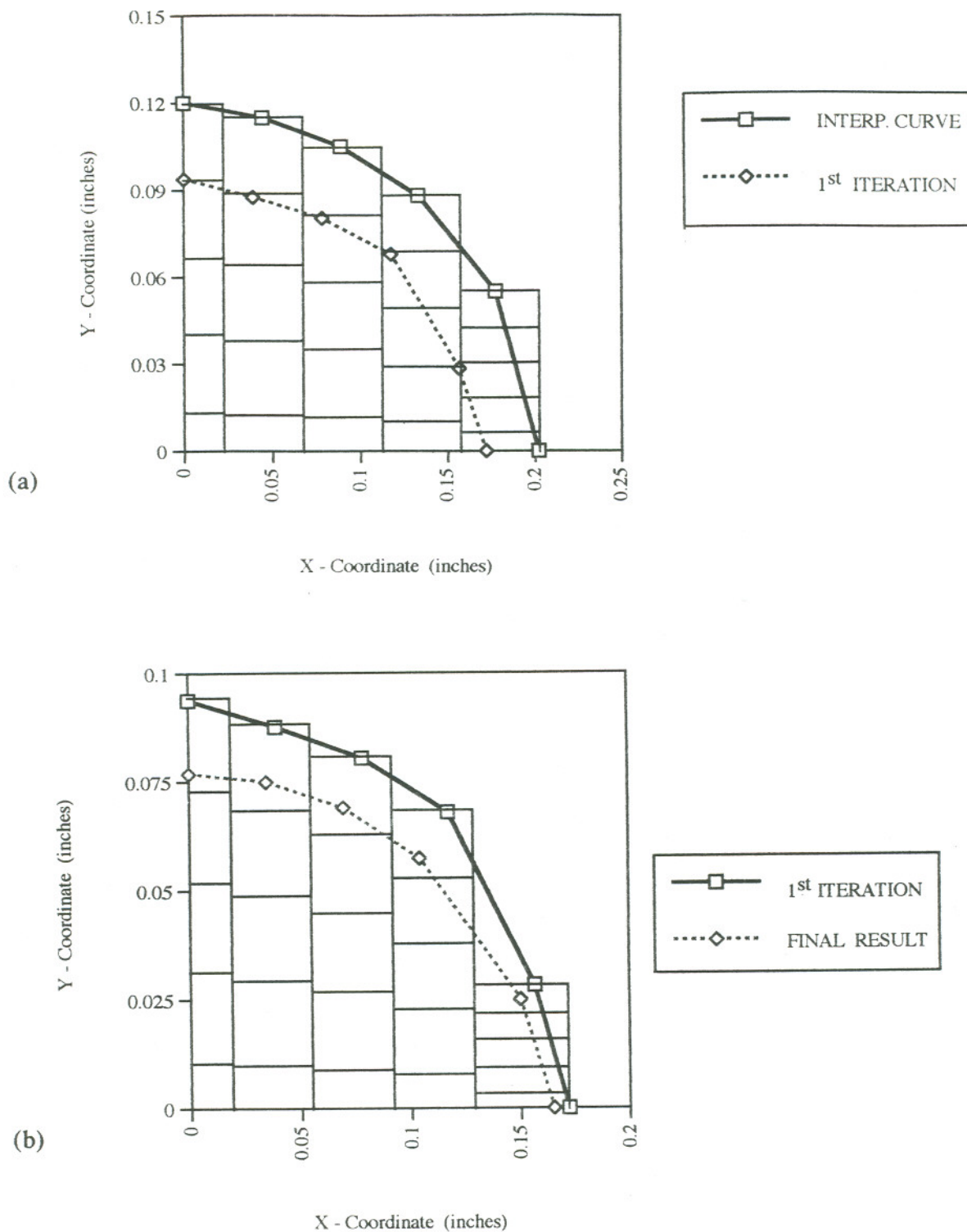


Figure 3.2 Mesh development and contact boundary (a) interpenetration curve and first iteration; and (b) first iteration and final boundary.

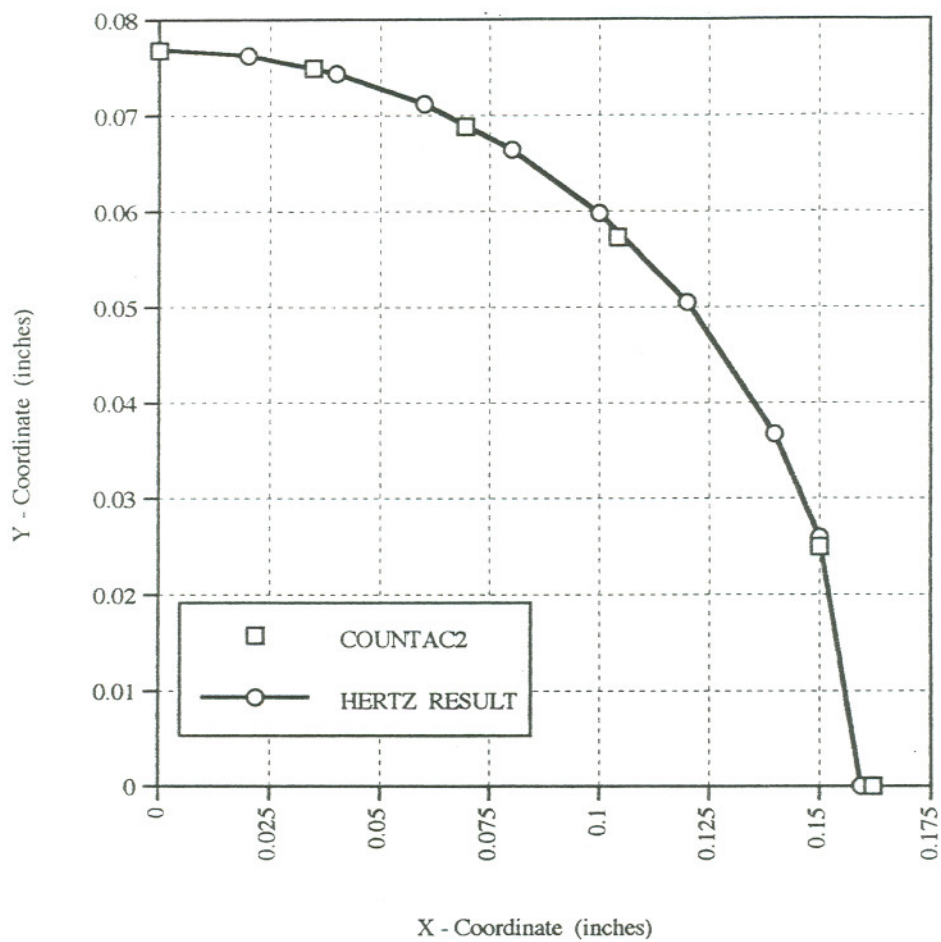


Figure 3.3 Comparison of contact patch geometry as predicted by COUNTAC2 and Hertz theory.

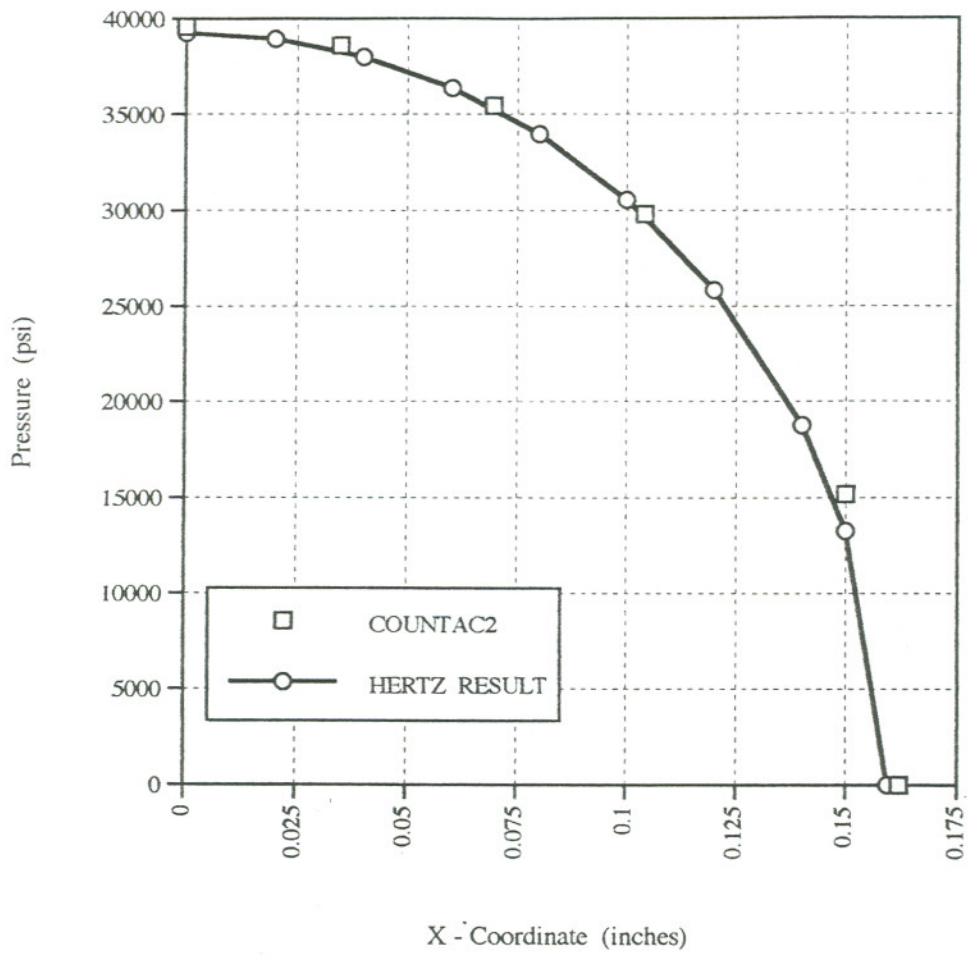


Figure 3.4 Comparison of contact patch pressure distribution as predicted by COUNTAC2 and Hertz theory.

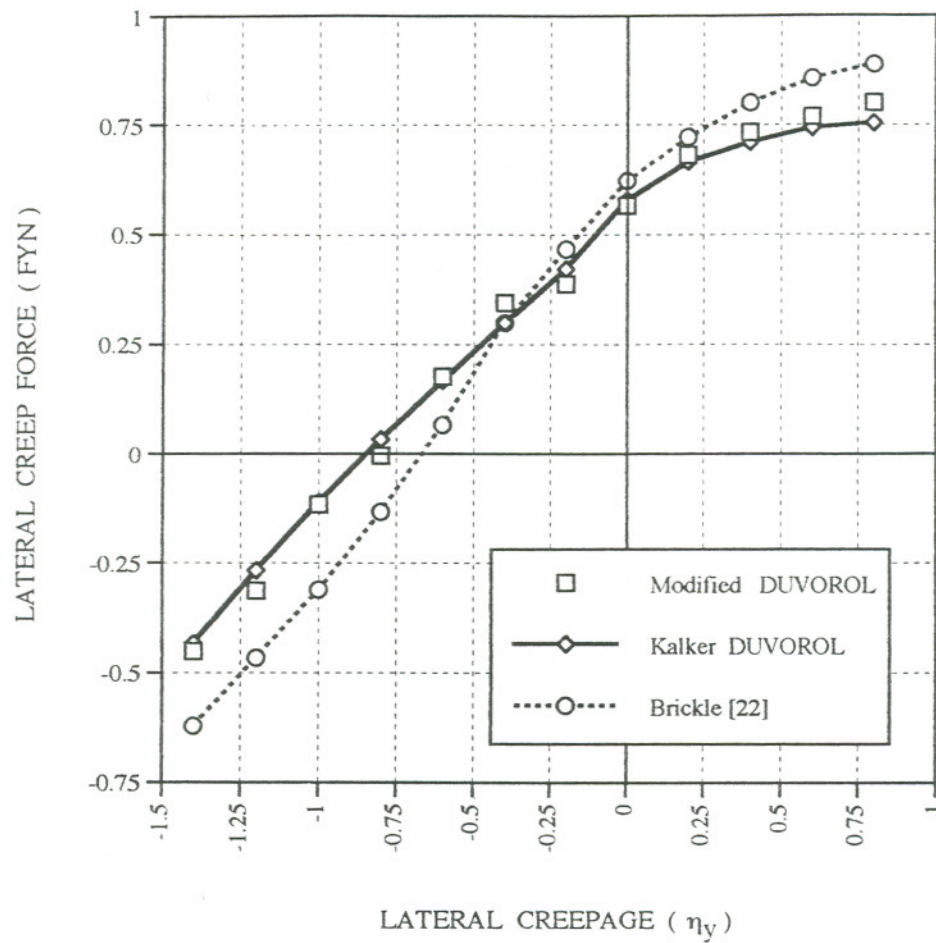


Figure 3.5 Lateral creep force - creepage curve comparison between modified DUVOROL and Kalker's original data [53].

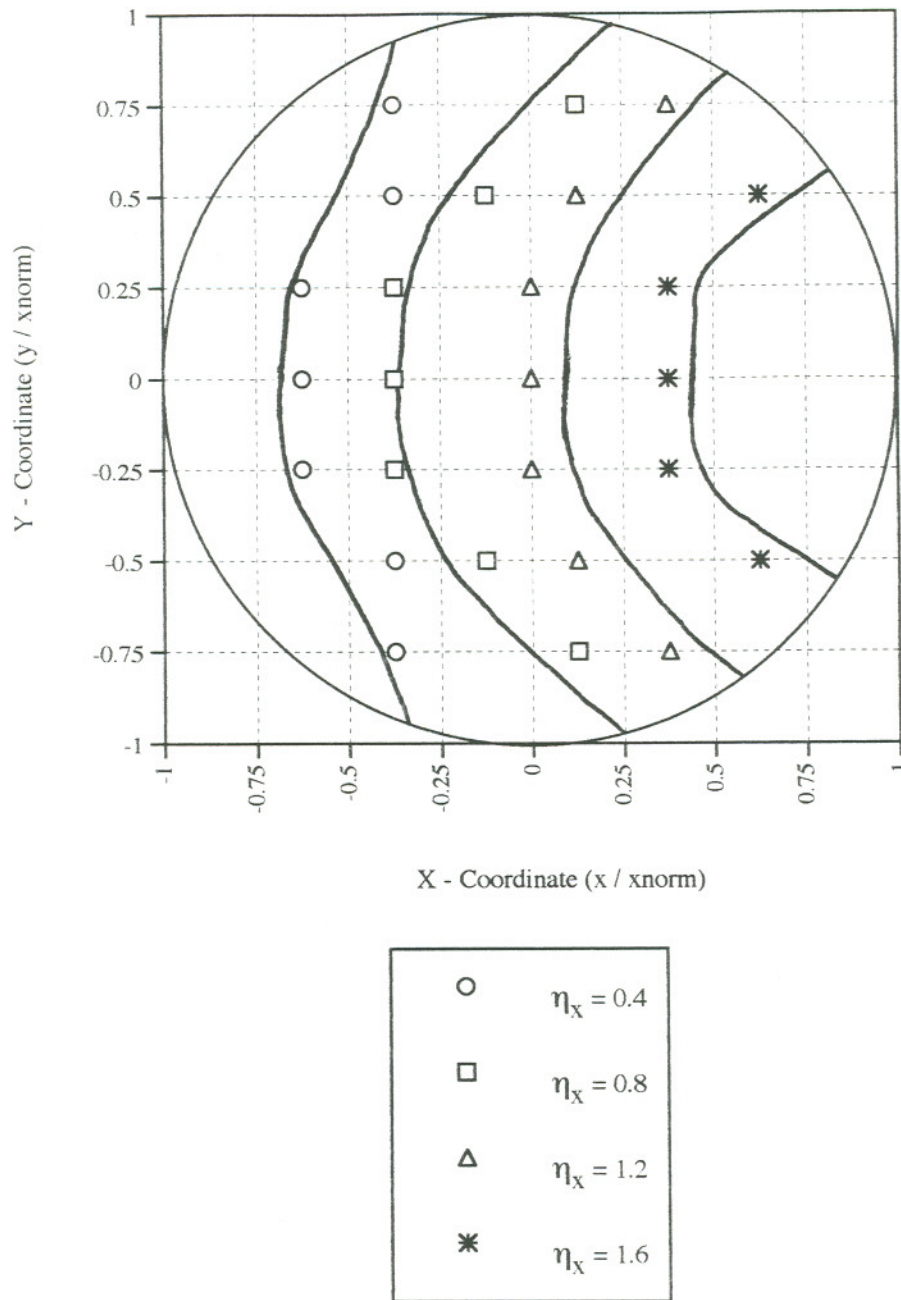


Figure 3.6 Comparison of separatrix locations for a circular contact as predicted by modified DUVOROL, data from Liu [35]

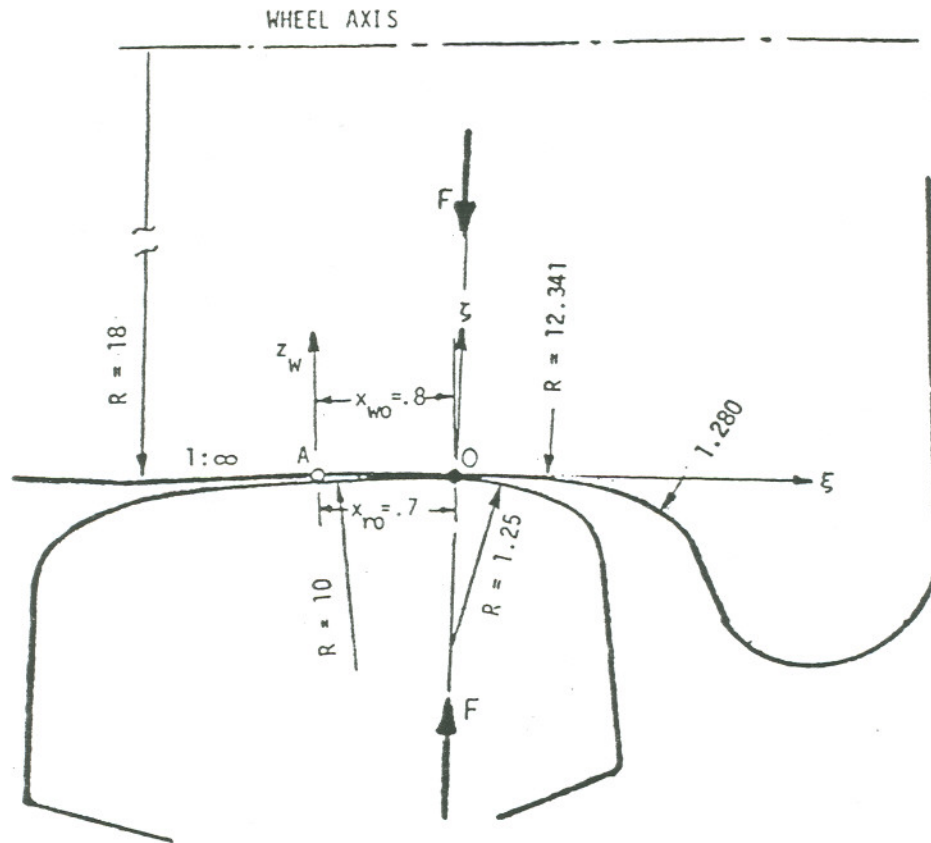


Figure 3.7 Rail and wheel profiles for a 140 RE X SIG (Schweizerische Industriel-Gesellschaft) Metroliner.

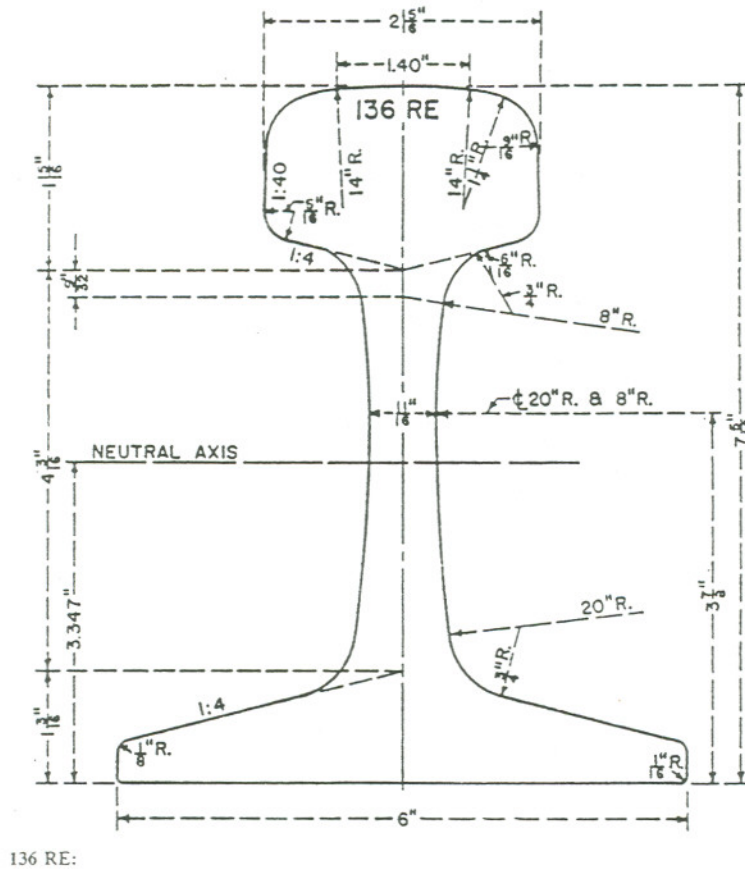


Figure 3.8 Profile of a new 136RE (136 pound per yard) rail.

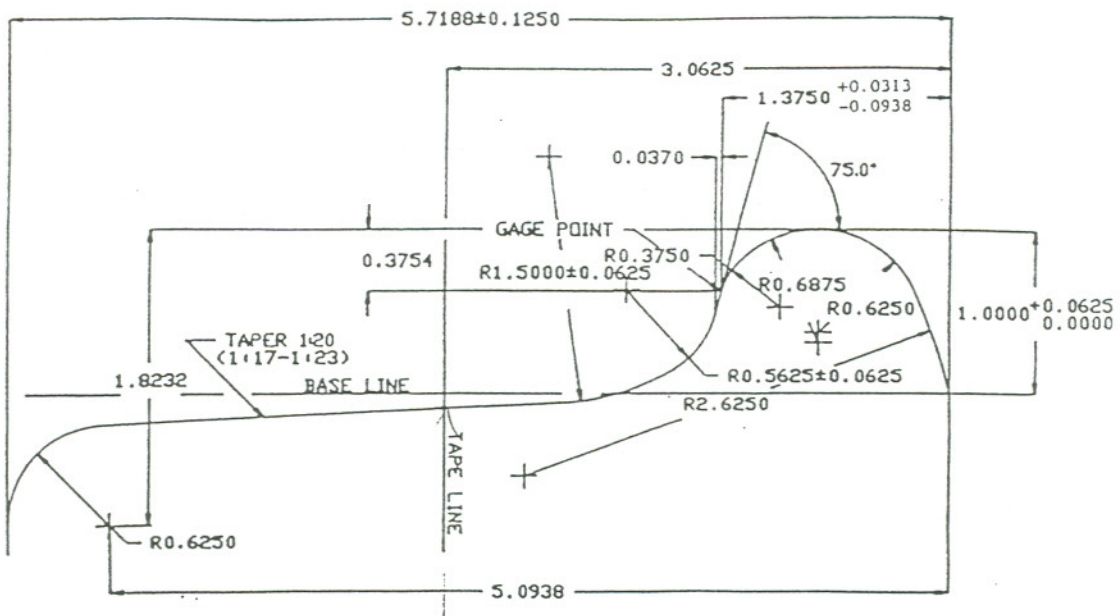


Figure 3.9 Profile of a new AAR1-B wide flange wheel.

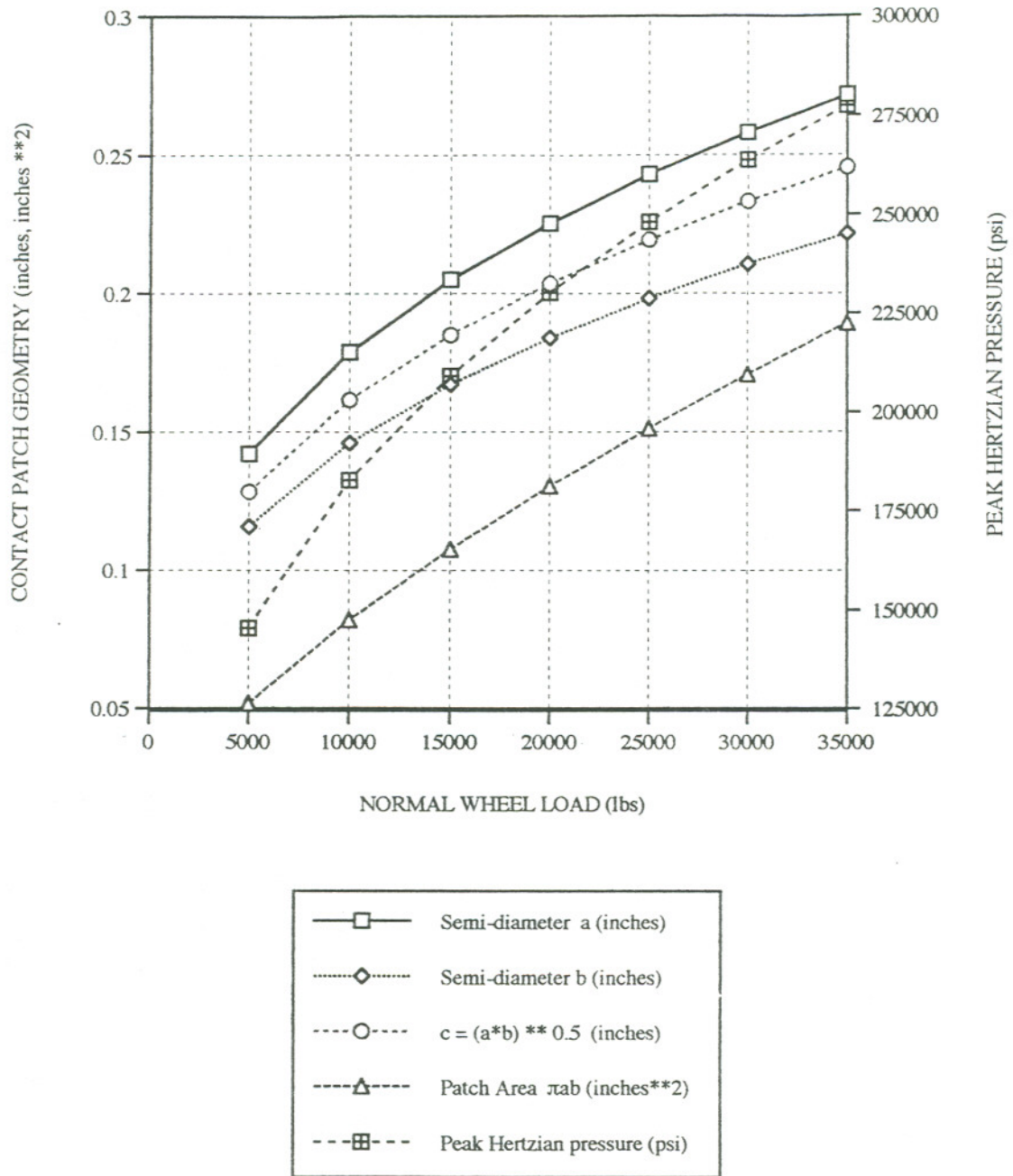


Figure 3.11 Results of the *normal* Hertzian solution as a function of wheel load for contact position #1.

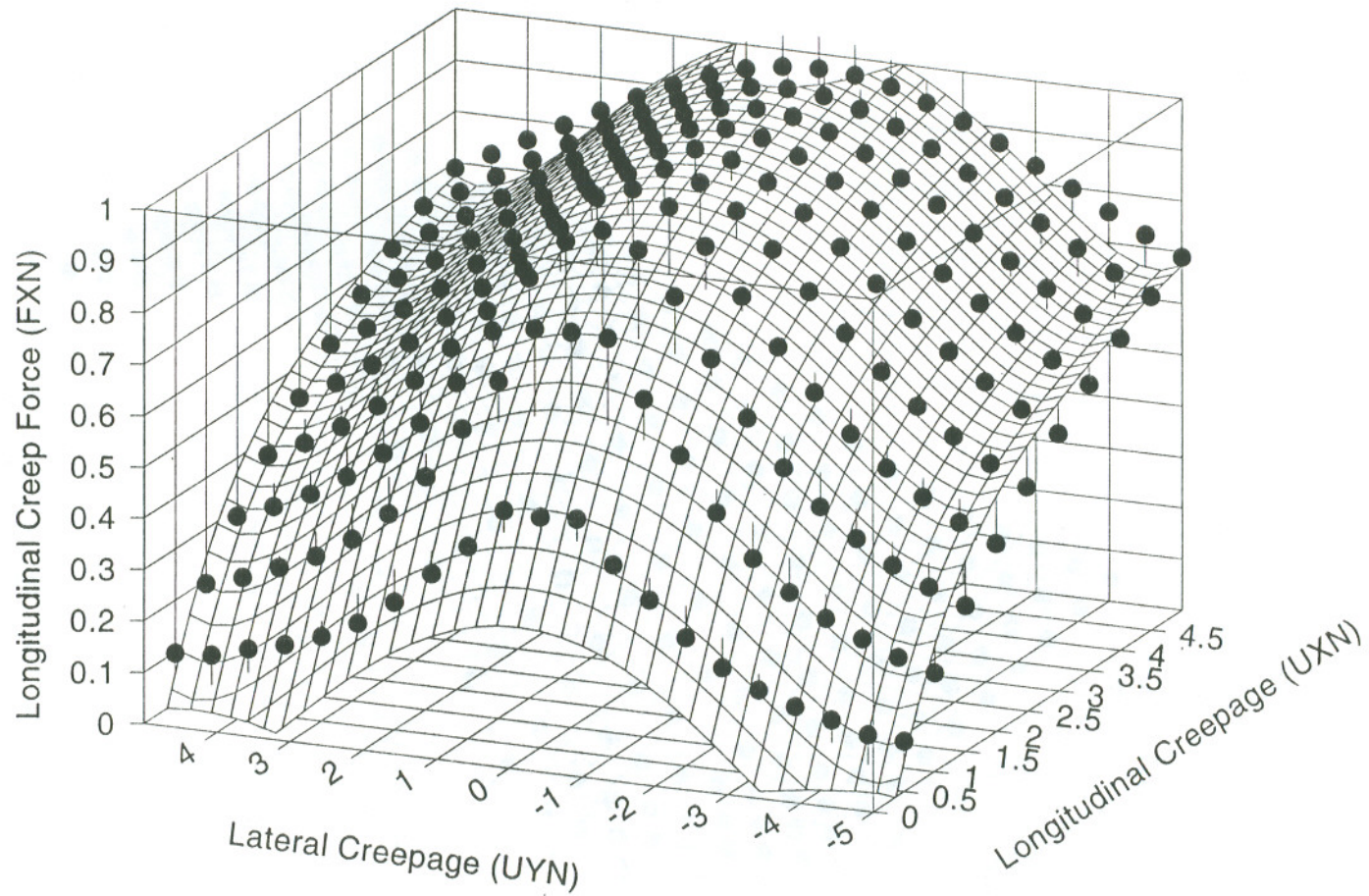


Figure 3.12 Longitudinal creep force - creepage surface plot for contact position #1 ($a/b = 1.22$)
 ($UXN = \eta_x$, $UYN = \eta_y$).

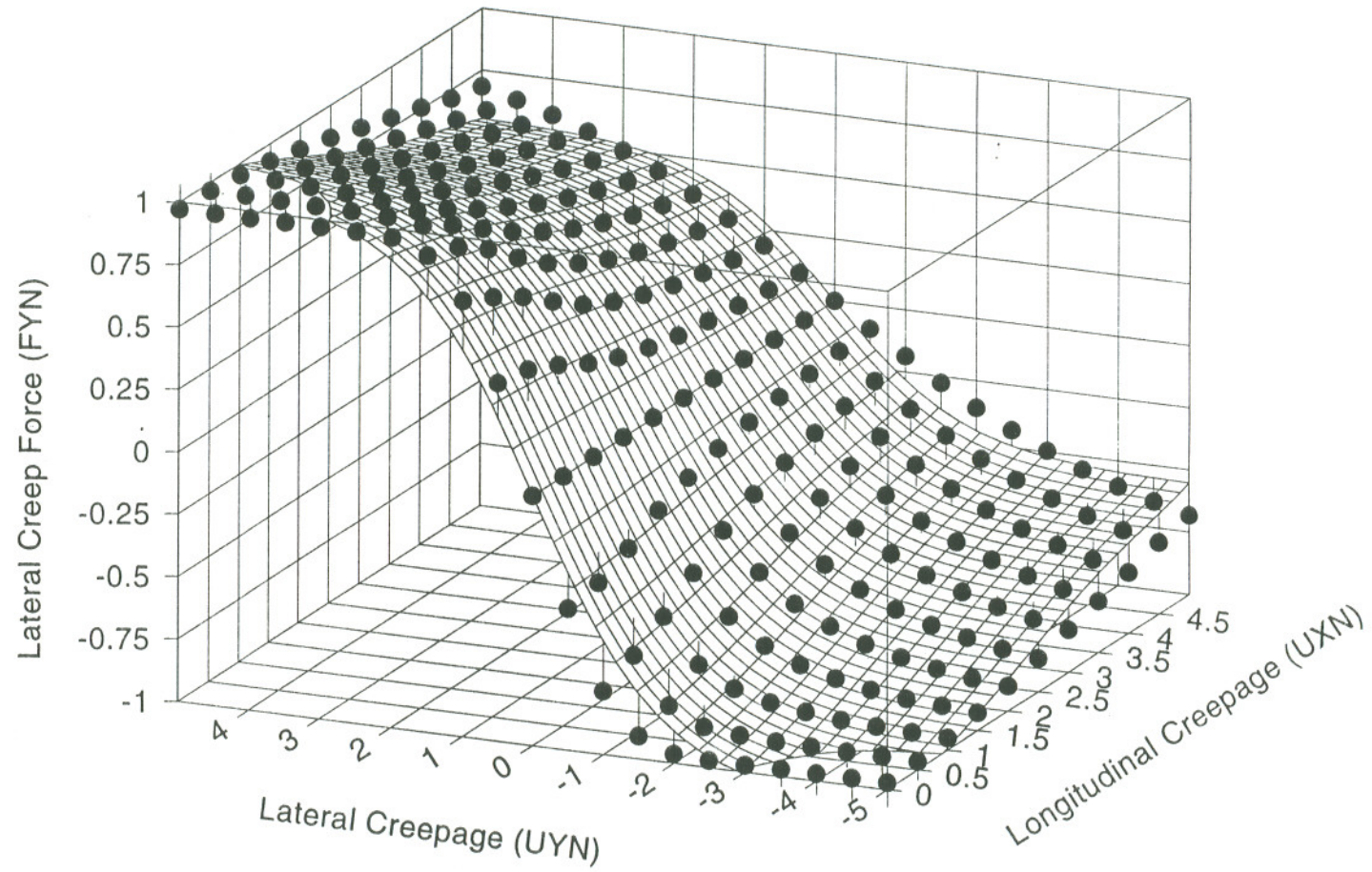


Figure 3.13 Lateral creep force - creepage surface plot for contact position #1 ($a/b = 1.22$) ($UXN = \eta_x$, $UYN = \eta_y$).

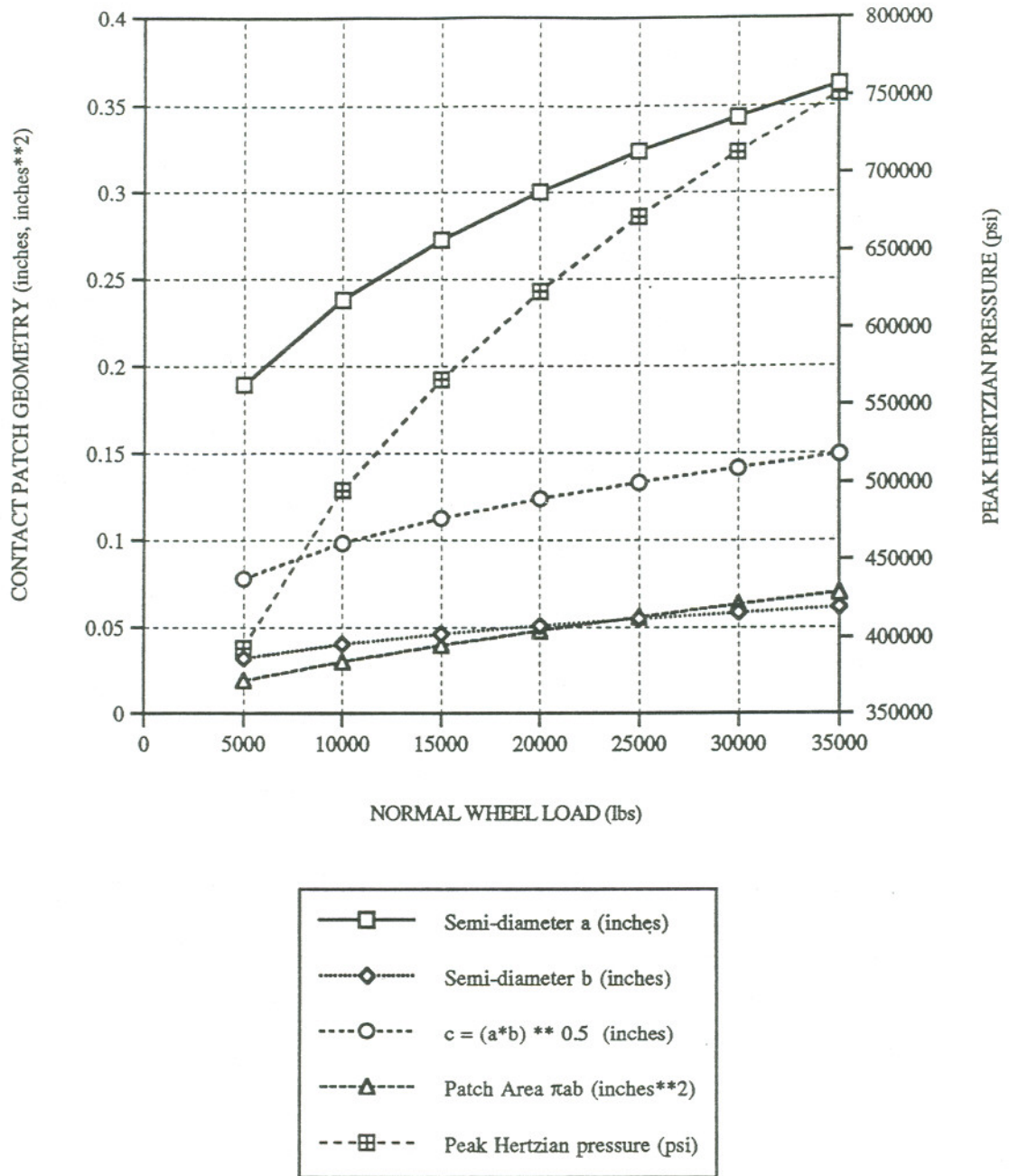


Figure 3.14 Results of the *normal* Hertzian solution as a function of wheel load for contact position #3.

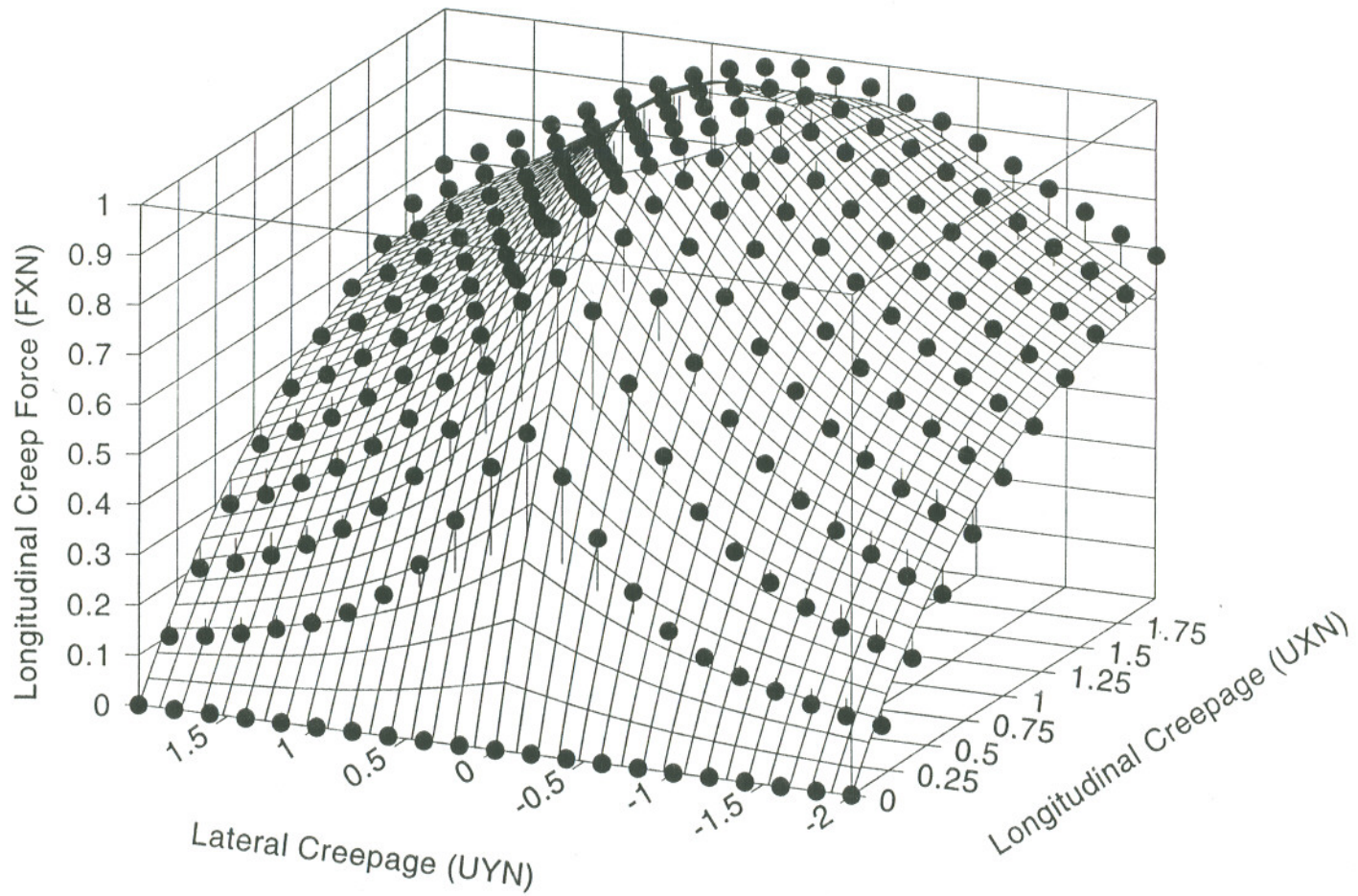


Figure 3.15 Longitudinal creep force - creepage surface plot for contact position #3 ($a/b = 5.88$)
 $(UXN = \eta_x, UYN = \eta_y)(UXN - \eta_x, UYN = \mu_y)$.

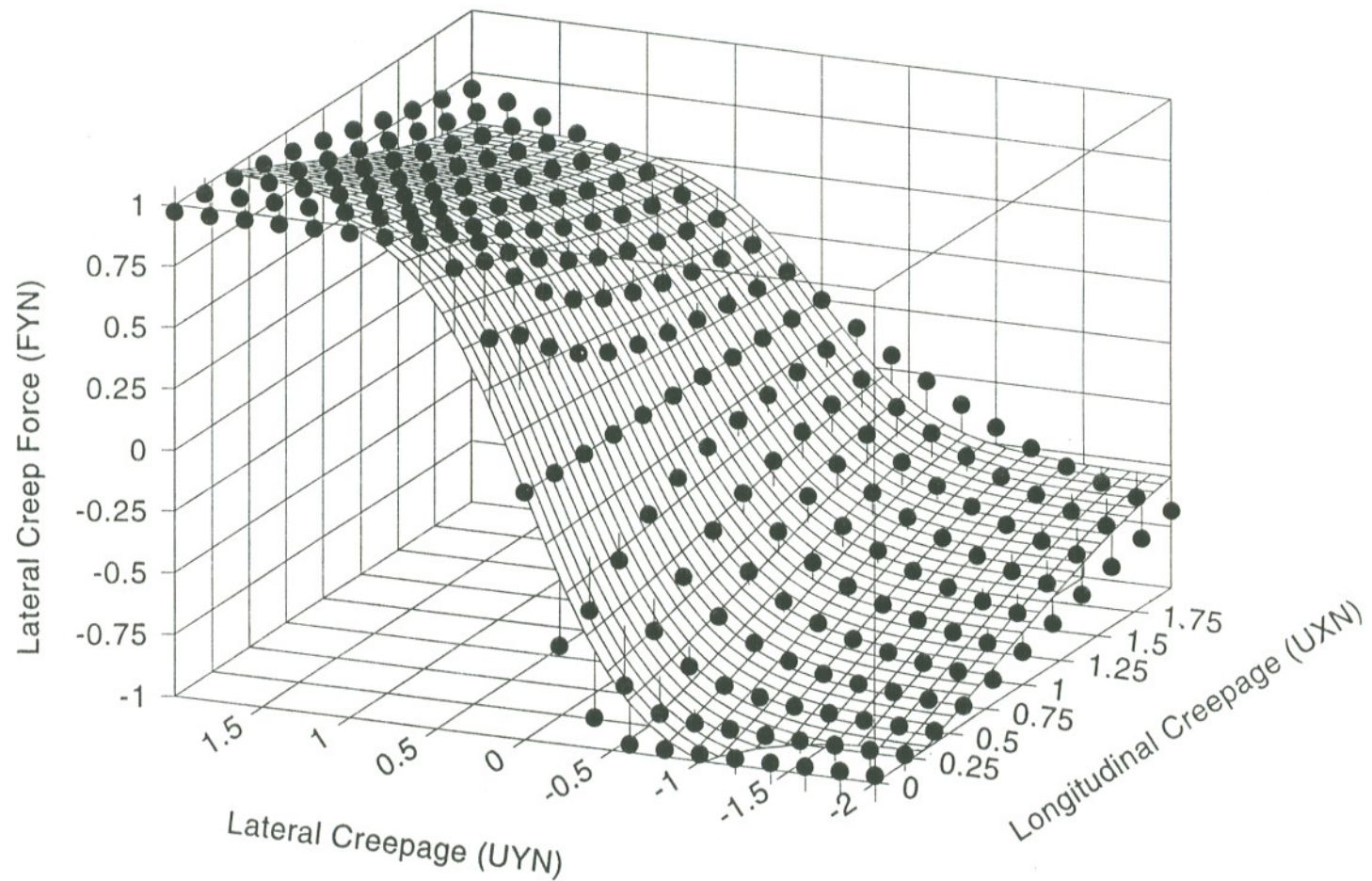


Figure 3.16 Lateral creep force - creepage surface plot for contact position #3 ($a/b = 5.88$)
 ($UXN = \eta_x$, $UYN = \eta_y$).

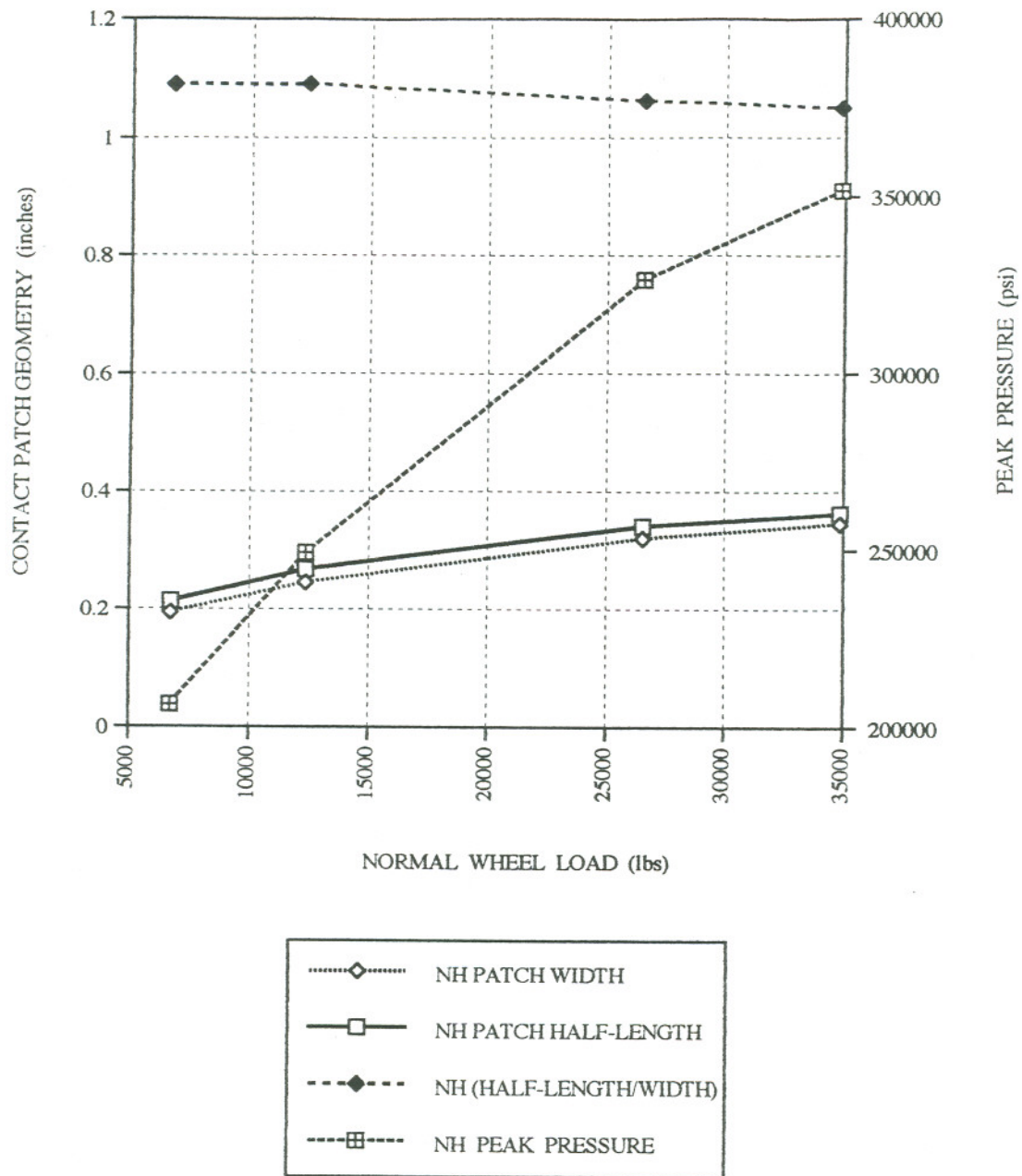


Figure 3.17 Results of the *normal* non-Hertzian solution as a function of wheel load for contact position #2.

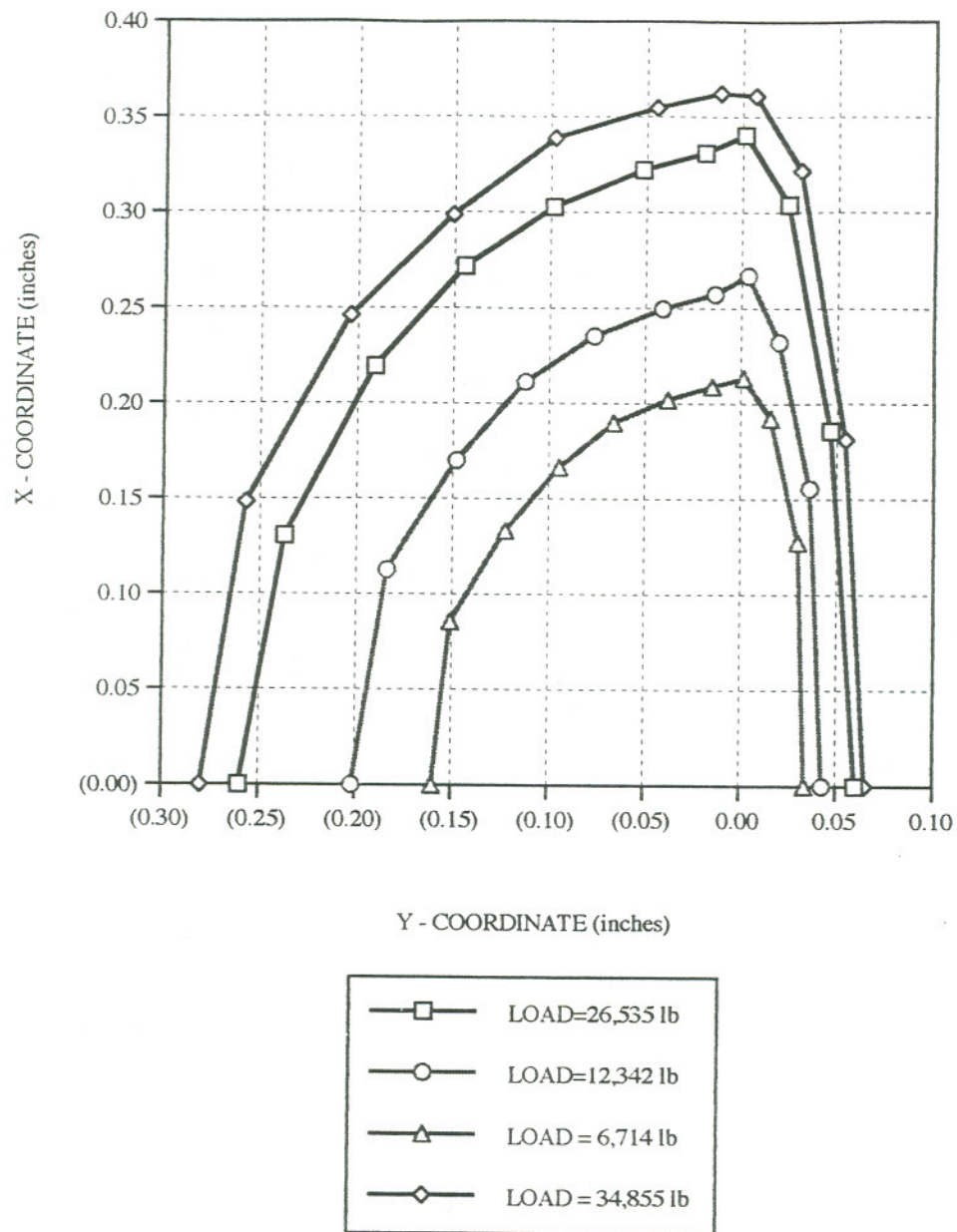


Figure 3.18 Non-Hertzian contact patch geometries as a function of wheel load for contact position #2 (half symmetry).

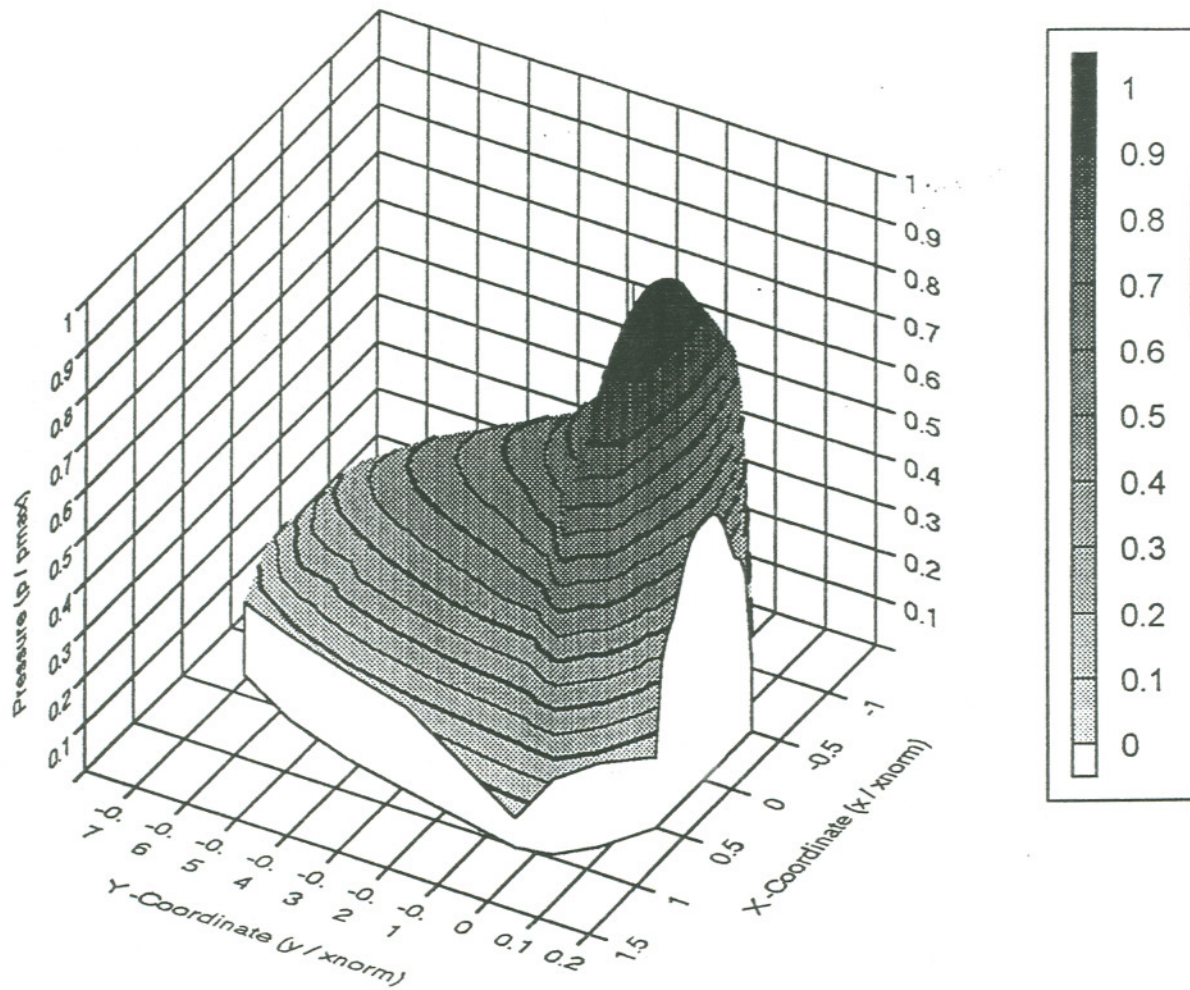


Figure 3.19 Non-Hertzian contact patch pressure distribution (3-D) for a 12,342 pound wheel load at position #2 ($p_{max} = 0.255 \times 10^6$ psi, $x_{norm} = 0.2591$ in.).

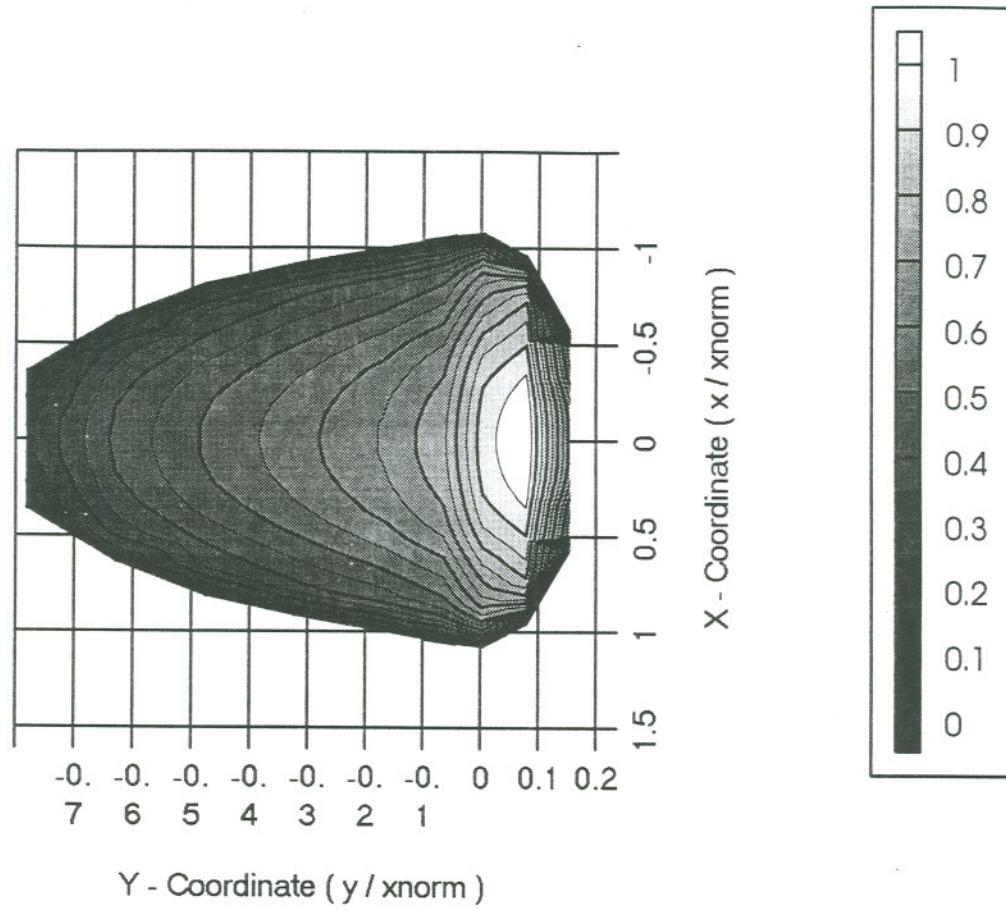


Figure 3.20 Non-Hertzian contact patch pressure distribution (2-D) for a 26,535 pound wheel load at position #2 ($x_{norm} = .3038$ inches, legend signifies variation in $\frac{P}{p_{max}}$).

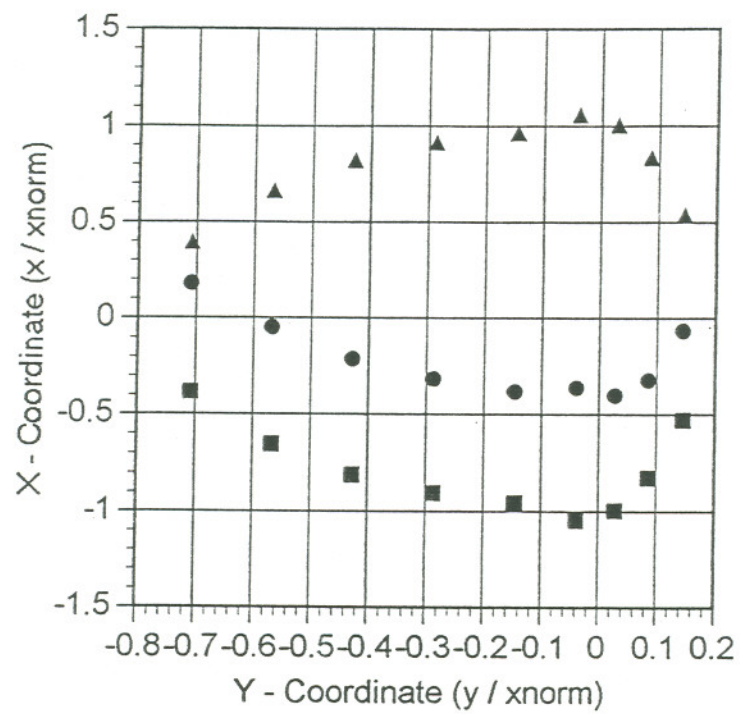


Figure 3.21 Separatrix location for a non-Hertzian contact of position #2 with a wheel load of 12,342 pounds ($v_x = 0.15\%$, $v_y = \phi = 0.0$, $x_{norm} = .259$ inches, triangle - leading edge; square - trailing edge; dots - separatrix).

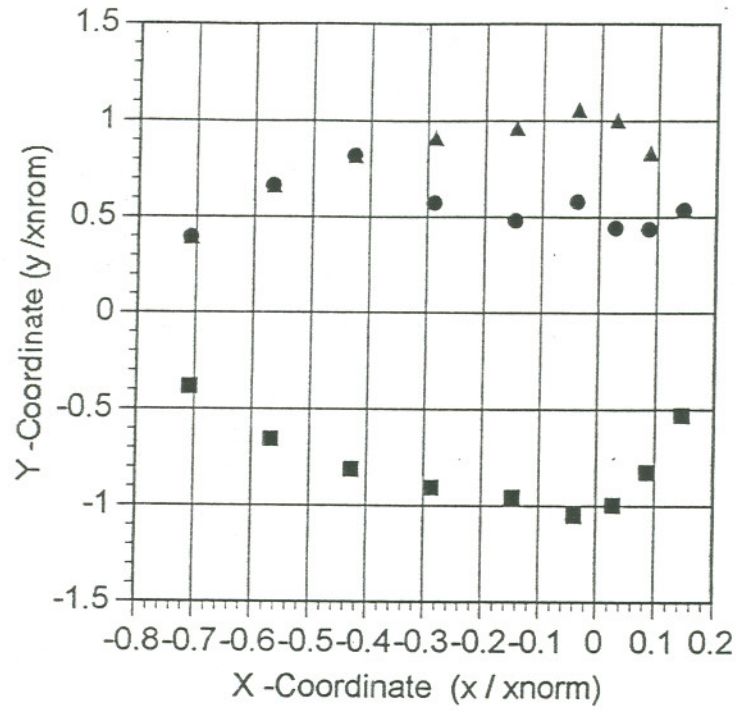


Figure 3.22 Separatrix location for a non-Hertzian contact of position #2 with a wheel load of 12,342 pounds ($v_x = 0.35\%$, $v_y = \phi = 0.0$ $x_{norm} = .259$ inches, triangle - leading edge; square - trailing edge; dots - separatrix).

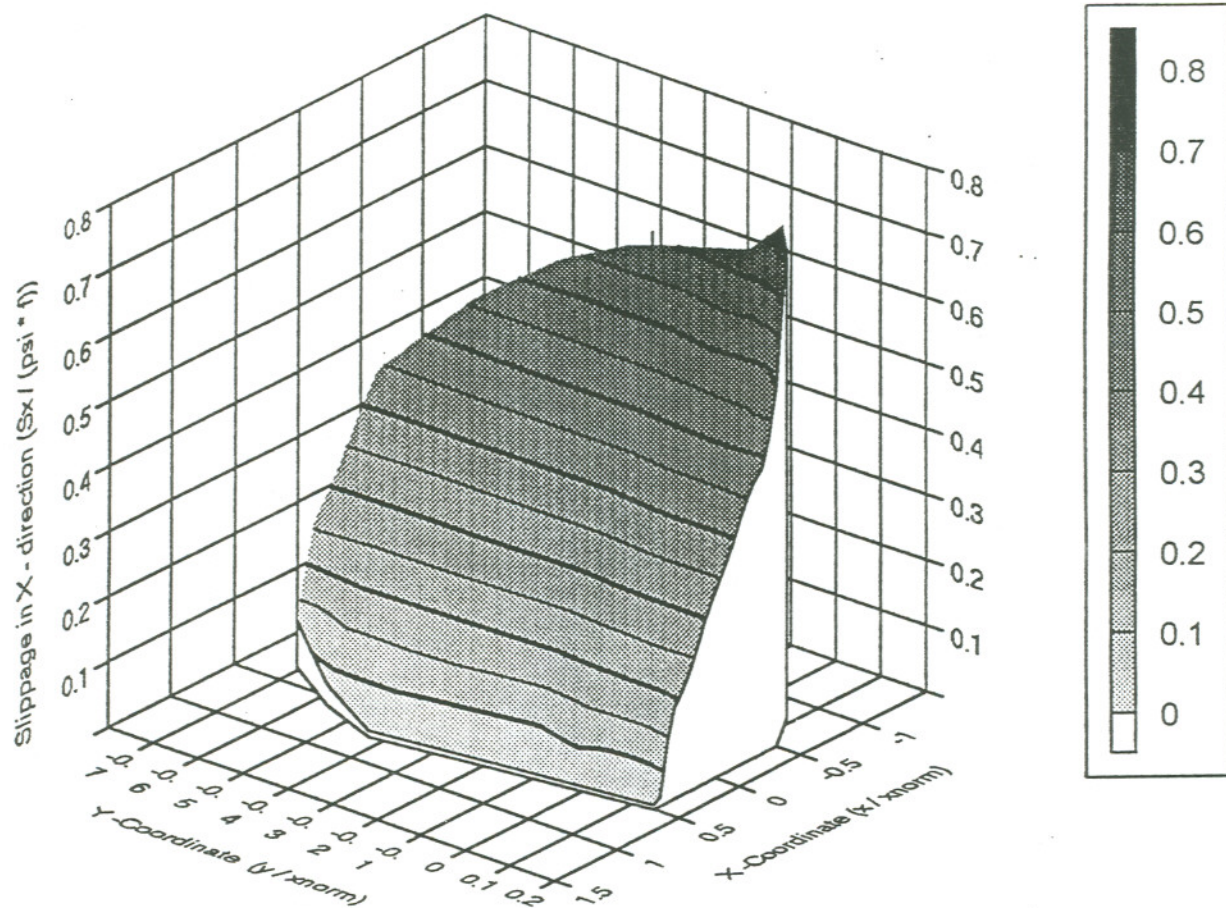


Figure 3.23 Longitudinal slippage distribution for non-Hertzian contact of position #2 with a wheel load of 12,342 pounds ($v_x = 0.35\%$, $v_y = \phi = 0.0$, $x_{norm} = 2591$ inches, $f=0.3$, $\psi=0.0035$).

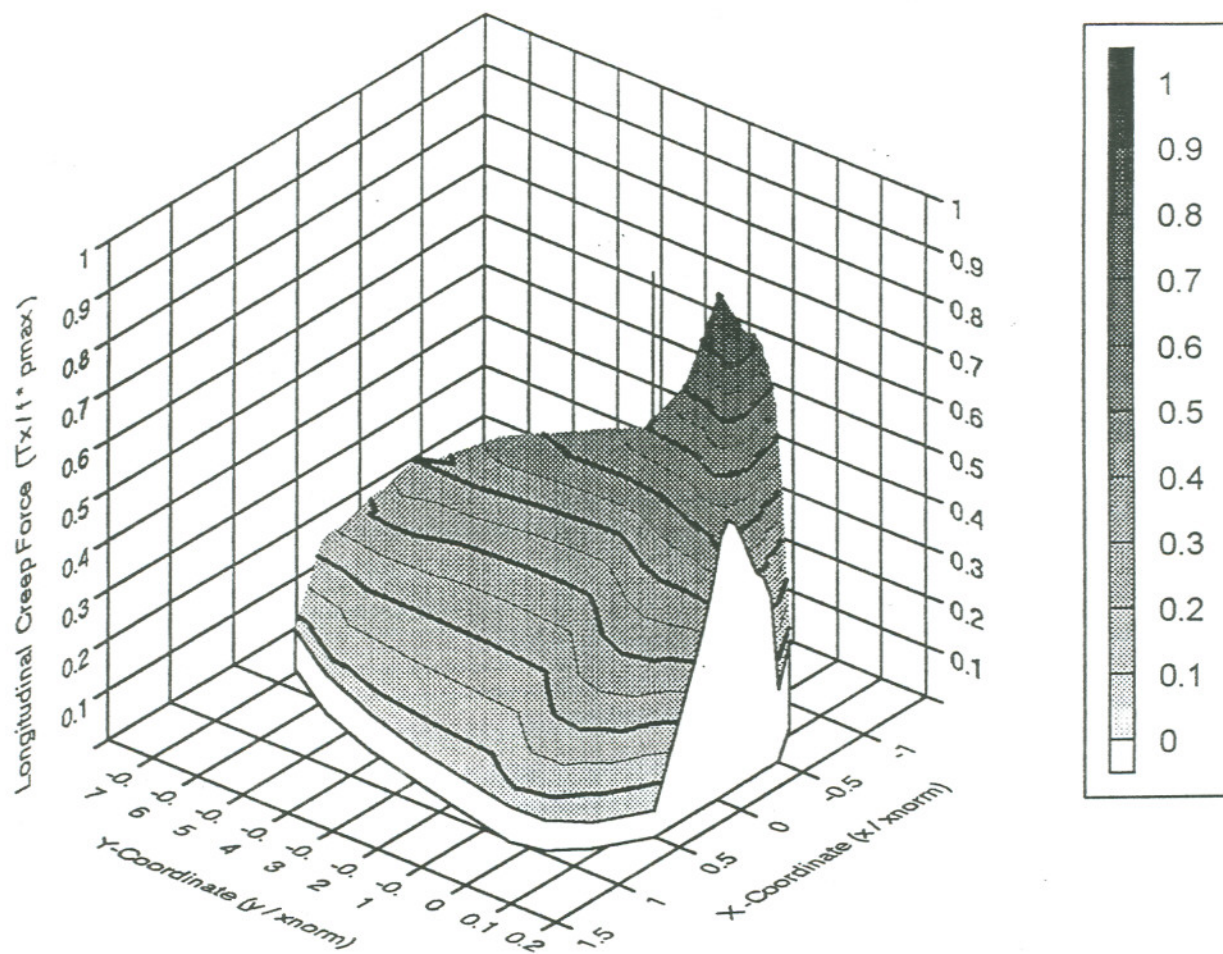


Figure 3.24 Longitudinal surface shear traction distribution for non-Hertzian contact of position #2 with a wheel load of 12,342 pounds ($\nu_x = 0.15\%$, $\nu_y = \phi = 0.0$, $x_{norm} = 0.2591$ inches, $f = 0.3$, $p_{max} = .255 \cdot 10^6$ psi).

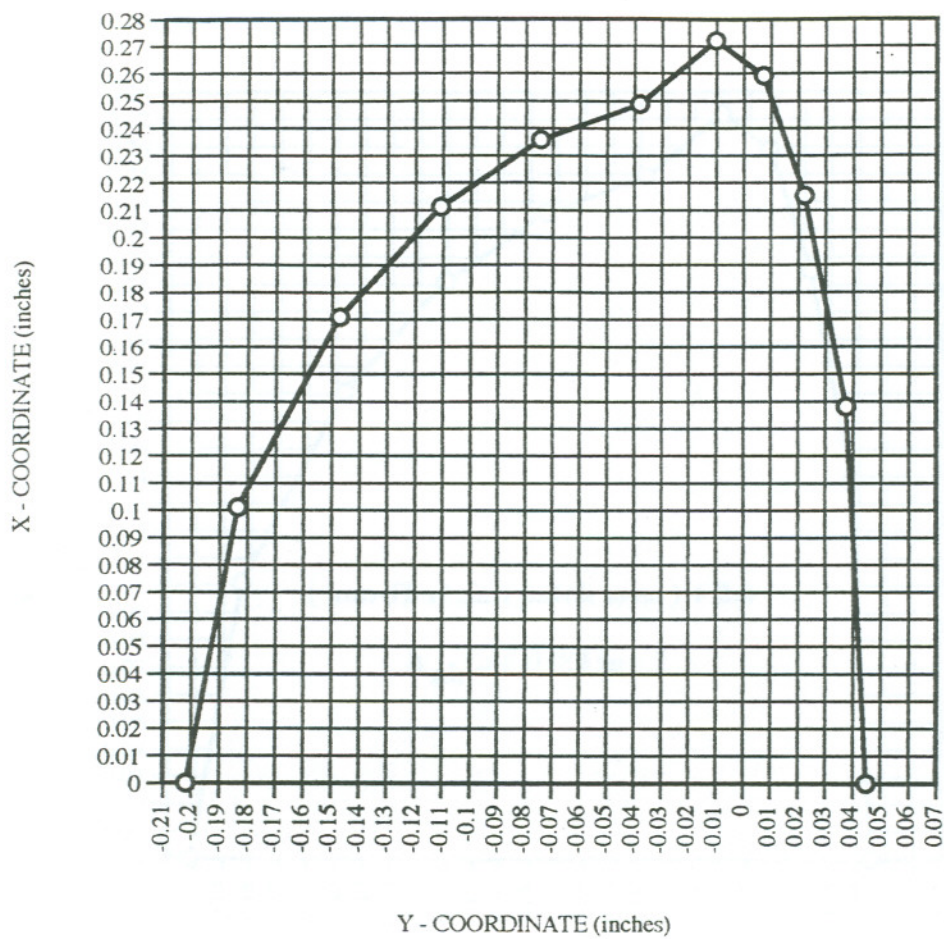


Figure 3.25 Non-Hertzian contact patch geometry for a wheel load of 12,342 pounds at position #2 - half symmetry with grid.

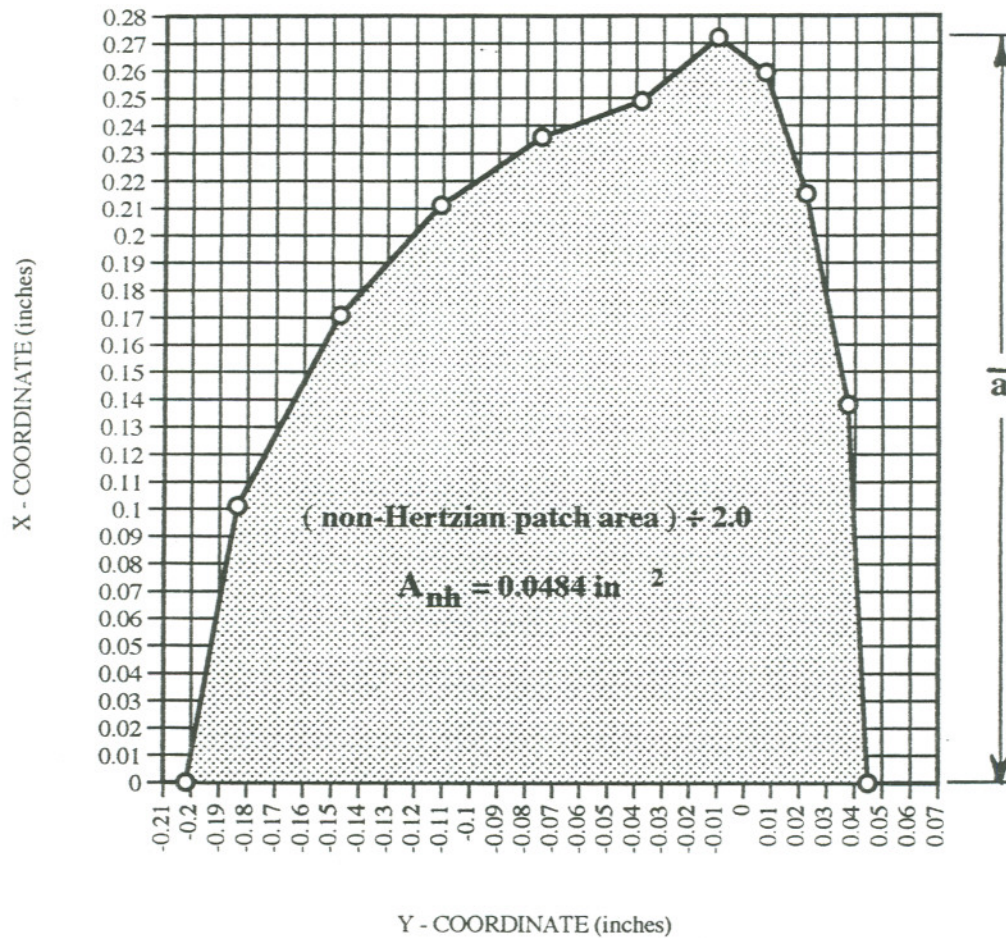


Figure 3.26 Non-Hertzian contact patch geometry for a wheel load of 12,342 pounds at position #2 - half symmetry showing actual area.

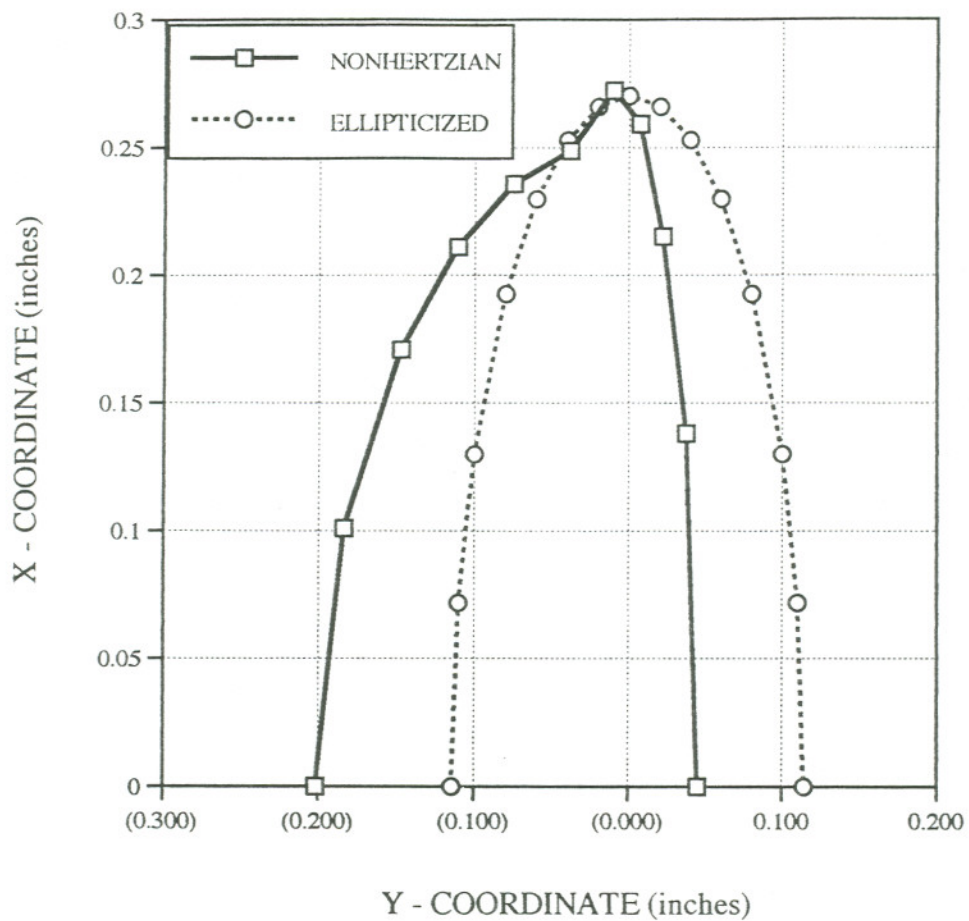


Figure 3.27 Contact patch geometry for both actual non-Hertzian and ellipticized contact for position #2 at 12,342 pounds of wheel load.

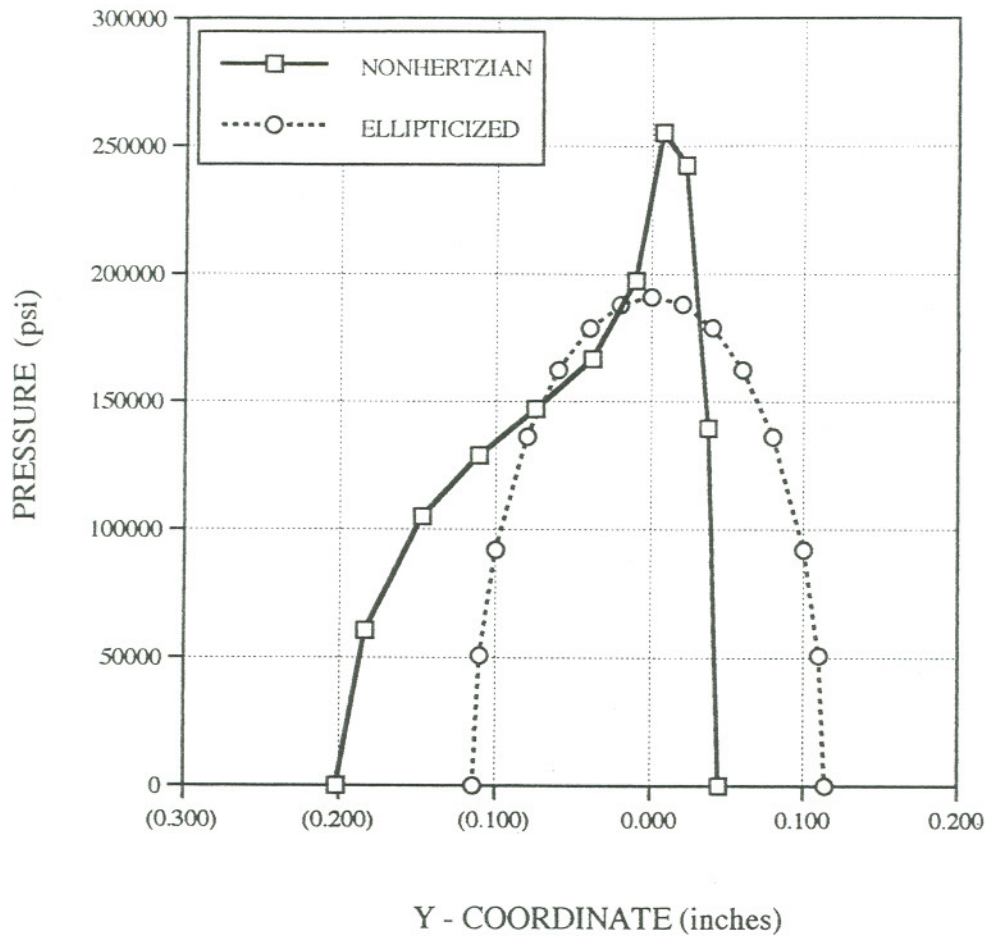


Figure 3.28 Contact patch pressure distribution for both actual non-Hertzian and ellipticized contacts for position #2 at 12,342 pounds of wheel load.

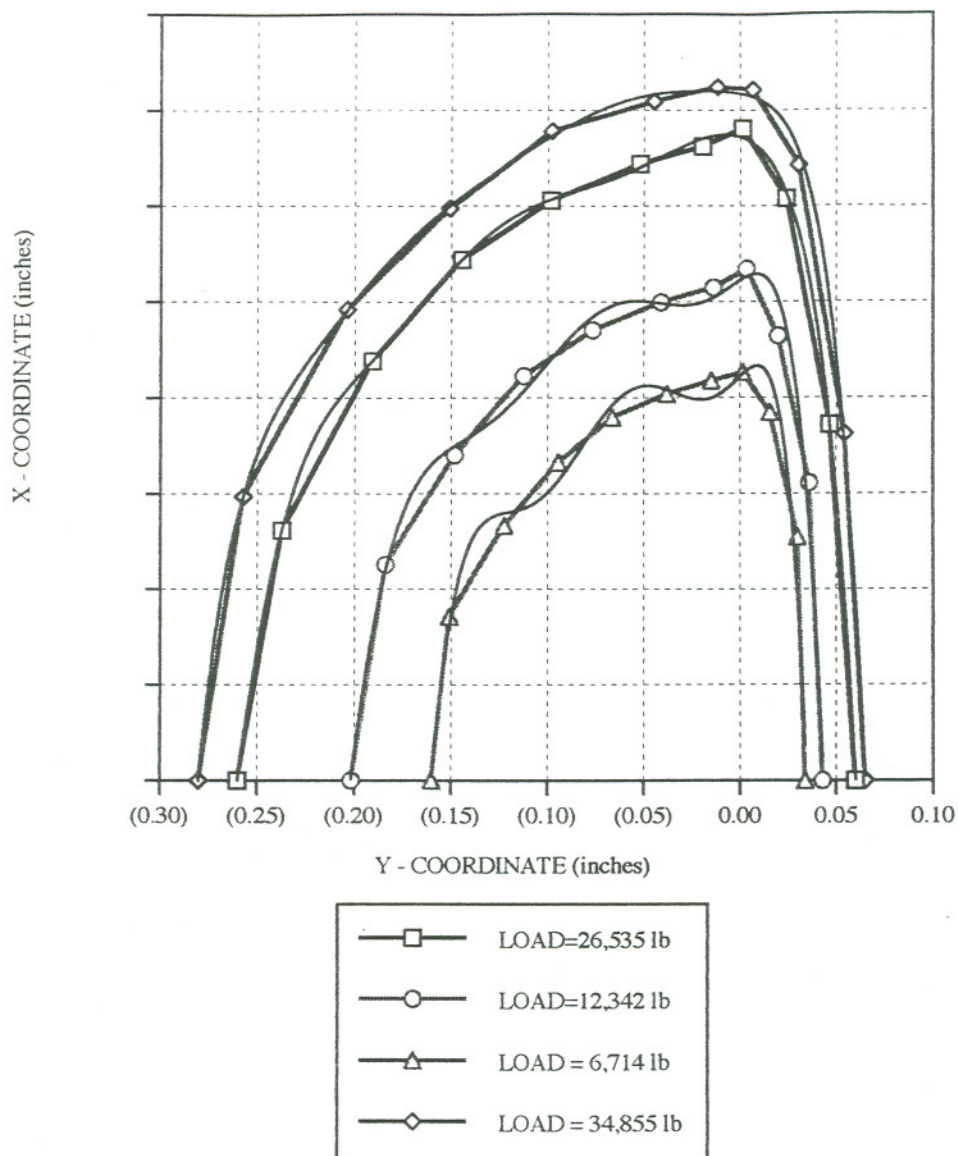


Figure 3.29 Polynomial curve fit of non-Hertzian contact geometries for position #2.

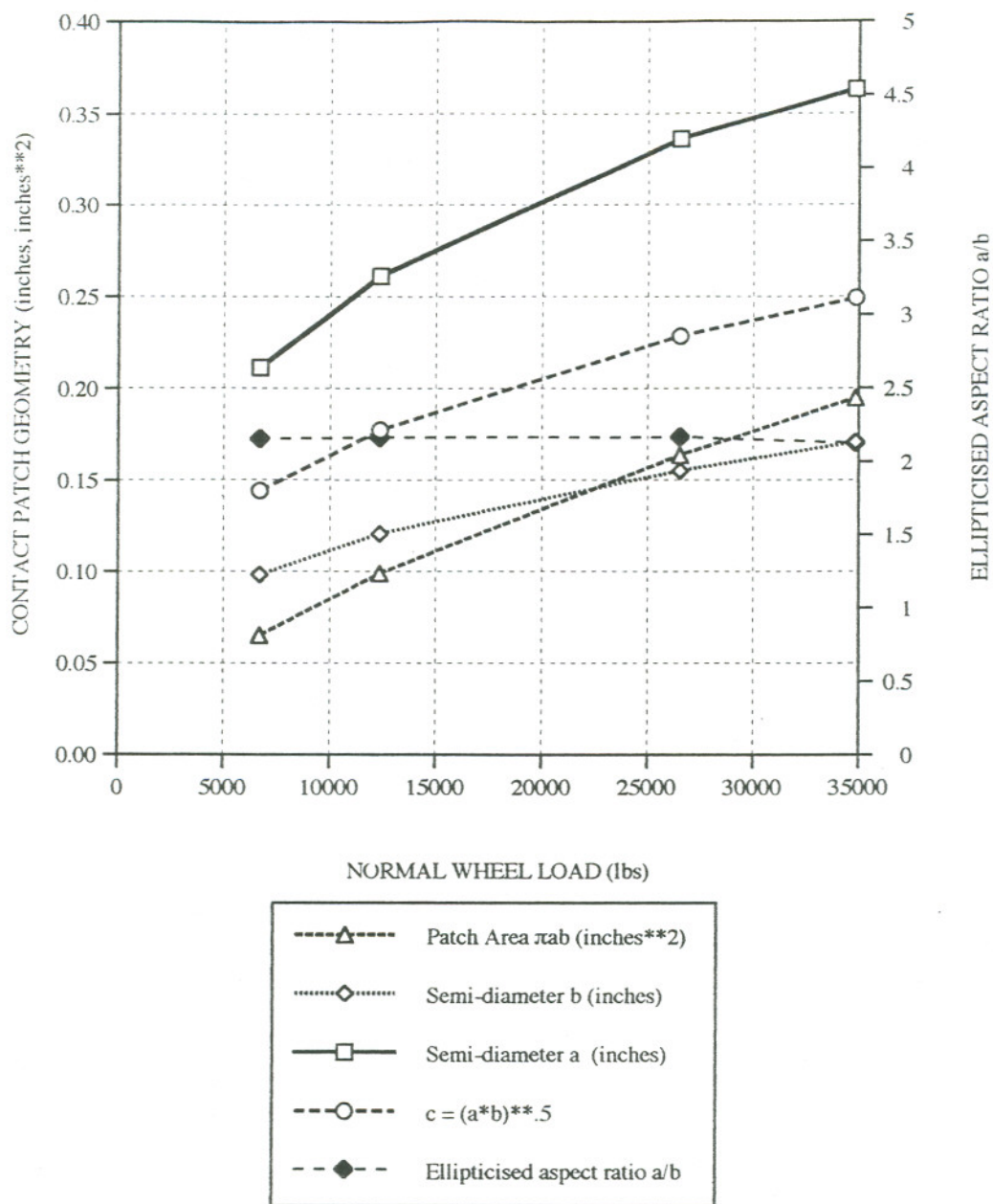


Figure 3.30 Effect of wheel load on non-Hertzian contact patch geometric parameters for position #2.

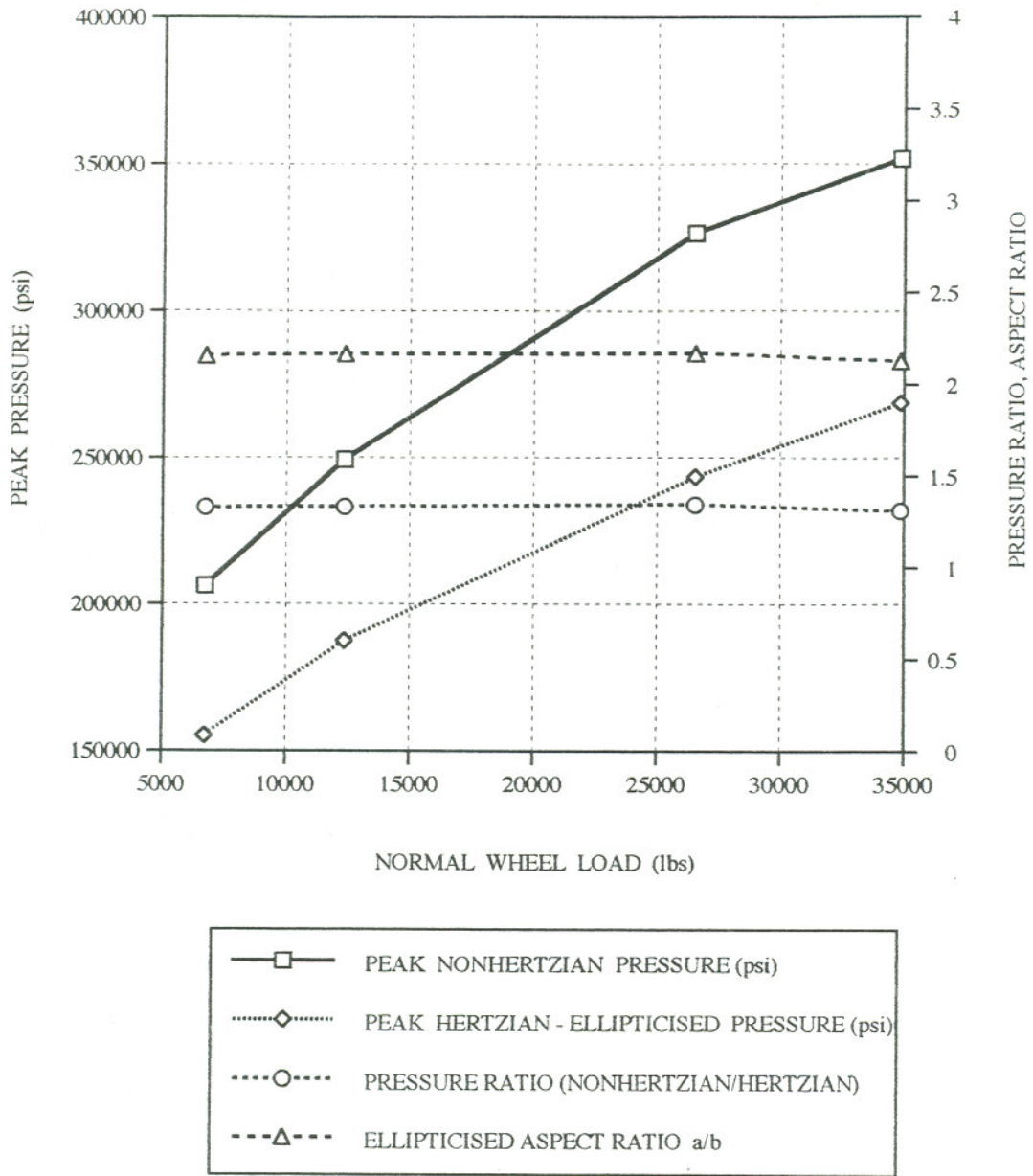


Figure 3.31 Effect of wheel load on non-Hertzian contact patch pressure for position #2.

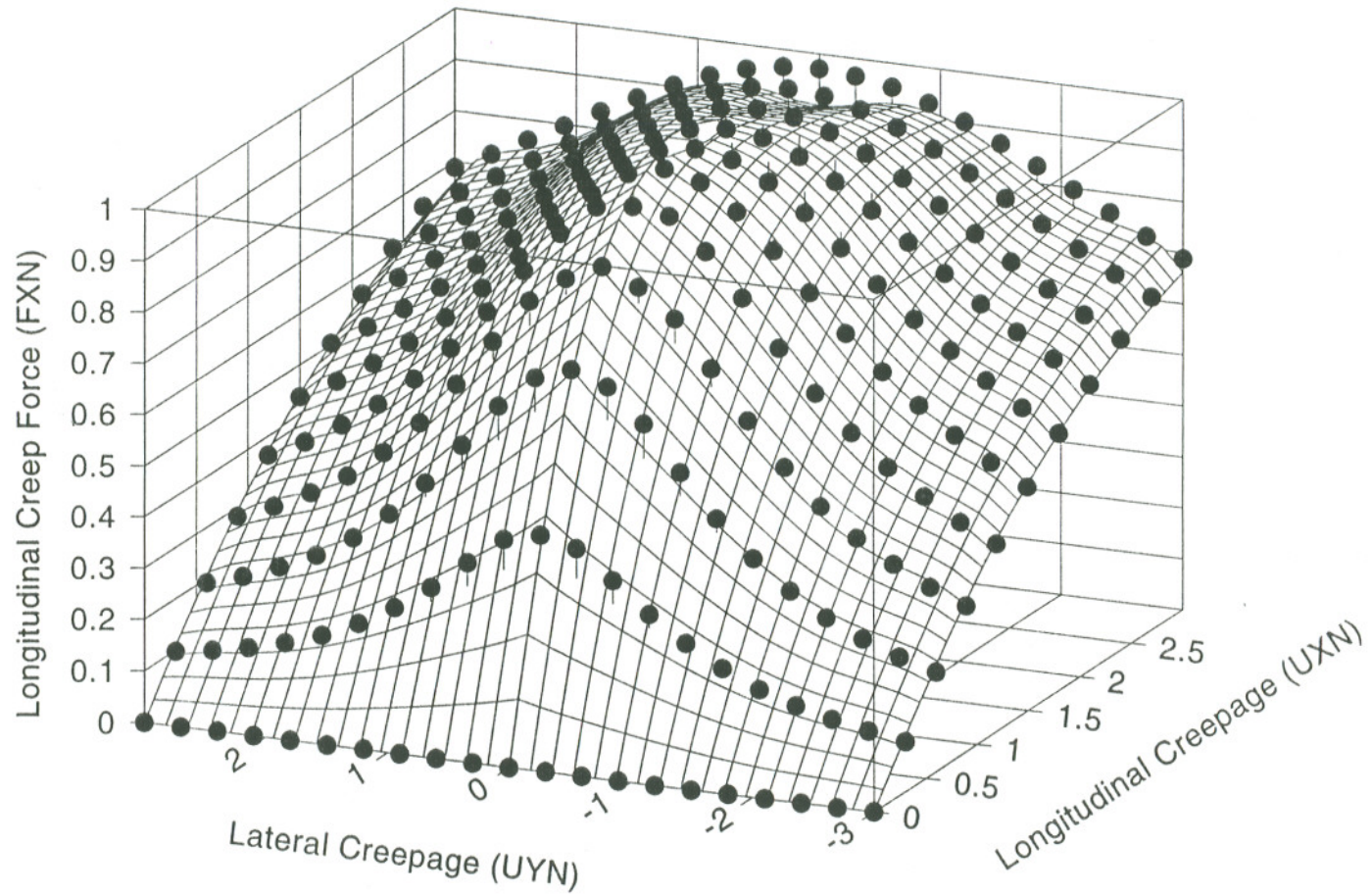


Figure 3.32 Longitudinal creep force - creepage surface plot for ellipticized contact position #2
 ($a/b = 2.16$) ($UXN = \eta_x$, $UYN = \eta_y$).

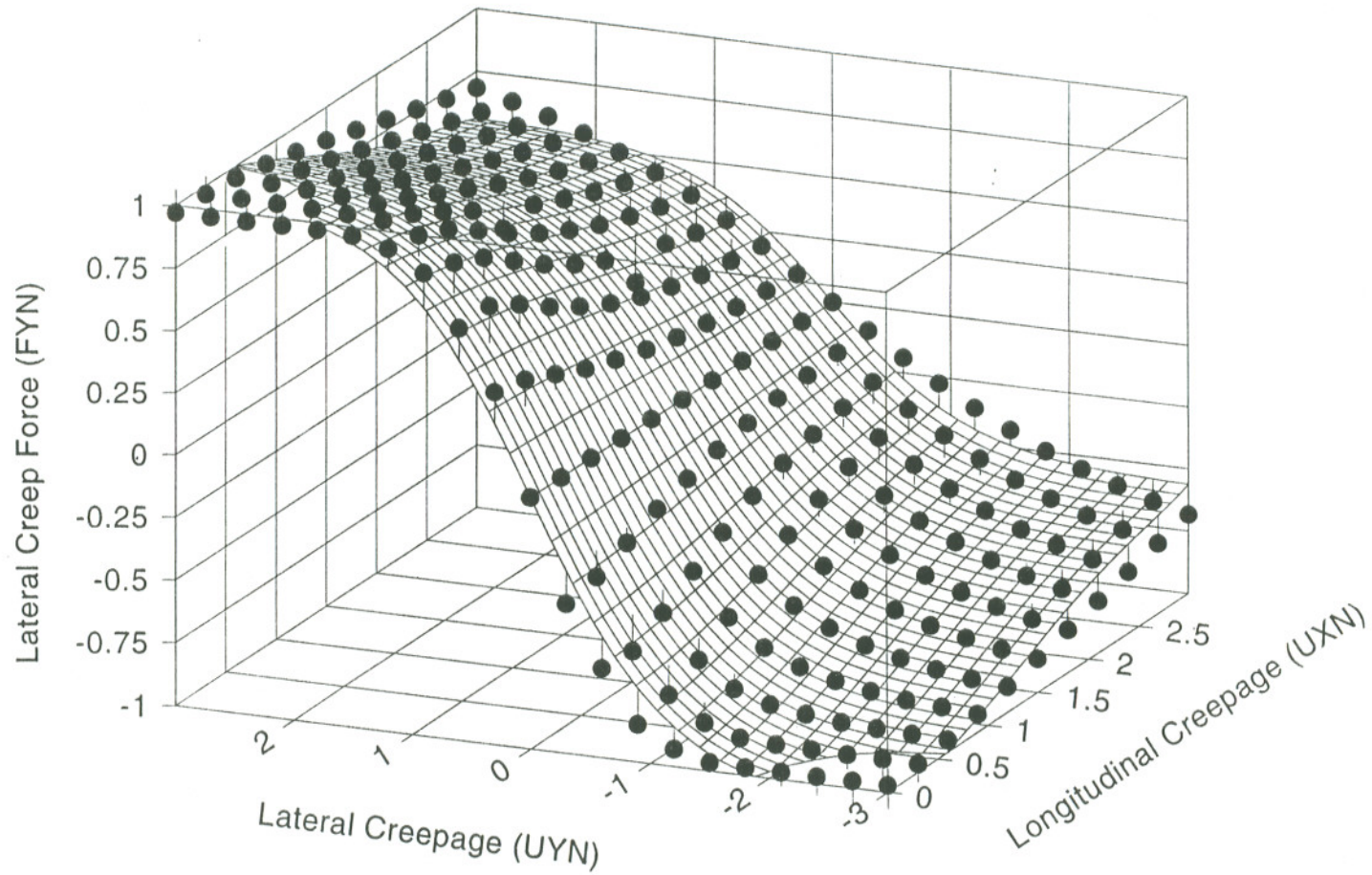


Figure 3.33 Lateral creep force - creepage surface plot for ellipticized contact position #2
 ($a/b = 2.16$) ($UXN = \eta_x$, $UYN = \eta_y$).

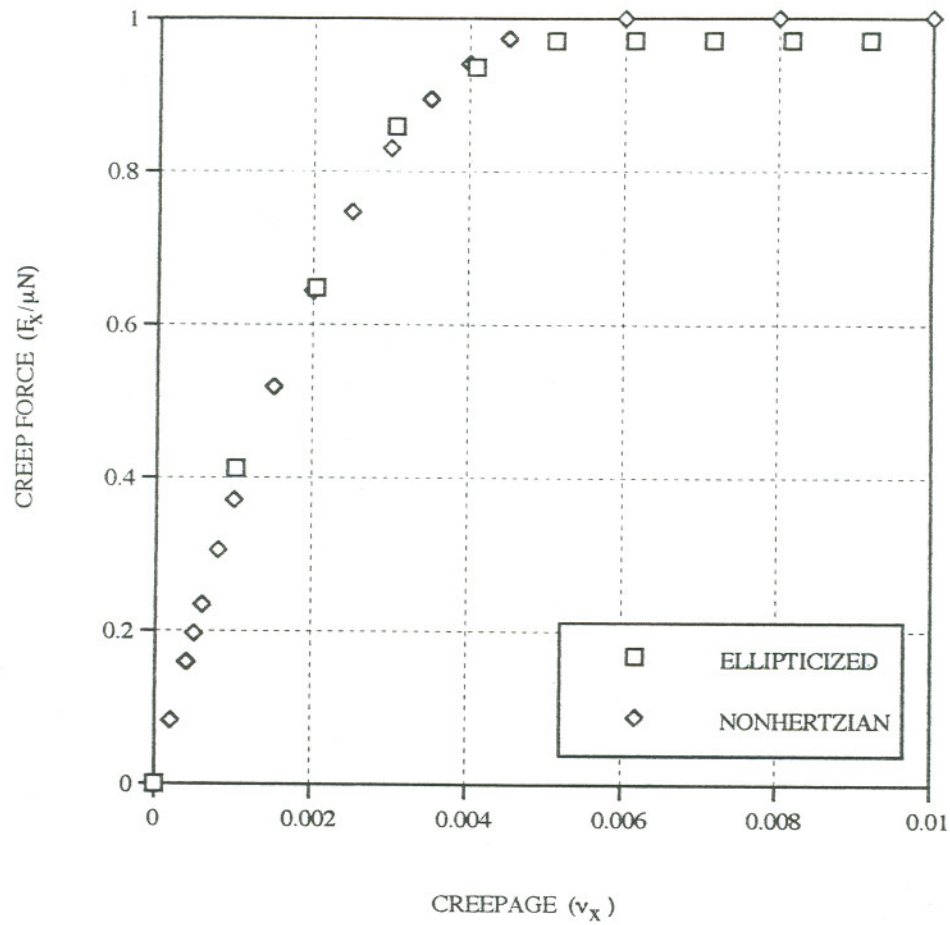


Figure 3.34 Comparison of creep force - creepage behavior for ellipticized and non-Hertzian contact at position #2 (load = 26,535 pounds, $v_y = \phi = 0$).

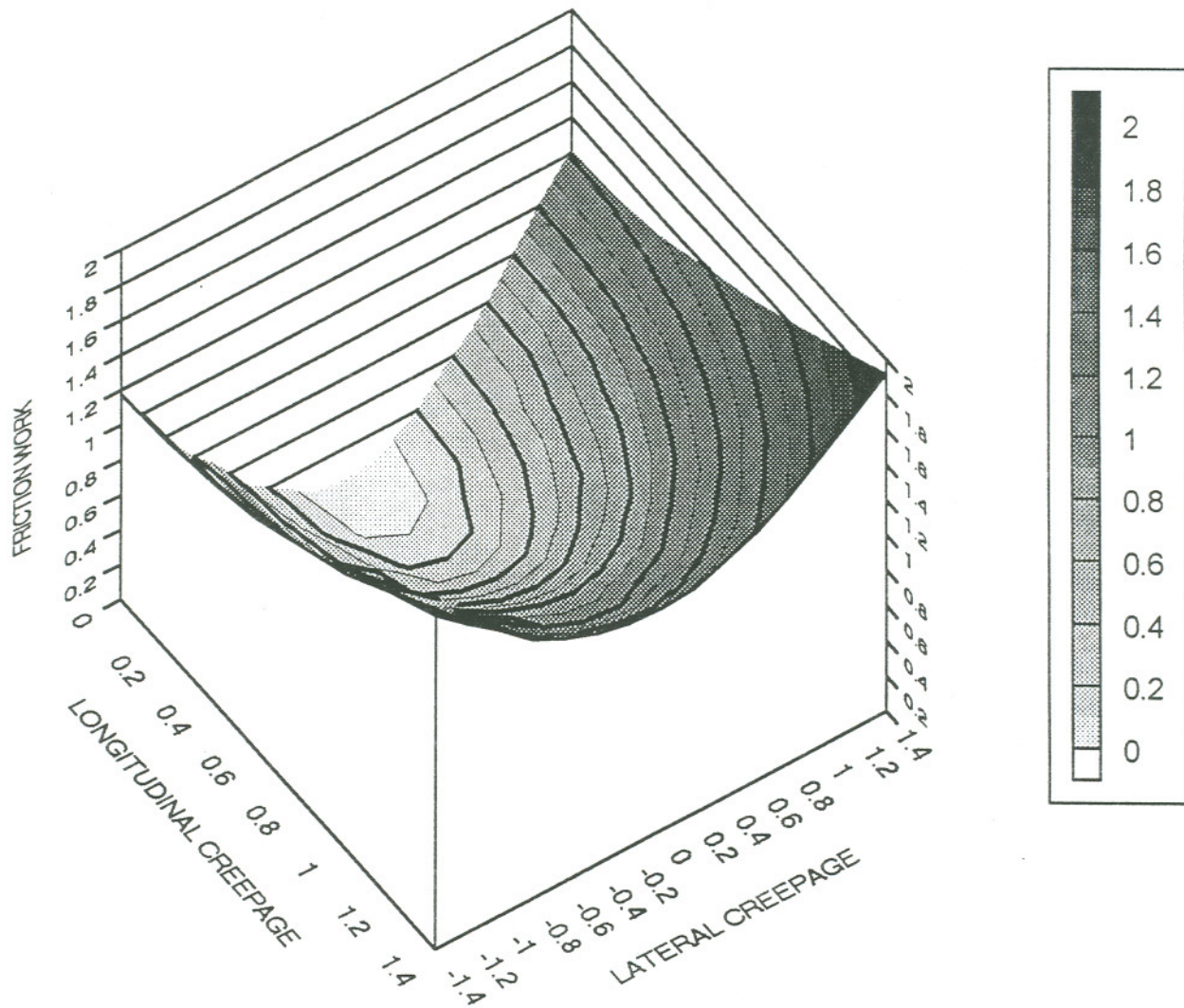


Figure 3.35 Global friction work surface plot ($a/b = 1.0$, $\chi_z = 0.2$, longitudinal creepage = η_x , lateral creepage = η_y , friction work = W'_{gd} (J/M)).

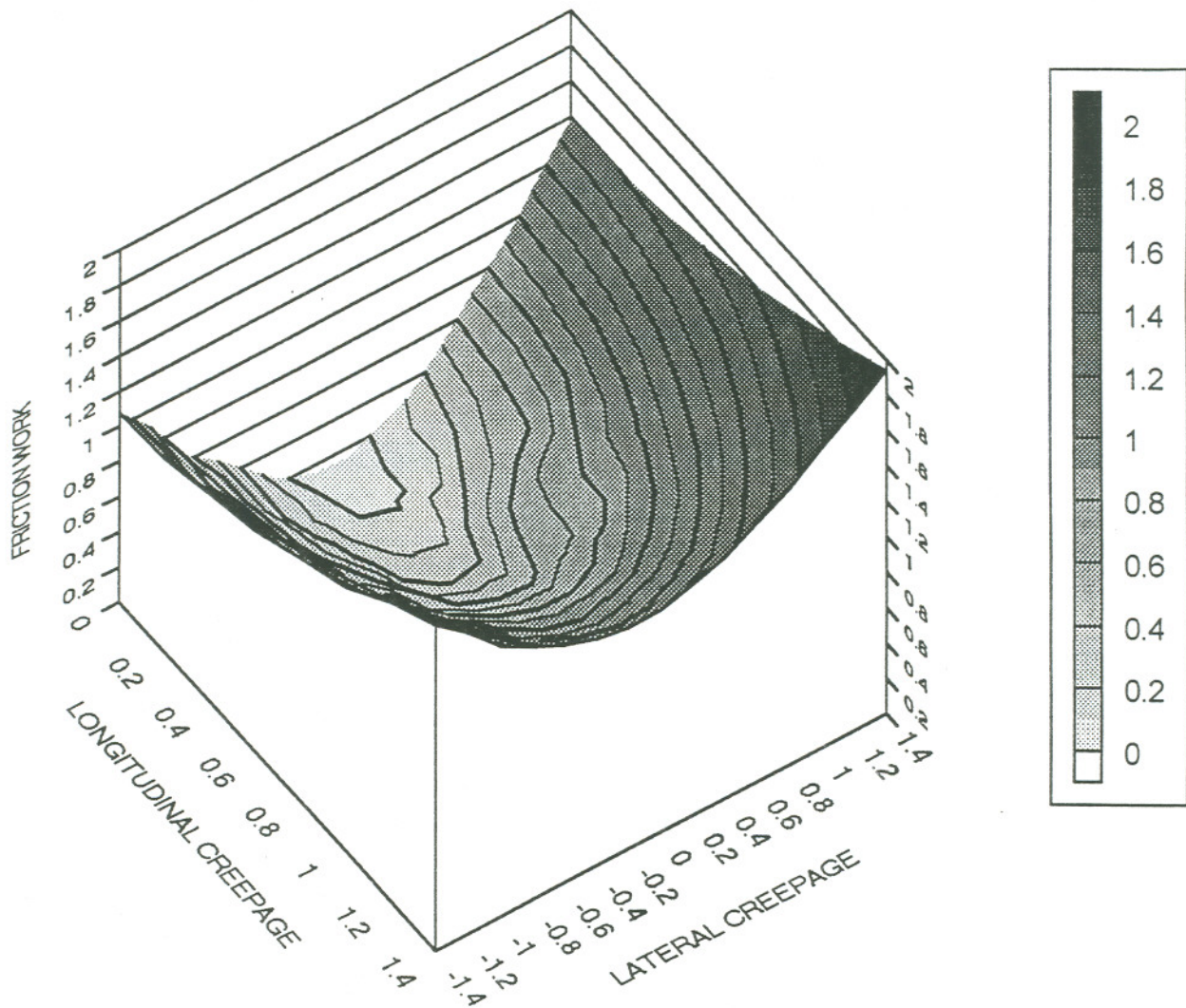


Figure 3.36 Global friction work surface plot ($a/b = 1.0$, $\chi_z = 0.8$, longitudinal creepage = η_x , lateral creepage = η_y , friction work = W'_{gd} (J/M)).

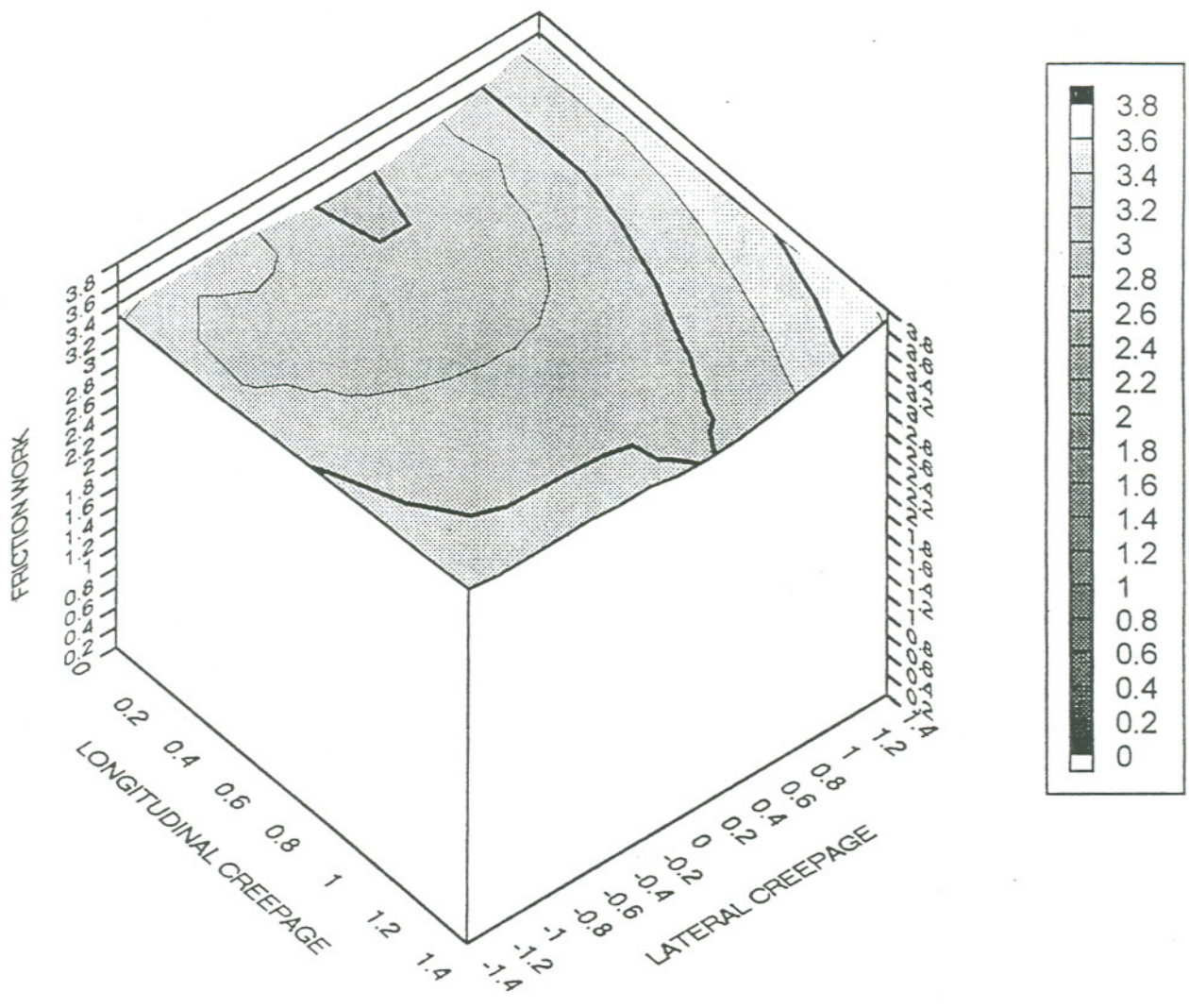


Figure 3.37 Global friction work surface plot ($a/b = 1.0$, $\chi_z = 6.5$, longitudinal creepage = η_x , lateral creepage = η_y , friction work = W'_{gd} (J/M)).

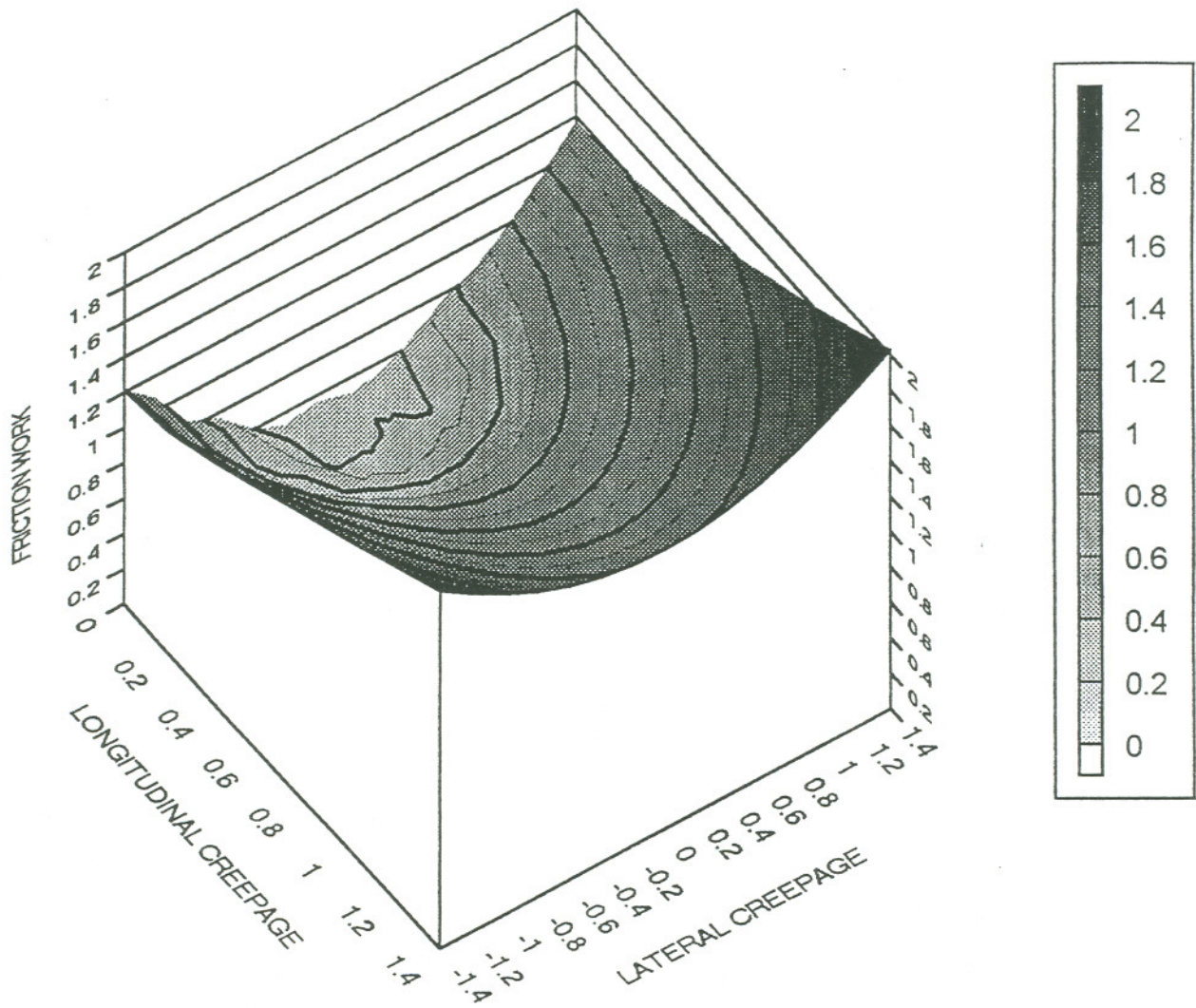


Figure 3.38 Global friction work surface plot ($a/b = 6.75$, $\chi_z = 0.8$, longitudinal creepage = η_x , lateral creepage = η_y , friction work = W'_{gd} (J/M)).

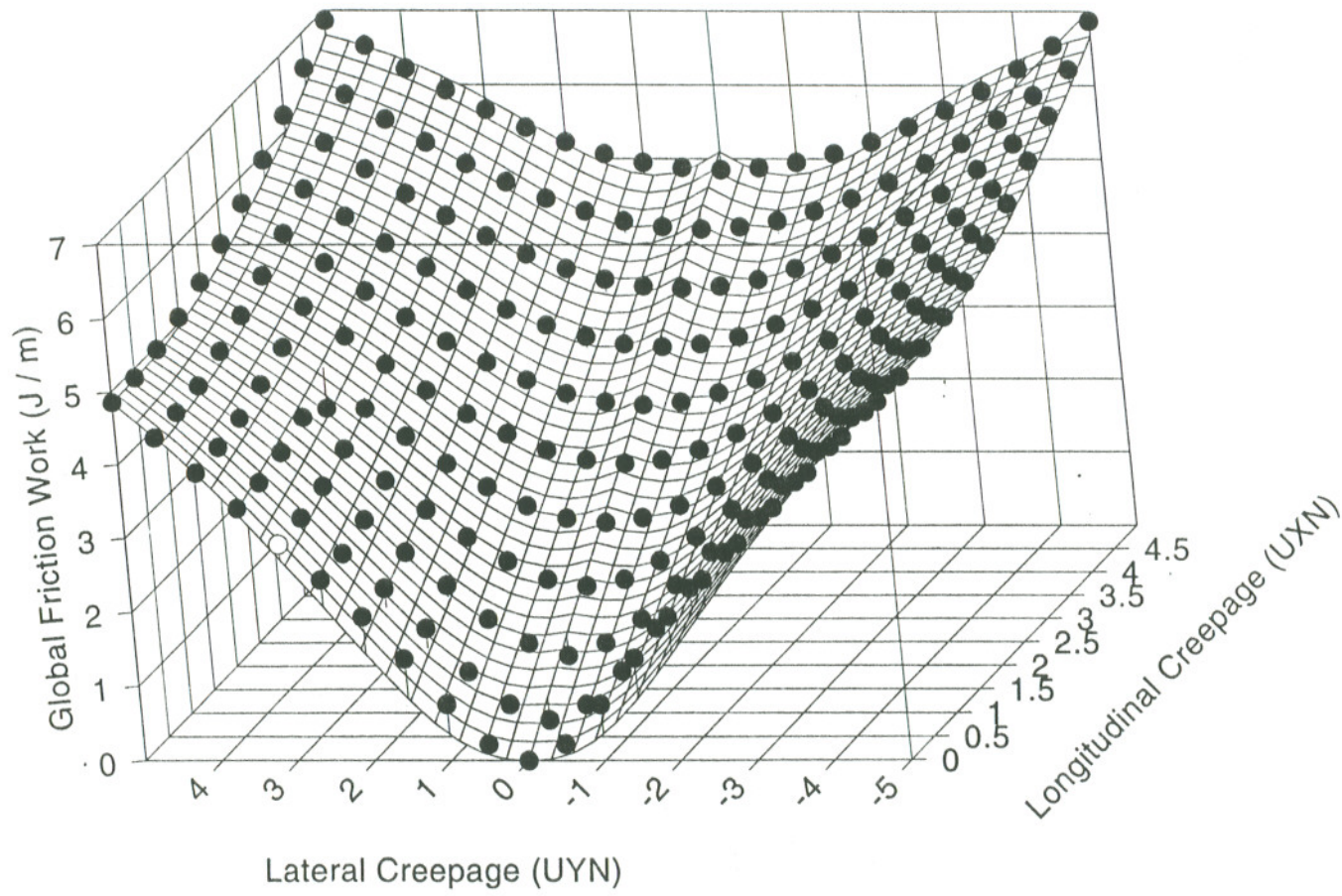


Figure 3.39 Generalized global friction work surface for position #1 ($UXN = \eta_x$, $UYN = \eta_y$).

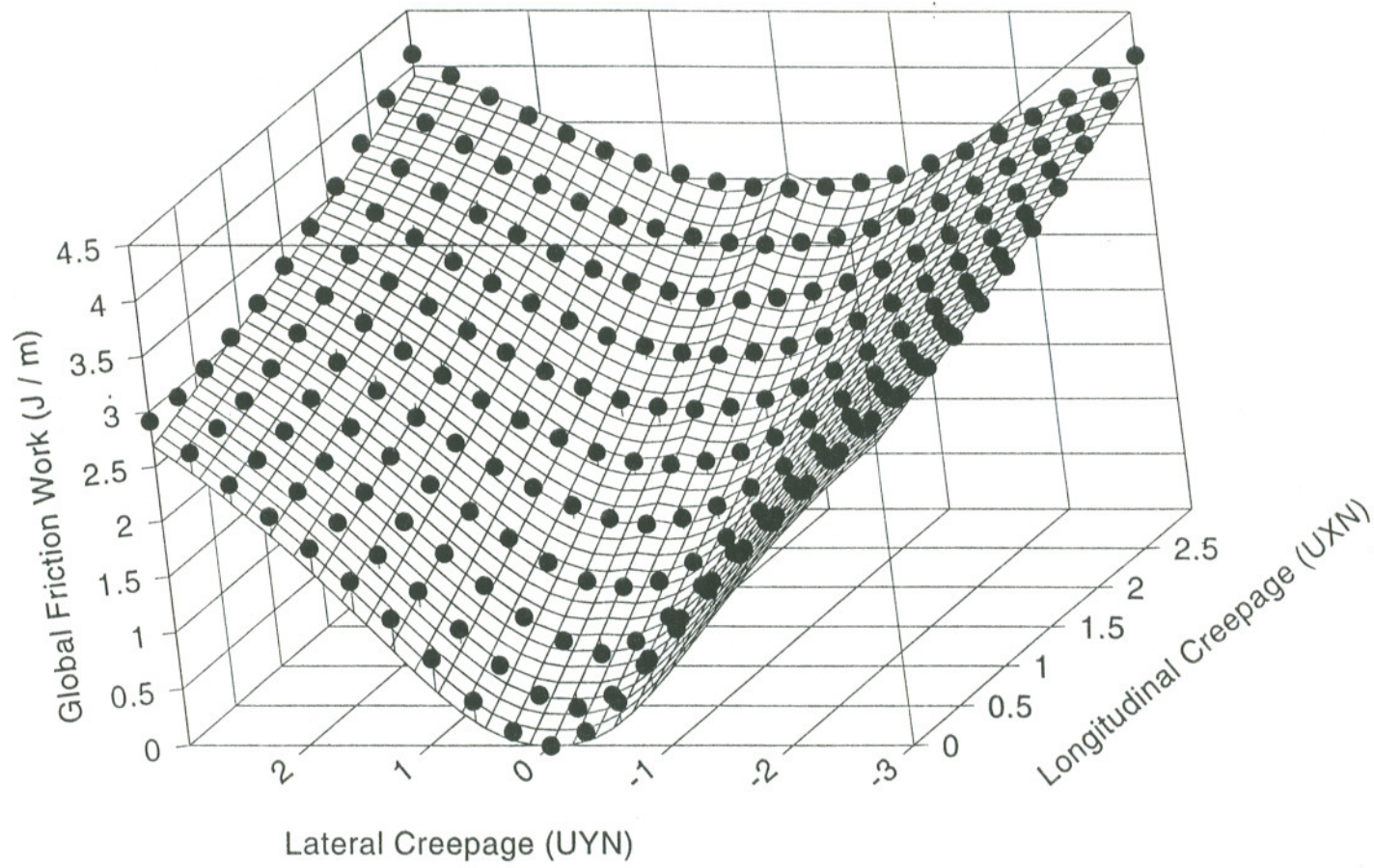


Figure 3.40 Generalized global friction work surface for position #2 ($UXN = \eta_x$, $UYN = \eta_y$).

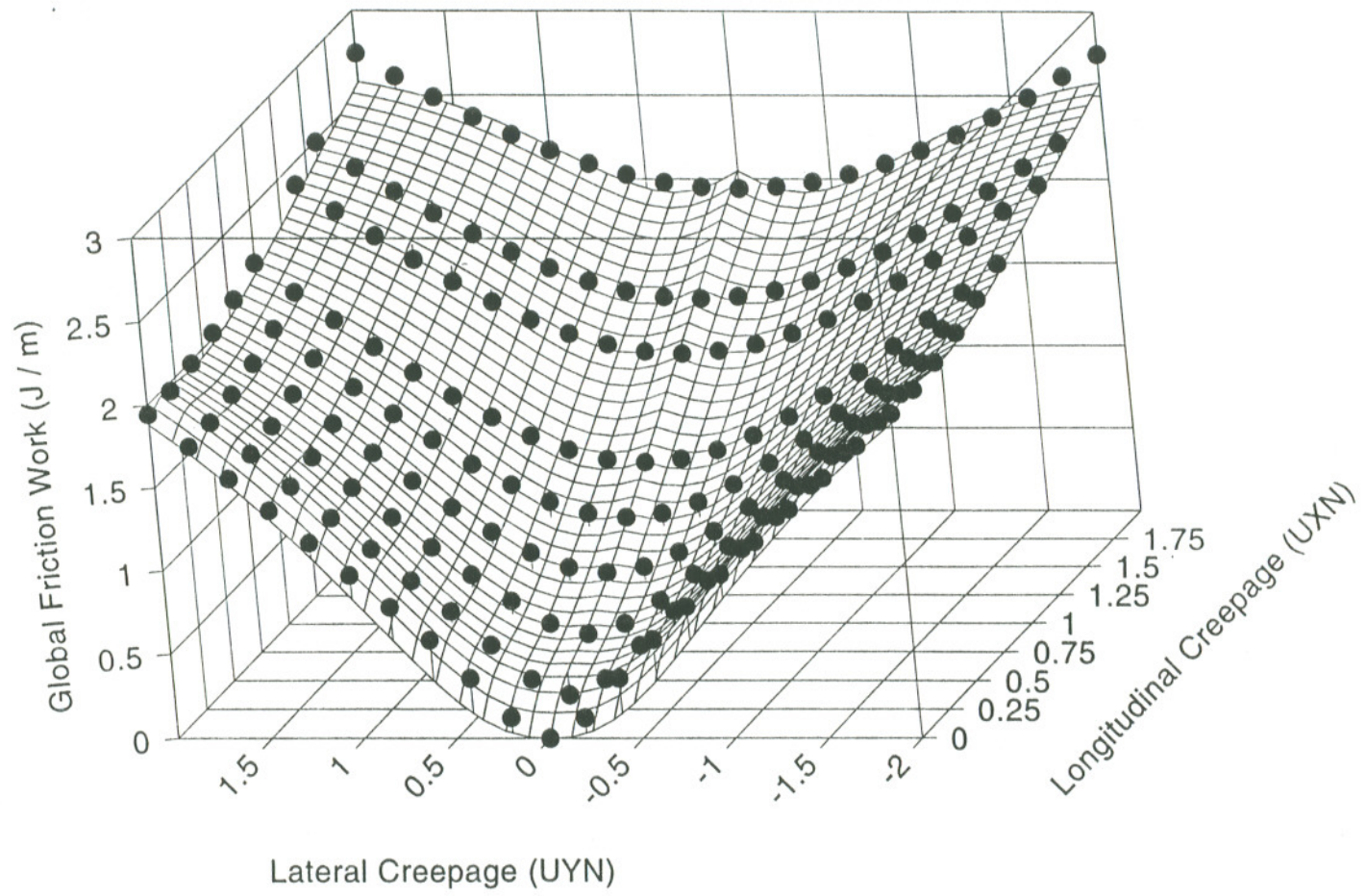


Figure 3.41 Generalized global friction work surface for position #3 ($UXN = \eta_x$, $UYN = \eta_y$).

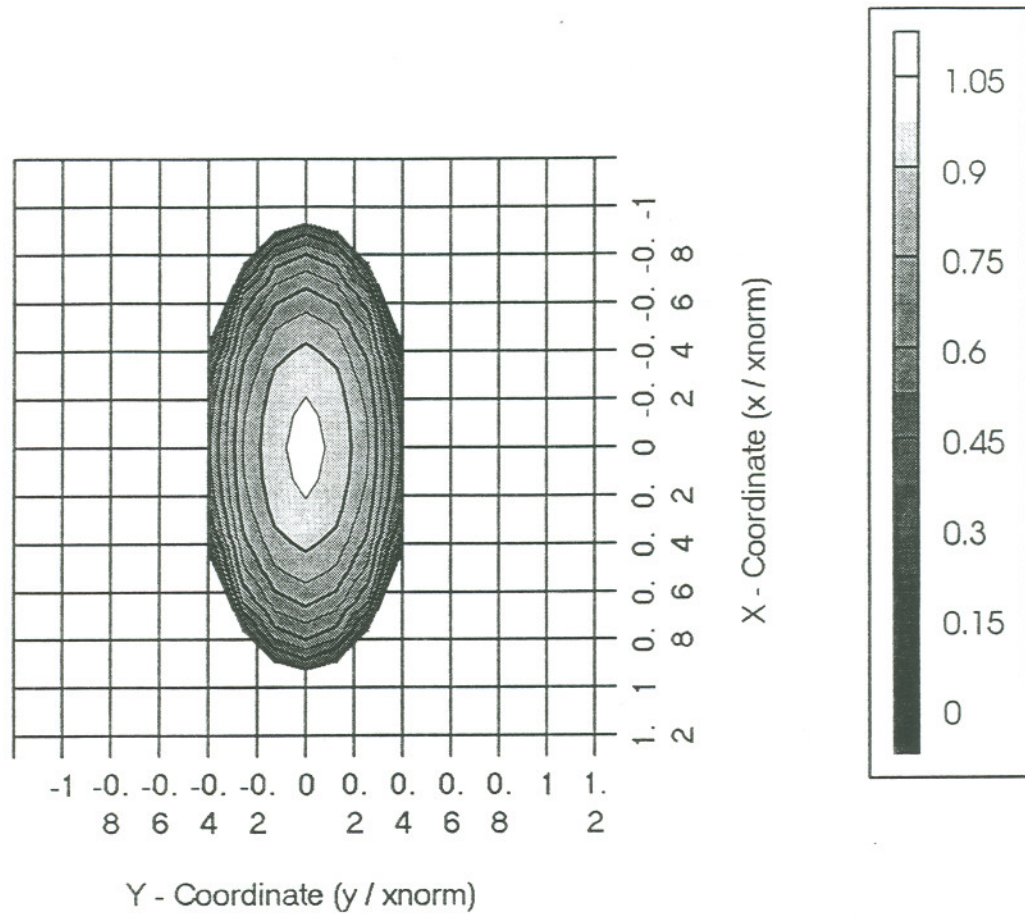


Figure 3.42 Local traction distribution for ellipticized contact of position #2 (load = 26,535 pounds, $a/b = 2.16$, $\nu_x = 0.6\%$, $\nu_y = f = 0.0$, $x_{norm} = 0.3360$ inches, legend signifies variations in local traction T_x).

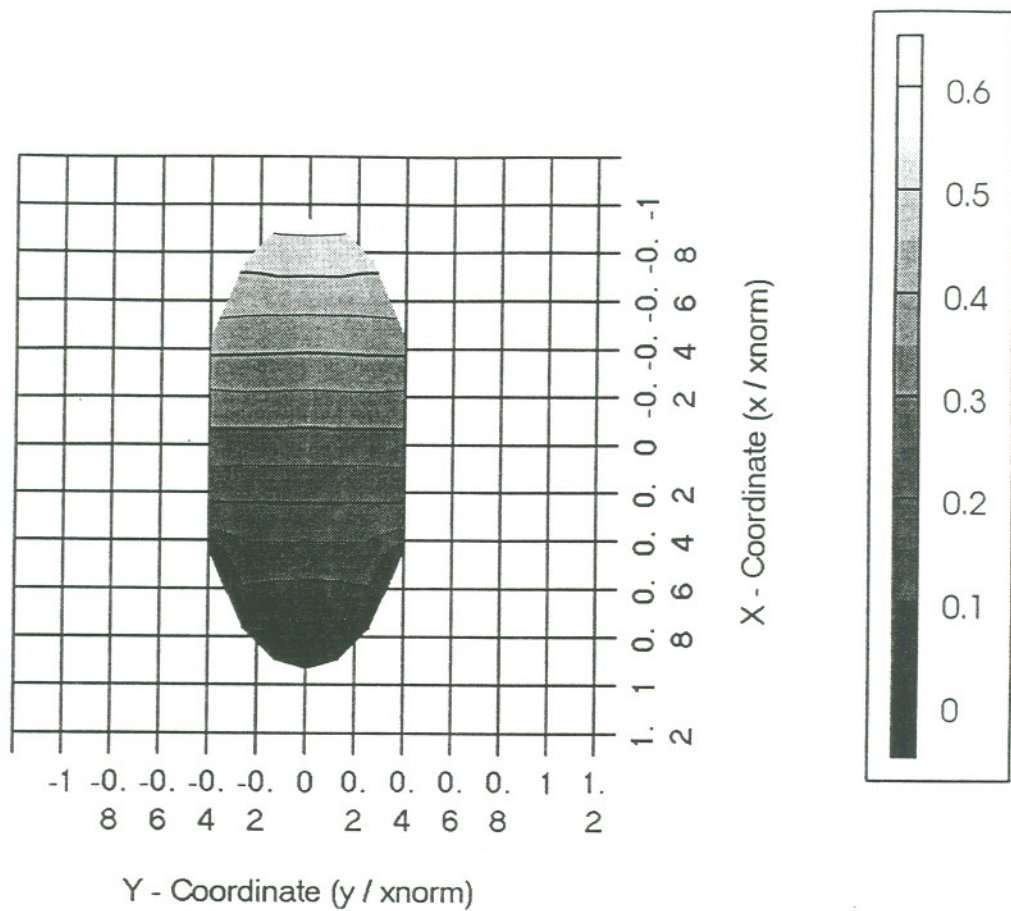


Figure 3.43 Longitudinal slippage distribution for ellipticized contact of position #2 (load = 26,535 pounds, $\nu_x = 0.6\%$, $\nu_y = \phi = 0.0$, $x_{norm} = 0.3360$ inches, legend signifies variations in local slippage s_x).

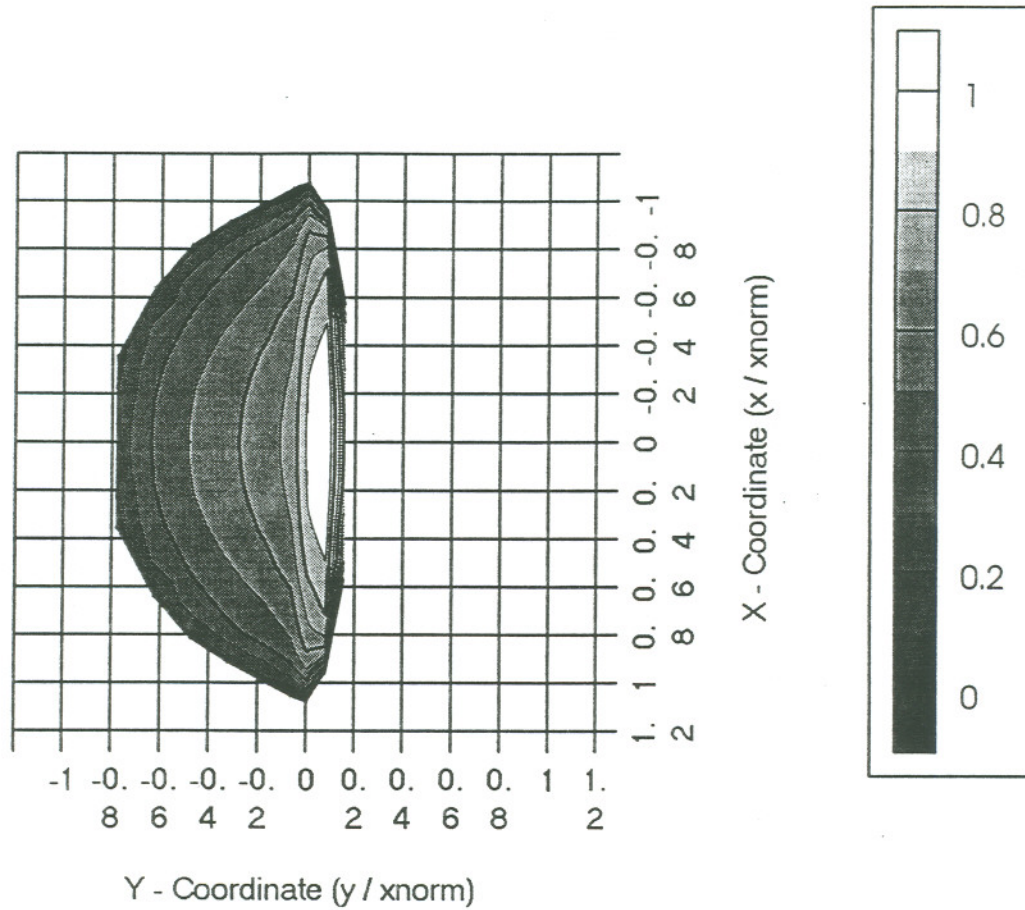


Figure 3.44 Local traction distribution for non-Hertzian contact of position #2 (load = 26,535 pounds, $\nu_x = 0.6\%$, $\nu_y = \phi = 0.0$, $x_{norm} = 0.3038$ inches, legend signifies variations in local traction T_x).

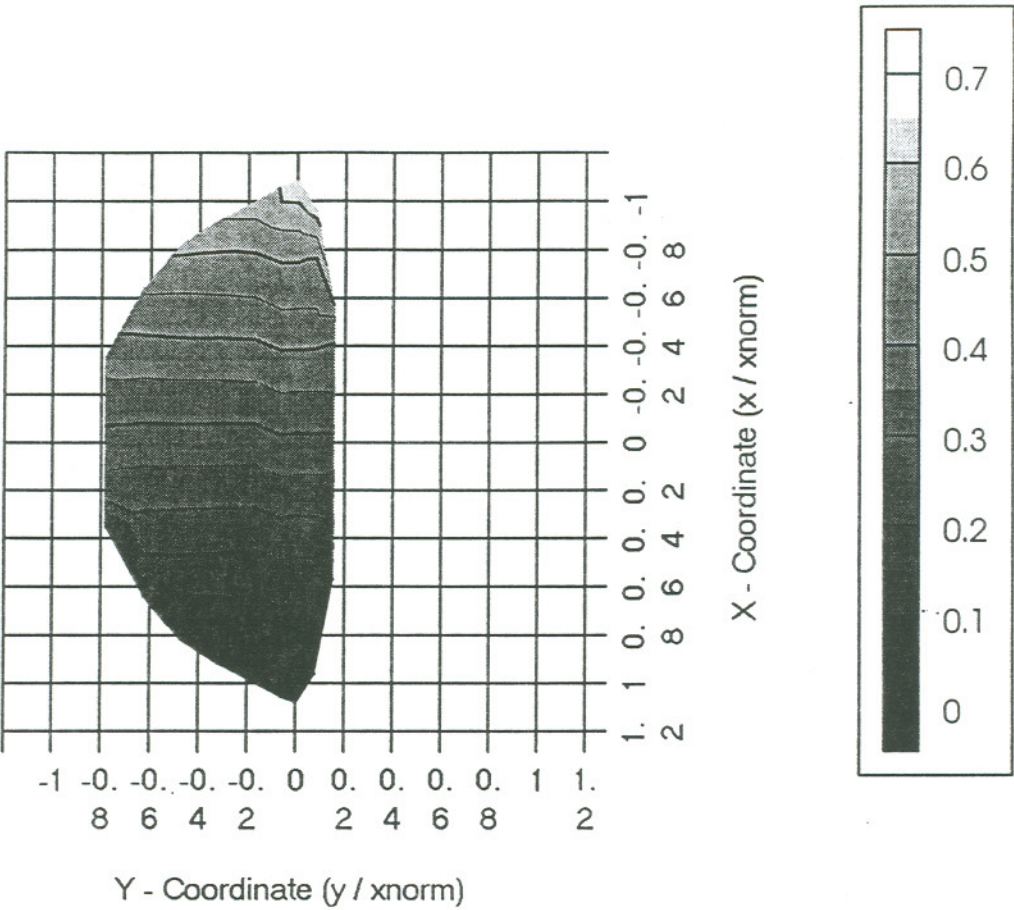


Figure 3.45 Longitudinal slippage distribution for non-Hertzian contact of position #2 (load = 26,535 pounds, $\nu_x = 0.6\%$, $\nu_y = \phi = 0.0$, $x_{norm} = 0.3038$ inches, legend signifies variations in local slippage s_x).

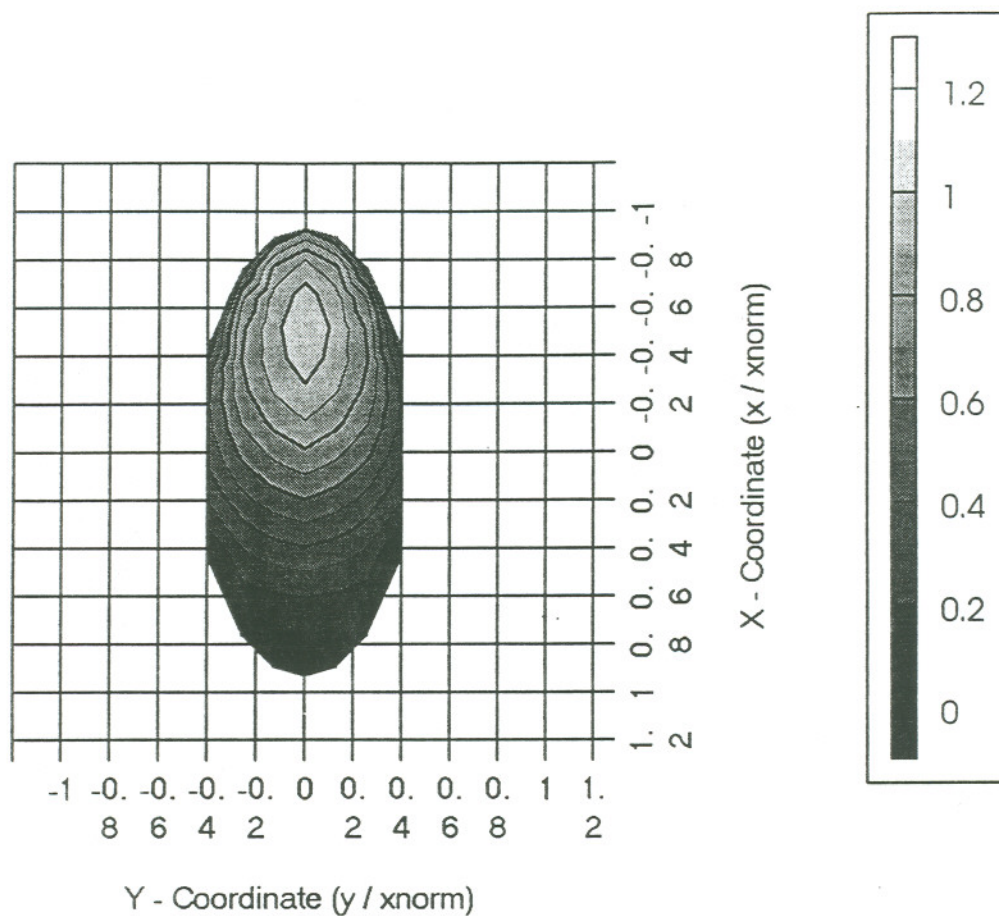


Figure 3.46 Local friction work distribution for ellipticized contact of position #2 (load = 26,535 pounds, $v_x = 0.6\%$, $v_y = \phi = 0.0$, $x_{norm} = 0.3360$ inches, legend signifies variations in local friction work W_{ij}).

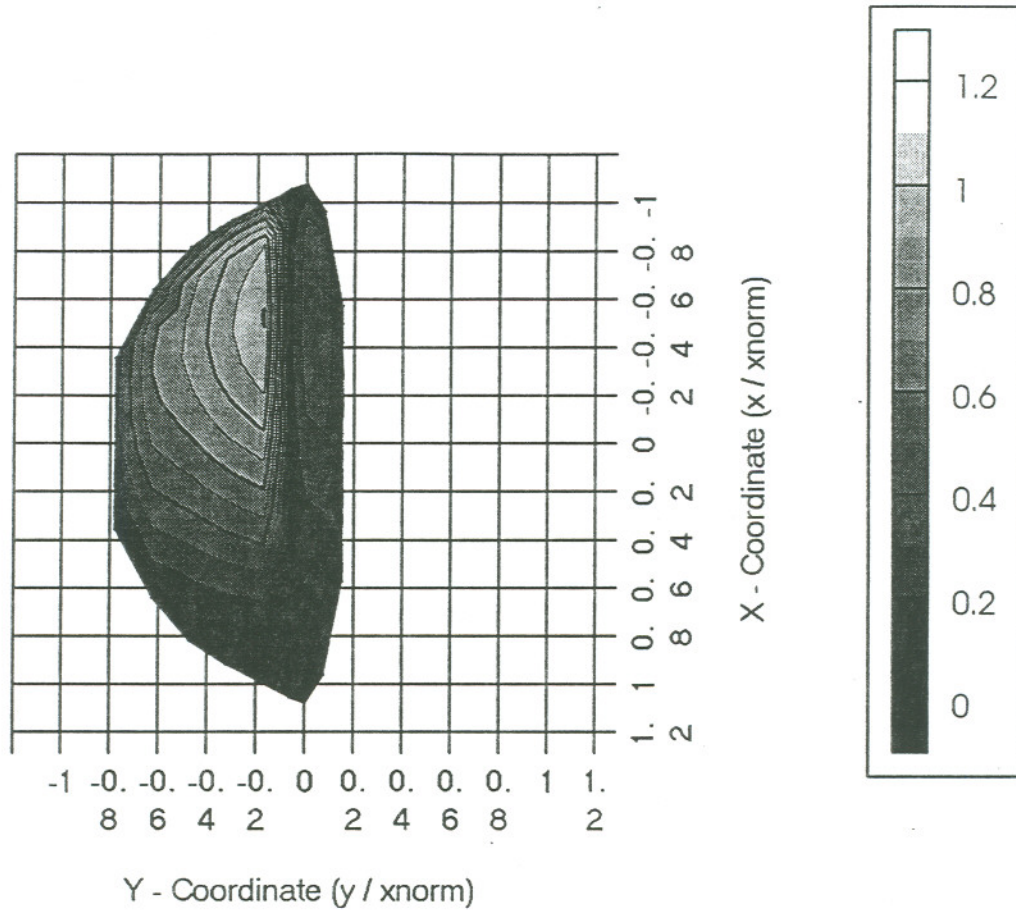


Figure 3.47 Local friction work distribution for non-Hertzian contact of position #2 (load=- 26,535 pounds, $\nu_x = 0.6\%$, $\nu_y = \phi = 0.0$, $x_{norm} = 0.3038$ inches, legend signifies variations in local friction work W_{ij}).

CHAPTER 4

DISCUSSIONS

4.1 Generalized Creep Force - Creepage Behavior

Numerical simulation of the nonlinear dynamics of railway vehicles requires the evaluation of the contact patch creep forces between the wheel and rail at every time step of integration. As summarized in Table 2.2, a variety of attempts have been made to develop complete creep force - creepage algorithms for this purpose. To date however, even the most advanced dynamic simulation codes commercially available remain limited in their application due primarily to the disproportionate amount of time required to compute the wheel-rail creep forces. One of the most successful of these codes (NUCARS), alleviates the need for excessive creep force computational effort by calling on a look-up table of creep force - creepage values which was developed by British Rail using Kalker's exact theory [50].

Interpolating within a look-up table was a novel approach that greatly reduced the time required to obtain values of creep force. It did however, necessitate excessive amounts of computer storage. Granted that the current cost of computer memory is only a fraction of what it was twenty years ago, the expectations of the dynamic simulation community have nonetheless seemed to increase by an inverse proportion. It was precisely these expectations (in light of the speed and simplicity of the look-up table approach) which provided the motivation to initiate a parametric investigation into the general nature of creep force - creepage behavior.

By studying the theory of Kalker and the trends of numerous two - dimensional creep force - creepage plots available in the literature, several general observations could be made.

1. The dimensionless creep forces FXN and FYN are defined from theory as being dependent only upon the dimensionless creepages, spin, and patch aspect ratio.

$$FXN = f(\eta_x, \eta_y, \chi_z, a/b) \quad (4.1)$$

$$FYN = g(\eta_x, \eta_y, \chi_z, a/b) \quad (4.2)$$

2. For conditions of vanishing spin, the dimensionless creep forces FXN and FYN may be described by very similar functions, where η_1 and η_2 are permuted (Figure 4.1 a, b)
3. The dimensionless creep force functions are antisymmetric to the line $FXN(0, \eta_2) = 0$ for longitudinal creep force and to $FYN(\eta_1, 0) = 0$ for the lateral forces.
4. The influence of patch aspect ratio is such that as a/b decreases the dimensionless creep force functions tend to become more linear with reduced slopes. (Figure 4.2)
5. The influence of dimensionless spin creepage is such that as χ_z increases the dimensionless creep force functions tend to become more linear with reduced slopes. (Figure 4.3).

Based on the above observations, it was proposed that a set of analytic functions be sought which could be combined in such a way that they describe the observed creep force - creepage behavior. By exercising the computer models of DUVOROL, COUNTAC 1

and 2, and ROLCREEP for the geometries, loads and creepage conditions of section 3.3, longitudinal and lateral creep force data were obtained. These data appear as the dots in the surface plots of Figures 3.12, 3.13, 3.15, 3.16 and 3.32 and 3.33.

Given the regularity and repeatability of the “shape” of the surface data for the variety of operating conditions ($1.22 \leq (a/b) \leq 5.88$), several characteristic trends were identified which provided the necessary insight into the choice of analytic function to be used for approximation purposes. The first trend common to both creep force functions was that as the creepage in a given direction increased above zero, the creep force function for that direction tended toward +1. A similar trend was observed for the opposite situation, that as the creepage in a given direction was decreased below zero, the creep force function tended toward -1. These trends are known to be characteristic of the hyperbolic tangent function and it was therefore selected as the primary shape function for each creepage direction as indicated in equations (4.3) and (4.4) [131].

$$FXN = f(\tanh(\eta_x), \eta_y, \chi_z, a/b) \quad (4.3)$$

$$FYN = g(\tanh(\eta_y), \eta_x, \chi_z, a/b) \quad (4.4)$$

Additional trends which were identified as the result of the parametric analysis were that the lateral creep force appeared to be dependent upon some polynomial function of longitudinal creepage and in a similar way the longitudinal creep force appeared to be some polynomial function of the lateral creepage. There appeared as well to be some “crossover” effects which were exponential in nature, providing a nonlinear “growth” of lateral creep force due to increasing longitudinal creepage and visa-versa.

By selecting the additional analytic functions (polynomials, exponentials and power functions) in a sufficiently general manner, and subjecting them to the parametric data along

with the surface fitting algorithm of section 3.3.3.2, the approximating functions of equations (3.8) and (3.9) were obtained. As indicated by the magnitudes and polarities of the coefficients a_0 to a_7 and b_0 to b_6 listed in Tables 3.2 through 3.4, although the general form of the functions (3.8) and (3.9) fit all of the parametric surface data quite well (average $r^2 = 0.9827$), the specific coefficients necessary for each of these fits differed.

The coefficients are listed by patch aspect ratio in Tables 4.1 and 4.2 for the purposes of comparison. Since it was postulated in equations (4.1) and (4.2) that the patch aspect ratio also was an independent parameter in the creep force functions, along with η_x and η_y it should be expected that the coefficients responsible for fitting the data to a given functional format in terms η_x and η_y , would depend on the a/b ratio alone, (since the parametric analysis was performed for the case of vanishing spin).

This trend can be observed by considering the manner in which any given coefficient changes with respect to increasing a/b . For the longitudinal creep force function of equation (3.8), it appears that coefficients a_0 , a_2 , a_3 , and a_7 are increasing in some direct proportion to a/b , while coefficients a_4 and a_5 are inversely proportional, and the trend for a_1 and a_6 appears unclear. Trends of some direct proportion exist for the coefficients b_0 and b_1 and there exists an inverse relationship for coefficients b_4 and b_5 , of the lateral creep force approximating function (3.9). In order to obtain the exact functional relationships between each of the coefficients and a/b , additional contacts would need to be analyzed over a wider range of a/b , and then the resultant coefficient trends with respect to patch aspect ratio could be approximated with a higher degree of confidence. The result would

be a pair of fully generalized creep force - creepage approximating functions valid over a wide range of a/b and creepages for the longitudinal and lateral directions.

The possibility of obtaining generalized creep force - creepage approximating functions has been demonstrated for both true Hertzian and *ellipticized non-Hertzian* contact patches. Although a *completely* general function set was not obtained in this study, it has been shown clearly that the characteristic shape is hyperbolic tangent in form, and that for the range of operating conditions studied, an excellent approximation to the model results of Kalker can be achieved. As a final consideration regarding the utility of a generalized creep force function, the ellipticized contact of position #2 was analyzed. The speed and accuracy of the approximating function was tested against the fastest creep force code available (SHE.FOR) as well as the exact code DUVOROL. Results are shown in Table 4.3 for the following input conditions: $a/b = 2.16$, $\eta_x = 2.0$, $\eta_y = 2.5$, and a normal wheel load of 26,535 pounds. As indicated the approximating functions are about 8.5 times faster than the SHE code and provide an accuracy (with respect to DUVOROL) of about 8%.

4.2 Ellipticized Non-Hertzian Contacts

When consideration is given to the different rail and wheel design profiles available, the variety of rail grinding procedures employed, and the myriad of rail and wheel wear patterns which develop under various payload and traffic conditions, the possibility of contact patch geometries which frequently envelope two different radii of curvature at any one location would seem inevitable. Although much of the literature appeared to be in agreement with this statement (to some degree), no quantitative work has been reported

which addresses the question: “How much difference is there between the actual non-Hertzian creep forces which develop within a non-Hertzian contact patch and the Hertzian creep forces which are typically assumed to exist there?”

In an attempt to answer this question, the possibility of representing a non-Hertzian contact with an equivalent “ellipticized” patch was considered. The assumptions and methodology necessary for ellipticizing a non-Hertzian contact patch have been outlined in section 3.3.5.3. Regarding the *normal* results, it has been shown in Figure 3.30 that the aspect ratio of the ellipticized contact is independent of load. This is significant for two reasons; the first being more fundamental in nature and the second, more a matter of convenience. The first reason is that a similar result was shown in Figure 3.17 for true non-Hertzian geometries. Thus for the sake of continuity between the two “equivalent” patch representations, this result provides supporting evidence that similitude is being preserved. Of additional interest, was that a load - independent patch aspect ratio would allow for a more convenient tangential analysis using dimensionless input parameters.

Another important result of the *normal* analysis is shown quite dramatically in Figure 3.28. As might be expected, the pressure experienced by a non-Hertzian contact geometry is distributed in an asymmetric manner over the patch domain, and has a peak value which is significantly higher than its ellipsoidal counterpart. Although this result did not seem problematic in and of itself, there was some concern that if variations in the peak pressure ratios for patches of different wheel loads were realized, then the validity of the similitude approach could come into question. After completing the *normal* analysis for the four non-Hertzian as well as ellipticized contacts for position #2, this concern was alleviated. As indicated in Figure 3.31, the peak pressure ratio (non-Hertzian / Hertzian) was found to be constant with a magnitude of 1.333. This is shown in equation (4.5).

$$P_{nh} = 4/3 P_h \quad (4.5)$$

This relationship is also significant in that it provides a convenient way to approximate the peak non-Hertzian pressure that could exist at any given location, provided wheel load and the Hertzian elliptic semi-diameters a and b are known, as shown by equation (4.6) (where the relationship for P_h was given in equation (2.16)).

$$P_{nh} = 4/3 \left\{ (3/2) (\text{Load} / \pi ab) \right\} = 2 (\text{Load} / \pi ab) \quad (4.6)$$

This result implies that the peak non-Hertzian pressure would simply be twice the average Hertzian pressure.

In order to answer the question regarding creep forces, which had been posed earlier in this section, the *tangential* analysis of both the ellipticized non-Hertzian as well as the true non-Hertzian contact geometries was performed with the aid of the *normal* results. The ellipticized contact was analyzed using the Hertzian code DUVOROL, while the non-Hertzian geometry was modeled via COUNTAC1 and ROLCREEP. The results are shown in Figure 3.34. As indicated, excellent agreement exists between these two methods, with a possible exception being taken for the data presented within the full slip regime. Nonetheless, as there have been no other comparative analysis reported in the literature, these results are indeed significant, for they imply that the creep forces which develop within a non-Hertzian contact patch may be predicted with the same degree of reliability by simply ellipticizing the patch and treating it with classical Hertzian analysis.

Having resolved what appeared to be an important, yet unanswered question, it became apparent that the agreement between the ellipticized creep force behavior and that of its non-Hertzian counterpart may be dependent upon the “degree of conformity” or “geometric agreement” between the two contact domains. In other words, it is possible that there may

be some limit to the geometric distortion of a given non-Hertzian patch, beyond which the physics of the problem may defy the imposed similitude conditions, such that the ellipticized patches although similar to the non-Hertzian ones in a geometric sense (ie. equivalent areas, $a = \bar{a}$), no longer display an equivalent creep force behavior.

Although this consideration was not fully explored, a parameter which could be used for such a study was developed. The geometric distortion parameter (Γ) was designed to provide a quantitative measure of “included area” between an ellipticized contact geometry and a non-Hertzian (non-elliptic) one. Two such geometries which have been subject to the similitude conditions of section 3.3.5.3 are shown in Figure 4.4 . If the area of the ellipticized contact geometry is defined by the term AE, and the total area which is *not* included within both geometries is defined by the term ANI, then the geometric distortion parameter may be described by equation (4.7).

$$\Gamma = \left[1 - \left(\frac{AE - ANI}{AE} \right) \right] * 100\% \quad (4.7)$$

As indicated from the equation, when both geometries of area $A = AE$ completely conform, then $ANI = 0$ and $\Gamma = 0\%$, in other words there is no distortion with respect to the ellipse.

As suspected, when the original non-Hertzian contact becomes less elliptical and has a highly asymmetric pressure distribution, then ANI increases significantly, resulting in large values of Γ .

In order to obtain a measure of the geometric distortion for the results of Figure 3.34, the non-Hertzian and ellipticized geometries were plotted in Figure 4.5. The area of the ellipticized patch was obtained from Figure 3.30 ($AE = 0.1635$ square inches) and the

amount of “area-not-included” ANI, was obtained by approximating the patch geometries (note half symmetry) with polynomial expressions and integrating them via the Romberg integration algorithm of Appendix E. The four segments of area which account for ANI/2 (A1, A2, A3, A4) are shown in Figure 4.6, where ANI = 0.1053 square inches. The resulting value for Γ was 64.4%, and as a consequence, it may be stated that the creep force behavior for non-Hertzian contacts may be accurately predicted by an ellipticized contact treated with classical Hertzian techniques, provided that $\Gamma \leq 64.4\%$.

4.3 Contact Patch Friction Work

Interest in the behavior of contact patch friction work and the ability to describe it quantitatively, has been motivated both by vehicle dynamicists who use it for predicting curving performance and derailments, as well as by tribologists who have experimentally found it to be a reliable wear index under certain operating conditions [17, 109, 132]. Since the wear process alters rail and wheel profiles, it thus modifies the patch geometry and resultant creep forces. These in turn have a strong influence on the rail car - track dynamics, and so the two effects become a coupled phenomenon.

In an attempt to better understand the behavior of contact patch friction work, an algorithm for predicting the dot product of the creep force and creepage vectors was developed and integrated into each of the computational tools which were used for Hertzian and non-Hertzian contact patch analysis. The details of this procedure have been outlined in section 3.4 for both global and local distributions of frictional work.

The surface plots of global patch work shown in Figures 3.35 through 3.38, demonstrate an interesting series of results from this study. For the circular contact

geometry of Figures 3.35 to 3.37, several general observations can be made. The first observation is with regard to the “dished shape” characteristic of the work surfaces. Although such a shape might have been expected if a term-wise multiplication of creepage and creep force were carried out for the coordinates along a classic two dimensional creep force - creepage curve, a complete picture of the global friction work behavior is difficult to envisage without the aid of the third dimension. Since friction work is the result of non-conservative forces, it is by definition equal to the change in the total mechanical energy of the system. If one considers the contact patch and the adjoining materials to be the system, then these plots provide a qualitative picture of potential material damage.

With regards to the spin parameter (χ_z) it was observed that as χ_z was increased it tended to “lift” the entire work surface. This seemed reasonable in light of equation (3.22), which indicated that the only independent parameter which was changing from Figures 3.35 to 3.37 was the spin. In addition, it was reasoned that for $\eta_x = \eta_y = 0$ the only slip zone generated should be that due to spin, and as the spin is reduced to zero so was the surface plot minima. As indicated in Figure 3.37, at extreme values of spin, the friction work became basically independent of creepage for the range of η_x and η_y considered. Presumably this was just an “order of magnitude” effect, in that if η_x and η_y were also drastically increased, then the characteristic shape would be regained.

When the results of Figure 3.36 and 3.38 were compared, the effect of contact patch aspect ratio on friction work behavior could be discerned, as a/b was the only independent parameter that was changed. As indicated, an increase in the aspect ratio from 1.0 to 6.75 tended to raise the surface minima from a dimensionless work value of about 1.8 to almost

6.0, with only a slight alteration in the surface plot perimeter values. This effect might best be explained in light of Figure 4.2, which displayed the trend of increasing creep force - creepage slope with increasing a/b values. The consequence of this would be that for a given creepage, the steeper slope provides a higher creep force value, and thus a larger creep force * creepage product term. This effect is most dramatic for the vanishing creepage regime and becomes almost negligible under full slip conditions.

The global work surface data for the 136RE X AA1-B rail - wheel combination was shown for contact regimes #1 - #3 in Figures 3.39 - 3.41. As indicated, since the surface minima drops to zero at $\eta_x = \eta_y = 0$, these were analyzed for conditions of vanishing spin ($\chi_z = 0$). The approximating equation responsible for the “mesh” in these figures (equation 3.24) was fit to the data with an average coefficient of determination (r^2) equal to 0.987 (where $r^2 = 1$ is a perfect fit). Other than the fact that this approximating equation appears to be some type of a modified ellipsoid (which should stand to reason since the contact domain was elliptical and the pressure distribution was ellipsoidal) the functional “form” does not seem to carry any physical meaning. With the spin set to zero, the equation parameters identified in (3.22) for a global work function should be η_x , η_y and a/b . Since the only parameters in the approximating equation (3.24) were η_x and η_y , it seemed reasonable therefore, that the specific coefficients responsible for the “fit” of each data set, would be dependent upon a/b . By studying the data of Tables 3.6 through 3.8, it became clear that the coefficients c_1 and c_2 are in some direct proportion to a/b , while c_5 relates in an inverse fashion (recall a/b increases from 1.22 at position #1, to 5.88 at position #3). It is unclear how c_3 , c_4 and c_6 relate to patch aspect ratio. In order to determine the exact

relationships of these coefficients to a/b , additional contact geometries would need to be analyzed. The result would be a fully general global work approximating function valid for a wide range of a/b and creepages in the lateral and longitudinal directions.

The possibility of obtaining a generalized global work approximating function has been demonstrated for both true Hertzian and ellipticized non-Hertzian contact patches. Although a *completely* general function was not obtained in this study, it has been shown (with sufficient generality) that a strong possibility for this exists by utilizing the functional form of equation (3.24) derived in this work. The utility of such a generalized function could be realized by those interested in curving performance and incipient derailment, in that for any set of creepages and wheel - rail contact location (a/b) they could have virtually instantaneous feedback regarding the work index. For those interested in wheel - rail profile design, such a generalized function could increase design efficiency if they are concerned with the Type II wear regime, (wherein the wear rate can be estimated as a direct proportion to contact patch work).

The final study regarding contact patch friction work focused on the local behavior of work distribution within the contact domain. This necessitated using the contact algorithm ROLCREEP for both Hertzian and non-Hertzian contact geometries, due to the finer discretization which was available. There were two primary motivations for this study, both of which were related to the asymmetry of non-Hertzian geometries. The first was to provide data on a non-Hertzian work distribution for those involved in wear modeling, as often times either a uniform or parabolic work profile has been assumed over the contact domain [89, 90]. The other motivation stemmed from an interest in tribo-energetics (the study of thermal - mechanical rubbing), where the local work distribution is related to the non-uniform heat flux boundary condition (section 2.4.3) of a moving heat source having a

velocity V_0 [93-102].

The contact geometry chosen for this work was one resulting from a 26,535 pound wheel load at position #2. Both an ellipticized patch ($a/b = 2.16$) and the true non-Hertzian one were analyzed using the modified ROLCREEP. In order to check the accuracy of the computational algorithm which was developed for predicting local work distribution, equation (2.37) was employed. It seemed reasonable that the equality of the global contact patch work and the summation of the local work for all contact domain locations should prevail. It became apparent, however, that at times this was true (for certain rolling conditions) and under other conditions for the same patch, an inequality existed. In an attempt to resolve this issue the contact patch of position #2 was analyzed for a wide range of longitudinal creepage values. After the results had been plotted (Figure 4.7) a trend of the work ratio ($k = \text{global/local sum}$) revealed the nature of the inequality. As indicated, the work ratio (a measure of the equality of equation (2.37)) quickly approached unity within the first 0.25% creepage, but did not appear to fully achieve a constant value until about 0.5% creepage. Since the slip region increases with increasing creepage, and it is *only* the slip region which contributes to frictional work, it became apparent that the exact behavior of the slipped area should be investigated. The results are included in Figure 4.8. As shown, a direct correlation exists between the percent slipped area and number of slipped cells within the contact domain, as would be expected. What was more interesting, however, was that the work ratio became entirely constant at the same creepage value ($v_x = 0.6\%$) where full slip was achieved. It is suspected that this effect is purely a function of the discretization of the contact domain, which was similar to work reported for a Hertzian analysis [89]. The resultant local traction and slip distributions are shown in Figures 3.42 and 3.43 for the ellipticized contact, and in 3.44 and 3.45 for the non-Hertzian patch for a

pure longitudinal creeping of 0.6%. As might be expected, the uniform slip distribution of Figure 3.43 tended to “push” the traction distribution peak of Figure 3.42 back toward the trailing edge of the ellipticized contact as shown in Figure 3.46. However, it is interesting to note how the asymmetric slip of Figure 3.45 influenced the very non-uniform traction distribution of Figure 3.44, causing the bi-modal friction work distribution of Figure 3.47 for the non-Hertzian case.

There have been no results published before for non-Hertzian frictional work distribution. Although a complete understanding of all of the possible consequences related to the bi-modal results of a non-Hertzian work profile are not clear at this time, it would seem reasonable that they could influence certain applications of Type II wear models, as well as the transient temperature distributions predicted for some thermal-mechanical rolling/sliding systems.

Table 4.1 Coefficients for the Longitudinal Creep Force Approximating Function of Equation (3.8)

Position #	a/b	a_0	a_1	a_2	a_3	a_4	a_5	a_6	a_7	r^2
1	1.22	.0353	-0.717	-0.121	-3.834	17.052	28.044	0.817	0.100	0.964
2	2.16	.0618	-0.537	-0.216	-4.394	15.896	19.304	1.067	0.139	0.994
3	5.88	.075	-1.053	-0.474	-5.095	13.081	18.660	0.951	0.414	0.971

Table 4.2 Coefficients for the Lateral Creep Force Approximating Function of Equation (3.9)

Position #	a/b	b_0	b_1	b_2	b_3	b_4	b_5	b_6	r^2
1	1.22	0.019	0.558	-0.310	-4.784	26.808	56.856	2.384	0.989
2	2.16	0.080	0.881	-0.366	-3.31	10.849	13.291	1.321	0.991
3	5.88	0.207	1.598	0.271	0.692	1.018	5.205	75.544	0.984

Table 4.3 Speed and Accuracy Test Data for Computer Codes

Code	Execution time (sec.)	FXN	FYN	(% error) [*] _{avg.}
SHE	0.06	.7931	.6090	26.1
Equations (3.8) and (3.9)	0.007	.6189	.6950	7.7
DUVOROL	1200	.6109	.7533	0

* as compared to DUVOROL

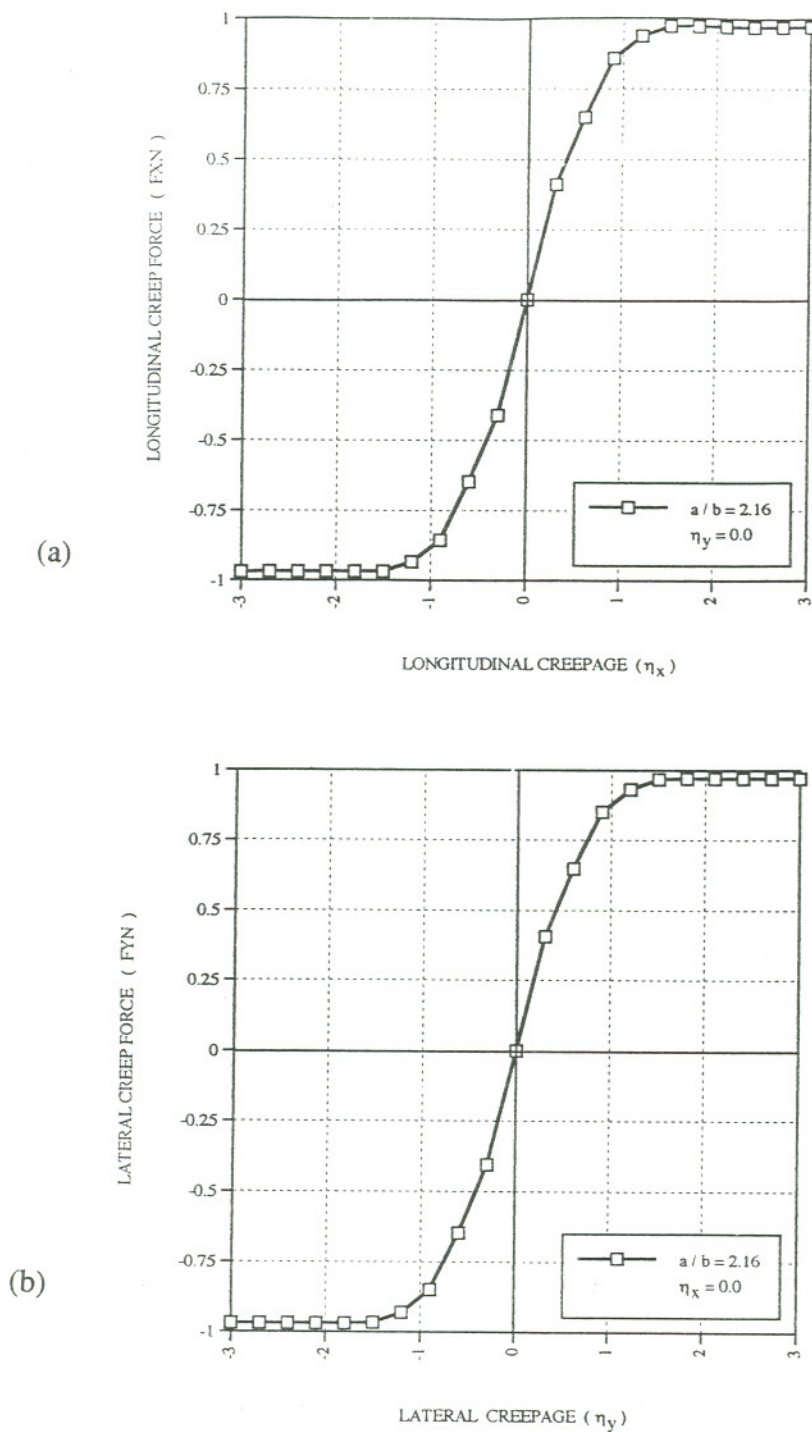


Figure 4.1 General behavior of dimensionless creep forces (a) F_{XN} versus η_x ; and (b) F_{YN} versus η_y .

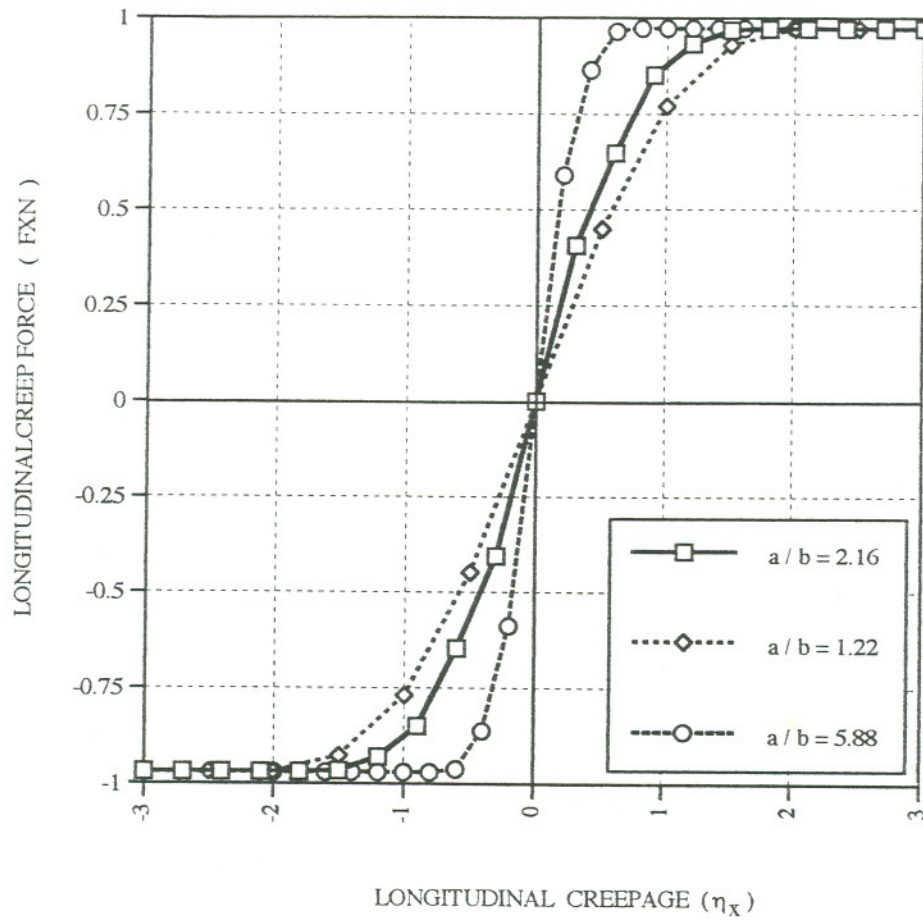


Figure 4.2 Effect of patch aspect ratio (a/b) on the creep force - creepage curve.

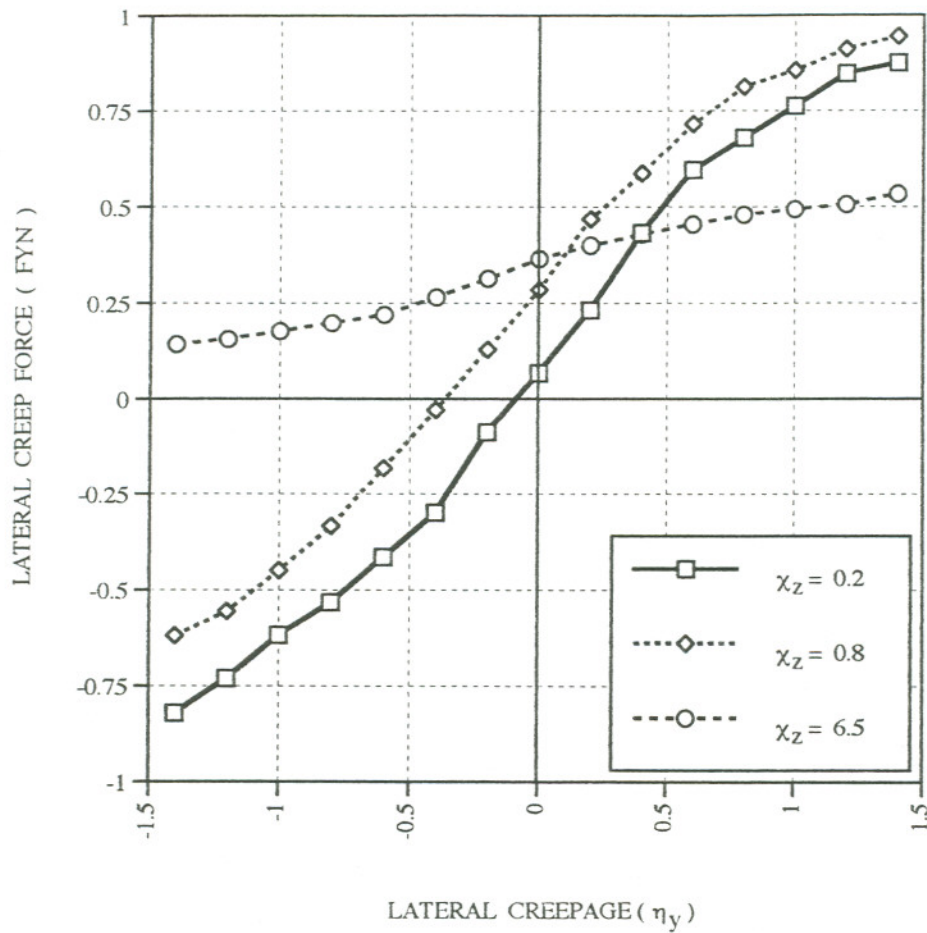


Figure 4.3 Effect of the dimensionless spin parameter χ_z on the creep force - creepage curve.

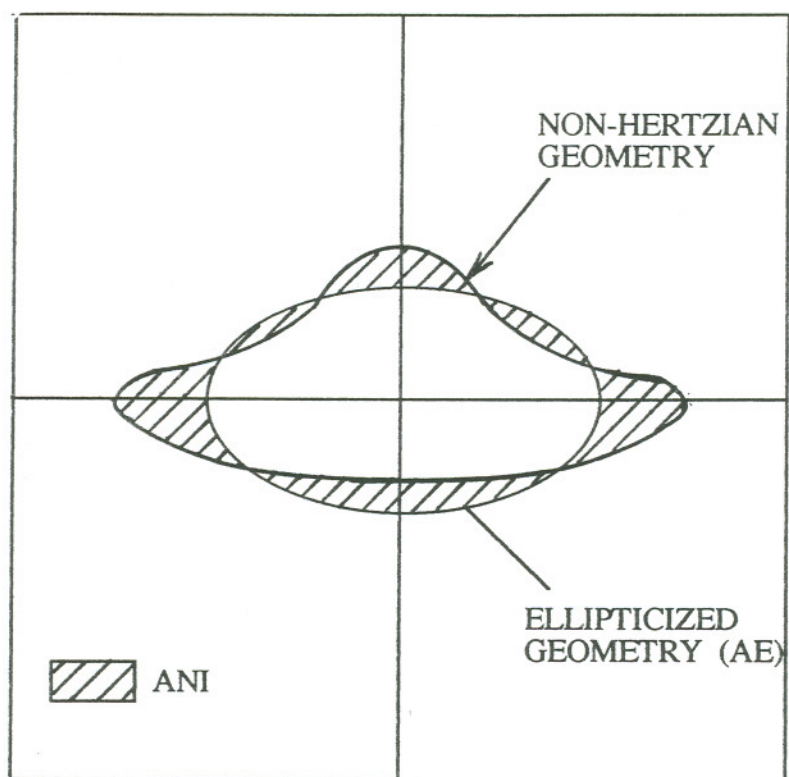


Figure 4.4 The idea of the geometric distortion parameter Γ .

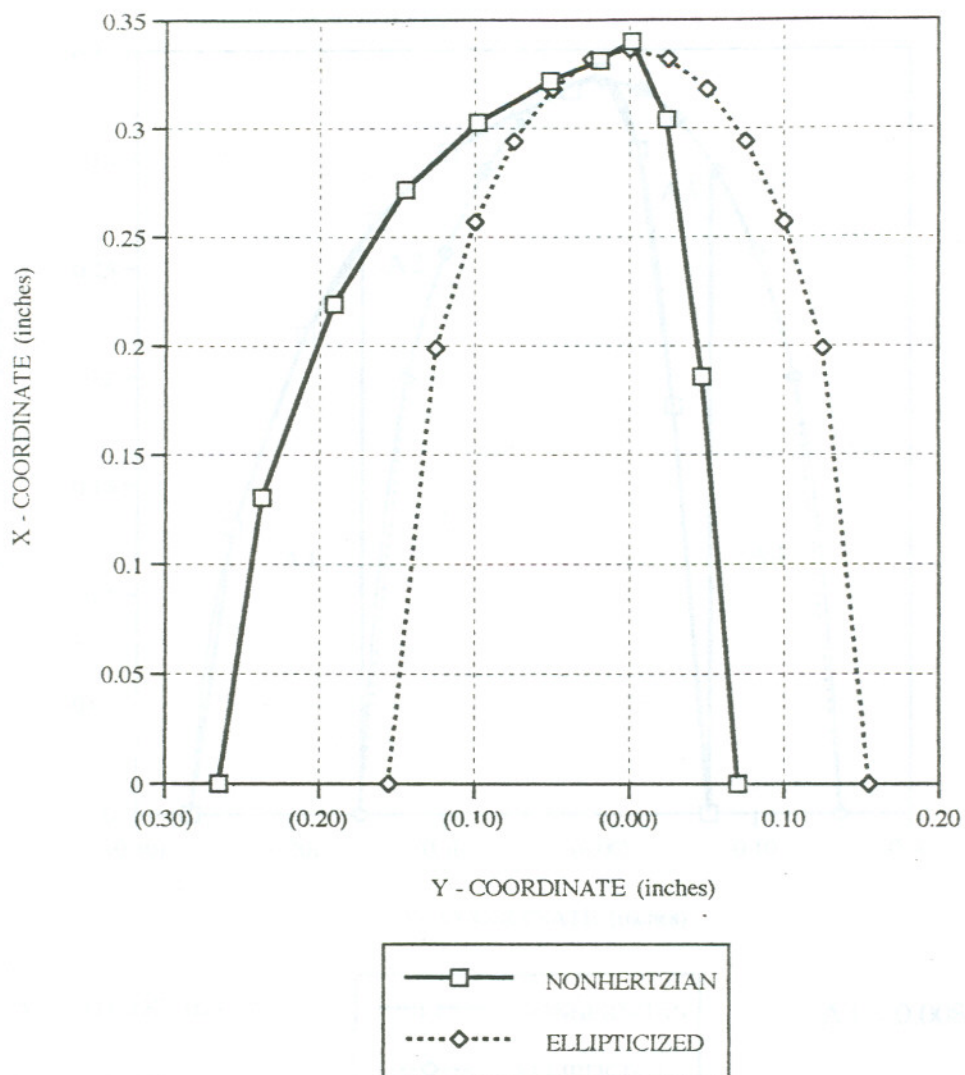
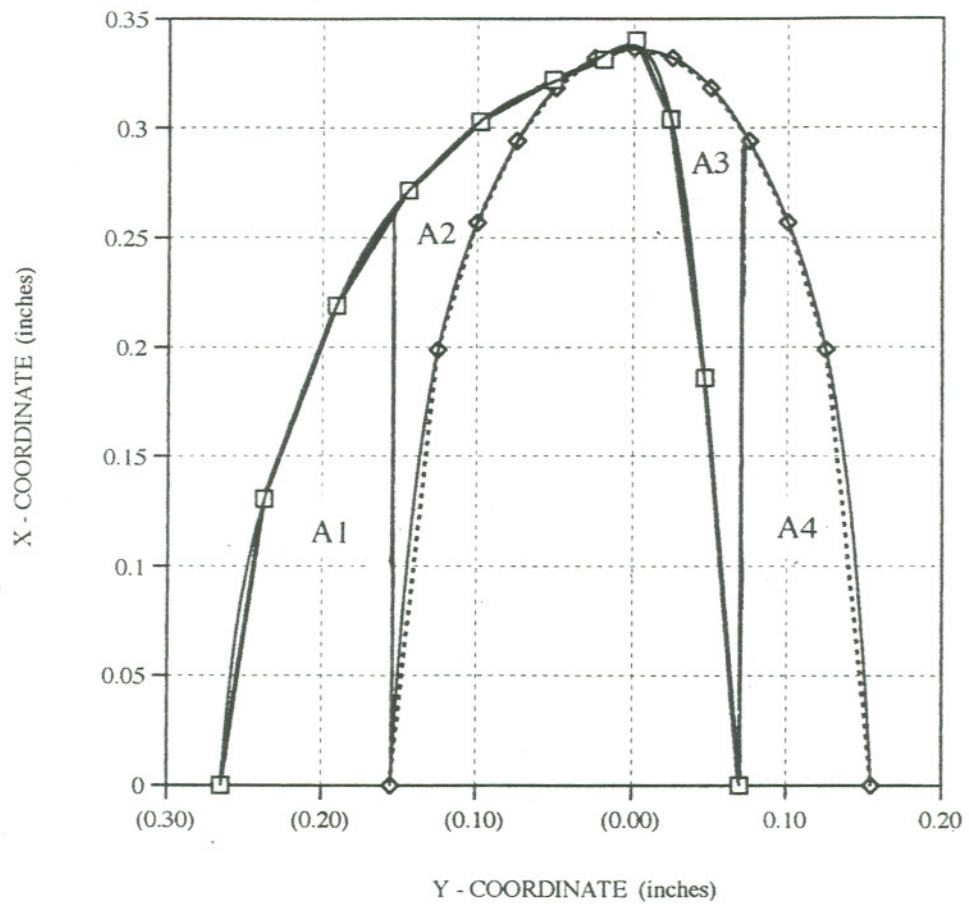
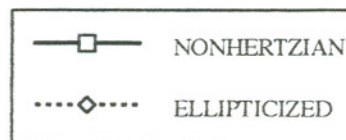


Figure 4.5 Non-Hertzian and ellipticized contact patch geometry for position #2 at a wheel load of 26,535 pounds.



A1 = 0.0187 in²

A2 = 0.0073 in²



A3 = 0.0087 in²

A4 = 0.0178 in²

Figure 4.6 Polynomial curve fits and ANI for ellipticized and non-Hertzian contact of position #2 at a wheel load of 26,535 pounds.

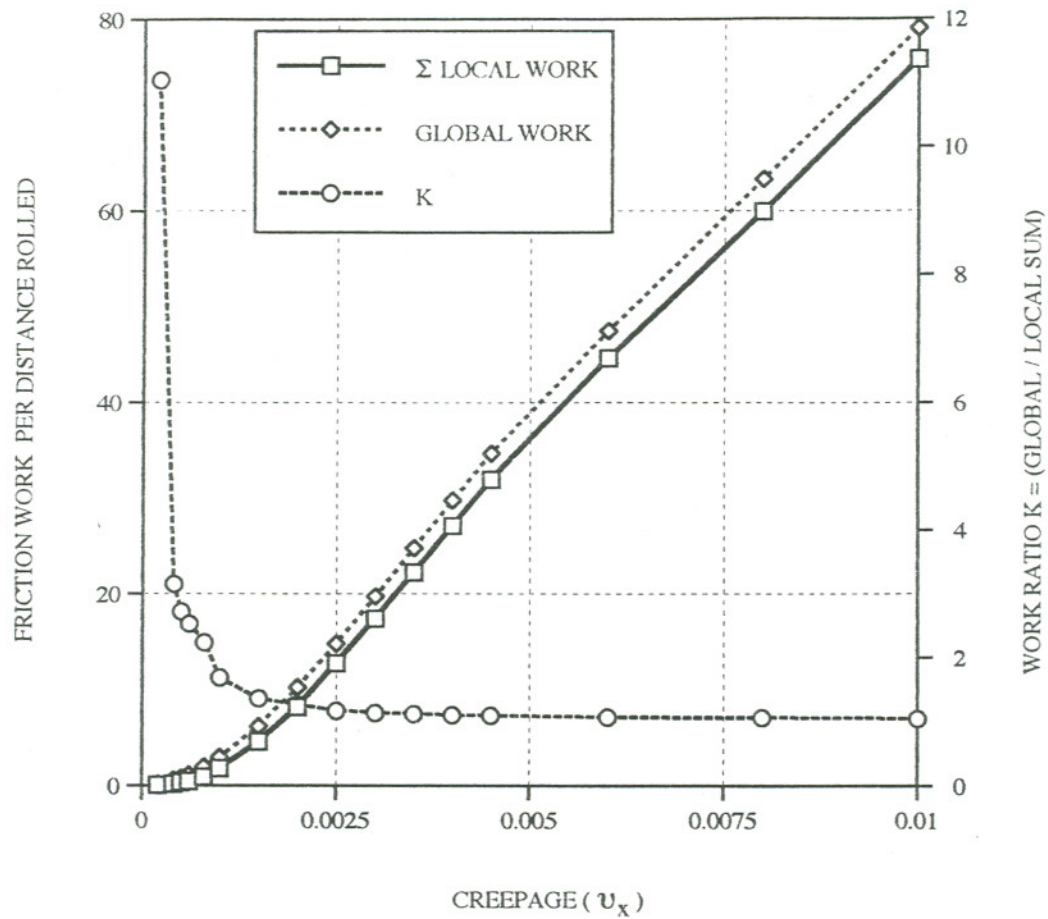


Figure 4.7 Non-Hertzian contact patch friction work comparison of local summation to global work (position #2, load = 26,535 pounds, $v_y = \phi = 0.0$).

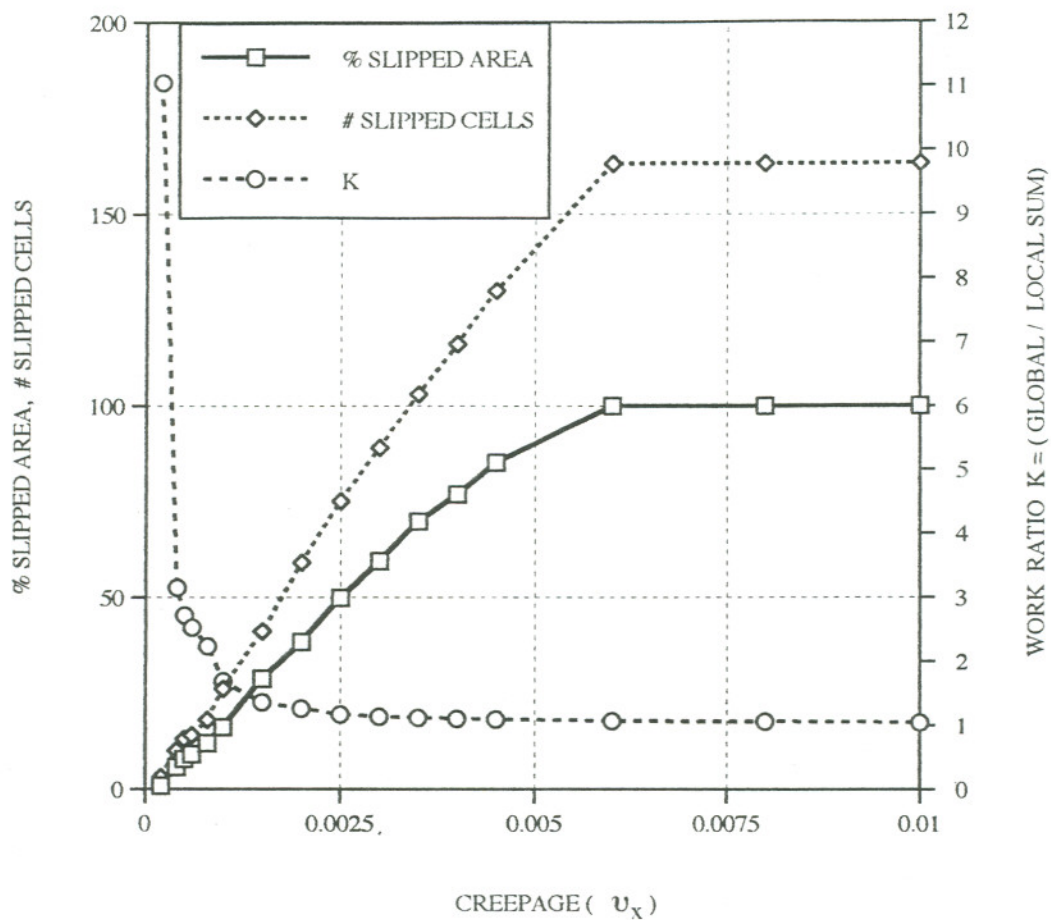


Figure 4.8 Non-Hertzian contact patch creepage effects on slip region (position #2, load = 26,535 pounds, $v_y = \phi = 0.0$).

CHAPTER 5

CONCLUSIONS

In this study, a numerical investigation of wheel-rail contact behavior was carried out. The numerical study of both Hertzian and non-Hertzian contact geometries, can be broadly divided into three main parts: generalized creep force - creepage behavior; ellipticized non-Hertzian contacts; and global and local contact patch friction work distributions. The results obtained in this study lead to the following conclusions:

- (1) Generalized creep force - creepage functions which were predominantly hyperbolic tangent in form provided a good approximation of creep force - creepage behavior over a wide range of tangent track operating conditions.
- (2) Computations of creep force using the generalized approximating functions were on the order of 8 times faster than those predicted by using the "very fast" algorithm of Shen, Hendrick and Elkins [57].
- (3) Computations of creep force using the generalized approximating functions were within 8% of those predicted using the "exact" theory of Kalker.
- (4) The ratio of peak pressures between non-Hertzian and ellipticized contacts was found to be independent of wheel load and equal to a value of 1.3 for the new 136RE X AAR1-B geometry.
- (5) The ellipticized non-Hertzian contact patch aspect ratio was found to be load independent.

- (6) The creep force behavior for non-Hertzian contacts may be accurately predicted by an ellipticized contact treated with classical Hertzian analysis, provided that the geometric distortion (Γ) is below 64.4%.
- (7) A generalized global contact patch friction work function was developed which provided a good approximation of the friction work - creepage behavior over a wide range of tangent track operating conditions.
- (8) Global values of contact patch friction work approach those of the local work summation as creepage values were increased.
- (9) The distribution of shear traction and slippage within a non-Hertzian contact were found to be very non-uniform.
- (10) The local contact patch friction work within non-Hertzian contacts was found to be very non-uniform and was shown to result in a bi-modal work distribution.

CHAPTER 6

SUGGESTIONS FOR FUTURE WORK

This investigation has raised several interesting questions regarding the behavior of Hertzian and non-Hertzian wheel - rail contacts. Some of the subject areas that could be explored in future research - studies are as follows:

- (1) Attempt to obtain a completely generalized set of creep force - creepage approximating functions. This could be realized by extending the current analysis procedures for a larger range of a/b ratio in order to describe adequately the coefficient dependence on patch aspect ratio, and by accounting for the influence of spin parameter χ_z utilizing a similar process.
- (2) Perform an experimental investigation into the geometric behavior of non-Hertzian contacts in order to verify the predictive capabilities of COUNTAC1. This could be accomplished under the static conditions using different scale models of wheel - rail profiles with known curvatures, and by utilizing prescaled color encapsulated pressure sensitive film. An alternative approach would be to use an electronic tactile pressure detecting system such as the Tekscan™ device.
- (3) Obtain a wide variety of non-Hertzian contact patch geometries for both new and worn wheel-rail profiles and test the applicability of using the ellipticized tangential results in place of the true non-Hertzian solution over a wider range of Γ . In addition, test the peak pressure ratio of non-Hertzian to ellipticized in order to check the generality of the constant value of $4/3$ obtained in this study.

- (4) Locomotive wheel slip and correction systems are basically designed to minimize wheel slip. Unless wheel slip is detected and corrected immediately, the wheels would accelerate and spin out of control [133]. The control system necessary for this balanced operation utilizes inputs from both the adhesion - creepage as well as creepage - velocity curves. It is suspected that in both the modeling of this process, as well as during its real time operation, the generalized creep force - creepage approximations as well as percent slipped area data for different patches resulting from various wheel-rail geometries would prove beneficial and their utility in this regard should be explored.
- (5) Attempt to obtain a completely generalized global friction work approximating function by extending the parameter range of the current study to include a wider range of aspect ratio, as well as the "lifting" behavior of the spin parameter χ_z .
- (6) In order to better understand the development of worn wheel - rail profiles and the influence of various rail grinding practices on surface degradation, local contact patch work distributions for different sets of typical curvatures could be systematically computed and analyzed. For certain regimes of contact this could necessitate the need to revive the CONFORM algorithm of B. Paul [75], as the contacts would no longer be counterformal.
- (7) Significant effort has been invested into the study of white etching layer (WEL) in rolling - sliding systems, however the basic questions regarding the mechanisms responsible for its development remain unanswered. Of specific dispute, is the existence of a thermal phase transformation process [31, 110-113]. By using the frictional work distributions for Hertzian and non-Hertzian contact geometries as heat flux boundary conditions, a thermal - mechanical finite element analysis is

recommended. This approach is expected to provide temperature profile data useful for helping resolve the role of thermal transformations under certain rolling - sliding conditions.

- (8) By incorporating the non-Hertzian contact patch pressure and traction distributions as boundary conditions into an elastic-plastic finite element analysis near the rail gauge corner, subsurface stress distributions can be obtained which would assist in understanding the development of rail shells (subsurface stress concentrations). To date only rectangular or "equivalent" Hertzian contact patch areas have been assumed in this type of FEA work [116].

REFERENCES

- [1] Office of Technology Assessment, *An Evaluation of Railroad Safety*, U.S. Government Printing Office, Washington, D.C., 1978.
- [2] Pilkey, W. D., "Review and Summary of Computer Programs for Railway Vehicle Dynamics", Technical Report No. FRA/ORD - 81/17, PB810183857, NTIS, Springfield, VA., February, 1981.
- [3] Wickens, A.H., "Non-Linear Dynamics of Railway Vehicles", Vehicle System Design, vol. 15, no. 5, 1986, pp. 289-301.
- [4] Hawthorne, V.T. and Manos, W.P., "Railroad Vehicle Analysis Models for the Personal Computer", paper no. 85-WA/RT-10, ASME Winter Annual Meeting, Chicago, IL, November, 1985.
- [5] Abbott, P.W., Morosow, G., and Macpherson, J., "Track-Train Dynamics", SAE paper no. 751058, S.A.E. Conference, Detroit, MI, 1975.
- [6] Rama Chandran, P.V., Gilchrist, A.J., El Madany, M.M., and Cappel, K., "Validation of rail vehicle system dynamic models", International Journal of Vehicle Design, vol. 3, no. 2, 1982, pp. 202-233.
- [7] Bell, C.E., Horak, D., and Hendrick, J.K., "Stability and Curving Mechanics of Rail Vehicles", Journal of Dynamic Systems, Measurement, and Control, vol. 103, no. 9, September, 1981, pp. 181-189.
- [8] Martin, L.M., and Giménez, J.G., "Railway Vehicle Modelling by the Constraint Equation Method", Vehicle Systems Dynamics, vol. 13, no. 5, 1984, pp. 281-287.
- [9] Sinha, P.K., Wormley, D.N., and Hendrick, J.K., "Rail Passenger Vehicle Lateral Dynamic Performance Improvement Through Active Control", Transactions of the ASME, vol. 100, no. 12, December, 1978, pp. 270-283.
- [10] Meijaard, J.P. and DePater, A.D., "Railway Vehicle Systems Dynamics and Chaotic Vibrations", International Journal of Non-Linear Mechanics, vol. 24, no. 1, 1989, pp. 1-17.
- [11] Malstrom, C.W., Heller, R., and Khan, M.S., "Hybrid Computation - An Advanced Computational Tool for Simulating the Non-Linear Dynamic Response of Railroad Vehicles", Advanced Technology in Track-Train Dynamics and Design Conference, Chicago, IL, September, 1977, pp. 241-260.
- [12] Ionescu, T.G. and Spirea, E.A., "Aspects of Experimental Analysis of Locomotive Dynamics", Applied Mechanics Rail Transportation Symposium, ASME Winter Annual Meeting, Chicago, IL, December, 1988, pp. 169-179.

- [13] Cooperrider, N.K. and Law, E.H., "A Survey of Rail Vehicle Testing for Validation of Theoretical Dynamic Analysis", Transactions of the ASME, vol. 100, no. 12, December, 1978, pp. 238-251.
- [14] Cox, J.J., Hendrick, J.K. and Cooperrider, N.K., "Optimization of Rail Vehicle Operating Speed with Practical Constraints", Transactions of the ASME, vol. 100, no. 12, December, 1978, pp. 260-269.
- [15] Xiaogang, Q., "Computer Simulation of Comprehensive Train Action and Motion", Applied Mechanics Rail Transportation Symposium, ASME Winter Annual Meeting, Chicago, IL, December, 1988, pp. 161-168.
- [16] Sparrow, R. W., "Vehicle and Track Dynamics Research on British Railways", Technical Proceedings of the 10th Railroad Engineering Conference, Depaw, NY., September 5-7, 1973, pp. 14-19.
- [17] Wormley, D. N., Hendrick, J. K. and Nagurka, M. L., "Analysis of Rail Transit Vehicle Dynamic Curving Performance", DOT Technical Report, no. UMTA - MA - 06 - 0025 - 84 - 1, PB85-112 845, NTIS, Springfield, VA, June, 1984, pp. 1-232.
- [18] Bell, C.E., Horak, D., and Hendrick, J.K., "Stability and Curving Mechanics of Rail Vehicles", Journal of Dynamic Systems, Measurement, and Control, vol. 103, no. 9, September, 1981, pp. 181-189.
- [19] Jingjun, Z. and Fuda, L., "A Simulation Study of Derailment Safety of a Freight Car on Transition Curves", Applied Mechanics Rail Transportation Symposium, ASME Winter Annual Meeting, Chicago, IL, December, 1988, pp 119-126.
- [20] Blader, F.B., Elkins, J.A., Wilson, N.G., and Klauser, P.E., "Development and Validation of a General Railroad Vehicle Dynamics Simulation (NUCARS)", 1989 IEEE/ASME Joint Railroad Conference, Philadelphia, PA, April, 1989, pp. 39-46.
- [21] Kortüm, W., "Analysis of Railway Vehicle System Dynamics with the Multibody Program MEDYNA:", 1990 ASME/IEEE Joint Railroad Conference, Chicago, IL, April, 1990, pp. 57-63.
- [22] Gilchrist, a. D. and Brickle, B. V., "A Re-Examination of the Proneness to Derailment of a Railway Wheel-Set", Journal of Mechanical Engineering Science, vol. 18, no. 3, 1976, pp. 131-141.
- [23] Blader, F. B., "Assessing Proximity to Derailment from Wheel/Rail Forces: A Review of the State of the Art", in Rail Transportation, ASME Winter Annual Meeting, Chicago, IL, December, 1989, pp. 179-188.
- [24] Elkins, J. A. and Wilson, N. G., "Rail Rollover Derailments Caused by Large Truck Turning Moments on Improperly Lubricated Track", in Rail Transportation, ASME Winter Annual Meeting, Chicago, IL, December, 1989, pp. 13-18.

- [25] Sweet, L. M. and Karmel, A., "Evaluation of Time-Duration Dependent Wheel Load Criteria for Wheelclimb Derailment", Journal of Dynamic Systems, Measurement and Control, vol. 103, no. 9, September, 1981, pp. 219-227.
- [26] Hayes, W. F. and Tucker, J. G., "Wheelset-track Resonance as a Possible Source of Corrugation Wear", Wear, vol. 144, no. 2, 1991, pp. 211-226.
- [27] Cooperrider, N. K., Law, E. H., Hull, R., Kadala, P. S. and Tuten, J. M., "Analytical and Experimental Determination of Nonlinear Wheel/Rail Geometric Constraints", Railroad Equipment Dynamics Symposium, 1976 Joint ASME-IEEE Railroad Conference, Chicago, IL, April, 1976, pp. 41-69.
- [28] Duffek, W., "Contact Geometry in Wheel Rail Vehicles", Proc. Int. Symp. on Contact Mechanics and Wear of Rail/Wheel Systems I, Vancouver, B.C., July, 1982, University of Waterloo Press, Waterloo, Ontario, 1983, pp. 161-181.
- [29] Tevaarwerk, J. L., "Traction in Lubricated Contacts", Proc. Int. Symp. on Contact Mechanics and Wear of Rail-Wheel Systems I, Vancouver, B.C., July, 1982, University of Waterloo Press, Waterloo, Ontario, 1983, pp. 121-132.
- [30] Elkins, J. A. and Allen, R. A., "Testing a Transit Vehicle for Wheel and Rail Wear", A.S.M.E. Transactions, Paper 81-WA/DSC, 1981.
- [31] Johnson, K. L., Contact Mechanics, Cambridge University Press, Cambridge, 1985.
- [32] Hashemi, J., and Paul, B., "Contact Stresses in bodies with Arbitrary Geometry, Applications to Wheels and Rails," Technical Report no. 7, FRA/ORD-79/23, PB 299409, Contract DOT-OS-60144, NTIS, Springfield, VA, April, 1979.
- [33] Kalker, J. J., "On the rolling contact of two elastic bodies in the presence of dry friction", Ph. D. Thesis, Delft University, Delft, The Netherlands, 1967.
- [34] de Pater, A.D., "On the reciprocal pressure between two elastic bodies in contact", in Rolling Contact Phenomena, Ed. by J. Birdwell, Elsevier, New York, 1964.
- [35] Liu, C., "Rolling Contact with Friction and Non-Hertzian Pressure Distributions", Ph.D. Thesis, Department of Mechanical Engineering and Applied Mechanics, University of Pennsylvania, Philadelphia, PA., 1988.
- [36] Hertz, H., "On the contact of rigid elastic solids and on hardness", Verhandlungen des Vereins zur Beförderung des Gewerbefleisses, Leipzig, Nov, 1882. (translation of the original)
- [37] Timoshenko, S., and Goodier, J.N., Theory of Elasticity, 3rd Ed., McGraw-Hill, New York, 1951, pp. 377-382.

- [38] Reynolds, O. "On Rolling Friction", Philosophical Transactions of the Royal Society, London, vol. 166, no. 1, 1876, pp. 155-174.
- [39] Carter, F. W., "On the Action of a Locomotive Driving Wheel", Proceedings of the Royal Society, vol. 112, no. 1, 1926, p. 151.
- [40] Paul, B., "A Review of Rail-Wheel Contact Stress Problems," Technical Report no. 1, FRA/ORD-76 141, PB 251238, Contract DOT-OS-40093, April, 1975.
- [41] Johnson, K. L., "The Effect of a Tangential Contact Force Upon the Rolling Motion of an Elastic Sphere on the Plane", ASME Journal of Applied Mechanics, vol. 25, no. 2, 1958, p. 339.
- [42] Johnson, K. L., "The Effect of Spin Upon the Rolling Motion of an Elastic Sphere on a Plane", ASME Journal of Applied Mechanics, vol. 25, no. 2, 1958, p. 332.
- [43] Johnson, K. L., "The Influence of Elastic Deformation upon the Motion of a Ball Rolling Between Two Surfaces", Proceedings Institution of Mechanical Engineers, vol. 173, no. 4, 1953, p. 795.
- [44] Kalker, J. J., "Wheel-Rail Rolling Contact Theory", Wear, vol. 144, no. 2, 1991, pp. 243-261.
- [45] Vermeulen, P. J. and Johnson, K. L., "Contact of Non-spherical Elastic Bodies Transmitting Tangential Forces", ASME Journal of Applied Mechanics, vol. 31, no. 2, 1964, p. 338.
- [46] Haines, D. J., and Ollerton, E., "Contact Stress Distributions on Elliptical Contact Surfaces Subjected to Radial and Tangential Forces", Proceedings, Institution of Mechanical Engineers, vol. 177, no. 1, 1963, p. 98.
- [47] Fries, R.H., Cooperrider, N.K., and Law, E.H., "Experimental Investigation of Freight Car Lateral Dynamics", Journal of Dynamic Systems, Measurement, and Control, vol. 103, no. 9, September, 1981, pp. 201-210.
- [48] Johnson, K. L., "The Effect of a Tangential Contact Force Upon the Rolling Motion of an Elastic Sphere on a Plane", ASME Journal of Applied Mechanics, vol. 25, no. 2, 1958, p. 339.
- [49] Liu, C. and Paul, B., "Fully Developed Sliding of Rough Surfaces", Applied Mechanics Rail Transportation Symposium, ASME Winter Annual Meeting, Chicago, IL, December, 1988, pp. 77-86.
- [50] Kalker, J. J., "The Computation of 3-D Rolling Contact with Dry Friction", International Journal of Numerical Methods in Engineering, vol. 14, no. 9, 1979, pp. 1293-1307.

- [51] Duvaunt, G. and Lions, J.L. Les inéquations en mécanique et en physique, Paris, Dunod, 1972.
- [52] Kalker, J. J., Three Dimensional Elastic Bodies in Rolling Contact, Kluwer Academic Publishers, Dordrecht, The Netherlands, 1990.
- [53] Goree, J. G., "User's Manual for Kalker's "Exact" Nonlinear Creep Theory", Technical Report, FRA/ORD - 78/50, PB 287 472, NTIS, Springfield, VA., August, 1978.
- [54] Kalker, J. J., "A Fast Algorithm for the Simplified Theory of Rolling Contact", Vehicle System Dynamics, vol. 11, no. 1, 1982, pp. 1-13.
- [55] Goree, J. G. and Law, E. H., "User's Manual for Kalker's Simplified Nonlinear Creep Theory", Technical Report, FRA/ORD - 78/06, PB 279503, NTIS, Springfield, IL, December, 1977.
- [56] Hung, Le The, "Normal - und Tangentialpannungsberechnung beim rollenden Kontakt für Relationskörper mit nichtelliptischen Kontaktflächen", Fortschrittberichte VDI, vol. 12, no. 87, 1987.
- [57] Shen, Z. Y., Hendrick, J. K., and Elkins, J. A., "A Comparison of Alternative Creep-force models for Rail Vehicle Dynamic Analysis" in : The Dynamics of Vehicles, Ed. by J.K. Hendrick, Proceedings of the 8th IAVSD Symposium, MIT, Cambridge, MA, Swets and Zeitlinger, Lisse, The Netherlands, 1984.
- [58] Kalker, J. J., "Simplified Theory of Rolling Contact", Delft Progress Report, Series C, vol. 1, no. 1, 1973, pp. 1-10.
- [59] Elkins, J. A. and Elckoff, B. M. "Advances in Nonlinear Wheel-Rail Prediction Methods and Their Validation", Journal of Dynamic Systems, Measurement, and Control, vol. 104, no. 2, June, 1982, pp. 308-406.
- [60] Boyd, P. J., Zaiko, J. P., and Jordan, W. L., "Wheel/Rail Force Measurement at the Washington Metropolitan Area Transit Authority - Phase II, Test Report," DOT - TSC - UMTA - 83 - 1, NTIS, Springfield, VA, June, 1983.
- [61] Paul, B., "A Review of Rail-Wheel Contact Stress Problems," Technical Report No. 1, FRA/ORD-76 141, PB 251238, Contract DOT-OS-40093, NTIS, Springfield, VA, April, 1975.
- [62] Woodward, W., and Paul, B., "Contact Stresses for Closely Conforming Bodies - application to Cylinders and Spheres," Technical Report no. 2, DOT/TST/77-48, PB 271033/AS, Contract DOT-OS-40093, NTIS, Springfield, VA, December, 1976.

- [63] Paul, B., and Hashemi, J., "An Improved Numerical Method for Counterformal contact Stress Problems," Technical Report no. 3, FRA/ORD-78/27, PB286228, Contract DOT-OS-60144, NTIS, Springfield, VA, July, 1977.
- [64] Paul, B., and Hashemi, J., "User's Manual for Program COUNTACT COUNTERformal contact stress problems", Technical Report no. 4, FRA/ORD-78/27, PB286097, Contract DOT-OS-60144, NTIS, Springfield, VA, September, 1977.
- [65] Paul, B., and Hashemi, J., "User's Manual for Program CONFORM (CONFORMal contract stresses between wheels and rails", Technical Report no. 5, FRA/ORD-78/40, PB288927, Contract DOT-OS-60144, NTIS, Springfield, VA, June, 1978,.
- [66] Paul, B., and Hashemi, J., "Rail-Wheel Geometry Associated with Contact Stress Analysis," Technical Report no. 6, FRA/ORD-78/41, PB80142656, Contract DOT-OS-60144, NTIS, Springfield, VA, September, 1979,.
- [67] Paul, B., and Hashemi, J., "Numerical Determination of Contact Pressures Between Closely Conforming Wheels and Rails", Technical Report no. 8, FRA/ORD-79/41, PB80120462, Contract DOT-OS-60144, NTIS, Springfield, VA, July, 1979.
- [68] Singh, K. P., and Paul, B., "A Method for Solving Ill-Posed Integral Equation of the First Kind," Computer Methods in Applied Mechanics and Engineering, vol. 2, no. 3, 1973, 339-348.
- [69] Singh, K. P., and Paul, B., "Numerical Solution of Non-Hertzian Elastic Contact Problems", ASME Journal of Applied Mechanics, Series E. vol. 96, no. 2, June, 1974, pp. 484-490.
- [70] Singh, K. P., and Paul, B., "Stress Concentration in Crowned Rollers," ASME Journal of Engineering for Industry, Series B., vol. 97, no. 3, 1975, pp. 990-994.
- [71] Paul, B., K. P. Singh., and Woodward, W., "Contact Stresses for Multiply-Connected Regions-The Case of Pitted Spheres," Proceedings of the Symposium on the Mechanics of Deformable bodies, Delft University Press, Delft, The Netherlands, 1975, pp. 264-281.
- [72] Paul, B., "A Review of Rail-Wheel Contract Stress Problems," Proceedings of the Symposium Railroad Track Mechanics, Pergamon Press, 1978, Ed. by A. Kerr, pp. 323-351.
- [73] Paul, B., and Hashemi, J., "An Improved Numerical Method for Counterformal Contact Stress Problems.:", in Computational Techniques for Interface Problems, AMD-vol. 30, Ed. by K.C. Park and D.K. Gartlung, American Society of Mechanical Engineers, N.Y., 1978, pp. 165-180.

- [74] Paul, B., "Description of Program COUNTACT," in Review of Track-Train Dynamics Computer Programs, A Report to Federal Railroad Administration by W. Pilkey, 1980.
- [75] Paul, B., "Description of Program CONFORM," in Review of Track-Train Dynamics Computer Programs, A Report to Federal Railroad Administration by W. Pilkey, 1980.
- [76] Paul, B., and Hashemi, J., "Contact Pressures on Closely Conforming Elastic Bodies", in Solid Contact and Lubrication, AMD-Vol. 39, Ed. by H. S. Cheng and L. M. Keer, American Society of Mechanical Engineers, NY., 1980, pp. 67-78.
- [77] Paul, B., and Hashemi, J., "Contact Geometry Associated with Arbitrary Wheel and Rail Profiles,," in The General Problem of Rolling Contact., AMD-Vol 40, Ed. by A. L. Browne and N. T. Tsai, American society of Mechanical Engineers, NY., 1980, pp. 93-105.
- [78] Paul, B., "Fundamental Studies Related to Wheel-Rail Contact Stress", Final Report, FRA / ORD - 81/05, PB81-1943200, NTIS, Springfield, VA, January, 1981.
- [79] Kalker, J. J., "Wheel-rail Wear Calculations with the Program CONTACT", in Proc. Int. Symp. on Contact Mechanics and Wear of Rail/Wheel Systems II, Kingston, RI, July, 1986, University of Waterloo Press, Waterloo, Ontario, 1987, pp. 3-26.
- [80] Kalker, J. J., "Two Algorithms for the Contact Problem, in Elastostatics" in Proc. Int. Symp. on Contact Mechanics and Wear of Rail-Wheel Systems I, Vancouver, B.C., July, 1982, University of Waterloo Press, Waterloo, Ontario, 1983, pp. 101-120.
- [81] Greenwood, J. A., "The Contact of Real Surfaces" in Proc. Int. Symp. on Contact Mechanics and Wear of Rail-Wheel Systems I, Vancouver, B.C., July, 1982, University of Waterloo Press, Waterloo, Ontario, 1983, pp. 21-35.
- [82] Greenwood, J. A. and Tripp, J. H., "The Elastic Contact of Rough Spheres", ASME Journal of Applied Mechanics, Vol. 34, no. 1, 1967, pp. 153-159.
- [83] O'Conner, J. J., and Johnson, K. L., "The Role of Surface Asperities in Transmitting Tangential Forces Between Metals", Wear, vol. 6, no. 1, 1963, p. 118.
- [84] Krause, H., and Poll, G., "The Influence of Real Material and System Properties on the Traction/Creep Relationships in Rolling Contact", Proc. Int. Symp. on Contact Mechanics and Wear of Rail-Wheel Systems I, Vancouver, B.C., July 1982, University of Waterloo Press, Waterloo, Ontario, 1983, pp. 353-372.

- [85] Beaglely, T. M., McEwen, I. J. and Pritchard, C., "Wheel/Rail Adhesion - The Influence of Railhead Debris", Wear, vol. 33, no. 1, 1975, pp. 141-152.
- [86] Pearce, T. G., and Rose, K. A., "Tangential Force - Creepage Relationships in Theory and Practice", Proc. Int. Symp. on Contact Mechanics and Wear of Rail-Wheel Systems I, Vancouver, B.C., July, 1982, University of Waterloo Press, Waterloo, Ontario, 1983, pp. 183-196.
- [87] Gilchrist, A. O., "The Effect of Surface Condition on Rolling Contact Behavior", British Rail Research Laboratories, Derby, England, April 1976.
- [88] Haque, I., and Law, E.H., "Estimation of Creep Coefficients from Tests of the SOAC Vehicle on the Roll Dynamics Unit", Proc. Int. Symp. on Contact Mechanics and Wear of Rail-Wheel Systems I, Vancouver, B.C., July 1982, University of Waterloo Press, Waterloo, Ontario, 1983, pp. 229-245.
- [89] Wang, B. T. and Fries, R. H., "Determination of Creep Force, Moment and Work Distribution in Rolling Contact with Slip", Applied Mechanics Rail Transportation Symposium, ASME Winter Annual Meeting, December, 1988, pp. 19-27.
- [90] Fries, R.H. and Davila, C.G., "Wheel Wear Predictions for Tangent Track Running", Journal of Dynamic Systems, Measurement and Control, vol. 109, no. 3, 1987, pp 397-404.
- [91] Private communication with Greg Saxton, Gunderson, Inc., 1993.
- [92] Johnson, K. L., "Tangential Traction and Micro-Slip in Rolling Contact", in Rolling Contact Phenomena, Ed. by J. Bidwell, 1962, Elsevier Publishing Co., The Netherlands, pp. 6-24.
- [93] Kennedy, F. E., "Thermal and Thermomechanical Effects in Dry Sliding", Wear, vol. 100, no. 3, 1984, pp. 453-476.
- [94] Ashby, M. F., Abulawi, J. and Kong, H. S., "Temperature Maps for Frictional Heating in Dry Sliding", Tribology Transactions, vol. 34, no. 4, 1991, pp. 577-587.
- [95] Uetz, H. and Föhl, J. "Wear as an Energy Transformation Process", Wear, vol 49, no. 2, 1978, pp. 253-264.
- [96] Spurr, R. T., "Temperatures Reached During Sliding", Wear, vol. 55, no. 2, 1979, pp. 289-293.
- [97] Ling, F. F., Surface Mechanics, John Wiley and Sons Publishers, New York, 1973, pp. 208-212.

- [98] Kennedy, F. E., "Thermomechanical Phenomena in High Speed Rubbing", Wear, vol. 59, no. 1, 1980, pp. 149-163.
- [99] Burton, R. A., "Thermal Deformation in a Frictionally Heated Contact", Wear, vol. 59, no. 1, 1980, pp. 1-20.
- [100] Kannel, J. W., and Barber, S. A., "Estimate of Surface Temperatures During Rolling Contact", Tribology Transactions, vol. 32, no. 3, 1989, pp. 305-310.
- [101] Ting, B. Y., and Winer, W. O., "A Proposed Thermomechanical Wear Theory", in Approaches to Modeling of Friction and Wear, Eds. F. F. Ling and C.H.T. Pan, Springer-Verlag Publishers, 1988, pp.125-131.
- [102] Barber, J. R., "The Transient Thermoelastic Contact of a Sphere Sliding on a Plane, Wear, vol. 59, no. 1, 1980, pp. 21-29.
- [103] Johnson, K. L., "Inelastic Contact: Plastic Flow and Shakedown", Proc. Int. Symp. on Contact Mechanics and Wear of Rail/Wheel Systems I, Vancouver, B.C., July, 1982, University of Waterloo Press, Waterloo, Ontario, 1983, pp. 79-101.
- [104] Bower, A. F., "The Influence of Strain Hardening on the Cumulative Plastic Deformation Caused by Repeated Rolling and Sliding Contact", Cambridge University Engineering Department Report CUED / C-Mech / TR.39, 1987, pp. 1-30.
- [105] Johnson, K. L., "Plastic Flow Residual Stresses and Shakedown in Rolling Contact", Proc. Int. Symp. on Contact Mechanics and Wear of Rail/Wheel Systems II, Kingston, RI, July, 1986, University of Waterloo Press, Waterloo, Ontario, 1987, pp. 83-97.
- [106] Kalousek, J., Rosval, G. and Ghonem, H., "Lateral Creepage and its Effect on Wear in Rail Wheel Interface", Proc. Int. Symp. on Contact Mechanics and Wear of Rail/Wheel Systems I, Vancouver, B.C., July, 1982, University of Waterloo Press, Waterloo, Ontario, 1982, pp. 373-393.
- [107] Barber, J.R., "Thermal Effects in Elastic Contact", Proc. Int. Symp. on Contact Mechanics and Wear of Rail/Wheel Systems II, Kingston, RI, July, 1986, University of Waterloo Press, Waterloo, Ontario, 1987, pp. 41-57.
- [108] McEwen, I.J., and Harvey, R.F., "Full Scale Wheel-on-Rail Wear Testing: Comparisons with Service Wear and a Developing Theoretical Predictive Method", Lubrication Engineering, vol. 41, no. 2, Feb. 1985.
- [109] Bolton, P., "Wear of BSII Rail Steels in Rolling/Sliding Contact with class "D" tyre Steel", British Rail Technical note no. TN MET 21, February, 1980.

- [110] Clayton, P. and Allery, M.B., "Metallurgical Aspects of Surface Damage Problems in Rails", Canadian Metallurgical Quarterly, vol. 21, no. 1, 1982, pp. 31-46.
- [111] Griffiths, B.J., "Mechanisms of White Layer Generation with Reference to Machining and Deformation Processes", Journal of Tribology, vol. 109, no. 7, 1987, pp. 525-530.
- [112] Newcomb, S.B., and Stobbs, W.M., "A Transmission Electron Microscopy Study of the White-Etching Layer on a Rail Head", Material Science Engineering, vol 66, no. 4, 1984, pp. 195-204.
- [113] Dikshit, V., Clayton, P. and Christensen, D., "Investigation of Rolling Contact Fatigue in a Head-Hardened Rail", Wear, vol. 144, no. 1, 1991, pp. 89-102.
- [114] Frederick, C.O., "A Rail Corrugation Theory", Proc. Int. Symp. on Contact Mechanics and Wear of Rail/Wheel Systems II, Kingston, RI, July, 1986, University of Waterloo Press, Waterloo, Ontario, 1987, pp. 181-212.
- [115] Lieurade, H.P., Deroche, R.Y., Derboule, B., and Conti, R., "A Study of the Shelling Mechanism of Rails" Proc. Int. Symp. on Contact Mechanics and Wear of Rail/Wheel Systems II, Kingston, RI, July, 1986, University of Waterloo Press, Waterloo, Ontario, 1987 pp. 379-396.
- [116] Hellier, A.K., Corderoy, D.J.H., and McGirr, M.B., "A Study of Subsurface Rail/Wheel Contact Stresses with Application to Modelling Rail Fatigue", Proc. Int. Symp. on Contact Mechanics and Wear of Rail/Wheel Systems II, Kingston, RI, July, 1986, University of Waterloo Press, Waterloo, Ontario, 1987, pp. 421-434.
- [117] Meekisho, L.L., "Thermal-Stress Analysis of contact Problems by the Finite Element Method", Ph.D. Thesis, Carleton University, Ottawa, Canada, 1988.
- [118] Kennedy, F.E., Colin, F., Floquet, A., and Glovsky, R.P., "Improved Techniques for Finite Element Analysis of Sliding Surface Temperatures", Proc. 10th Leeds - Lyon Symposium on Tribology, Butterworths, London, 1984.
- [119] Tournay, H.M. and Nulder, J.M., "Wheel/Rail Interaction: The Transition from the Wear to the Stress Regime", Proc. Int. Symp. on Contact Mechanics and Wear of Rail/Wheel Systems III, Vancouver, B.C., July, 1993, University of Waterloo Press, Waterloo, Ontario, 1995, p. 201.
- [120] Private communication with Dr. Burton Paul, Univ. of Pennsylvania, 1993.
- [121] IMSL, Library Vol. 1, Chapter 1 & 2, IMSL, Inc., 14141 Southwest Freeway, Sugarland, Texas, 1991.

- [122] Private Communication with Wes Smith, Shattuck Hall, Portland, State University, Portland, OR, 1993.
- [123] Faries, J.D. and Burden, R.L., Numerical Methods, PWS-Kent Publishing Co., Boston, MA, 1993.
- [124] Varga, R., Matrix Iterative Techniques, J. Wiley & Son, New York, 1962.
- [125] Jandel Scientific Corp., 2591 Kerner Blvd., San Rafael, CA, 94901, 1993.
- [126] Wang, Y., Yan, M., Li, X. and Lei, T., "Frictional Temperature Field and Wear Behavior of Steel 52100 with Different Microstructures", Journal of Tribology, vol. 116, no. 4, p. 255-259, 1994.
- [127] Bolton, P.J. and Clayton, P., "Rolling-Sliding Wear Damage in Rail and Tyre Steels", Wear, vol. 93, no. 1, p. 145-165, 1984.
- [128] Harder, R.F. and Meekisho, L.L., "Generalized Creep Force - Creepage Behavior for Hertzian and Non-Hertzian Wheel-Rail Contact Geometries", Journal of Engineering for Industry, (in press).
- [129] AREA Manual for Railway Engineering, volume 92, 1991, p. 49.
- [130] Fischer, R.C. and Ziebur, A.D., Calculus and Analytic Geometry, 3rd Edition, Prentice-Hall Publishers, Englewood Cliffs, N.J., 1975.
- [131] Duffek, W. and Jaschinski, A., "Efficient Implementation of Wheel-Rail Contact Mechanics in Dynamic Curving", in The Dynamics of Vehicles, Ed. by A.H. Wickens, Proc. of the 7th IAVSD Symposium, Cambridge, U.K., Swets and Zeitlinger, Lisse, The Netherlands, 1982.
- [132] Pearce, T.G. and Sherratt, M.D., "Prediction of Wheel Profile Wear", Wear, vol. 144, no. 1, 1991, pp. 343-351.
- [133] Logston, C.G. and Itami, G.S., "Locomotive Friction-Creep Studies", Journal of Engineering for Industry, vol. 102, no. 3, 1980, pp. 275-281.

APPENDIX A

Fortran Source Code for Modified COUNTAC2

```

C PROGRAM COUNTACT-2
C BY J. HASHEMI, JULY 1977, MODIFIED BY R.F. HARDER, JUNE 1993
C FOR BATCH MODE OPERATION WITH IMSL SUBROUTINES DL2TRG AND
DLFSRG
C REPLACING LEQTIF FOR IBM 486 OPERATION.
C FOR STRESS ANALYSIS OF COUNTERFORMAL CONTACT OF TWO BODIES
HAVING
C TWO AXIS OF SYMMETRY IN CONTACT PATCH.
C FOR UP TO 50 EQUATIONS (FIELD POINTS).
C PROGRAM REQUIRES THE FOLLOWING USER-SUPPLIED SUBROUTINE.
cc *****
cc *** good for hertzian contacts! ***
cc *****
CC
CC *****
CC *** NOTICE! BE SURE TO ADJUST A AND B IN INSEP SUBROUTINE! ***
CC *****
IMPLICIT REAL*8 (A-H,O-Z)
CC character*4 ipfn,opfn
DIMENSION B(100,100),F(100,1),WKAREA(100),X SX(100),YSY(100)
DIMENSION P(20,5),XB(20),YB(20),HX(20),HY(20),XBN(20),YBN(20)
DIMENSION AR(20)
DIMENSION TITLE(20)
CC EXTERNAL LSLRG
cc write(*,38)
cc read(*,*)ipfn
cc write(*,39)
cc read(*,*)opfn
open(unit=5,file='count2.dat',status='old')
open(unit=6,file='count2.out',status='old')
READ (5,226) TITLE
READ (5,225) IAI,IDGT,ITM,NC
READ (5,218) E1,ANU1,E2,ANU2
READ (5,225) MX1,MX2,MX3,MX4
READ (5,225) MX,MY
READ(5,218) XX1,XX2,XX3,XX4
READ (5,218) (XB(I),YB(I),I=1,MX)
READ (5,218) EPS,SB
READ (5,218) D
C *** WRITE INPUT DATA.
*****
WRITE (6,227) (TITLE(I),I=1,20)
WRITE (6,219) IAI,IDGT,ITM,NC,eps

```

```
WRITE (6,212) E1,ANU1,E2,ANU2
WRITE (6,220) MX1,MX2,MX3,MX4
WRITE (6,224) XX1,XX2,XX3,XX4
WRITE (6,229) MX,MY,d
PI=3.141592654
CK=(1.-ANU1**2)/(PI*E1)+(1.-ANU2**2)/(PI*E2)
IT=1
DO 4 I=1,MX
4 HY(I)=YB(I)/(MY-.5)
H=XX1/(MX1-.5)
DO 7 I=1,MX1
7 HX(I)=H
IF (MX2.EQ.0) GO TO 15
I=MX1+1
MX12=MX1+MX2
H=XX2/MX2
DO 9 J=I,MX12
9 HX(J)=H
IF (MX3.EQ.0) GO TO 15
J=MX12+1
H=XX3/MX3
MX123=MX12+MX3
DO 11 I=J,MX123
11 HX(I)=H
IF (MX4.EQ.0) GO TO 15
I=MX123+1
H=XX4/MX4
DO 13 J=I,MX
13 HX(J)=H
15 WRITE (6,223) IT
WRITE (6,213)
WRITE (6,214)
WRITE (6,222) (XB(I),YB(I),I=1,MX)
J=0
DO 100 IS=1,MX
XS=XB(IS)
HXS=HX(IS)
HYS=HY(IS)
AR(IS)=HYS*HXS
DO 100 JS=1,MY
YS=HYS*(JS-1)
J=J+1
XSX(J)=XS
YSY(J)=YS
CALL INSEP (XS,YS,FZ)
F(J,1)=(D-FZ)/CK
I=0
DO 100 IFF=1,MX
```



```

XF=XB(IFF)
DO 100 JF=1,MY
YF=HY(IFF)*(JF-1)
I=I+1
IF (J.EQ.1) GO TO 30
IF (IS.EQ.1) GO TO 50
IF (JS.EQ.1) GO TO 70
  B(I,J)=DAOR(XF,YF,XS,YS,HXS,HYS)+DAOR(XF,YF,XS,-YS,HXS,HYS)+
  1DAOR(XF,YF,-XS,YS,HXS,HYS)+DAOR(XF,YF,-XS,-YS,HXS,HYS)
GO TO 100
30 B(I,J)=DAOR(XF,YF,XS,YS,HXS,HYS)
GO TO 100
50 B(I,J)=DAOR(XF,YF,XS,YS,HXS,HYS)+DAOR(XF,YF,XS,-YS,HXS,HYS)
GO TO 100
70 B(I,J)=DAOR(XF,YF,XS,YS,HXS,HYS)+DAOR(XF,YF,-XS,YS,HXS,HYS)
100 CONTINUE
C SOLVE THE SYSTEM OF LINEAR EQUATIONS
N=J
CALL DL2TRG(N,B,IAI,B,IAI,FPVT,WKAREA)
CALL DLFSRG(N,B,IAI,FPVT,F,1,F)
C WRITE THE SOLUTION (PRESSURE DISTRIBUTION).
WRITE (6,211)
WRITE (6,215) (I,XSX(I),YSY(I),F(I,1),I=1,N)
RY=YB(NC)
C CHECK FOR PRESSURE TO BE ALL POSITIVE AND FIND NEW
BOUNDARY OF CONTACT
C AND PROPER LOAD CONDITION.
IFP=0
IJ=0
DO 180 I=1,MX
DO 150 J=1,MY
IJ=IJ+1
P(I,J)=F(IJ,1)
IF (P(I,J).LT.0.0) GO TO 160
150 CONTINUE
Y1=YSY(IJ)
F1=F(IJ,1)
IJ1=IJ-1
Y2=YSY(IJ1)
F2=F(IJ1,1)
IJ2=IJ-2
Y3=YSY(IJ2)
F3=F(IJ2,1)
YB(I)=PARAB(Y1,Y2,F1,F2)
GO TO 180
160 IF (J.EQ.1) GO TO 200
IJ1=IJ-1
YB(I)=(F(IJ,1)*YSY(IJ1)-F(IJ1,1)*YSY(IJ))/(F(IJ,1)-F(IJ1,1))

```

```

IJ=I*MY
180 CONTINUE
IFP=1
I1=MX-1
F1=P(MX,1)
F2=P(I1,1)
X1=XB(MX)
X2=XB(I1)
I2=I1-1
X3=XB(I2)
F3=P(I2,1)
if(f2.gt.f1) then
  XBR=PARAB(X1,X2,F1,F2)
else
  if(f3.gt.f2) then
    XBR=PARAB(X2,X3,F2,F3)
  else
    go to 470
  end if
end if
I1=MX+1
XB(I1)=XBR
YB(I1)=0.0
IF (IFP.EQ.0) GO TO 340
C  START CALCULATING TOTOA FORCE AND MOMENT.
FT=0.0
DO 199 I=1,MX
DO 199 J=1,MY
IF (J.EQ.1) GO TO 196
IF (I.EQ.1) GO TO 196
C=1.
GO TO 198
196 C=.5
198 FTT=P(I,J)*AR(I)*C
FT=FT+FTT
199 CONTINUE
FT=4.*FT-F(1,1)*AR(1)
C  WRITE THE LOADING SITUATION.
WRITE (6,216) FT
GO TO 340
200 I1=I-1
XBR=(P(I,J)*XB(I1)-P(I1,J)*XB(I))/(P(I,J)-P(I1,J))
YB(I)=0.0
XB(I)=XBR
340 WRITE (6,221) XBR,D
C  LOOK FOR CONVERGENCE.
IF (DABS(1.-RY/YB(NC)).LE.EPS) GO TO 450
IF (IT.GT.ITM) GO TO 450

```

```

IT=IT+1
C  START TO GENERATE NEW MESH LAY OUT.
  IF (XBR.GT.XX1) GO TO 402
401 H=XBR/(MX1-.5)
    MM=1
    MMM=MX1
    X=0.0
    IIL=1
    GO TO 430
402 IF (MX2.EQ.0) GO TO 401
    XX12=XX1+XX2
    IF (XBR.GT.XX12) GO TO 405
403 MM=MX1+1
    MMM=MX12
    H=(XBR-XX1)/MX2
    DO 404 I=1,MX1
404 HY(I)=YB(I)/(MY-.5)
    X=XB(MX1)+H/2.
    IIL=MM
    GO TO 430
405 IF (MX3.EQ.0) GO TO 403
    XX123=XX1+XX2+XX3
    IF (XBR.GT.XX123) GO TO 408
406 MM=MX12+1
    MMM=MX123
    H=(XBR-XX12)/MX3
    DO 407 I=1,MX12
407 HY(I)=YB(I)/(MY-.5)
    X=XB(MX12)+H/2.
    IIL=MM
    GO TO 430
408 IF (MX4.EQ.0) GO TO 406
    H=(XBR-XX123)/MX4
    MM=MX123+1
    MMM=MX
    DO 409 I=1,MX123
409 HY(I)=YB(I)/(MY-.5)
430 DO 440 I=MM,MMM
    HX(I)=H
431 IF(X-XB(IIL))433,434,432
432 IIL=IIL+1
    GO TO 431
433 J=IIL-1
    YBN(I)=(YB(J)-YB(IIL))*(X-XB(J))/(XB(J)-XB(IIL))+YB(J)
    HY(I)=YBN(I)/(MY-.5)
    XBN(I)=X
    X=X+H
    IIL=J

```

```

GO TO 440
434 XBN(I)=X
    YBN(I)=YB(IIL)
    HY(I)=YBN(I)/(MY-.5)
    X=X+H
440 CONTINUE
    DO 441 I=MM,MMM
    YB(I)=YBN(I)
441 XB(I)=XBN(I)
    MX=MMM
    GO TO 15
450 WRITE (6,214)
    WRITE (6,222) (XB(I),YB(I),I=1,MX)
    GO TO 500
470 WRITE (6,228)
C  FORMAT STATEMENTS .
211 FORMAT (//(25X,'NODE',11X,'X',17X,'Y',17X,'P'))
212 FORMAT(20X,'E1=',E13.7,2X,'ANU1=',F5.3,2X,'E2=',E13.7,2X,'ANU2=',
1F5.3)
213 FORMAT (//(40X,'BOUNDARY OF CONTACT REGION'))
214 FORMAT (/(19X,'X',14X,'Y',14X,'X',14X,'Y',14X,'X',14X,'Y'))
215 FORMAT (/(25X,I5,3E18.7))
216 FORMAT (//(46X,'FORCE = ',F10.3))
218 FORMAT (8F10.0)
219 FORMAT (20X,'IAI=',I3,2X,'IDGT=',I3,2X,'ITM=',I3,2X,'NC=',I3,
&2x,'EPS=',e11.4)
220 FORMAT (20X,'MX1=',I3,2X,'MX2=',I3,2X,'MX3=',I3,2X,'MX4=',I3,2X,'
1MY=',I3)
221 FORMAT (/(28X,'RIGHT X-BOUNDARY=',F10.7,5X,' APPROACH=', F10.8))
222 FORMAT (/(10X,6E15.7))
223 FORMAT (//(46X,'ITERATION =',I2))
224 FORMAT (20X,'XX1=',F7.5,3X,'XX2=',F7.5,3X,'XX3=',F7.5,3X,'XX4=',
1F7.5)
225 FORMAT(16I5)
226 FORMAT (20A4)
227 FORMAT (1H1,20A4/)
228 FORMAT (20X,'ERROR DUE TO F2<F1')
229 FORMAT (20X,'MX=',I3,15X,'MY=',I3,15x,'approach=',e11.4)
500 STOP
cc 38 format('Please enter input file name and then hit return')
cc 39 format('Please enter output file name and then hit return')
END
C  PROFILE FUNCTION OF RAIL & WHEEL COUNTERFORMAL CONTACT
STRESSES.
SUBROUTINE INSEP(X,Y,FZ)
IMPLICIT REAL*8 (A-H,O-Z)
A=.00948
B=.02769

```

```

      FZ=A*X**2+B*Y**2
50 RETURN
      END
      DOUBLE PRECISION FUNCTION DAOR(XF,YF,XS,YS,HXS,HYS)
C
C-----
C  FUNCTION DAOR(XF,YF,XS,YS,HXS,HYS)
C
C  PURPOSE.....
C  TO CALCULATE INTEGRAL OF DA OVER R.
C
C  METHOD.....
C  BY USING LURE,S FORMULA APPLIED TO A RECTANGLE CELL WHEN
C  THE DISTANCE BETWEEN THE SOURCE AND FIELD POINT IS LESS THAN
C  1.5 TIMES THE MAXIMUM DIMENSION OF CELL, AND APPROXIMATELY
C  AS DA/R , OTHERWISE.
C
C  DESCRIPTION OF ARGUMENT VARIABLES....
C  XF,YF  COORDINATES OF THE FIELD POINT
C  XS,YS  COORDINATES OF THE SOURCE POINT
C  DAOR   VALUE FOR THE FUNCTION TO BE RETURNED
C-----
C
      IMPLICIT REAL*8 (A-H,O-Z)
      EPS=1.E-10
      PI=3.141592654
      C=1.
      YYSF=YS-YF
      R=DSQRT((XF-XS)**2+YYSF**2)
      IF (HXS-HYS) 1,1,2
1  H=HYS
      GO TO 3
2  H=HXS
3  IF (R-1.5*H) 6,6,4
4  DAOR=HXS*HYS/R
      GO TO 50
6  H1=YYSF+.5*HYS
      IF (DABS(H1)-EPS) 10,10,5
5  H4=H1-HYS
      IF (DABS(H4)-EPS) 10,10,20
10 C=.5
      H1=HYS
      H4=-HYS
20 H2=XS-XF+.5*HXS
      H3=H2-HXS
      T1=DATAN(H2/H1)
      B1=DATAN(H3/H1)
      T2=DATAN(H1/H2)

```

```

B2=DATAN(H4/H2)
T3=DATAN(H1/H3)
B3=DATAN(H4/H3)
T4=DATAN(H2/H4)
B4=DATAN(H3/H4)
AT1=DABS(T1)
AT2=DABS(T2)
AT3=DABS(T3)
AT4=DABS(T4)
AB1=DABS(B1)
AB2=DABS(B2)
AB3=DABS(B3)
AB4=DABS(B4)
C11=DLOG(DTAN(PI/4.+AT1/2.))
C12=DLOG(DTAN(PI/4.+AB1/2.))
C21=DLOG(DTAN(PI/4.+AT2/2.))
C22=DLOG(DTAN(PI/4.+AB2/2.))
C31=DLOG(DTAN(PI/4.+AT3/2.))
C32=DLOG(DTAN(PI/4.+AB3/2.))
C41=DLOG(DTAN(PI/4.+AT4/2.))
C42=DLOG(DTAN(PI/4.+AB4/2.))
C1=T1/AT1*C11-B1/AB1*C12
C2=T2/AT2*C21-B2/AB2*C22
C3=T3/AT3*C31-B3/AB3*C32
C4=T4/AT4*C41-B4/AB4*C42
DAOR=DABS(DABS(H1)*C1+DABS(H2)*C2-DABS(H3)*C3-DABS(H4)*C4)*C
50 RETURN
END
DOUBLE PRECISION FUNCTION PARAB(SM,SL,PM,PL)
*****
***
***subroutine parab3 is missing in the original program,
***this subroutine is parab taken from program COUNTACT-1
*****
***
C  PARAB(SM,SL,PM,PL)
C  -----
C
C  PURPOSE.....
C  TO EXTRAPOLATE BETWEEN TWO POINTS AND FIND ORDINATE
C  WHEN ABSESSIA IS ZERO
C
C  METHOD.....
C  PARABOLIC EXTRAPOLATION BETWEEN THE TWO POINTS AND
C
C  DESCRIPTION OF ARGUMENTS.....
C  (SM,PM) COORDINATES OF POINT M
C  (SL,PL) COORDINATES OF POINT L

```

```
C   PARAB   VALUE OF THE ORDINATE TO BE RETURNED TO THE  
C           CALLING PROGRAM.
```

```
C-----
```

```
C  
C   IMPLICIT REAL*8 (A-H,O-Z)  
C   PARAB=(PL**2*SM-PM**2*SL)/(PL**2-PM**2)  
C   RETURN  
C   END
```

APPENDIX B

Fortran Source Code for SHE Model

```

C*****
C***** THIS PROGRAM HAS BEEN DESIGNED TO IMPLEMENT THE CREEP-
*****
C***** FORCE / CREEPAGE RELATIONSHIP AS DEVELOPED BY SHEN,
*****
C***** HENDERICK AND ELKINS. KALKER'S LINEAR TABLE IS USED.
*****
C***** PROGRAM WRITTEN BY R.F. HARDER, MARCH 1993 *****
C*****
C
C
C
C
C DIMENSION C11(20), C22(20), C23(20), AR(20), E(20,4)
OPEN(UNIT=7,FILE='LINTABL.DAT',STATUS='OLD')
C
C*****
C***** NOMENCLATURE - CONSTANT DEFINITION *****
C*****
C XN = NORMAL FORCE (WHEEL LOAD) (Newtons) *
C PHI = SPIN CREEPAGE ( 1 / mm ) *
C YNU = LATERAL CREEPAGE non-dimensional*
C XNU = LONGITUDINAL CREEPAGE non-dimensional*
C RMU = POISSON'S RATIO non-dimensional*
C FMU = COEFFICIENT OF SLIDING FRICTION *
C A = CONTACT ELLIPSE SEMI-DIAMETER (ROLLING DIR.) (mm)*
C B = CONTACT ELLIPSE SEMI-DIAMETER (TRANSVERSE DIR.) (mm)*
C GG = MODULUS OF RIGIDITY (SHEAR MODULUS) (Newtons/mm2)*
C C11 = LONGITUDINAL CREEP COEFF. - KALKER non-dimensional*
C C22 = LATERAL CREEP COEFF. - KALKER non-dimensional*
C C23 = SPIN CREEP COEFF. - KALKER non-dimensional*
C FX = LONGITUDINAL CREEP FORCE - KALKER (Newtons) *
C FY = LATERAL CREEP FORCE - KALKER (Newtons) *
C FRPRIME = RESULTANT LINEAR CREEP FORCE (Newtons) *
C FR = RESULTANT NON-LINEAR CREEP FORCE (Newtons) *
C EPS = REDUCTION COEFFICIENT non-dimensional*
C FXNL = LONGITUDINAL NON-LINEAR CREEP FORCE (Newtons) *
C FYNL = LATERAL NON-LINEAR CREEP FORCE (Newtons) *
C FNORM = NORMALIZED RESULTANT CREEP FORCE non-dimensional*
C TAU = NORMALIZED CREEPAGE FACTOR non-dimensional*
C ALPHA = NORMALIZED SPIN FACTOR (%) non-dimensional*
C*****
C

```



```

C ** INPUT CONTACT DATA **
C
  XN=55000.0
  PHI=0.002
  YNU=0.0003
  XNU=0.005
  RMU=0.300
  FMU=0.300
  A=4.00
  B=2.00
  GG=82733.0
  SG=A/B
C
C ** READ IN THE CREEPAGE COEFFICIENTS OF KALKER'S LINEAR THEORY
**
C
  DO 60 I=1,19
60  READ(7,*)(E(I,J),J=1,4)
  DO 65 I=1,19
  AR(I)=E(I,1)
  C11(I)=E(I,2)
  C22(I)=E(I,3)
65  C23(I)=E(I,4)
  DO 70 I=1,19
  IF(SG.LE.AR(I)) GO TO 80
70  CONTINUE
  GO TO 85
C
C ** PERFORM LINEAR INTERPOLATION ON CREEPAGE COEFFICIENTS **
C
80  CC11=C11(I-1)+(C11(I)-C11(I-1))*((SG-AR(I-1))/(AR(I)-AR(I-1)))
  CC22=C22(I-1)+(C22(I)-C22(I-1))*((SG-AR(I-1))/(AR(I)-AR(I-1)))
  CC23=C23(I-1)+(C23(I)-C23(I-1))*((SG-AR(I-1))/(AR(I)-AR(I-1)))
C
C ** COMPUTE CREEP FORCES AS PER KALKER LINEAR CODE **
C
85  FX=-A*B*GG*CC11*XNU
  FY=-A*B*GG*((CC22*YNU)+(((A*B)**0.5)*CC23*PHI))
  FRPRIME=(FX**2.0+FY**2.0)**0.5
  PAR=3.0*FMU*XN
  IF(FRPRIME.GT.PAR) GO TO 100
C
C ** REDUCE LINEAR RESULT TO THE NON-LINEAR VIA VERMEULEN-
JOHNSON **
C
  RATIO=(FRPRIME/(FMU*XN))
  FR=(FMU*XN)*(RATIO-(0.333*(RATIO**2.0))+(0.037037*(RATIO**3.0)))
  GO TO 150

```

```
100 FR=FMU*XN
150 EPS=FR/FRPRIME
    FXNL=FX*EPS
    FYNL=FY*EPS
    FNORM=FR/(FMU*XN)
C
C ** COMPUTE NORMALIZED CREEPAGE AND SPIN FACTORS **
C
    TAU=((A*B*GG)/PAR)*((CC11*XNU)**2.0+((CC22*YNU)+(CC23*(A*
    .B)**0.5)*PHI)**2.0)**0.5
    ALPHA=(ABS(CC23*SQRT(A*B)*PHI)/((CC11*XNU)**2.0+(CC22
    .YNU)**2.0+(CC23*SQRT(A*B)*PHI)**2.0)**0.5)*100.0
    WRITE(*,*) 'FXNL=',FXNL,' ', 'FYNL=',FYNL
    WRITE(*,*) 'FR/MUN=',FNORM,' ', 'TAU=',TAU,' ', 'ALPHA=',ALPHA
    WRITE(*,*) 'C11=',CC11,' ', 'C22=',CC22,' ', 'C23=',CC23
CLOSE(7)
STOP
END
```

APPENDIX C

Fortran Source Code for Modified DUVOROL Code

```

C   DUVOROL  Keyed in by D. G. Pringle for R. F. Harder's PhD
c   thesis research studies. For use on fortran 77 and modified
c   so that data can be read in batch mode.
c
c   See " on the rolling contact of two elastic bodies in the
c   presence of dry friction, " by J.J. Kalker, PhD thesis,
c   Delft University (1967). The program is an improvement on
c   method described in the above thesis and is presented in
c   rolling. I, description," by J.J. Kalker and " II,
c   programme description, " by H. Goedings (1972).
c   unpublished, obtained from professor Kalker in private
c   communication.
c
c
c   The input is described in the following section
c
c
c   Data #1  NV1
C           TYPICAL: 1
C
c           NV1 (solves nv1 complete problems), integer
c
c   Data #2  A,B,NU,LXN,LYN,KAPPA
c           TYPICAL: 2.5980 0.3849 0.28 0.00 0.00 0.00
C
C           ( A and B are the normalized contact ellipse
c           dimensions, where if A1 and B1 are the actual
c           dimensions then  $A=A1/\sqrt{A1*B1}$  and
c            $B=B1/\sqrt{A1*B1}$ . note  $A/B \geq 0.1$ 
C           NU IS THE COMBINED POISSON'S RATIO. WHERE
C            $NU = G/2*(NU+/G+ + NU-/G-)$ , WHERE THE + AND
C           - SIGNS REFER TO POISSON'S RATIO AND THE
C           SHEAR MODULUS FOR THE LOWER AND UPPER
C           REGION RESPECTIVELY. THE CONSTANT G IS THE
C           COMBINED MODULUS,  $1/G=1/2*1/G+ + 1/G-$ .
C           THE VALUES OF A,B,NU PROVIDE THE NECESSARY
C           INFORMATION NEEDED TO COMPUTE (INTERNALLY) FROM
C           SUBROUTINE CONST ), THE NORMALIZED MODULUS, GS
C           THE CONSTANT  $GS = G*(C^{**3})/(RHO*N)$ , WHERE  $C =$ 
C            $\sqrt{A1*B1}$ ,  $1/RHO=1/4*R1+ + 1/R1- + 1/R2+ +$ 
C            $1/R2-$ ), AND N=RESULTANT NORMAL FORCE.
C           LXN AND LYN ARE NORMALIZED INVERSE STIFFNESSES
C           OF A THIN ELASTIC LAYER COVERING THE SURFACE.

```

```

C      .XN=LX*RHO*N/C**4, LYN=LY*RHO*N/C**4.
C      FOR NO LAYER TAKE LXN=LYN=0.0
C      KAPPA IS THE ELASTIC DIFFERENCE PARAMETER
C      KAPPA=G/4*(1-2*NU+)/G+-(1-2*NU-)/G-).
C
C      DATA #3  N1,M1,NS
C      TYPICAL: 12,6,2
C
C      N1,M1 (LATTICE POINTS IN CONTACT REAGION,
C      NS (TO PRINT OUTPUT ON THE CONTACT REGION, NS=1,
C      TO DUPPRESS ALL OUTPUT EXCEPT THE RESULTANT
C      FORCES AND MOMENT , TAKE NX=2), INTEGER
C      FOTE: FXN=FX/(MU*N), FYN=FY/MU*N),
C      MZN=MZ*C/MU*N), WHERE N IS THE RESULTANT NORMAL
C      FORCE AND MU IS THE COEFFICIENT OF FRICTION
C
C      DATA #4  NV2
C      TYPICAL: 1
C
C      SOLVES NV2 PROBLEMS FOR DISTINCT VALUES OF
C      CREEPAGE AND SPIN GIVEN ON NV2 DATA #5), INTEGER
C
C      DATA #5  UXN,UYN,PHN
C      TYPICAL: 0.0 2.0 0.4
C
C      UXN AND UYN ARE NORMALIXED CREEPAGES, PHN
C      IS THE NORMALIZED SPIN), REAL
C      UXN=UX*RHO/(MU*C), UYN=UY*RHO/(MU*C),
C      PHN=PH*RHO/MU
C
C      ***** NOTE: ALL VARIABLES HABE BEEN NORMALIXED SUCH
C      ***** THAT THE COEFFICIENT OF FRICTION, MU, DOES NOT
C      ***** APPEAR EXPLICITLY.
C
C      DIMENSION XS(38),XT(400),YT(400),ZT(400),XU(400),YU(400),ZU(400)
C      DIMENSION RZT(120,1),RZU(120,1),F1(60,60),F2(60,60),F3(60,60)
C      DIMENSION S(60),U1(1,120),U2(120,120),FDACC(120,120),FACC(1,120)
C      REAL KAPPA
C      INTEGER C(38),C1(9),C2(9),TMA(200)
C      INTEGER PMA,QMA,FAC1,FAC2
C      DIMENSION XTU(60),YTU(60)
C      DIMENSION ARR(120,120),T(120,1),U(120,1),RT(120),TT(120),P(120)
C      DIMENSION RU(120)
C      REAL MU,KPG,K1,K2,K3,MZS,LXN,LYN
C      INTEGER FAC1P,FAC2P,WP
C      REAL MZ

```

```

EXTERNAL SIGN
REAL K
REAL NU
  DATA C1/1,0,-1,-2,0,2,1,0,-1/,C2/1,-2,1,-2,4,-2,1,-2,1/
DATA PI/3.14159/
  OPEN(UNIT=3,FILE='DUVO.OUT',STATUS='OLD')
  OPEN(UNIT=9,FILE='DEBUG.OUT',STATUS='OLD')
  OPEN(UNIT=4,FILE='FDACC.OUT',STATUS='OLD')
  OPEN(UNIT=5,FILE='SHEAR.OUT',STATUS='OLD')
  OPEN(UNIT=6,FILE='FACC2.OUT',STATUS='OLD')
  OPEN(UNIT=7,FILE='TIJ.OUT',STATUS='OLD')
  OPEN(UNIT=15,FILE='SLIP.OUT',STATUS='OLD')
CC   OPEN(UNIT=17,FILE='TX.OUT',STATUS='OLD')
CC   READ(1,*)NV1
      IKKKK=0
      NV1=1
      DO 999 II1=1,NV1
C
CC   READ(1,*)A,B,NU,LXN,LYN,KAPPA
CC   READ(1,*)N1,M1,NS
CC   A=2.4257
CC   B=0.41229
CC   A=1.0
CC   B=1.0
      A=1.47
      B=0.68
      NU=0.28
      LXN=0.00
      LYN=0.00
      KAPPA=0.00
      N1=8
      M1=8
      NS=1
C
      SX=LXN
      SY=LYN
      IF(A/B.LT.0.1) GO TO 998
C
C
C       SUBROUTINE CONST COMPUTES THE NORMALIZED MODULUS
C       FROM KALKER'S TABLES AND ASYMPTOTIC EXPANSIONS.
C       VALID FOR A/B EQUAL TO OR GRATER THEN 0.1.
C
C
      CALL CONST(A,B,NU,GS)
      G=GS
      SIGMA=NU

```

```

F00=3.0/(2.0*PI)
MU=1.0
H= A/FLOAT(N1)
K= (2.0*B)/FLOAT(M1)
WRITE(3,968)
N=0
M=0
AA=A*A
Y=B
MM=M1/2
L3=0
L4=0
DO 100 I=1,MM
L1=0
L2=0
Y=B-I*K
YB=(Y*Y)/(B*B)
XS(M1-I)=-A*SQRT(1.0-YB)
XS(I)=XS(M1-I)
X=-XS(I)/(2*H)
J=X
IF((-2.*J*H-XS(I))/H.LE.0.02) J=J-1
L=2*J+1
X=-L*H
IF(X.LT.XS(I))GO TO 50
M=M+1
L2=1
XU(M)=X
YU(L+M)=Y
YU(M)=Y
ZU(L+M)=F00*SQRT(1.0-(X*X)/AA-YB)
ZU(M)=ZU(L+M)
XU(L+M)=-X
50  N=N+1
X=X+H
IF(X.LE.-.1*H) GO TO 200
X=0.0
XT(N)=0.0
YT(N)=Y
ZT(N)=F00*SQRT(1.0-YB)
GO TO 60
200  L=N+2*(J-L1)
ZT(L)=F00*SQRT(1.0-(X*X)/AA-YB)
ZT(N)=ZT(L)
XT(N)=X
XT(L)=-X
YT(L)=Y
YT(N)=Y

```

```
X=X+H
M=M+1
L=M+2*(J-L1)-1
XU(M)=X
XU(L)=-X
YU(M)=Y
YU(L)=Y
ZU(M)=F00*SQRT(1.0-(X*X)/AA-YB)
ZU(L)=ZU(M)
L1=L1+1
GO TO 50
60  N=N+J
    M=M+J+L2
    C(2*I-1)=N-L3
    C(2*I)=M-L4
    L3=N
    L4=M
100 CONTINUE
    NN=N+1
    MM=M+1
    L=0
    N=2*N-N1+1
    M=2*M-N1
    I=N
301  L=L+1
    XT(I)=-XT(L)
    YT(I)=-YT(L)
    ZT(I)=ZT(L)
    I=I-1
    IF(I.GE.NN) GO TO 301
    L=0
    I=M
401  L=L+1
    XU(I)=-XU(L)
    YU(I)=-YU(L)
    ZU(I)=ZU(L)
    I=I-1
    IF(I.GE.MM) GO TO 401
    L=3
    H=2.*H
    ISTART=M1/2+1
    IEND=M1-1
    DO 500 I=ISTART,IEND
    IF(ISTART.GT.IEND)GO TO 500
    C(2*I-1)=C(M1-L)
    C(2*I)=C(M1-L+1)
500  L=L+2
    WRITE(3,901)
```

```

901 FORMAT(1H1)
   WRITE(3,969)
   WRITE(3,970)A,B,NU,LXN,LYN,KAPPA
   WRITE(3,972)N1,M1,NS
   WRITE(3,973)GS,N,M
   MAX=M
   IF(N.GT.M) MAX=N
C
C   IN-LINE MRZ
C
C   F4=F1, F5=F2, RZ=RZU, CMRZ=0.5
MN=M
DO 8110 I=1,M
  XTU(I)=XU(I)
  RZU(2*I-1,1)=0.0
  RZU(2*I,1)=0.0
8110 YTU(I)=YU(I)
8130 DO 8140 I=1,MN
  DO 8140 J=1,N
    L=0
    P4=0.0
    P5=0.0
    Q4=0.0
    Q5=0.0
    X1=XT(J)-XTU(I)
    Y1=YT(J)-YTU(I)
    X=X1-H
8131 Y=Y1-K
8132 L=L+1
    T1=ALOG(X*X+Y*Y+H*1.E-10)
    T2=X*ATAN(Y/(X+H*1.E-10))
    T3=Y*ATAN(X/(Y+K*1.E-10))
    P4=P4+C1(L)*(.5*Y*T1+T2)
    P5=P5+C1(L)*(.5*X*T1+T3)
    Q4=Q4+C2(L)*((X*X+Y*Y)*(T1-1)-(.5*Y*T1+T2)*Y1*4.0)
    Q5=Q5+C2(L)*(X*Y+Y*T3-X*T2-(.5*X*T1+T3)*Y1*2.0)
    Y=Y+K
    IF(Y.LE.Y1+K+.5*K) GO TO 8132
    X=X+H
    IF(X.LE.X1+H+.5*H) GO TO 8131
    F1(I,J)=P4/H+Q4/H/K/4.0
    F2(I,J)=P5/H+Q5/H/K/2.0
8140 CONTINUE
    LEND=2*MN-1
    DO 8150 I=1,LEND,2
      DO 8150 J=1,N
        RZU(I,1)=RZU(I,1)+F1((I+1)/2,J)*ZT(J)
8150 RZU(I+1,1)=RZU(I+1,1)+F2((I+1)/2,J)*ZT(J)

```



```

C  IN-LINE MRZ
C  F4=F1, F5=F2, RZ=RZT, CMRZ=.E-5
8220 MN=N
      DO 8225 J=1,N
          XTU(J)=XT(J)
          RZT(2*J-1,1)=0
          RZT(2*J,1)=0.0
8225 YTU(J)=YT(J)
8230 DO 8240 I=1,MN
      DO 8240 J=1,N
          L=0
          P4=0.0
          P5=0.0
          Q4=0.0
          Q5=0.0
          X1=XT(J)-XTU(I)
          Y1=YT(J)-YTU(I)
          X=X1-H
8231 Y=Y1-K
8232 L=L+1
          T1=ALOG(X*X+Y*Y+H*1.E-10)
          T2=X*ATAN(Y/(X+H*1.E-10))
          T3=Y*ATAN(X/(Y+K*1.E-10))
          P4=P4+C1(L)*(.5*Y*T1+T2)
          P5=P5+C1(L)*(.5*X*T1+T3)
          Q4=Q4+C2(L)*((X*X+Y*Y)*(T1-1)-(.5*Y*T1+T2)*Y1*4.0)
          Q5=Q5+C2(L)*(X*Y+Y*T3-X*T2-(.5*X*T1+T3)*Y1*2.0)
          Y=Y+K
          IF(Y.LE.Y1+K+.5*K) GO TO 8232
          X=X+H
          IF(X.LE.X1+H+.5*H) GO TO 8231
          F1(I,J)=P4/H+Q4/H/K/4.0
          F2(I,J)=P5/H+Q5/H/K/2.0
8240 CONTINUE
          LEND=2*MN-1
          DO 8250 I=1,LEND,2
              DO 8250 J=1,N
                  RZT(I,1)=RZT(I,1)+F1((I+1)/2,J)*ZT(J)
8250 RZT(I+1,1)=RZT(I+1,1)+F2((I+1)/2,J)*ZT(J)
          DO 83100 I = 1,M
              DO 83100 J=1,N
                  L=0
                  P1=0
                  P2=0
                  P3=0
                  Q1=0
                  Q2=0
                  Q3=0

```

```

X1=XT(J)-XU(I)
Y1=YT(J)-YU(I)
Y1END=Y1+K+.5*K
X1END=X1+H+.5*H
X=X1-H
8310 Y=Y1-K
8320 L=L+1
R=ABS(X/(Y+K*1.E-10))
SS=ABS(Y/(X+H*1.E-10))
T1=SIGN(X)*Y*ALOG(R+SQRT(1.+R*R))
T3=SIGN(Y)*X*ALOG(SS+SQRT(1.+SS*SS))
T2=SQRT(X*X+Y*Y+H*K*1.E-20)
P1=P1+C1(L)*(T1+T3)
P2=P2-C1(L)*T2
P3=P3+C1(L)*T1
Q1=Q1+C2(L)*(Y*T1+X*T2-(T1+T3)*Y1*2.)
Q2=Q2+C2(L)*(X*T3-Y*T2+T2*Y1*2.)
Q3=Q3+C2(L)*(Y*T1-X*T2-T1*Y1*2.)
Y=Y+K
IF(Y.LE.Y1END) GO TO 8320
X=X+H
IF(X.LE.X1END) GO TO 8310
F1(I,J)=P1/H+Q1/H/K/2.
F2(I,J)=P2/H+Q2/H/K/2.
F3(I,J)=P3/H+Q3/H/K/2.
83100 CONTINUE
C
C
CC  READ(1,*)NV2
    NV2=21
cc  NV2=1
    UYN=-3.30
    WRITE(3,974) NV2
    DO 997 L2K=1,NV2
CC  READ(1,*,END=9999)UXN,UYN,PHN
    UXN=-3.0
    UYN=UYN+0.30
    PHN=0.0
    UX=UXN
    UY=UYN
    PHI=PHN
    WRITE(3,975)UXN,UYN,PHN
    L3=0
    L4=N
    L5=M
    IF(ABS(UX).LT.1.E-8.AND.ABS(KAPPA).LT.1.E-8) L3=1
    IF(ABS(UY).LT.1.E-8.AND.ABS(PHI).LT.1.E-8) L3=2
    IF(L3.EQ.0) GO TO 8410

```

```

C   IN-LINE KAPAF *****
      N=0
      M=0
      J=M1/2
      DO 8420 I=1,J
      M=M+C(2*I)
      N=N+C(2*I-1)
8420 CONTINUE
8410 CONTINUE
C
C
C   IN-LINE MA *****
      PMA=2*M-1
      QMA=2*N-1
      PIG=PI*G
      IF(L3)8520,8510,8520
8510 DO 8515 J=1,QMA,2
      DO 8515 I=1,PMA,2
      I1=(I+1)/2
      J1=(J+1)/2
      ARR(I,J)=((1.-SIGMA)*F1(I1,J1)+SIGMA*F3(I1,J1))/PIG
      ARR(I,J+1)=(SIGMA*F2(I1,J1))/PIG
      ARR(I+1,J)=ARR(I,J+1)
8515 ARR(I+1,J+1)=(2.-SIGMA)*F1(I1,J1)/PIG-ARR(I,J)
      GO TO 85100
8520 TMA(1)=1
      LEND=M1-2
      DO 8530 I=1,LEND
8530 TMA(I+1)=TMA(I)+C(2*I-1)*2
      IF(L3.NE.1)GO TO 8540
      FAC1=-1
      FAC2=1
8540 IF(L3.NE.2) GO TO 8550
      FAC1=1
      FAC2=-1
8550 DO 8560 J=1,QMA,2
      J1=(J+1)/2
      IF(J.GE.TMA(M1/2)) GO TO 85200
      I=2
8552 IF(J.LT.TMA(I))GO TO 85301
      I=I+1
      IF(I.LE.M1/2)GO TO 8552
85301 J2=(TMA(M1-I+1)+J-TMA(I-1)+1)/2
      DO 85400 I=1,PMA,2
      I1=(I+1)/2
      ARR(I,J)=((1.-SIGMA)*(F1(I1,J1)+FAC1*F1(I1,J2))
      $+SIGMA*(F3(I1,J1)+FAC1*F3(I1,J2)))/PIG
      ARR(I+1,J)=(SIGMA*(F2(I1,J1)+FAC1*F2(I1,J2)))/PIG

```

```

      ARR(I,J+1)=(SIGMA*(F2(I1,J1)+FAC2*F2(I1,J2)))/PIG
      ARR(I+1,J+1)=(F1(I1,J1)+F1(I1,J2)*FAC2-SIGMA*(F3(I1,J1)
      $+F3(I1,J2)*FAC2))/PIG
85400 CONTINUE
      GO TO 8560
85200 DO 8559 I=1,PMA,2
      I1=(I+1)/2
      ARR(I,J)=((1.-SIGMA)*F1(I1,J1)+SIGMA*F3(I1,J1))/PIG
      ARR(I,J+1)=(SIGMA*F2(I1,J1))/PIG
      ARR(I+1,J)=ARR(I,J+1)
8559 ARR(I+1,J+1)=(2.-SIGMA)*F1(I1,J1)/PIG-ARR(I,J)
8560 CONTINUE
85100 CONTINUE
C
C
      IF(ABS(SX).GT.1.E-4.OR.ABS(SY).GT.1.E-4) GO TO 86111
      GO TO 86100
C
C  IN-LINE ADS  *****
86111 M2=M1-1
      J=1
      I=1
      NN=0
      SXH=LXN/H
      SYH=LYN/H
      IF(L3.NE.0)M2=M1/2
      DO 87100 I1=1,M2
      L1=2*I1-1
      L=0
      L2=L1+1
      IF(C(L1).GE.C(L2))GO TO 8710
      L=1
      ARR(I,J)=ARR(I,J)+SXH
      ARR(I+1,J+1)=ARR(I+1,J+1)+SYH
      II=I+C(L1)*2
      JJ=J+(C(L1)-1)*2
      ARR(II,JJ)=ARR(II,JJ)-SXH
      ARR(II+1,JJ+1)=ARR(II+1,JJ+1)-SYH
8710 MM=L+NN+1
      NN=NN+C(L2)-L
      IF(MM.GE.NN)GO TO 8730
      DO 8729 I2=MM,NN
      IF(MM.GT.NN)GO TO 8729
      I3=2*I2-1
      I4=I3+1
      ARR(I3,J)=ARR(I3,J)-SXH
      ARR(I3,J+2)=ARR(I3,J+2)+SXH
      ARR(I4,J+1)=ARR(I4,J+1)-SYH

```

```
      ARR(I4,J+3)=ARR(I4,J+3)+SYH
8729 J=J+2
8730 CONTINUE
87100 CONTINUE
C
86100 KPG=KAPPA/PI/G
      WRITE(3,901)
      IEND=2*M-1
      DO 86110 I=1,IEND,2
        L=(I+1)/2
        RU(I)=UX-PHI*YU(L)+KPG*RZU(I,1)
        RU(I+1)=UY+PHI*XU(L)+KPG*RZU(I+1,1)
86110 CONTINUE
      JEND=2*N-1
      DO 86120 J=1,JEND,2
        L=(J+1)/2
        RT(J)=UX-PHI*YT(L)+KPG*RZT(J,1)
        RT(J+1)=UY+PHI*XT(L)+KPG*RZT(J+1,1)
86120 CONTINUE
      IF(L3.EQ.0) GO TO 86130
      L=0
      J=0
      IEND=IFIX(FLOAT(M1)/2.0-0.9)
      DO 86129 I=1,IEND
        J=J+C(2*I-1)*2
        L=L+C(2*I)
86129 CONTINUE
      DO 86128 I=1,J
86128 RT(I)=RT(I)*2
        DO 86127 I=1,L
86127 ZU(I)=ZU(I)*2
86130 JEND=2*N
      DO 86140 J=1,JEND
86140 T(J,1)=0
        RE=.2
        RB=.2
        MM=0
        B=1.0
        E=.5
86150 JEND=2*N
      DO 86155 J=1, JEND
86155 TT(J)=T(J,1)
        MM=MM+1
        L1=0
86160 NN=0
C   DX=1.0, EX=E, PX=P, T=T, MU=MU
C
86170 DXP=1.0
```

```

DO 8799 I=1,N
GX=MU*MU*ZT(I)*ZT(I)-T(2*I-1,1)*T(2*I-1,1)-T(2*I,1)*T(2*I,1)
IF(GX)8703,8702,8702
8702 P(2*I-1)=-2*E/(GX+DXP*E)
P(2*I)=4.*E/((GX+DXP*E)*(GX+DXP*E))
GO TO 8799
8703 P(2*I-1)=-2./DXP+2.*GX/(DXP*DXP*E)
P(2*I)=4./(DXP*DXP*E)
8799 CONTINUE
C
C
JEND=2*N-1
DO 86175 J=1,JEND,2
IF (P(J).LT.-1.E10)GO TO 86180
86175 CONTINUE
GO TO 86190
C PW3: *****
86180 IF(L1.NE.1)GO TO 86200
WRITE(3,904)
904 FORMAT('PROCESS INTERRUPTED, RESULTS MIGHT NOT BE
SIGNIFICANT')
C
IPCODE=0
C IN-LINE PRINT *****
4145 LL=L3
9001 IF(NS.GT.1) GO TO 499
WRITE(3,9004)
9004 FORMAT(//,20X,'***** CONTACT REGION FOLLOWS *****',/,
$10x,'X AND Y ARE NORMALIZED COORDINATES, X IN THE ROLLING',/,
$10X,'DIRECTION, X,Y=X1/C1,Y1/C1 WHERE X1,Y1 ARE DIM. COORD.',/,
$10X,'TZH=HERTZ STRESS =3/(2*PI)*SQRT(1.0-X*X/(A*A)-Y*Y/(B*B))',
$,10X,'TX AND TY ARE NORMALIZED SHEAR STRESSES',/,10X,'TX=-
TAUXZ*
$C**3/(RHO*N), TY=-TAUYZ*C**3/(RHO*N)',/,
$10X,'ABS(TX,TY) LESS THEN TZH FOR NO SLIP, EQUAL TO TZH FOR
SLIP',
$,10X,'VX,BY ARE NORMALIXED SLIP COMPONENTS,
VX=VX1/V*FHO/(MU*C)',
$,10X,'VY=VY1/V*RHO/(MU*C), WHERE VX1,VX2=REL. VEL.
BETWEEN',/,10X
$, 'ADJACENT POINTS AND V=ROLOLING VEL.',////)
499 CONTINUE
LU=1
LT=1
J1=1
FAC1P=1
FAC2P=1
WP=0

```

```

      J=M1/2
      IF(LL.EQ.0)J=M1-1
C   V2:      *****
8802 DO 8801 I=J1,J
      IF(J1.GT.J)GO TO 8801
      MAX=C(2*I-1)
      L3P=2
      IF(C(2*I-1).GE.C(2*I)) GO TO 8803
      MAX=C(2*I)
      L3P=1
8803 CONTINUE
909  FORMAT(/)
      IF(WP.NE.1)GO TO 8804
      LU=LU-C(2*I-2)-C(2*I)
      LT=LT-C(2*I-3)-C(2*I-1)
8804 FIX1=YT(LT)*FAC1P*FAC2P
      IBLANK=0
      DO 8801 I1=1,MAX
      IF(L3P.EQ.2)GO TO 8812
C   SS1:      *****
8800 TX=U(2*LU-1,1)*FAC1P
      TY=U(2*LU,1)*FAC2P
      FIX3=SQRT(TX*TX+TY*TY)
      IF(ABS(U(2*LU-1,1)).LT.1.E-20)TX=1.E-20
      FIX2=180./PI*ATAN(TY/TX)+(1.0-SIGN(TX))*90.
      IF(NS.GT.1) GO TO 501
      IF(IBLANK.EQ.0)WRITE(3,9006)FIX1
      IF(IBLANK.EQ.0) WRITE(3,9009)
      WRITE(3,9008) XU(LU),FIX3,FIX2
      WRITE(15,9112) UYN,FIX1,FIX1A,TX,TY
9112  FORMAT(1X,'UYN=',F6.2,4X,'Y=',F11.4,4X,'X=',F11.4,4X,'VX=',F11.4
      $,4X,'VY=',F11.4)
9008  FORMAT(1X,1F11.4,33X,2F11.4)
501  CONTINUE
      IBLANK=1
      LU=LU+1
      IF(MAX.EQ.C(2*I).AND.I1.EQ.MAX)GO TO 8813
C   SS2:      *****
8812 FIX1A=XT(LT)
      TX=T(2*LT-1,1)*FAC1P
      TY=T(2*LT,1)*FAC2P
      FIX2=TX
      FIX3=TY
CC   WRITE(17,*) 'XU=',XU(LU),'XT=',XT(LT),'TX=',TX,'TY=',TY
      FIX4=SQRT(TX*TX+TY*TY)
      IF(ABS(T(2*LT-1,1)).LT.1.E-20)TX=1.E-20
      FIX5=180./PI*ATAN(TY/TX)+(1.-SIGN(TX))*90.
      FIX6=MU*ZT(LT)

```

```

TXX=(COS(FIX5))*FIX4
TYY=(SIN(FIX5))*FIX4
IF(NS.GT.1) GO TO 502
IF(IBLANK.EQ.0)WRITE(3,9006)FIX1
IF(IBLANK.EQ.0) WRITE(3,9009)
WRITE(3,9011) FIX1A,FIX6,FIX4,FIX5
WRITE(5,9111) UYN,FIX1,FIX1A,FX,TY
9111 FORMAT(1X,'UYN=',F6.2,4X,'Y=',F11.4,4X,'X=',F11.4,4X,'TX=',F11.4
$,4X,'TY=',F11.4)
9011 FORMAT(1X,4F11.4)
502 CONTINUE
IBLANK=1
LT=LT+1
L3P=1
C SS3: *****
8813 CONTINUE
8801 CONTINUE
IF(LL.EQ.1.AND.WP.EQ.0) GO TO 8859
GO TO 8850
8859 FAC1P=-1
WP=1
J1=M1/2+1
J=M1-1
GO TO 8802
8850 IF(LL.EQ.2.AND.WP.EQ.0)GO TO 5188
GO TO 8851
5188 FAC2P=-1
WP=1
J1=M1/2+1
J=M1-1
GO TO 8802
8851 MZ=0
TX=0
TY=0
IF(LL.NE.0)GO TO 8852
JLAST=2*N-1
DO 8853 J=1,JLAST,2
TX=TX+T(J,1)
TY=TY+T(J+1,1)
MZ=MZ+XT((J+1)/2)*T(J+1,1)-YT((J+1)/2)*T(J,1)
8853 CONTINUE
GO TO 8855
8852 LT=1
ILAST=FLOAT(M1)/2.0-0.9
DO 8856 I=1,ILAST
JLAST=2*C(2*I-1)
DO 8856 J=1,JLAST,2
TX=TX+(1+FAC1P)*T(LT,1)

```



```

TY=TY+(1+FAC2P)*T(LT+1,1)
MZ=MZ+XT((LT+1)/2)*T(LT+1,1)*(FAC2P+1)-YT((LT+1)/2)*
$T(LT,1)*(-FAC1P+1)
LT=LT+2
8856 CONTINUE
JLAST=2*C(M1-1)
DO 8858 J=1,JLAST,2
TX=TX+T(LT,1)
TY=TY+T(LT+1,1)
MZ=MZ+XT((LT+1)/2)*T(LT+1,1)-YT((LT+1)/2)*T(LT,1)
LT=LT+2
8858 CONTINUE
8855 TX=TX*H*K
TY=TY*H*K
MZ=MZ*H*K
RES=SQRT(TX**2+TY**2)
WRITE(3,905)
905 FORMAT(///)
WORK=(TX*UXN)+(TY*UYN)+(MZ*PHN)
WRITE(3,977)TX,TY,RES,WORK
WRITE(3,978)MZ
IF(IPCODE.EQ.1)GO TO 6470
GO TO 9999
86200 L1=1
JLAST=2*N
DO 7110 J=1,JLAST
7110 T(J,1)=TT(J)
RB=SQRT(RB)
RE=SQRT(RE)
B=B/RB
E=E/RE
GO TO 86160
86190 MM=2*M-1
NNN=2*N-1
N2=NNN+1
EPS=1.E-7
C
CALL ARRAY(2,2*M,2*N,120,120,ARR,ARR)
CALL ARRAY(2,2*N,1,120,1,T,T)
CALL GMPRD(ARR,T,U,2*M,2*N,1)
CALL ARRAY(1,2*M,2*N,120,120,ARR,ARR)
CALL ARRAY(1,2*N,1,120,1,T,T)
CALL ARRAY(1,2*M,1,120,1,U,U)
C ABOVE IS EQUIVALENT TO ALL TO MATVER(A,T,U) *****
DO 6910 I=1,MM,2
II=(I+1)/2
U(I,1)=U(I,1)+RU(I)
U(I+1,1)=U(I+1,1)+RU(I+1)

```

```

S(II)=SQRT(U(I+1,1)*U(I+1,1)+U(I,1)*U(I,1)+B)
U1(1,I)=(MU*ZU(II)*U(I,1))/S(II)
U1(1,I+1)=(MU*ZU(II)*U(I+1,1))/S(II)
6910 CONTINUE
C
CALL ARRAY(2,1,2*M,1,120,U1,U1)
CALL ARRAY(2,2*M,2*N,120,120,ARR,ARR)
CALL GMPRD(U1,ARR,FACC,1,2*M,2*N)
CALL ARRAY(1,1,2*M,1,120,U1,U1)
CALL ARRAY(1,2*M,2*N,120,120,ARR,ARR)
CALL ARRAY(1,1,2*N,1,120,FACC,FACC)
C ABOVE IS EQUIVALENT OT MATVER(U1,A,FACC)
DO 6920 J=1,NNN,2
FACC(1,J)=-FACC(1,J)+RT(J)+P(J)*T(J,1)
FACC(1,J+1)=-FACC(1,J+1)+RT(J+1)+P(J)*T(J+1,1)
6920 CONTINUE
DO 6940 I=1,M
I2=2*I
I1=I2-1
SS=S(I)*S(I)
MZS=(MU+ZU(I))/S(I)
K1=MZS*(1-U(I1,1)*U(I1,1))/SS)
K2=-MZS*U(I1,1)*U(I2,1)/SS
K3=MZS*(1-U(I2,1)*U(I2,1))/SS)
DO 6930 J=1,N2
U2(J,I1)=K1*ARR(I1,J)+K2*ARR(I2,J)
U2(J,I2)=K2*ARR(I1,J)+K3*ARR(I2,J)
6930 CONTINUE
6940 CONTINUE
CALL ARRAY(2,2*N,2*M,120,120,U2,U2)
CALL ARRAY(2,2*M,2*N,120,120,ARR,ARR)
CALL GMPRD(U2,ARR,FDACC,2*N,2*M,2*N)
CALL ARRAY(1,2*N,2*M,120,120,U2,U2)
CALL ARRAY(1,2*M,2*N,120,120,ARR,ARR)
CALL ARRAY(1,2*N,2*N,120,120,FDACC,FDACC)
C ABOVE IS EQUIVALENT TO MATVER(U2,A,FDACC)
DO 6950 I=1,NNN,2
FDACC(I,I)=FDACC(I,I)-P(I)+P(I+1)*T(I,1)*T(I,1)
TEMP=FDACC(I,I+1)+P(I+1)*T(I,1)*T(I+1,1)
FDACC(I,I+1)=TEMP
FDACC(I+1,I)=TEMP
FDACC(I+1,I+1)=FDACC(I+1,I+1)-P(I)+P(I+1)*T(I+1,1)*T(I+1,1)
6950 CONTINUE
IF (L3.EQ.0) GO TO 6960
J=1
ILAST=FLOAT(M1)/2.0-0.9
DO 6980 I=1,ILAST
6980 J=J+C(2*I-1)*2

```

```

I2=1
IF(L3.EQ.1)I2=0
IFIRST=J+I2
ILAST=J+C(M1-1)*2-1
DO 6970 I=IFIRST,ILAST,2
IF(IFIRST.GT.ILAST)GO TO 6970
FACC(1,I)=0
DO 6970 I1=1,N2
FDACC(I,I1)=0
FDACC(I1,I)=0
FDACC(I,I)=1
6970 CONTINUE
C PAS:      *****
6960 CONTINUE
      CALL ARRAY(2,1,2*N,1,120,FACC,FACC)
CC      CALL ARRAY(2,2*N,2*N,120,120,FDACC,FDACC)
CC      CALL GELG(FACC,FDACC,N2,1,EPS,IER)
CC      CALL ARRAY(1,1,2*N,1,120,FACC,FACC)
CC      CALL ARRAY(1,2*N,2*N,120,120,FDACC,FDACC)
CC      do 517 lp=1,N2
CC      write(4,*) (FDACC(LP,KO), KO=1,N2)
CC      WRITE(5,*) FACC(LP,1)
CC 517 CONTINUE
CC      WRITE(5,*) 'N2=',N2,'N=',N,'M=',M
      IKKKK=IKKKK+1
      CALL SORR(FDACC,FACC,N2,EPS,IKKKK,UYN)
CC      DO 518 LZ=1,N2
CC      WRITE(6,*) FACC(LZ,1)
CC 518 CONTINUE
      CALL ARRAY(1,1,2*N,1,120,FACC,FACC)
C      ABOVE IS EQUIVALENT TO ADGELG(FACC,FDACC,N2,1,EPS,IER)
      IER=0
      IF(IER) 6989,6990,6989
6989 WRITE(3,6901)
6901 FORMAT('// SINGULAR MATRIX, NO RESULTS//)
      GO TO 9999
6990 DO 6999 J=1,N2
      WRITE(7,*) 'J=',J,'T(J,1)=' ,T(J,1),'FACC(1,J)=' ,FACC(1,J)
      T(J,1)=T(J,1)+FACC(1,J)
      L=1
      DO 6999 I=1,N2
      IF(ABS(FACC(1,I)).GE.1.E-4) L=0
6999 CONTINUE
C      END OF NEWTON *****
C
      NN=NN+1
      IF(NN.LT.20) GO TO 86191
      GO TO 86180

```

```

86191 IF(L.EQ.0) GO TO 86170
      IF(B.LT.1.E-8.AND.E.LT.1.E-8)GO TO 29168
      GO TO 86192
29168 IPCODE=1
      GO TO 4145
6470 CONTINUE
      GO TO 9999
86192 IF(B.GT.1.E-8)B=B*RB
      IF(E.GT.1.E-8)E=E*RE
      GO TO 86150
C VOLG:      *****
9999 L6=L3
      IF(L3.EQ.0)GO TO 9991
      L=0
      J=0
      ILAST=FLOAT(M1)/2.-.9
      DO 9990 I=1,ILAST
      J=J+C(2*I-1)*2
      L=L+C(2*I)
9990 CONTINUE
      DO 9992 I=1,J
9992 RT(I)=RT(I)*.5
      DO 9993 I=1,L
9993 ZU(I)=ZU(I)*.5
9991 CONTINUE
      N=L4
      M=L5
997 CONTINUE
      GO TO 999
998 WRITE(3,979)
999 CONTINUE
9006 FORMAT(/3X,'*** Y=',1F11.4)
9009 FORMAT( 7X,'X',10X,'TZH',      5X,'ABS(TX,TY)',1X,'ARG(TX,TY)',
      $ 1X,'ABS(VX,VY)',1X,'ARG(VX,VY)')
968 FORMAT('1'///,T63,'PROGRAM WISK-SRT',/,T54,'GENERAL THEORY OF
      $ROLLING CONTACT',/,T64,'BY J.J. KALKER',/,T66,'CLEMSON, SC',/)
969 FORMAT(////,58X,'***** INPUT PARAMETERS *****',/)
970 FORMAT(16X,'NORMALIZED CONTACT DIMENSIONS  A=',1PE11.4,10X,'(
      $ A=A1/C1, B=B1/C1, WHERE C1=SQRT(A1*B1)',/,32X,'(DATA #2)'
      $,11X,'B=',1PE11.4,10X,'( A1,B1 ARE ACTUAL CONTACT DIMENSIONS',/,
      $19X,' COMBINED POISSON S RATIO  NU=',1PE11.4,/,33X,'(DATA #2)'
      $,/,28X,'LAYER STIFFNESSES  LXN=',1PE11.4,/,33X,'(DATA #2)',
      $ 8X,'LYN=',1PE11.4,/,21X,' ELASTIC DIFFERENCE  KAPPA=',1PE11
      $,4,/,33X,'(DATA #2)',/)
972 FORMAT( 26X,'NUMERICAL CONSTANTS  N1=',I3,/,31X,'(DATA $3)',
      $11X,'M1=',I3,/,51X,'NS=',I3,/)
973 FORMAT(47X,'***** PARAMETERS COMPUTED AND USED IN PROGRAM
      *****'

```

```

$,//, 21X,'NORMALIZED SHEAR MODULUS   GS=',1PE11.4,/,22X,'(CO
$MBINED)',//,52X,'N=',I3,5X,'N=NUMBER OF TRACTION POINTS',/,
$52X,'M=',I3,5X,'M=NUMBER OF SLIP POINTS',//)
974 FORMAT(42X,'***** NV2=',I2,' DISTINCT PROBLEMS FOLLOW FOR
DIFFEREN
$T *****',/,45X,'***** VALUES OF NORMALIZED CREEPAGE AND SPIN
*****
$',//)
975 FORMAT(//,17X,'NORMALIXED CREPAGE AND SPIN   UXN=',1PE11.4,/,
$23X,'(INPUT ON DATA #5)',
$ 9X,'UYN=',1PE11.4,/,50X,'PHN=',1PE11.4,//)
977 FORMAT( 24X,'NOMALIZED FORCES ARE   FXN=',1PE11.4,/,29X,
$(COMPUTED)',11X,'FYN=',1PE11.4,//,24X,'RESULTANT FORCE
$RES=',1PE11.4,/,14X,'(RES=SQRT(FXN**2+FYN**2))', 'WRK=',1PE11.4,//)
978 FORMAT( 25X,'NORMALIZED MOMENT IS   MZN=',1PE11.4,/,
$30X,'(COMPUTED)',//)
979 FORMAT(//,58X,'***** A/B LESS THEN 0.1 *****',/,
$58X,'***** WORK NEXT PROBLEM *****',//)
CLOSE(3)
REWIND(3)
CLOSE(9)
REWIND(9)
REWIND(4)
REWIND(5)
REWIND(15)
CLOSE(4)
CLOSE(5)
CLOSE(15)
STOP
END

C ***** FUNCTION SIGN *****
FUNCTION SIGN(X)
IF(X)10,20,30
10 SIGN=-1.0
RETURN
20 SIGN=0
RETURN
30 SIGN=1.0
RETURN
END

C ***** SUBROUTINE CONST *****

SUBROUTINE CONST(A,B,NU,GS)
DIMENSION D(3),E(3,20),AR(20)
C ***** DATA E(I,J) GIVES THE VALUES OF GS FROM
C ***** KALKER'S TABLE, VALID FOR A/B EQUAL TO OR GREATER THEN

```

```

0.1
  REAL NU
  DATA E/
    $ 0.7670, 0.5752, 0.3835, 0.5608, 0.4206, 0.2804, 0.4779, 0.3584,
    $ 0.2390, 0.4343, 0.3257, 0.2172, 0.4089, 0.3066, 0.2044, 0.3934,
    $ 0.2950, 0.1967, 0.3840, 0.2880, 0.1920, 0.3785, 0.2839, 0.1892,
    $ 0.3758, 0.2818, 0.1879, 0.3750, 0.2812, 0.1875, 0.3758, 0.2818,
    $ 0.1879, 0.3785, 0.2839, 0.1892, 0.3840, 0.2880, 0.1920, 0.3934,
    $ 0.2950, 0.1967, 0.4089, 0.3066, 0.2044, 0.4343, 0.3257, 0.2172,
    $ 0.4779, 0.3584, 0.2390, 0.5608, 0.4206, 0.2804, 0.7670, 0.5752,
    $ 0.3835, 0.7918, 0.5938, 0.3959/
    DATA AR / 0.1,0.2,0.3,0.4,0.5,0.6,0.7,0.8,0.9,1.0,1.111111,
    $1.25,1.428571,1.666667,2.0,2.5,3.333333,5.0,10.0,11.0/
    PI=3.14159
    RG=A/B
    IF(RG.GT.AR(20)) GO TO 14
    GO TO 15
14  SG=B/A
    GS=3.0*(1.0-NU)/(4.0*PI*SQRT(SG))
    GO TO 80
15  DO 20 I=2,20
    IF(RG.LE.AR(I)) GO TO 25
20  CONTINUE
25  J=I
    DO 30 I=1,3
30  D(I)=E(I,J-1)+(E(I,J)-E(I,J-1))*(RG-AR(J-1))/(AR(J)-AR(J-1))
    AL=8.0*(D(3)-2.0*D(2)+D(1))
    BE=2.0*(-D(3)+4.0*D(2)-3.0*D(1))
    GS=AL*NU**2+BE*NU+D(1)
80  CONTINUE
    RETURN
    END
C
C ***** SUBROUTINE ARRAY *****
C
  SUBROUTINE ARRAY(MODE,I,J,N,M,S,D)
  DIMENSION S(1), D(1)
cc  DOUBLE PRECISION S(120),D(120)
  NI=N-I
C  TEST TYPE OF CONVERSION
  IF(MODE-1) 100, 100, 120
C  CONVERT FROM SINGLE TO DOUBLE DIMENSION
100  IJ=I*J+1
    NM=N*J+1
    DO 110 K=1,J
    NM=NM-NI
    DO 110 L=1,I
    IJ=IJ-1

```

```

      NM=NM-1
110 D(NM)=S(IJ)
      GO TO 140
C CONVERT FROM DOUBLE TO SINGLE DIMENSION
120 IJ=0
      NM=0
      DO 130 K=1,J
      DO 125 L=1,I
      IJ=IJ+1
      NM=NM+1
125 S(IJ)=D(NM)
130 NM=NM+NI
140 RETURN
      END

```

```

C
C *****SUBROUTINE GMPRD*****
C

```

```

      SUBROUTINE GMPRD(A,B,R,N,M,L)
      DIMENSION A(1), B(1), R(1)
cc  DOUBLE PRECISION A(120),B(120),R(120)
      IR=0
      IK=-M
      DO 10 K=1,L
      IK=IK+M
      DO 10 J=1,N
      IR=IR+1
      JI=J-N
      IB=IK
      R(IR)=0
      DO 10 I=1,M
      JI=JI+N
      IB=IB+1
10  R(IR)=R(IR)+A(JI)*B(IB)
      RETURN
      END

```

```

C*****
      SUBROUTINE SORR(A,B,N,EPS,IK,KKK,UYN)
      DIMENSION A(120,120), B(120), X(120),XN(120),ERR(120)
C*****
cc  Note omega = 1.35 provides fast convergence on + creeps
cc  better convergence on - creeps with omega = 1.08
cc  OMGA=1.35
cc *****
      OMGA=1.08
      SUMAX1=0.0
      SUMAX2=0.0
      ITMAX=30000

```

```

      IF(IK K K K.EQ.1) THEN
      DO 100 NN=1,N
      X(NN)=1.00
100  CONTINUE
      ELSE
CC    DO 105 NR=1,N
CC    X(NR)=X(NR)+B(NR)
CC 105  CONTINUE
      ENDIF
      K=1
101  IF(K.GT.ITMAX) GO TO 200
      DO 150 I=1,N
      DO 125 J=1,I-1
      SUMAX1=A(I,J)*X(J)+SUMAX1
125  CONTINUE
      DO 130 JJ=I+1,N
      SUMAX2=A(I,JJ)*X(JJ)+SUMAX2
130  CONTINUE
      XN(I)=((1.-OMGA)*X(I))+((OMGA/A(I,I))*(B(I)-SUMAX1-SUMAX2))
      SUMAX1=0.0
      SUMAX2=0.0
      ERR(I)=ABS(X(I)-XN(I))
      X(I)=XN(I)
150  CONTINUE
      IJ=1
160  IF(ERR(IJ).LE.EPS) THEN
      IJ=IJ+1
      GO TO 170
      ELSE
      K=K+1
      GO TO 101
      ENDIF
170  IF(IJ.NE.N) GO TO 160
      WRITE(*,*)'UYN=',UYN,'SOLN. WITHIN TOL., IK K K K=',IK K K K,'K=',K
      GO TO 250
200  WRITE(*,*) ' MAX. ITERATIONS EXCEEDED, QUESTIONABLE
ACCURACY'
250  DO 255 KP=1,N
      B(KP)=X(KP)
255  CONTINUE
      RETURN
      END

```


APPENDIX D

Fortran Source Code for Modified COUTAC1 Code

Source Code

```

C
C-----
C PROGRAM COUNTACT-1
C BY B. PAUL AND J. HASHEMI, MODIFIED BY R.F. HARDER, DECEMBER
C 1993
C TO ACCOUNT FOR BATCH MODE OPERATION WITH IMSL SUBROUTINES
C DL2TRG AND DLFSRG REPLACING THE ORIGINAL LEQT1F, FOR IBM 486
C OPERATION.
* This program has modified section of mesh generation
C
C PURPOSE.....
C TO SOLVE FOR PRESSURE DISTRIBUTION, BOUNDARY OF CONTACT
C PATCH,
C AND LOAD WHEN THE TWO BODIES IN COUNTERFORMAL CONTACT
C UNDERGO
C A RIGID BODY APPROACH DELTA.
C
C METHOD.....
C THE MODIFIED SIMPLY DISCRITIZED METHOD OF CONTACT PATCH IS
C USED TO SOLVE THE GOVERNING INTEGRAL EQUATIONS. FOR MORE
C DETAILS SEE "AN IMPROVED NUMERICAL METHOD FOR
C COUNTERFORMAL
C CONTACT PROBLEMS" BY B. PAUL AND J. HASHEMI.
C
C STANDARD SUBPROGRAMS.....
C SUBFUNCTION DAOR (XF,YF,XS,YS,HXS,HYS)
C SUBFUNCTION PARAB (SM,SL,SK,PM,PL,PK)
C
C INPUT VARIABLES.....
C TITLE ANY TITLE DESCRIBING PROBLEM (UP TO 80 CHARACTERS)
C IAI MAX. DIMENSION USED FOR B AND F
C IDGT A PARAMETER USED IN IMSL SURROUTINE LEQT1F
C ITM MAXIMUM NO. OF ITERATIONS
C NC THE STRIP NO. THAT CONTROLS THE CONVERGENCE
C E1,ANU1 ELASTIC PROPERTIES OF BODY 1
C E2,ANU2 ELASTIC PROPERTIES OF BODY 2
C MX1,MX2,MX3 NO. OF STRIPS IN FIRST,SECOND,THIRD
C MX4,MX5 FOTH AND FIFTH SEGMENTS
C MX,MY TOTAL NO. OF STRIPS AND NO. OF CELLS
C IN EACH STRIP

```

```

C   XX1,XX2,XX3  LENGTH OF FIRST,SECOND,THIRD
C   XX4,XX5     FORTH AND FIFTH SEGMENT
C   XB(I),YB(I) COORDINATES OF THE POINTS ON THE BOUND. CURVE
C   EPS         ANO. TO CONTROL THE TOLERANCE
C   D           RIGID BODY APPROACH

```

```

C   INPUT ARRANGEMENTS.....
C   CARD ID FORMAT VARIABLES
C   A (20A4) TITLE
C   B (4I5) IAI,IDGT,ITM,NC
C   C (4F10.0)E1,ANU1,E2,ANU2
C   D1 (5I5) MX1,MX2,MX3,MX4,MX5
C   D2 (2I5) MX,MY
C   D3 (5F10.0)XX1,XX2,XX3,XX4,XX5
C   E (8F10.0)XB(I),YB(I) I=1,MX
C   F (F10.0) EPS
C   G (F10.0) D

```

```

C-----
C
C   IMPLICIT REAL*8 (A-H,O-Z)
C   character*4 cnverg
C   DIMENSION B(100,100),F(100,1),WKAREA(100),XSY(100),YSY(100)
C   DIMENSION P(20,5),XB(20),YB(20),HX(20),HY(20),XBN(20),YBN(20)
C   DIMENSION YBM(20),AR(20)
C   DIMENSION TITLE(20)
C   dimension yy(10,10),pp(10,10)
C   OPEN(UNIT=5,FILE='NHZ1364.DAT',STATUS='OLD')
C   OPEN(UNIT=6,FILE='NH136TT.OUT',STATUS='OLD')
C   open(unit=7,file='rcpnip2.dat',status='old')

```

```

C
C.....INPUT DATA
C   1 READ (5,226,END=999) TITLE
C   READ (5,225) IAI,IDGT,ITM,NC
C   READ (5,218) E1,ANU1,E2,ANU2
C   READ (5,225) MX1,MX2,MX3,MX4,MX5
C   READ (5,225) MX,MY
C   READ (5,218) XX1,XX2,XX3,XX4,XX5
C   READ (5,218) (XB(I),YB(I),I=1,MX)
C   READ (5,218) EPS
C   READ (5,218) D

```

```

C
C.....PRINT OUT INPUT DATA
C   WRITE (6,227) (TITLE(I),I=1,20)
C   WRITE (6,219) IAI,IDGT,ITM,NC,EPS
C   WRITE (6,212) E1,ANU1,E2,ANU2
C   WRITE (6,220) MX1,MX2,MX3,MX4,MX5
C   WRITE (6,224) XX1,XX2,XX3,XX4,XX5
C   WRITE (6,229) MX,MY,D

```

```

C
C.....CALCULATE SOME OF THE CONSTANT VARIABLES
N=MX*MY
PI=3.141592654
CK=(1.-ANU1**2)/(PI*E1)+(1.-ANU2**2)/(PI*E2)
IT=1
C
  do 2 i=1,mx
2 ybm(i)=yb(i)
  xtot=xx1+xx2+xx3+xx4+xx5
  do 3 i=1,5
  rxx1=xx1/xtot
  rxx2=xx2/xtot
  rxx3=xx3/xtot
  rxx4=xx4/xtot
  rxx5=xx5/xtot
  3 continue
C.....CALCULATE AND STORE HY(I)
  DO 4 I=1,MX
4 HY(I)=YB(I)/(MY-.5)
  I=1
  IF (MX1.EQ.0) GO TO 7
  H=XX1/MX1
C
C.....CALCULATE AND STORE HX(I) FOR FIRST STRIP
  DO 6 I=1,MX1
6 HX(I)=H
  I=MX1+1
7 MX12=MX1+MX2
  H=XX2/MX2
C
C.....CALCULATE AND STORE HX(I) FOR SECOND STRIP
  DO 8 J=I,MX12
8 HX(J)=H
  J=MX12+1
  H=XX3/MX3
  MX123=MX12+MX3
C
C.....CALCULATE AND STORE HX(I) FOR THIRD STRIP
  DO 9 I=J,MX123
9 HX(I)=H
  I=MX123+1
  MX1234=MX123+MX4
  H=XX4/MX4
C
C.....CALCULATE AND STORE HX(I) FOR FOURTH STRIP
  DO 10 J=I,MX1234
10 HX(J)=H

```

```

IF (MX5.EQ.0) GO TO 14
H=XX5/MX5
J=MX1234+1
C
C.....CALCULATE AND STORE HX(I) FOR FIFTH STRIP
DO 12 I=J,MX
12 HX(I)=H
14 xblm=xb(1)-hx(1)/2.0
   xbrm=xb(mx)+hx(mx)/2.0
   xbr=xbrm
   xbl=xblm
C
C.....SOURCE POINT DO-LOOP
15 J=0
   cnverg='yes'
DO 100 IS=1,MX
   XS=XB(IS)
   HXS=HX(IS)
   HYS=HY(IS)
   AR(IS)=HXS*HYS
DO 100 JS=1,MY
   J=J+1
C
C.....FIELD POINT DO LOOP
I=0
DO 100 IFF=1,MX
   XF=XB(IFF)
DO 100 JF=1,MY
   I=I+1
   IF (J.GT.1) GO TO 60
   XSX(I)=XB(IFF)
   YSY(I)=HY(IFF)*(JF-1)
   YY=YSY(I)
   XX=XSX(I)
C
C.....CALCULATE THE INITIAL SEPARATION AND THE RIGHT HAND SIDE OF
EQ.
CALL INSEP(XX,YY,FZ)
F(I,1)=(D-FZ)/CK
60 IF (I.GT.1) GO TO 65
   HXS=HX(IS)
   YS=YSY(J)
65 YF=YSY(I)
   IF (JS.EQ.1) GO TO 80
C
C.....FIND B(I,J) FOR CELLS AWAY FROM THE X-AXIS
B(I,J)=DAOR(XF,YF,XS,YS,HXS,HYS)+DAOR(XF,YF,XS,-YS,HXS,HYS)
GO TO 100

```

```

C
C.....FIND B(I,J) FOR CELLS ON THE X-AXIS
      80 B(I,J)=DAOR(XF,YF,XS,YS,HXS,HYS)
      100 CONTINUE
C
C.....SOLVE SYSTEM OF LINEAR EQUATIONS
CC   CALL LEQT1F(B,1,N,IAI,F,IDGT,WKAREA,IER)
      CALL DL2TRG(N,B,IAI,B,IAI,FPVT,WKAREA)
      CALL DLFSRG(N,B,IAI,FPVT,F,1,F)
C
C.....PRINT OUT ITERATIONS WITH POINTS ON THE BOUND. CURVE
      WRITE (6,223) IT
      WRITE (6,213)
      WRITE (6,214)
      WRITE (6,222) (XB(I),YB(I),I=1,MX)
      WRITE (6,211)
      WRITE (6,215) (I,XSX(I),YSY(I),F(I,1),I=1,N)
      WRITE (6,221) XBL,XBR
      RY=YB(NC)
C
C.....TEST FOR ALL PRESSURES TO BE POSITIVE
      IFP=0
      IL=0
      IJ=0
      DO 180 I=1,MX
      DO 150 J=1,MY
      IJ=IJ+1
      P(I,J)=F(IJ,1)
      IF (P(I,J).LT.0.0) then
         cnverg='no'
         go to 160
      else
         end if
      IF (IL.NE.1) GO TO 150
      I1=I-1
      XBL=(P(I,J)*XB(I1)-P(I1,J)*XB(I))/(P(I,J)-P(I1,J))
      XB(I1)=XBL
      YB(I1)=0.0
      IL=2
      150 CONTINUE
C
C.....LOCATE THE CELLS FOR EXTRAPOLATION TO GET THE NEW YB(I)
      F1=F(IJ,1)
      IJ1=IJ-1
      F2=F(IJ1,1)
      F3=F(IJ1-1,1)
      Y1=YSY(IJ)
      Y2=YSY(IJ1)

```

```

Y3=YSY(IJ1-1)
C
C.....FIND YB(I) BY PARABOLIC EXTRAPOLATION
if(f2.gt.f1) then
  YBN(I)=PARAB (Y1,Y2,F1,F2)
else
  cnverg='no'
  if(f3.gt.f2)then
    ybn(i)=parab(y2,y3,f2,f3)
  else
    go to 155
  end if
end if
IF (YBN(I).LE.YBM(I)) GO TO 180
if(ybm(i).eq.0.0) go to 180
155 YBN(I)=(YBN(I)+YBM(I))/2.
GO TO 180
160 IF (J.GT.1) GO TO 170
  IF (XB(I).GT.0.0) GO TO 200
  IL=1
  IIL=I
  GO TO 179
170 Y1=YSY(IJ)
  IJ1=IJ-1
  Y2=YSY(IJ1)
C
C.....FIND YB(I) WHEN PRESSURE CHANGES SIGN
  YBN(I)=(F(IJ,1)*Y2-F(IJ1,1)*Y1)/(F(IJ,1)-F(IJ1,1))
  YBM(I)=Y1
179 IJ=I*MY
  IFP=1
180 CONTINUE
  IIL=1
  IF (IIL.EQ.2) GO TO 183
C.....FIND THE LEFT X-BOUNDARY BY PARABOLIC EXTRAPLATION
  F1=P(1,1)
  F2=P(2,1)
  F3=P(3,1)
  X1=XB(1)
  X2=XB(2)
  X3=XB(3)
  if(f2.gt.f1) then
    XBLN=PARAB(X1,X2,F1,F2)
  else
    cnverg='no'
    if(f3.gt.f2) then
      xbln=parab(x2,x3,f2,f3)
    else

```

```

        go to 182
    end if
end if
C
IF (XBLN.LT.XBLM) GO TO 182
XBL=XBLN
GO TO 183
182 XBL=(XBL+XBLM)/2.
C.....FIND THE RIGHT X-BOUNDARY BY PARABOLIC EXTRAPOLATION
183 I1=MX-1
    F1=P(MX,1)
    F2=P(I1,1)
    F3=P(I1-1,1)
    X1=XB(MX)
    X2=XB(I1)
    X3=XB(I1-1)
    if(f2.gt.f1) then
        XBRN=PARAB(X1,X2,F1,F2)
    else
        cnverg='no'
        if(f3.gt.f2) then
            xbrn=parab(x2,x3,f2,f3)
        else
            go to 185
        end if
    end if
end if
C
IF (XBRN.GT.XBRM) GO TO 185
XBR=XBRN
GO TO 186
185 XBR=(XBR+XBRM)/2.
186 I1=MX+1
    XB(I1)=XBR
    YBN(I1)=0.0
    IF (IFP.EQ.1) GO TO 340
C
C.....INITIALIZE SOME OF THE VARIABLES
FT=0.0
TORK=0.0
DO 199 I=1,MX
DO 199 J=1,MY
IF (J.EQ.1) GO TO 196
C=1.
GO TO 198
196 C=.5
C
C.....FIND THE LOAD.
198 FTT=P(I,J)*AR(I)*C

```

```

    FT=FT+FTT
    TORK=TORK+FTT*XB(I)
199 CONTINUE
    FT=2.*FT
    TORK=2.*TORK
    WRITE (6,216) FT,TORK,D
    GO TO 340
200 I1=I-1
    XBR=(P(I,J)*XB(I1)-P(I1,J)*XB(I))/(P(I,J)-P(I1,J))
    YBN(I)=0.0
    XB(I)=XBR
    if (il.eq.2) go to 340
    ILL=2
    F1=P(1,1)
    F2=P(2,1)
    F3=P(3,1)
    X1=XB(1)
    X2=XB(2)
    X3=XB(3)
C
C.....FIND THE X-LEFT BOUND WHEN ALL PRESSURES ARE +VE.
    if(f2.gt.f1) then
        XBLN=PARAB(X1,X2,F1,F2)
    else
        cnverg='no'
        if(f3.gt.f2) then
            xbln=parab(x2,x3,f2,f3)
        else
            go to 250
        end if
    end if
    IF (XBLN.LT.XBLM) GO TO 250
    XBL=XBLN
    GO TO 340
250 XBL=(XBL+XBLM)/2.
340 IF(DABS(1.-RY/YBN(NC)).LE.EPS.and.cnverg.eq.'yes')GO TO 450
    IF (IT.GT.ITM) GO TO 450
    IT=IT+1
    xtot=xbr-xbl
    xbl=xbl
* mesh generation of first strip
    if(mx1.eq.0)then
        xx1=0.0
    else
        xx1=xtot*rx1
        h=xx1/real(mx1)
        do 400 i=1,mx1
            hx(i)=h

```



```

    xbn(i)=xb1+(real(i)-0.5)*h
400 continue
    end if
    xb1=xb1+xx1
    j1=mx1+1
    j2=mx1+mx2
* mesh generation of second strip
    if(mx2.eq.0)then
        xx2=0.0
    else
        xx2=xtot*rxx2
        h=xx2/real(mx2)
        do 405 i=j1,j2
            hx(i)=h
            xbn(i)=xb1+(real(i-j1+1)-0.5)*h
405 continue
        end if
        xb1=xb1+xx2
        j1=j1+mx2
        j2=j2+mx3
* mesh generation of third strip
        if(mx3.eq.0)then
            xx3=0.0
        else
            xx3=xtot*rxx3
            h=xx3/real(mx3)
            do 410 i=j1,j2
                hx(i)=h
                xbn(i)=xb1+(real(i-j1+1)-0.5)*h
410 continue
            end if
            xb1=xb1+xx3
            j1=j1+mx3
            j2=j2+mx4
* mesh generation of fourth strip
            if(mx4.eq.0)then
                xx4=0.0
            else
                xx4=xtot*rxx4
                h=xx4/real(mx4)
                do 415 i=j1,j2
                    hx(i)=h
                    xbn(i)=xb1+(real(i-j1+1)-0.5)*h
415 continue
                end if
                xb1=xb1+xx4
                j1=j1+mx4
                j2=j2+mx5

```

```

* mesh generation of fifth strip
  if(mx5.eq.0)then
    xx5=0.0
  else
    xx5=xtot*rx5
    h=xx5/real(mx5)
    do 420 i=j1,j2
      hx(i)=h
      xbn(i)=xb1+(real(i-j1+1)-0.5)*h
420 continue
    end if
* interpolate new yb when xb are known
  do 435 i=1,mx
    xarg=xbn(i)
    xb1=xb(1)
    xbm=xb(mx)
    if(xarg.lt.xb1) then
      yb(i)=0.0+(xarg-xb1)/(xb1-xb1)*(ybn(1)-0.0)
    else if(xarg.gt.xbm) then
      yb(i)=0.0+(xbr-xarg)/(xbr-xbm)*(ybn(mx)-0.0)
    else
      do 430 j=1,mx-1
        if(xarg.lt.xb(j)) go to 430
        yb(i)=ybn(j)+(xarg-xb(j))/(xb(j+1)-xb(j))*(ybn(j+1)-ybn(j))
430 continue
      end if
435 continue
* calculate hy
  do 440 i=1,mx
    xb(i)=xbn(i)
    hy(i)=yb(i)/(real(my)-0.5)
440 continue
C
C.....REPEAT THIS PROCESS AS MANY TIMES AS REQUIRED.
  GO TO 15
450 WRITE (6,214)
  WRITE (6,222) (XB(I),YB(I),I=1,MX)
C.....SOLVE THE NEXT PROBLEM IF ANY.
  GO TO 1
460 WRITE (6,230)
  GO TO 1
999 WRITE (6,1000)
cc
*****
cc **add logic for writing the ycoord and pressures in a rolcrepn format**
cc
*****
NI=5

```

```

GK=1.0
DO 4200 NN=1,9
KT=2
DO 4290 MM=1,9
IF(MM.LT.5) GK=-1.0
IF(MM.EQ.5) GO TO 4280
IF(MM.GT.5) GO TO 4285
YY(NN,MM)=GK*YSY((NN*NI)+1-MM)
PP(NN,MM)=F(((NN*NI)+1-MM),1)
GO TO 4287
4280 YY(NN,MM)=0.0
PP(NN,MM)=F(((NN*NI)+1-MM),1)
GO TO 4287
4285 YY(NN,MM)=- (YY(NN,MM-KT))
PP(NN,MM)=PP(NN,MM-KT)
KT=KT+2
4287 GK=1.0
4290 CONTINUE
4200 CONTINUE
DO 4300 IW=1,9
WRITE(7,4299)(YY(IW,IV),IV=1,9)
4299 FORMAT(1X,9(F8.6,','))
4300 CONTINUE
DO 4301 IQ=1,9
WRITE(7,4302)(PP(IQ,IA),IA=1,9)
4302 FORMAT(1X,9(F8.1,','))
4301 CONTINUE
C
*****
****
500 STOP
211 FORMAT (//(25X,'NODE',11X,'X',17X,'Y',17X,'P'))
212 FORMAT(20X,'E1=',E13.7,2X,'ANU1=',F5.3,2X,'E2=',E13.7,2X,'ANU2=',
$F5.3)
213 FORMAT (//(40X,'BOUNDARY OF CONTACT REGION'))
214 FORMAT (//(19X,'X',14X,'Y',14X,'X',14X,'Y',14X,'X',14X,'Y'))
215 FORMAT (//(25X,I5,3E18.7))
216 FORMAT
(//(25X,'FORCE=',F10.3,5X,'MOMENT=',F10.3,5X,'APPROACH=',E1
$2.7))
219 FORMAT (20X,'IAI=',I3,2X,'IDGT=',I3,2X,'ITM=',I3,2X,'NC=',I3
&,2X,'EPS=',E11.4)
220 FORMAT (20X,'MX1=',I3,2X,'MX2=',I3,2X,'MX3=',I3,2X,'MX4=',I3,2X,'
$MX5=',I3)
218 FORMAT (8F10.0)
221 FORMAT (//(28X,'LEFT X-BOUNDARY=',F10.7,5X,'RIGHT X-
BOUNDARY=',F10.
$7))

```

```

222 FORMAT ((10X,6E15.7))
223 FORMAT (///(46X,'ITERATION =',I2))
224 FORMAT (20X,'XX1=',F7.5,3X,'XX2=',F7.5,3X,'XX3=',F7.5,3X,'XX4=',
    $F7.5,3X,'XX5=',F7.5)
225 FORMAT(16I5)
226 FORMAT (20A4)
227 FORMAT (1H1,20X,20A4//)
228 FORMAT (20X,'ERROR DUE TO F2<F1')
229 FORMAT (20x,'MX=',I3,10x,'MY=',I3,10x,'APPROACH=',e11.4)
230 FORMAT(10X,'ERROR IN MESH LAY OUT OVER THE CONTACT PATCH.')
1000 FORMAT (1H1)
    END
    SUBROUTINE INSEP(X,Y,FZ)
    IMPLICIT REAL*8 (A-H,O-Z)
    B=0.026315
    IF(X.GT.0.0)GO TO 10
    A=0.035714
    GO TO 30
10 A=0.400
30 fz=a*x**2+b*y**2
    return
    end
    DOUBLE PRECISION FUNCTION DAOR(XF,YF,XS,YS,HXS,HYS)
C
C-----
C  FUNCTION DAOR(XF,YF,XS,YS,HXS,HYS)
C
C  PURPOSE.....
C  TO CALCULATE INTEGRAL OF DA OVER R.
C
C  METHOD.....
C  BY USING LURE,S FORMULA APPLIED TO A RECTANGLE CELL WHEN
C  THE DISTANCE BETWEEN THE SOURCE AND FIELD POINT IS LESS THAN
C  1.5 TIMES THE MAXIMUM DIMENSION OF CELL, AND APPROXIMATELY
C  AS DA/R , OTHERWISE.
C
C  DESCRIPTION OF ARGUMENT VARIABLES....
C  XF,YF  COORDINATES OF THE FIELD POINT
C  XS,YS  COORDINATES OF THE SOURCE POINT
C  DAOR   VALUE FOR THE FUNCTION TO BE RETURNED
C-----
C
    IMPLICIT REAL*8 (A-H,O-Z)
    EPS=1.E-10
    PI=3.141592654
    C=1.
    YYSF=YS-YF
    R=DSQRT((XF-XS)**2+YYSF**2)

```

```

      IF (HXS-HYS) 1,1,2
1  H=HYS
  GO TO 3
2  H=HXS
3  IF (R-1.5*H) 6,6,4
4  DAOR=HXS*HYS/R
  GO TO 50
6  H1=YYSF+.5*HYS
  IF (DABS(H1)-EPS) 10,10,5
5  H4=H1-HYS
  IF (DABS(H4)-EPS) 10,10,20
10 C=.5
    H1=HYS
    H4=-HYS
20 H2=XS-XF+.5*HXS
    H3=H2-HXS
    T1=DATAN(H2/H1)
    B1=DATAN(H3/H1)
    T2=DATAN(H1/H2)
    B2=DATAN(H4/H2)
    T3=DATAN(H1/H3)
    B3=ATAN(H4/H3)
    T4=DATAN(H2/H4)
    B4=DATAN(H3/H4)
    AT1=DABS(T1)
    AT2=DABS(T2)
    AT3=DABS(T3)
    AT4=DABS(T4)
    AB1=DABS(B1)
    AB2=DABS(B2)
    AB3=DABS(B3)
    AB4=DABS(B4)
    C11=DLOG(DTAN(PI/4.+AT1/2.))
    C12=DLOG(DTAN(PI/4.+AB1/2.))
    C21=DLOG(DTAN(PI/4.+AT2/2.))
    C22=DLOG(DTAN(PI/4.+AB2/2.))
    C31=DLOG(DTAN(PI/4.+AT3/2.))
    C32=LOG(DTAN(PI/4.+AB3/2.))
    C41=DLOG(DTAN(PI/4.+AT4/2.))
    C42=DLOG(DTAN(PI/4.+AB4/2.))
    C1=T1/AT1*C11-B1/AB1*C12
    C2=T2/AT2*C21-B2/AB2*C22
    C3=T3/AT3*C31-B3/AB3*C32
    C4=T4/AT4*C41-B4/AB4*C42
    DAOR=DABS(DABS(H1)*C1+DABS(H2)*C2-DABS(H3)*C3-DABS(H4)*C4)*C
50 RETURN
  END
  DOUBLE PRECISION FUNCTION PARAB(SM,SL,PM,PL)

```

```
C  PARAB(SM,SL,PM,PL)
C -----
C
C  PURPOSE.....
C  TO EXTRAPOLATE BETWEEN TWO POINTS AND FIND ORDINATE
C  WHEN ABSESSIA IS ZERO
C
C  METHOD.....
C  PARABOLIC EXTRAPOLATION BETWEEN THE TWO POINTS AND
C
C  DESCRIPTION OF ARGUMENTS.....
C  (SM,PM) COORDINATES OF POINT M
C  (SL,PL) COORDINATES OF POINT L
C  PARAB  VALUE OF THE ORDINATE TO BE RETURNED TO THE
C  CALLING PROGRAM.
C -----
C
C  IMPLICIT REAL*8 (A-H,O-Z)
C  PARAB=(PL**2*SM-PM**2*SL)/(PL**2-PM**2)
C  RETURN
C  END
```

APPENDIX E

Fortran Source Code for Romberg Integration Algorithm

```

*****
*****ROMBERG.FOR PERFORMS ROMBERG
INTEGRATION*****
*****FOR A GENERAL FUNCTION F(X) BETWEEN LIMITS A &
B*****
*****
CC
*-- ROMBERG.FOR was obtained from "NUMERICAL METHODS" by Faries &
*-- Burden. It integrates the function f(x) from x=a to x=b. The
*-- elements of the Romberg table are stored in T(K,M), where K denotes
*-- the order and M labels the level of the approximation, i.e.the
*-- number of panels,  $n = 2^{**k}$ , while  $M=0 \Rightarrow$  trapezoidal rule,  $M=1 \Rightarrow$ 
*-- Simpson's rule, etc. The calculation is terminated successfully
*-- when successive diagonal elements differ by less than the user
*-- supplied tolerance EPS. Round-off error is monitored by compu-
*-- ting the quantity R(K) which should be close to one. If signi-
*-- ficantly different from one, the calculation is halted, a mes-
*-- sage printed, and the most recent value returned. The calcula-
*-- tion is continued through a maximum user supplied order KMX. If
*-- the desired accuracy is not achieved after order KMX, a diag-
*-- nostic message is printed and the latest, most accurate, value
*-- is returned. If IPRNT=1, the complete Romberg table is printed
*-- before any return. If IFAIL = 1, the procedure has failed.
*=====
=====
* Variables
*--
  DOUBLE PRECISION T(0:15,0:15),R(0:15)
  CHARACTER FLAG*3
  INTEGER K,M,NPTS,KMX,IPRINT
  REAL DX,A,B,EPS,SUM,FRACT
CC  F(X)=2.*X
c  F(XZ)= -4405623.97*XZ**7-2815684.08*XZ**6-638948.149*XZ**5
c  $-63071.45*XZ**4-2430.308*XZ**3-10.164*XZ**2+0.964*XZ+0.211
c  F(X)=(-10093043.759*X**9-9568645.284*X**8-3495835.187*X**7
c  $-625712.645*X**6-61031.681*X**5-4467.105*X**4-380.101*X**3
c  $-24.632*X**2-0.311*X+0.336)
c  F(X)=(-10093043.759*X**9-9568645.284*X**8-3495835.187*X**7
c  $-625712.645*X**6-61031.681*X**5-4467.105*X**4-380.101*X**3
c  $-24.632*X**2-0.311*X+0.336)-(-1405435.799*x**8+36976.952*x**6
c  $-404.579*x**4-6.121*x**2+0.336)

```

```

f(x)=(-1405435.799*x**8+36976.952*x**6-404.579*x**4-6.121*x**2
$+0.336)-(-10093043.759*X**9-9568645.284*X**8-3495835.187*X**7
$-625712.645*X**6-61031.681*X**5-4467.105*X**4-380.101*X**3
$-24.632*X**2-0.311*X+0.336)
c f(x)=-29852179.6*x**8-19677576.5*x**7-4968358.9*x**6-589159.6*x**5
c $-31182.2*x**4-421.421*x**3+7.137*x**2+0.027*x+0.255
c f(x)=-213144280.22*x**8-112525458.477*x**7-22685827.124*x**6
c $-2118216.158*x**5-82207.8*x**4-119.306*x**3+46.6*x**2+.176*x+.202
*--
*-- A,B -- The integration interval [INPUT]
*-- EPS -- Convergence tolerance [INPUT]
*-- KMX -- The maximum order of the calc. [INPUT]
*-- IPRNT -- Print flag, if 1 print tables [INPUT]
*-- T(.) -- The elements of the Romberg table
*-- R(.) -- Table of round-off error flags
*-- K -- The current order of the calculation
*-- M -- The current level of the calculation
*-- NPTS -- Current number of sampling points
*-- SUM -- Sum of interior function values
*-- FRACT -- The fractional change in diagonal elements
*-- IFAIL -- If zero, no errors detected
*-----
* First compute the zero-th order/one panel trapezoidal rule value
* BE SURE TO USE THE NEW LIMITS OF A AND B FOR THE FUNCTION USED*
*
KMX=20
EPS=0.00001
IPRNT=1
A=0.0
B=.07
DX = (B-A)
T(0,0) = 0.5*DX*(F(A) + F(B))
R(0) = 1.
R(1) = 1.
IF(IPRNT .EQ. 1)THEN
WRITE(*,10)(I,I=0,KMX)
WRITE(*,11)' Order','-----',I=0,KMX)
WRITE(*,12)0,T(0,0)
WRITE(*,'(T7,"|-----|")')
ENDIF
*
* Next, for order K = 1 through KMX
*
DO 5 K = 1,KMX
*
* Compute the next order trapezoid rule value, i.e. step
* down the 1-st col. of the table by halving the intervals
* and doubling the number of sampling points.

```



```

*
  NPTS = 2**K
  DX = DX/2.
*
* Sum the function at all odd points, i.e., the midpoints of
* the previous intervals.
*
  SUM = 0.0
  DO 2 I = 1, NPTS-1, 2
    SUM = SUM + F(A+I*DX)
2  CONTINUE
*
* The next order trapezoid rule is given by
*
  T(K,0) = T(K-1,0)/2 + DX*SUM
*
* Next step across the table, M = 1,2, ..., K
*
  KSTOP = K
  DO 3 M = 0, K-1
    T(K,M+1) = T(K,M) + (T(K,M)-T(K-1,M))/(4.**M-1)
3  CONTINUE
  ROMBRG = T(K,K)
  IF(IPRNT .EQ. 1)THEN
    WRITE(*,12)K,(T(K,M),M=0,K)
    WRITE(*,11) ' ',('-----',I=0,K)
  ENDIF
*
* Test for errors or success in this pass
*
  IFAIL = 0
  IF(K .GE. 2)THEN
    FRACT = (T(K,K) - T(K-1,K-1))/T(K,K)
    IF(ABS(FRACT) .GT. EPS)THEN
      R(K) = (T(K-1,K-2) - T(K-2,K-2))/
+         (T(K ,K-2) - T(K-1,K-2))/(4.**K-1)
      IF(ABS(LOG(ABS(R(K)))) .GT. 2.)THEN
        WRITE(*,13)K,R(K),FRACT,T(K,K)
        IFAIL = 1
      CC      RETURN
        GOTO 1000
      ENDIF
    ELSE
      CC      RETURN
        GOTO 1000
      ENDIF
    ENDIF
  5 CONTINUE

```

```

*
* In KMX passes, the calculation has failed to obtain a
* sufficiently accurate value. Print a warning.
*
  WRITE(*,14)KMX,FRACT,ROMBRG
  IFAIL = 1
CC  RETURN
  GOTO 1000
* -----
* Formats
*--
10 FORMAT(/,T5,'The Romberg table',//,
  + T9,'Level =>',/,
  + T7,'|',7(3X,I2,4X,'|'))
*--
11 FORMAT(A6,'|',7A10)
*--
12 FORMAT(2X,I2,T7,'|',7(F9.6,'|'))
*--
13 FORMAT(/,
  + T5,'*=====ERROR in ROMBERG=====*/',/,
  + T5,'| In pass ',I2,' the calculation was halted ',T50,'|',/,
  + T5,'| due to round-off error. The round-off error',/,
  + T5,'| flag is ',E7.1,'. The latest fractional',T50,'|',/,
  + T5,'| change in diagonal terms = ',E7.1,T50,'|',/,
  + T5,'| The value returned = ',F12.8,T50,'|',/,
  + T5,'*=====IFAIL = 1=====*')

14 FORMAT(/,
  + T5,'*=====ERROR in ROMBERG=====*/',/,
  + T5,'| ROMBRG has failed due to excessive iterations*|',/,
  + T5,'| After ',I2,' passes, sufficient accruacy was not '|',/,
  + T5,'| acheived. The latest fractional change was '|',/,
  + T5,'| R = ',E7.1,T52,'|',/,
  + T5,'| The value returned was ',F12.8,T52,'|',/,
  + T5,'*=====IFAIL = 1=====*')
1000 STOP
  END

```

ROBERT F. HARDER
25060 N.W. Russell Creek Rd.
Yamhill, OR 97148
(503) 662-4047 (Home)
(503) 538-8383 ext. 2723 (Work)

**PROFESSIONAL
EXPERIENCE:**

Associate Professor
of Engineering

GEORGE FOX COLLEGE,
NEWBERG, OREGON

Responsibilities include development of 3:2 cooperative Engineering program, student advising and teaching courses in: General Physics, Statics, Dynamics, Strength of Materials, Electric Circuits, Logic Design and Engineering Graphics. August 1988 - Present.

Engineering Consultant

TEKTRONIX CORPORATION - CORPORATE
HEADQUARTERS,
BEAVERTON, OREGON

Responsibilities includes numerical modelling of conjugate heat transfer from discrete heat sources within electronic instrumentation enclosures.
August 1989 - October 1990

CASCADE STEEL CORPORATION,
MCMINNVILLE, OREGON

Responsibility includes process control engineering and thermal analysis for billet reheat furnace.
May 1990 - October 1992

U.P. ENGINEERING,
HOUGHTON, MICHIGAN

Responsibilities included design and drafting work for water treatment and distribution facility.
May 1989-August 1989

SMURFIT NEWSPRINT INC.,
NEWBERG, OREGON

Responsibilities included project design engineering for paper machine vacuum pump addition.
May 1988-January 1989.

- Furnace Engineer UNITED STATES STEEL CORPORATION-GARY WORKS,
GARY, INDIANA
Responsibilities included supervision of instrument repairmen in the testing and maintenance of a microprocessor based combustion control system for the 84" Hot Strip Mill reheat furnaces. Also responsible for thermographic surveys and furnace performance evaluation. September 1982-August 1984.
- Assistant Furnace Engineer GKN/BRITISH STEEL CORPORATION-CARDIFF ROD MILL, CARDIFF, WALES U.K.
Worked on the thermal enhancement of billet reheat furnaces. Responsibilities included assisting in the development and commissioning of a microprocessor based combustion control system. June 1982-September 1982.
- Co-op Student REPUBLIC STEEL CORPORATION-CLEVELAND DISTRICT, CLEVELAND, OHIO
Worked with the Combustion Engineering Department, assigned to the 84" Hot Strip Mill. Responsibilities included energy audits and the redesign of a laminar flow strip cooling system. May 1981-August 1981, March 1980-August 1980.

EDUCATION:

- OREGON GRADUATE INSTITUTE OF SCIENCE AND TECHNOLOGY, BEAVERTON, OREGON
Ph.D. candidate in Materials Science and Engineering Department, January 1992 to present. Research work includes numerical modeling of contact mechanics, thermoelastic rolling contacts and tribology. Courses include: Finite element analysis, Thermal Spray Systems, Wear and Tribology. Thesis defense - May 1995.
- PURDUE UNIVERSITY, WEST LAFAYETTE, INDIANA
Ph.D. candidate in Mechanical Engineering Department, August 1986 to 1988. Research work included the study of radiative heat transfer from combustion processes. Focus was on modeling indirectly heated industrial furnaces and gas-fired radiant tubes. Courses included: Radiation Heat Transfer, Numerical Modeling of Heat, Mass and Momentum Transfer, Combustion, Engineering Optics and Fluid Mechanics.

MICHIGAN TECHNOLOGICAL UNIVERSITY,
HOUGHTON, MICHIGAN

M.S. in Mechanical Engineering, August 1984-July 1986. Research included developing an optical method to determine the temperature and thermal properties of engine deposits in a fired two stroke engine. Course work concentrated on heat transfer, thermodynamics and fluid mechanics. Graduate Teaching Assistant for thermodynamics and heat transfer laboratory.

MICHIGAN TECHNOLOGICAL UNIVERSITY,
HOUGHTON, MICHIGAN

B.S. in Mechanical Engineering, course work concentrated on heat transfer and combustion, September 1978-May 1982. Member of ASME 1980-1982; Member of Sigma Tau Gamma Fraternity 1979-1982; Sigma Tau Gamma Fraternity - President 1981-1982; MTU Varsity Wrestling 1978-1979.

**PROFESSIONAL
SOCIETIES AND
CERTIFICATIONS:**

Member of the Association of Iron and Steel Engineers 1982-1984; certified "Engineer-in-Training" October 1983; certified Thermographer October 1983; currently a member of ASME, ASEE.

PERSONAL DATA:

Date of Birth: January 1, 1959
Family: Married, 5 children

**PROFESSIONAL
PUBLICATIONS:**

Harder, R.F. and Urda, M.V., "The Evolution of a State-of-the Art Combustion Control System of U.S. Steel's 84" Hot Strip Mill Reheat Furnaces" Advances in Instrumentation, Volume 39, Part 2, p. 867-876, Instrument Society of America, International Conference, October, 1984.

Harder, R.F., "An Investigation of Simulated and Real Combustion-Chamber Deposits in a Fired Engine Utilizing Radiation Thermometry", Michigan Technological University, M.S. Thesis, 1986.

Harder, R.F., Viskanta, R. and Ramadhyani, S., "Gas Fired Radiant Tubes: A Review of the Literature", GRI-Topical Report, No. GRI-87/0343, Gas Research Institute, Chicago, IL., 1987, pp. 76.

Harder, R.F., Ramadhyani, S. and Viskanta, R., "Evaluation and Modelling of Gas-Fired Radiant Tubes", Presented at the session for Modelling of Combustion Systems-25th National ASME Heat Transfer Conference, Houston, Texas; July, 1988.

Harder, R.F. and Anderson, C.L., "Investigation of Combustion-Chamber Deposit Thermal Behavior Utilizing Optical Radiation Measurements in a Fired Engine", Combustion Science and Technology, Vol. 60, 4-6, p 423, 1988.

Harder, R.F., Ramadhyani, S. and Viskanta, R., "On the Prediction of Natural Gas Burn-Up Rate in Confined Turbulent Diffusion Flames". Presented at the Fossil Fuels Combustion Symposium, ASME 12th Annual Energy-sources Technology Conference, Houston, Texas, January, 1989.

Chapman, K., Harder, R.F., Ramadhyani, S. and Viskanta, R., "Radiative Heat Transfer", GRI Annual Report No. GRI-88-0141, Gas Research Institute, Chicago, IL, 1988.

Harder, R.F., "A Theoretical Investigation of Natural Gas Burn-Up Rate in Enclosed Turbulent Diffusion Flames with Swirl", presented at the International Gas Research Conference, Tokyo, Japan, November, 1989.

Harder, R.F., "Nitric Oxide Reductions in a Multi-Zone Reheat Furnace", presented at the Spring Conference of the Association of Iron and Steel Engineers in Nashville, TN, May 3-5, 1993.

Harder, R.F., "Nitric Oxide Reductions in a Multi-Zone Reheat Furnace", Iron and Steel Engineer, April 1994. pp. 107-111.

Harder, R.F., "Reduced Nitric Oxide Emissions From Industrial Furnaces: A Control System Approach to Near-Stoichiometric Firing", presented at the American Society for Engineering Education Annual Conference in Edmonton, Alberta, Canada, June 26-29, 1994.